Thermally Isolated Microelectronic Devices for Gas Sensing Applications

Dissertation submitted to the Faculty of Science of the
University of Neuchâtel, in fulfillment of the requirements
for the degree of “Docteur ès Sciences”

by

Danick Briand

M. Sc. in Engineering Physics, École Polytechnique de Montréal

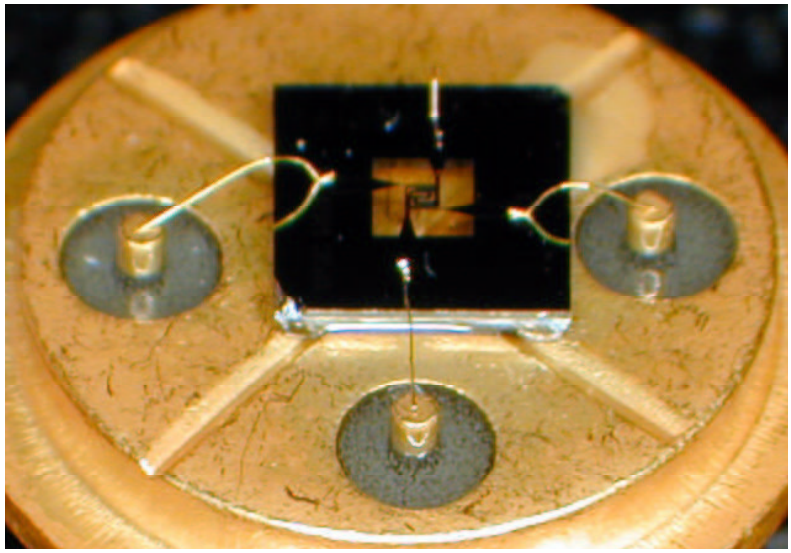

Institute of Microtechnology
University of Neuchâtel
Rue Jaquet-Droz 1, P.O. Box 3
CH-2007 Neuchâtel
Switzerland

2001

IMPRIMATUR POUR LA THESE

Thermally isolated microelectronic devices for gas sensing applications

de M. Danick Briand

UNIVERSITE DE NEUCHATEL

FACULTE DES SCIENCES

La Faculté des sciences de l'Université de Neuchâtel sur le rapport des membres du jury,

Mme. M. Koudelka-Hep,
MM. N. de Rooij (directeur de thèse),
B. van der Schoot et I. Lundström (Linköping S)

autorise l'impression de la présente thèse.

Neuchâtel, le 11 octobre 2001

Le doyen:

J.-P. Derendinger

Abstract

This thesis deals with the reduction of gas sensor power consumption. Systems named electronic noses and containing several non-specific gas sensors of the same or different types, in combination with some data processing, have appeared on the market over the last decade. The transducers of which these systems are composed are mainly chemo-resistors, MOSFETs, quartz microbalance (QMB) and surface acoustic wave (SAW) sensors. General speaking, all these transducers, when coated with a polymer gas-sensitive film, operate at a temperature which is slightly higher than room temperature and exhibit low-power consumption as a result.

In the case of chemo-resistors based on metal oxide gas-sensitive materials, and MOSFETs coated with catalytic metals, operating temperatures can be up to 400°C and 200°C, respectively. If made in a standard technology, these sensors are characterised by relatively high power consumption. They are not suitable for applications in portable electronic nose systems, a new trend in the market. Therefore, the work presented in this thesis focused on the reduction of the power consumption for these two types of gas sensing technology.

The combination of thin film and silicon micromachining processes was used to thermally isolate electronic devices on micro-hotplates. Drop-coated metal-oxide and MOSFET gas sensors requiring less than 100 mW were achieved. The design, fabrication, and optimisation of these devices, and thermal and gas sensing characteristics, are presented.

Résumé

Le sujet de cette thèse est principalement axé sur la diminution de la consommation d'énergie des capteurs de gaz. Les systèmes basés sur les nez électroniques, systèmes qui contiennent plusieurs capteurs de gaz non spécifiques combinés à un traitement des signaux, ont fait leur apparition sur le marché au début des années 90. Les transducteurs composant les capteurs de ces systèmes sont principalement basés sur des résistances électriques, des dispositifs à effet de champ ainsi que des résonateurs soit en quartz, soit utilisant des ondes acoustiques de surface. D'une manière générale, ces différents transducteurs, lorsque combinés à une couche sensible aux gaz de nature polymérique, fonctionnent à une température légèrement supérieure à la température ambiante et nécessitent ainsi un faible apport en énergie.

Dans le cas de capteurs de gaz de type résistif basés sur des couches sensibles composées d'oxydes métalliques, et dans le cas de capteurs de type MOSFET, c'est-à-dire à effet de champ, recouverts d'un métal ayant des propriétés catalytiques, leurs températures de fonctionnement peuvent s'élever respectivement jusqu'à 400°C et 200°C. Lorsqu'ils sont fabriqués à l'aide d'une technologie standard, ces capteurs sont caractérisés par une consommation d'énergie élevée. Ils ne remplissent donc pas les spécifications requises pour les applications dans le domaine des systèmes portatifs, un nouveau créneau sur le marché des nez électroniques. Cette thèse fut donc concentrée sur la réduction de la consommation d'énergie de ces deux types de technologie de capteurs.

Les procédés de dépôt et de structuration de couches minces et de micro-usinage du silicium ont été utilisés afin d'isoler thermiquement des dispositifs électroniques intégrés à des micro-plaques chauffantes sur silicium. Des micro-capteurs de gaz de type résistif à base d'un oxyde métallique en couche épaisse et de type MOSFET, qui présentent une consommation inférieure à 100 mW, ont été réalisés. Le design, la fabrication et l'optimisation de ces dispositifs, de même que leurs comportements thermiques et sous différentes atmosphères gazeuses, sont présentés dans cette thèse.

Contents

Preface

I have always liked to study and, especially, to learn. Knowledge is a precious treasure given by this world (with love!, but love can only be lived…), and many ways can be used to approach and touch it. Physics is a fascinating subject to discover, since it brings with it knowledge about the way this world behaves. A long time ago, I made the decision that I would explore this more deeply through doctoral research. That corresponded to the intellectual freedom I wanted to maintain and helped me avoid to make major decisions about my future.

There are possible reasons for why I ended up in Neuchâtel and in the field of microsystems. Some people who know me quite well would suggest that I followed Justin, or I was attracted by “la $ui$$e”. Nothing was really planned and these choices were more the result of a philosophy of life than anything else. The decisions I made at that time and context were based on what I felt would be best for my own personal growth and intellectual development. I could still keep in touch with physics, pursue an activity I enjoy very much teaching, and experience research and development in an industry- related environment.

This thesis presents the results of my efforts to this end, in the form of work performed within the Sensors, Actuators and Microsystem Laboratory (SAMLAB) at the Institute of Microtechnology, University of Neuchâtel, Switzerland, during the years 1997-2000.

The thesis consists of two parts. In the first part, an introduction to the field of gas sensing and microfabrication is presented. Gas sensing principles and electronic noses are described. This is followed by the presentation of the techniques used to fabricate silicon microstructures. The connection between gas sensors and the microfabrication techniques is then drawn in order to introduce the micromachined gas sensor technology. This first part gives an overview of the status of the research in the field and some technological basics that could help the reader to better appreciate the research papers. To finish the introductory section, a summary introduces the context within which the research presented in the papers was done, and points out the contributions to the field. The second part contains five separate research papers, studying various aspects of micromachined gas sensors: their design, fabrication, operation and optimisation. This represents the main body of the thesis, since I present there my own work and the subsequent contributions to the field.

This thesis gave some answers to few questions, answers that are considered as right now, but that could be wrong tomorrow… The value of these contributions to the field is not guarantee, but it was without doubt valuable for my scientific and personal development. Unfortunately, our society needs degrees and titles to recognise the path followed by a man. This thesis is surely the last one I will obtain and from now on, I will be almost fully self-taught.

Neuchâtel, december 4th, 2000

List of papers

This thesis is based on the following papers:

I. Design and fabrication of high temperature micro-hotplates for drop-coated gas sensors
D. Briand, A. Krauss B. van der Schoot, U.Weimar, N. Barsan, W. Göpel, and N.F. de Rooij
Sensors and Actuators, B 68, pp. 223-233, 2000.

II. Thermally isolated MOSFET for gas sensing application
D. Briand, H. Sundgren, B. van der Schoot, I. Lündström, and N.F. de Rooij
IEEE Electron Device Letters, 22(1), pp. 11-13, 2001.

III. A low-power micromachined MOSFET gas sensor
D. Briand, B. van der Schoot, H. Sundgren, I. Lundström, and N.F. de Rooij
Journal of Micro-Electro-Mechanical Systems, 9 (3), pp. 303-308, 2000.

IV. New modes of operation for MOSFET gas sensors using low-power devices

D. Briand, H. Windgrant, B. van der Schoot, H. Sundgren, L.-G. Ekedahl, I. Lundström, and N. F. de Rooij

Conf. Proc. of Eurosensors XIV, Copenhagen, Denmark, Aug. 2000, pp. 737-740, manuscript in preparation.

V. Thermal optimisation of micro-hotplates having a silicon island

D. Briand, S. Heimgartner, M.-A. Grétillat, B. van der Schoot, and N.F. de Rooij

Conf. Proc. of 3rd Int. Conf. on Modelling and Simulation of Microsystems, San-Diego, California, U.S.A., March 2000, pp. 640-643, manuscript in preparation.

Related papers, not included in this thesis

VI. Polymer Gate FET Sensor Array for Detecting Organic Vapours

J.A. Covington, D. Briand, J.W. Gardner, and N. F. de Rooij

Sensors and Actuators, B 77, pp. 155-162, 2001.

VII. Geometry optimisation of micro-hotplates for metal-oxide gas sensors

A.Krauss, D. Briand, N. Barsan, B. van der Schoot, U. Weimar, and N. F. de Rooij

Book of abstracts, 8th International Meeting on Chemical Sensors, Basel, Switzerland, 2-5 July 2000, p. 519, manuscript in preparation.

VIII. A Cabin Air Analyser

R. Tamadori, J.W. Gardner, A. Krauss, U. Weimar, D. Briand, B. van der Schoot, H. Sundgren, I. Besnard, P. Barttlet, L. Gier, and S. Cosensa

Book of abstract, 8th International Meeting on Chemical Sensors, Basel, Switzerland, 2-5 July 2000, p. 450, manuscript in preparation.

Acknowledgements

This thesis was done in collaboration with a number of external partners and involved many people at the Sensors, Actuators and Microsystem Laboratory (SAMLAB). Without all these people, this thesis would not have been as, let's say, "successful". The next paragraphs are dedicated to expressing my sincere gratitude to them. For those people I might have forgotten, you can be sure that this won't be forever. Your contribution will probably be remembered once in the future.

To start with, I want especially to thank Nico de Rooij for giving me the opportunity to work in this versatile, qualified and dynamic group, "le groupe de Rooij"! More than just offering me a motivating and multidisciplinary environment in the heart of the MEMS world, Nico provided me with a position in a very stimulating and exciting project, which after a while became projectS. As he usually says "we are flexible" and during these years I had the chance to learn, teach, supervise, go abroad, attend a lot of conferences, have my six weeks of holidays… And finally I ended up with this thesis. Thanks again, Nico.

Bart van der Schoot, my supervisor, played also an important role in this achievement. He set me on the track at the beginning. He also gave me the little push needed each time I had to change direction or I got stuck somewhere on my way. I have learned a lot from him about the way to manage research projects in collaboration with other partners. I really appreciated his "cool" attitude mixed with a high level of professionalism.

I have also got valuable scientific inputs from the partners involved in the different projects. I am grateful to the members of S-SENCE and AppliedSensor (former NST), Sweden, and to the people at the University of Tübingen, Germany, for the interest and the effort they put in these research projects. I would like to thank Ingemar Lundström for the helpful scientific discussions, the time he spent reviewing my manuscripts and for the honour to have him on the examiners' board of this thesis. Hans Sundgren and Per Martensson also contributed a lot to this work and deserve to be especially acknowledged. Some other people to whom I would like to offer many thanks for their scientific contributions are: Anita Lloyd-Spetz, Ingemar Grahn, Lars-Gunnar Ekedahl and Martin Holmberg from S-SENCE, Andreas Krauss, Nicolae Barsan and Udo Weimar from Tübingen, Martin Eihehag and Tomas Eklöv from AppliedSensor, Emmanuel Scheid from the Laboratory for Analysis and Architecture of Systems in Toulouse, and Jumana Boussey from the Institut National Polytechnique de Grenoble.

And now it is the time to say how I appreciated to work with all of you from SAMLAB. I am especially grateful to Milena for accepting to be an examiner of this thesis, to Sabeth for kindly reviewing my English, to Jean-Charles for the Ghost views, to Marc for introducing me to the field of simulation, to Olivier and Gregor for their fruitful collaborations, to Peter for sharing the same hobby, to KTS, Beni and PFI for the good ambience and all the people who organised "apéro". Great thanks to the members of the SAMLAB technical staff: Edith, Sabina, Bastien, Cleyron, Gianni, José and Sylvain, who processed so many runs for me during these years. I would not be surprised if they thought I was doing some smuggling. I would also like to mention the

willingness of the people responsible for the computer network to always answer my dummy questions.

Some students also participated in this work and helped it advance: Helena Wingbrant, Stephan Heimgartner and Thorsten Knoll. It was pleasant to work with them and my best wishes for their futures.

Some people contributed indirectly to this work. I would like to thank two friends who lived in Neuchâtel during the time this thesis was done: Steph and Justin, for their great contribution to my social life and for the discoveries made together in fields other than science. I think that I spent more time in their living rooms than in the clean room. Also many thanks to my roommate and friend, Jeanne, who withstood the two crazy guys mentioned above (and me of course), and with whom I could escape into a more spiritual world.

Finally, I am grateful to the bus drivers who drove me carefully to the Czech Republic more than once a month in average, and this over almost three years. The journeys were good sources of inspiration and relaxation. The Czech Republic is a country that provided me with the funny people, the warm atmosphere and the good beer missing in Switzerland. Most of all, the Czech Republic brought to me the “magic” woman with whom I am sharing my life and to whom I open my soul.

Take care,

1. Introduction

Human beings have existed a long time, that is to say, more than just a few years ! From the beginning, our ancestors relied on the sophisticated senses of hearing, smell, touch, taste and sight, which helped them to survive in the uncertain environment in which they lived. The knowledge they obtained from their sensing experiences over the generations stimulated, in a more efficient way, the development of another powerful tool than their senses: the brain. We have just to think of other animals and of people who have a deficiency in one or more of these senses, and as a consequence develop their remaining senses to above the average levels, to say that in general the human being does not use his senses with the utmost efficiency. The development of the brain over a long period of time, and the outbreak of science in our society made that the time dedicated to our senses was neglected for more creative processes. A consequence of this evolution is that our senses have been replaced in a lot of operations. Different transducers are used to attain higher accuracy and an increase in productivity, and certainly sometimes because of our laziness.

Nowadays, there is a lot of effort in the scientific community to mimick most of these senses in order to replace the traditional panels of human testers, which are expensive and not as always objective as we want them to be. Most of the applications may be found in quality control, environmental monitoring, safety and health screening. For instance, microphones, another growing field in microsystems technology, have been developed for people who are hard of

hearing. Optical inspection and/or recognition of components is used in many fields such as in microelectronics, and chemical sensor systems have appeared for quality control of products with respect to smell (emitted gases) and/or taste (extracted liquid). The latter field of multisensor analysis of both gaseous environments and chemically complex liquids has been growing rapidly during the last decade (the 90's), with the intention of replacing or complement advanced analytical instruments such as gas chromatographes and mass spectrometers [1]. These instruments reveal the identity and the concentration of the molecules giving rise to smell, but they are expensive and require trained personal. Moreover, the amount of data to evaluate in the analysis is extensive and it is a difficult task to relate a multitude of parameters to a certain state or odour.

The concepts of artificial sensing systems, capable of producing a digital fingerprint of a given gaseous or liquid ambient, have come to be known as electronic noses (Enoses) and electronic tongues (Etongues), respectively [2,3]. The electronic nose/tongues can be seen as the middle course between the human panel and the advanced analytical systems to analyse odours. In an electronic nose, the function of the olfactory bulb in the mammalian olfactory system is assumed by an array of non-specific gas sensors, and a computer is used for measuring, processing and evaluating the signals from the sensors [2-5]. Taking into account the large number of transducers and gas-sensitive materials that exist, a multitude of gas sensing devices can be developed [6]. At the moment, the main gas sensors used in the electronic noses are based on metal-oxides, conducting polymers, polymer composites (e.g. carbon black matrix) and catalytic metals materials, in combination with chemoresistor,

MOSFET, quartz microbalance (QMB) and surface acoustic waves (SAW) transducers [3].

A new trend in the electronic nose market is the development of hand held monitoring devices capable of performing on-site analysis. One limitation for such a device is power consumption, which should be low enough to allow battery operation. Looking at the list of sensors generally used, the metal-oxide and MOSFET sensors are generally operated at high temperature, 250–450°C and 140–200°C, respectively [6]. If made in a standard technology, their high power consumption is unsuitable for portable electronic nose systems.

Therefore, there is a need to reduce the power consumption in these two gas-sensing technologies. The thermal isolation of these electronic devices by their integration onto micro-hotplates using a combination of the thin-film and microfabrication processing is the subject of the thesis presented in the next chapters and research papers that follow.

Chapter 2 presents the different transducers used for gas sensing applications, and their incorporation in the gas sensing systems named electronic noses. The main focus is on the sensor technologies utilised in the papers, namely the metal-oxide and MOSFET sensors. Then in Chapter 3, the main microfabrication techniques to micromachine microstructures in silicon are described. Silicon is the material that was chosen to fabricate the micro-hotplates on which the gas sensitive devices were thermally isolated. Finally, Chapter 4 is an overview of the work performed so far in the field of micromachined gas sensors. Their design and fabrication are presented with respect to their thermal and mechanical behaviour.

Throughout these chapters, connections are drawn to both work previously published in the literature and the papers included in this thesis. Hopefully, these chapters will provide an introduction for the neophytes in the field, and guidance for the discerning reader when going through the papers forming the body of this thesis.

2. Gas sensor systems

A gas sensor is a chemical sensor that is operated in the gas phase. It converts chemical information, which is determined by different concentrations of gaseous chemical species, into an electrical signal [6]. Thus, a chemical sensor gives a signal that in some way is related to the chemical environment it is exposed to. The response, x, of a gas sensor to a single gas can be described as:

$$x = f_{gas}(c_{gas}) \tag{2.1}$$

where f_{gas} is a function (usually non-linear) and c_{gas} the concentration of the gas. The response is in most cases defined as the difference or ratio between the steady-state sensor response when exposed to the sample gas and the sensor response when exposed to a reference atmosphere (no sample gas). This is shown in Figure 2.1a.

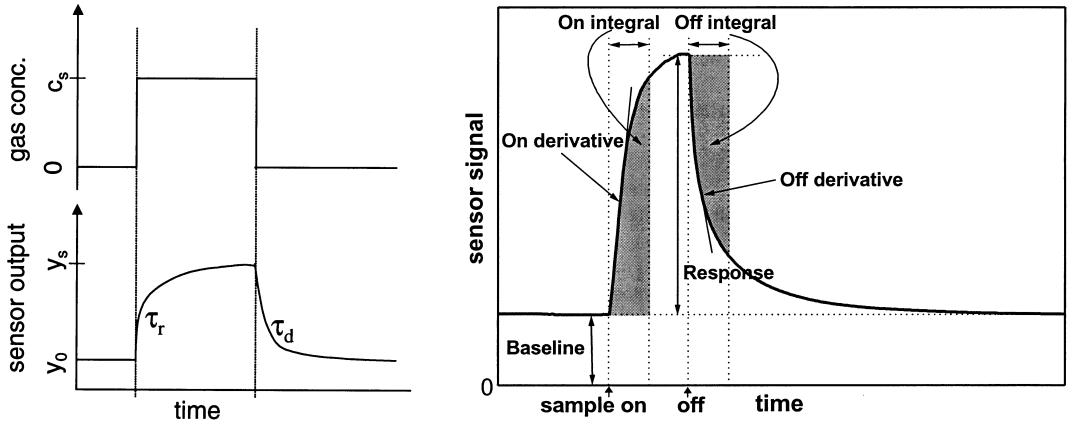

Figure 2.1. (a) Typical gas sensor response curve, (b) Possible parameters to extract from a gas response curve.

The concentration-response relationship for most gas sensors approximately exhibits either saturated linear behaviour, i.e. linear for low concentrations and saturated for higher concentrations, or logarithmic behaviour. Other values containing information about the kinetics of the reactions can also be extracted from the sensor response, such as the derivatives and integrals over certain time intervals (Fig. 2.1b). Three important parameters when describing the response of a sensor are the sensitivity, selectivity and stability. The sensitivity, γ_{gas}, of the sensor towards a specific gas is then defined as:

$$\gamma_{gas} = \frac{\partial x}{\partial c_{gas}} \tag{2.2}$$

In general, the sensitivity is a non-linear function of concentration. The selectivity, Ξ, of a single sensor is usually defined as the ratio of the sensitivity related to the gas concentration to be monitored in the linear region and the maximal sensitivity to all other interfering components:

$$\Xi = \frac{\gamma_{gas}}{\max\limits_{all\ other\ gases}(\gamma)} \tag{2.3}$$

The stability of the sensor response is defined as the reproducibility of the sensitivity and selectivity as a function of time. Most of the drawbacks of the commonly used gas sensing technologies come from of their lack of stability.
There are other demands to be met when producing gas sensors, such as short response time, good reversibility, low cost, small size and low power consumption. The work presented here concentrated on optimisation of the

last three points. The gas-sensing properties were evaluated in collaboration with our partners.

In order to be able to reach these requirements, it is important to have a clear view of how a gas sensor is made. It usually consists of two parts: the sensing material and the transducer. The sensing material interacts with the analyte, e.g. by adsorption/desorption or chemical reactions on the surface and/or the bulk of the material. The interaction changes some physical property or properties of the sensing material, such as the electrical conductivity or the mass, which can be detected using a transducer. The latter converts the variation of the physical properties, containing the chemical information, into an electrical signal. Different transducer principles can be used in chemical sensors, such as changes in conductivity as detected by the voltage drop over a series resistor, or changes in mass as detected by the shift in frequency of a resonator. A schematic description of the working principles of solid-state gas sensors is depicted in Figure 2.2 [7].

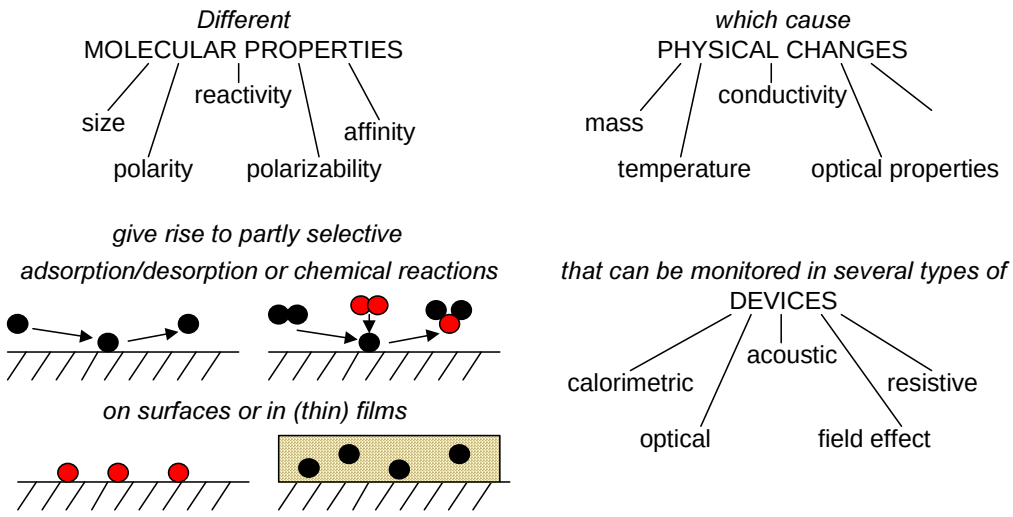

Figure 2.2. Principle of solid-state gas sensors..

In the following sections, different aspects of sensing materials and transducer principles are described, together with the description of some of the most common gas sensors.

2.1 SENSING MATERIALS

A large number of different materials have their physical properties modified after interaction with a chemical environment (Table 2.1). Properties of the analytes, such as molecular size, polarity, polarisability, and affinity, along with the matching characteristics of the sensing material, govern the interaction.

Table 2.1. Typical sensing materials used in gas sensors, adapted from [8]

Class of materials	**Example**
ionic compounds	electronic conductors (SnO_2, WO_3, TiO_2, In_2O_3, MoO_3, V_2O_5, ZnO, …)
	mixed conductors (Ga_2O_3, $SrTiO_3$, …)
	ionic conductors (ZrO_2, CeO_2, …)
metals	Pd, Pt, Ir, Ag, Au, …
polymers	polypyrrole, polytiophene, polyaniline, carbon-black composite…
supramolecular structures	calixarenes, porphyrins, phthalocyanines, …

Two main types of interaction between the analyte and the sensing material can be distinguished. One type is chemical sensing with inorganic materials. Reactions at the surface and/or in the sensing material may lead to chemisorption or catalytic reactions between the molecules present. Thus, the charge distribution, or the carrier concentration or mobility in the sensing material might change, which can be detected by several transducer principles.

This type of gas-sensitive material is often unspecific. Instead, different sensitivities for broad groups of molecules are achieved. The sensitivities of these materials can be tuned by addition of dopants or operation at different temperatures for example. Examples of this type of sensing material are semiconducting metal oxide and catalytic metals [9-12]. Another type of chemical sensing materials is based on lock-and-key-type interaction, which usually consists of organic materials. They can be arranged either as a monolayer of the recognition molecules or as specific recognition sites in a polymeric matrix [8]. Typical materials employed are cage-like molecules, such as calixarenes [13]. The recognition may be both geometric, depending on the size and shape of the material, and affinity-based between the key and lock molecules, via specific recognition sites in the sensing material.

2.2 TRANSDUCER PRINCIPLES

The change in the physical properties of the sensing material when interacting with the analyte might be monitored using different transducer principles. These transducers allow measurement of changes in the physical properties and their conversion into an electrical signal. The most common sensing material properties monitored are summarised in Table 2.2. The changes of different properties of the sensing material, due to its interaction with the analyte, can be measured using different detection principles. For instance, several physical properties have been suggested for monitoring in conjunction with tin oxide sensors, i.e. work function, conductivity and temperature, which can give additional information about the analytes present [14]. Conducting polymers are used mostly as chemoresistors [15], but they can also serve in

mass-sensitive devices [16], work-function sensitive MOSFET [17], capacitive sensors [18], optical thickness dependent devices [18], and temperature sensitive thermopiles [18]. Therefore, several different detection principles can be employed for a specific application, depending on the required characteristics for the sensors, such as the sensitivity, selectivity, linearity, and response time.

Table 2.2 Physical properties monitored in gas sensors [19]

Property		**Example of sensor type**
mass	Δm	Surface acoustic wave sensor and quartz microbalance
work function	$\Delta\Phi$	transistors, Schottky diodes
resistance	ΔR	metal oxide semiconductor resistors
impedance	ΔZ	conducting polymer chemoresistors
capacitance	ΔC	capacitors
potential difference	ΔE	voltametric electrochemical cell
current	ΔI	amperometric electrochemical cell
temperature	ΔT	thermistor
optical absorption	$\Delta\varepsilon$	optical CO_2 detector
optical thickness	$\Delta(n \cdot d)$	reflectometric interference sensors

2.3 SPECIFIC GAS SENSORS

A certain number of gas sensors are described in this section, with an emphasis on the two technologies utilised in this thesis work and presented in the publication chapters to follow: the metal-oxide sensor and the MOSFET sensor.

2.3.1 Metal-oxide sensors

2.3.1.1 Sensing Mechanisms

These sensors are based on the gas-sensitive properties of a semiconducting metal-oxide layer which is usually polycrystalline, and whose conductivity is modulated by the oxygen adsorbed at the surface and at grain boundaries [10]. These metal oxides change their conductivity in the presence of reducing or oxidising gases, such as O_2, H_2, CO, NO_x, C_2H_5OH and hydrocarbons [20]. The sensitivity and the selectivity of these sensors can be modified by changing the oxide microstructure and/or by using catalytic metals (dopants) as Pt, Pd, Au or Ag [20]. A schematic illustration of sensor operation is shown in Figure 2.3.

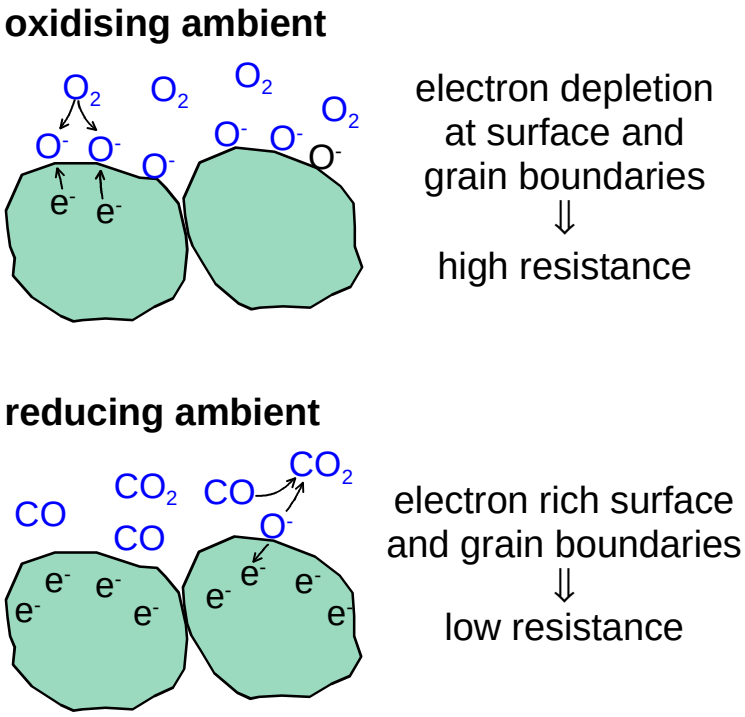

Figure 2.3. Principle of metal oxide sensor operation [19].

The detection principle of the n-type SnO_2 sensor presented in Paper 1 is closely related to the number of oxygen ions adsorbed on the SnO_2 grains. In air, oxygen is adsorbed on the surface of the grains, depleting the surface and the grain boundaries of electrons, which subsequently leads to a decreased conductivity of the device. Depending on the operating conditions, the nature of the oxygen ions formed can be O_2^-, O^-, or O^{2-}. Hydroxyl groups (OH) may also be present [10]. In the presence of reducing molecules, the number of adsorbed oxygen ions decreases, increasing the concentration of electrons in the material. The reverse occurs in the presence of oxidising molecules. The role of dopants is to promote the reaction between the reducing and oxidising gases with the sensor surface and grain boundaries. At low temperatures, physical adsorption can dominate the chemical sensing, while chemisorption becomes more influential at somewhat higher temperatures. For higher temperatures, catalysis and surface defects, and finally bulk effects, start to dominate the sensing mechanism. Since the chemical reactions are strongly dependent on temperature, the sensitivity and selectivity of the device can be tuned by the variation of the operating temperature from 200 to 450°C [20].

2.3.1.2 Technology

Metal-oxide sensors are fabricated as sintered powders or thin films with variable thickness [21]. The sintered powder is usually screen printed on top of an alumina substrate with previously integrated electrodes and heater on the front and on backside, respectively (Fig. 2.4). This thick film technology is considered as a relatively high power technology and does not allow a rapid variation of the operating temperature.

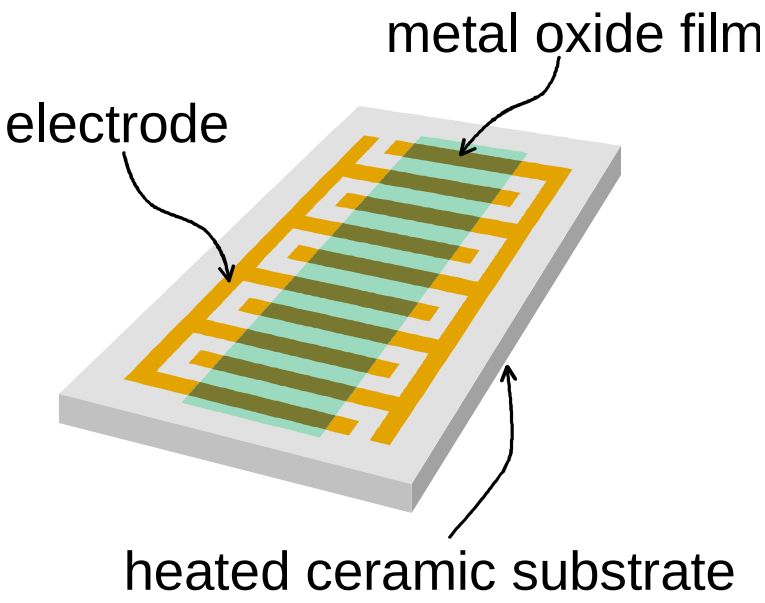

Figure 2.4. Thick film metal-oxide gas sensor structure [19].

The thin film technology is mostly utilised in combination with the micro-hotplate concept (Fig. 2.5) [21,22]. The devices are based on a micromachined hotplate on a silicon substrate (see Chapter 4). The gas-sensitive thin film material is deposited on top of the remaining thermally isolated membrane. The sensors show a low-power consumption compared to the thick sensors previously mentioned. Moreover their small thermal mass enables fast temperature variations. As noted earlier, the sensitivity and selectivity of a metal-oxide sensor is highly temperature dependent. Thus, a large amount of information can be obtained by modulating the temperature and conductance of the metal-oxide film. However, one of the major drawback of this technology is the poor stability (drift) of the gas-sensitive thin metal-oxide film.

Therefore, the technology presented in Paper 1 is based on the merging of thick film sensing technology with the micro-hotplate concept. The thick film

sensing material provides better gas sensing characteristics in term of stability and the hotplate substrate makes this technology suitable for markets where low-power consumption, low-cost and reliable devices are needed, such as in portable instrumentation and the automotive industry.

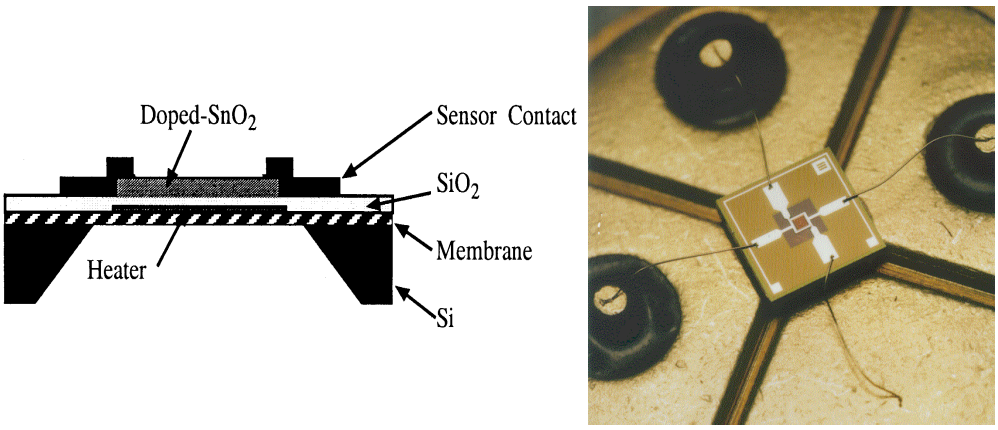

(a) (b)

Figure 2.5. Thin film metal-oxide gas sensor structure: (a) schematic cross-sectional view, (b) thin film micromachined gas sensor mounted on a standard TO type package (Courtesy of Microsens SA, Neuchâtel, Switzerland).

2.3.2 MOSFET sensors

2.3.2.1 MOSFET sensor structure

Metal-Oxide Semiconductor devices can be built as Schottky diodes, capacitors (MOSCAP) or transistors (MOSFET). The semiconductor is normally silicon and the insulator, silicon dioxide. Gas-sensitive field effect devices have been studied for over 25 years, since the original discovery of the

large sensitivity of palladium gate metal-oxide semiconductor structures to hydrogen [23]. A schematic illustration of a n-type Pd-MOSFET sensor structure is shown in Figure 2.6.

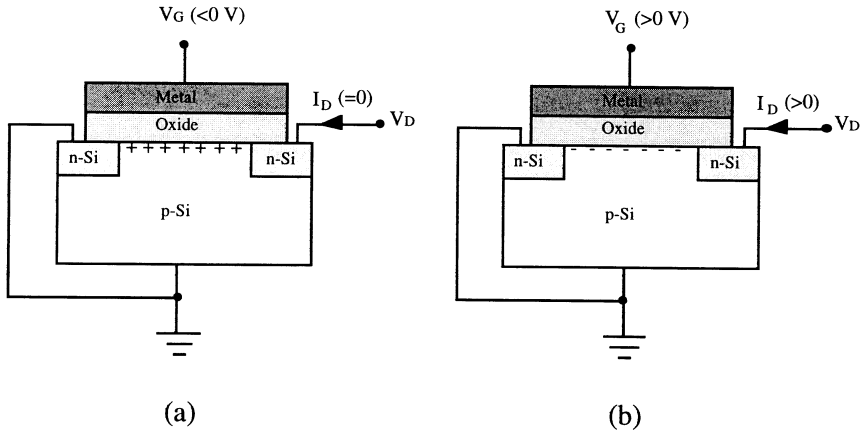

Figure 2.6. Schematic Pd-MOSFET structure.

The sensor is composed basically of three layers: doped silicon as substrate, a typically 100 nm-thick oxide film, topped by a continuous catalytic metal film forming the transistor gate. With a negative gate voltage, majority carriers (holes) are drawn towards the semiconductor-insulator interface (Fig. 2.6a). Because of the rectifying properties of p-n junctions, there will be no drain current (I_D) at a positive applied drain voltage (V_D). At positive gate voltage, electrons accumulate at the interface (Fig. 2.6b). At high enough positive voltage, the electrons outnumber the negative acceptor ions in a thin layer just below the interface. This is called an inversion layer, which makes it possible for current to flow between the two n-doped areas. In a field-effect transistor, a small change in applied gate voltage can give rise to a relatively larger change in conductance in the inversion layer.

In a sensor configuration, the gate and drain are connected together (V_G=V_D). The MOSFET operates at constant current between the source and drain. The voltage at the gate and drain constitutes the sensor signal (V_{GD}).

2.3.2.2 Sensing mechanisms

When exposed to the catalytic metal, hydrogen gas molecules dissociate and adsorb on the palladium surface as hydrogen atoms. Some of the atoms diffuse rapidly through the metal layer to be adsorbed at the metal-oxide interface, resulting in its polarisation. These atoms appear to be residing on the oxide side of the interface [24]. They give rise to a dipole layer, which is in equilibrium with the outer layer of adsorbed hydrogen and the gas phase. The dipole layer induces an abrupt step in charge and hence potential distribution in the structure (Fig. 2.7) [25].

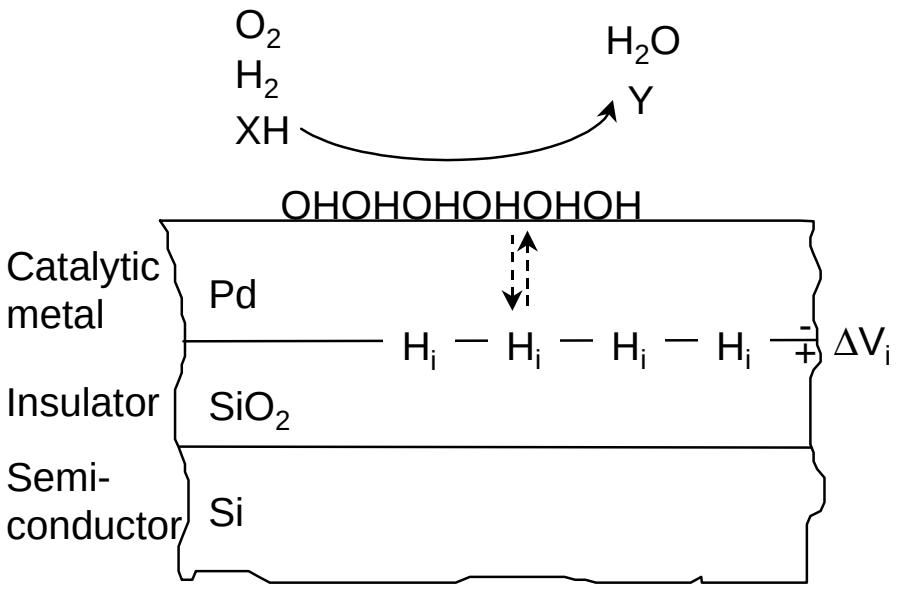

Figure 2.7. Detection principle for a thick metal gate MOSFET sensor [19].

The voltage drop, ΔV_i that appears at the interface is added to the externally applied voltage (V_{GD}) and a shift in the I-V curve towards lower voltages is obtained as an output signal (Fig. 2.8).

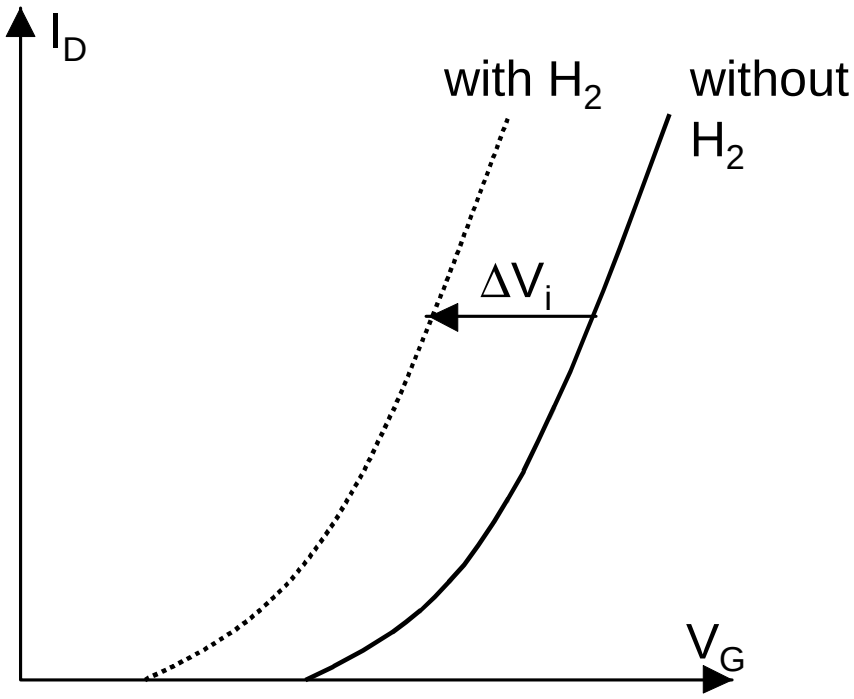

Figure 2.8. I-V characteristics for a MOSFET sensor with and without hydrogen exposure [19].

The voltage drop (ΔV_i) is proportional to the number of hydrogen atoms absorbed per unit area at the metal-oxide interface, and is used to monitor the hydrogen concentration in the ambient environment. When the hydrogen gas is not anymore present in the ambient, the hydrogen atoms at the metal-air interface recombine into molecules (or water if oxygen is present), and the metal-oxide interface, which is in equilibrium with the outer interface, is emptied. This shift in the I-V curve is therefore reversible [24,26].

Hydrogen containing molecules can also be detected with a Pd-MOSFET sensor if they can be dehydrogenated on the palladium surface, such that hydrogen atoms are released and diffuse through the metal layer to the metal-oxide interface [27]. This is valid for, e.g., alcohols, hydrogen sulphide and unsaturated hydrocarbons, but not ammonia and amines. By changing the temperature it is also possible to detect different molecules (tune the selectivity) with a single Pd-MOSFET sensor since they require different temperatures to start reacting on the catalytic metal. However, the temperature of operation is limited by the silicon technology to a value not higher than 200–225°C, due to leakage currents at p-n junctions increasing with temperature.

If the catalytic metal gate is made so thin that it is discontinuous with holes and cracks, but still useful as a gate electrode, a large sensitivity to e.g. ammonia is found [28,29]. In this case, it is believed that the voltage shift is not only due to the electrical polarisation phenomenon at the metal-oxide interface, ΔV_i, but also from charges/dipoles on the insulator surface, ΔV_a, and possibly on the metal surface, ΔV_s (Fig. 2.9).

Present work indicates that polarisation phenomena at the insulator surface, when they occur, together with the hydrogen dipoles at the metal-insulator surface, might give the most significant contributions to the voltage shift [30]. A detailed model for the generation of a voltage shift in thin metal films does not exist yet.

Thin discontinuous metal gates can therefore detect all kinds of molecules that give rise to polarisation phenomena in the thin metal film, including those detected by the thick film sensor, and some additional ones like ammonia and

amides. In order to increase the selectivity of these sensors, other catalytic metals, such as Pt and Ir, that have different response characteristics towards different molecules, can be used [11].

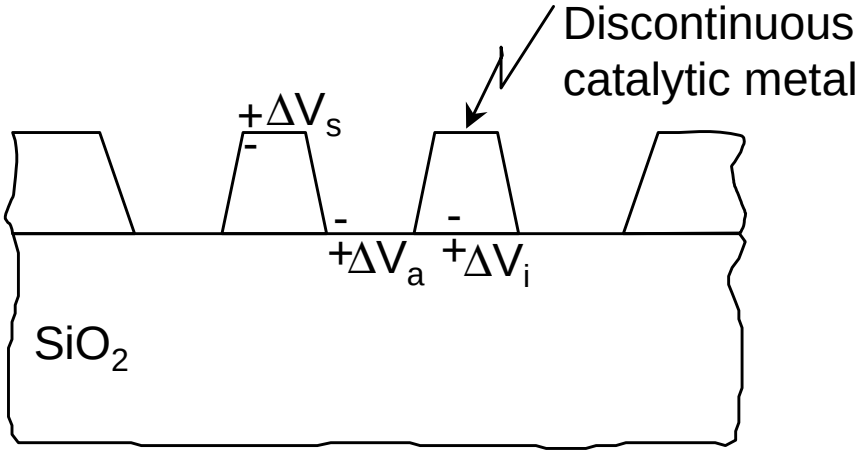

Figure 2.9. Detection principle for a thin metal gate MOSFET sensor [19].

2.3.2.3 Technology

The MOSFET transducer is fabricated using standard microelectronic processes on silicon, such as thin film deposition and patterning, and ion implantation [31]. As a kind of post-processing, the standard gate material is removed and replaced by a catalytic metal film. Multiple sensors can be fabricated simultaneously on a substrate, and batches processed. However, this technology is limited to operational temperatures of 200–225°C, and the power consumption is relatively high. The operation of the sensor in a modulated temperature mode and its application in hand held instruments are therefore practically not possible.

Another design based on the field-effect sensing mechanism is the suspended gate field-effect transistor structure (SGFET), with an insulating air gap

between the gate metal and the insulator [32]. In such devices, the response originates from the species adsorbed to the gate and insulator surface, but not from a metal-oxide interface as in the MOSFET sensor. The adsorbed molecules and occurring species give rise to a shift in the work function, which can be detected by a shift in the operating point of the MOSFET. For instance, the gate metal could be Pd and the sensor would have then approximately the same hydrogen sensing mechanism as the thick Pd-MOSFET, except that the response is smaller. Other conducting materials such as conducting polymers can also be used as gate sensitive materials [32]. These polymer films can also replace the catalytic metal in a MOSFET sensor structure to obtain a gas sensor based also on the principle of the work function variation [33]. These last two technologies, the SGFET and the polymer gate FET (PolFET) have the advantage that they manifest gas-sensitive properties at room temperature and therefore can be considered as low-power devices. Finally, the reduction of the power consumption of the common MOSFET sensors based on catalytic metals, to compete with the technologies mentioned above and also enable new modes of operation such as temperature modulation, is the subject of Papers 2 to 4 included in this thesis.

In the case of temperature limitation, it has been shown that Schottky diodes and transistors made on silicon carbide substrates can be used at temperatures up to 1000°C, due to the larger bandgap of SiC [34,35]. Using such structures, it is possible to detect e.g. saturated hydrocarbons, which is difficult with an ordinary MOSFET sensor. Another interesting feature is the short response time of the sensors, less than 10 ms at high temperature, which makes SiC devices useful for e.g. monitoring of the fuel-to-oxygen ratio in the exhausts

from individual cylinders in car and truck engines. In the following papers, we suggest silicon-on-insulator technology (SOI) as a possible candidate to reduce the power consumption of MOSFET sensors and increase their temperature of operation up to 300–350°C [36]. SOI could fill the gap left in temperature between the standard silicon and the more expensive SiC technologies.

2.3.3 Other sensor types

2.3.3.1 Mass sensitive devices [6]

The most frequently used mass sensitive transducers are quartz microbalances (QMB) and surface acoustic wave devices (SAW). The large number of potential gas-sensing coatings, like polymers, inorganic materials, and biomolecules, results in a broad availability of selectivity. SAW-devices can be operated at higher frequencies than QCM, resulting in higher sensitivity.

The working principle of these devices relies on the relation of the electric field with the dimensions/geometry of the piezoelectric materials. When an AC-field is applied to the electrodes, the piezoelectric crystal (quartz, $LiNbO_3$, $LiTaO_3$) oscillates at a characteristic frequency. In QMB, bulk acoustic waves are propagated in a transverse shear mode between the two faces bearing the electrodes, i.e. the atoms are displaced in the same direction as the wave propagates. In SAW devices, the particle displacement is perpendicular to the wave propagation direction. They are usually operated as delay lines in which a second pair of interdigitated electrodes is used to receive the signal launched from the first electrodes. Changes in mass and/or viscosity of the sensing layer

through adsorption of molecules decrease the frequency. The sensing layer determines the sensitivity profile.

2.3.3.2 Polymer sensors [6]

Polymers are used in a wide variety of gas sensor types, based on electrical (e.g. chemoresistors), electrochemical, mass sensitive and optical mechanisms [15,16]. A wide range of materials can be synthesised by changing the basic monomers, the attached functional groups, the polymeric structure, or by use of different dopants. Thus, sensitivity to a multitude of organic compounds can be obtained. Nonylphenylpolyethoxylate, poly(ethyleneimine), polypyrrole, polyaniline, phthalocyanine, and carbon black matrix, are among the polymers used to detect different analytes.

Chemoresistors are widely used with conducting polymers. They consist of two electrodes with the polymer film in between. They are usually operated at room temperature (low-power). A disadvantage of this technology is that most of these polymer films show a high sensitivity to humidity.

2.3.3.3 Optochemical sensors [6]

Optical sensors utilise changes in properties such as fluorescence, absorption, refractive index, and reflectance, caused by the interaction of the analyte with the sensing surface. A number of different molecules can be detected, with selectivity dependent on the sensing layer, and the excitation and detection wavelengths.

Carbon dioxide is an important indicator of biological and combustion activities. CO_2 monitoring is based on optical absorption at a CO_2-specific wavelength, and can give important information on the activity of the analysed

samples. Another interesting type of transducer for optical sensors is based on fiber optics [37]. They can be coated with different sensing materials such as polymers and catalytic metals. Surface plasmon resonance (SPR), which employs the evanescent electric field that penetrates the sensing layer (on a metal) under conditions of total reflection to probe that layer, can be also used as chemical sensor [38]. The detection of the reflected intensity can be correlated to the refractive index change induced by chemical incorporation into the sensing layer.

2.3.3.4 Electrochemical cells[6]

Solid-state electrochemical cells consist of a ZrO_2-Y_2O_3 tube, where the zirconium dioxide acts as an oxygen ion conductor at 600-800°C. This sensor type is one of the most widely used devices as a λ-probe in automobiles to monitor combustion efficiency. Solid-state thick and thin film electrochemical sensors for CO_2 have also been reported [39,40].

2.3.3.5 Pellistors

In thermal chemical sensors, commonly named pellistors, combustible gases are monitored by measuring the energy (temperature) liberated during their oxidation. For instance, these sensors have found applications in methane detection [41,42]. Volatile organic compounds can also be detected using a calorimetric sensor arrangement [43].

2.4 ELECTRONIC NOSES

2.4.1 Working principle

The concept of the electronic nose (ENose), that is to say the combination of gas sensor arrays and computerised data processing to model the human olfactory sense, was first proposed by Persaud and Dodd in 1982 [4]. The array of a few non-specific sensors “performs the function” of the huge number of non-specific receptor cells (the olfactory bulb) of the mammalian olfactory system, and the pattern recognition, with the help of a computer, has the “role” of the brain in treating the data [2,44]. Once the signals are analysed, the results are compared to previously acquired data in a database to classify and/or quantify the chemical clusters of volatile compound, in particular, odours. The system principle is illustrated in Figure 3.10.

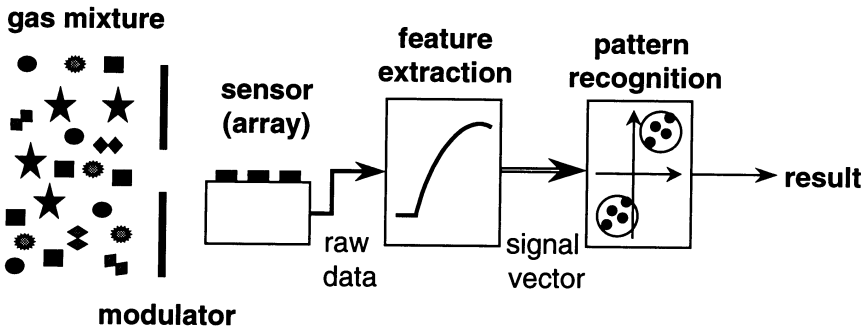

Figure 3.10. Principle of a system for analysis of volatile compounds using gas sensors [19].

The result obtainable by an ENose can be viewed as a chemical image or portrait of a given combination of volatile compounds [3]. For successful recognition of an odour, the sensors need to give a stable and reproducible

signal when exposed to the odours of interest. Moreover, an array of sufficiently different sensors (typically 4–20), with a certain sensitivity overlap, should be used to obtain a chemical image. It is worth pointing out that the sensor array may also include some specific solid-state sensors to be used as reference points in the data analysis procedure.

2.4.2 Data treatment

Data treatment is an important aspect in the use of an electronic nose. Two phases can be distinguished in the data treatment procedure: feature extraction, also called pre-processing, and pattern recognition [44-46].

Feature extraction reduces the data comprising the signal (baseline, response and recovery) of every sensor to one of a few typical values characteristic for the odour. The choice of feature extraction depends on the sensor type used. The common values extracted are the response, which is the difference or ratio between the steady-state value obtained for the sample gas and the value of the sensor when exposed to no sample gas, and the derivative and integrals over certain time intervals. The values of every sensor are then collected in a 'feature vector' or matrix that is used as input for the pattern recognition [44].

A formal definition of pattern recognition can be "the mapping of a pattern from a given pattern space into a class-membership space" [47]. In the case of gas analysis, it could involve molecular recognition of species present in a gas mixture, and less common, at what concentrations. The class-membership does not necessarily have to be the concentration of the molecules present, but can also be indirect properties of the gas mixture such as the freshness of ingredients and the quality class of air. Depending on the purpose and

characteristics of specific odour analysis, different pattern recognition techniques can be applied to the feature matrix. For some simple applications where the system is only used to detect an incidental outlyer, a simple visualisation with principle component analysis (PCA) might be sufficient [45,48,49]. This method allows the visualisation of a maximum of data variance using a base transformation [2,50,51]. When in a developed stage, with an optimised system and good discrimination between data sets, some data sets can be used to train the system. These training data sets can be modelled by a linear technique like partial least squares (PLS) [2,50], or with neural networks [47]. The choice of a more refined technique depends on the application and the required output format [52].

2.4.3 Applications and technology

Within the last 10 years, there has been rapid development in the electronic nose technology [53]. The principal sensors used initially were metal-oxide, organic conducting polymer sensors and quartz microbalance sensors. More recently, MOSFET and surface acoustic wave sensors have been used, and quadrupole mass spectrometry has been introduced in commercial systems.

Presently, electronic noses are mainly applied for quantitative or qualitative applications in various fields, e.g. food and beverage, tobacco, cosmetics, and packaging industries, environment control, and more recently, R&D studies for safety and health care purposes. More details on electronic nose technology can be found in review articles [5,44,54,55].

Miniaturisation is one future trend in the ENose market and some research institutions and companies are already at work on chip-based Enose. On-site

analysis and leakage detection require analysis to be performed with hand held devices. In terms of power consumption, the sensors based on polymer technology have an advantage over the other technologies. On-chip ENose based on carbon black matrix- or polymer- CMOS compatible chemo-capacitors, -calorimeters and -resonators are in an advanced state of development [56,57]. Modular miniaturised gas analysers, with integrated valves and pumps and using the surface acoustic wave or metal-oxide technology, have also been reported [58,59].

As stated in the previous section, the low-power thin film metal-oxide sensors suffer from a lack of stability, and MOSFET sensors from high power consumption. There is a need to improve both of these technologies with the aim of meeting the specifications for applications in the next generation of portable gas analytical systems. This thesis represents a step further in this direction. Micromachining of silicon is described in the next chapter. This technique of microfabrication was the main tool used to lower the power consumption of metal-oxide and MOSFET gas sensors.

2.5 CONCLUSION

In summary, many types of gas sensors can be made from the combination of the different sensing materials and transducers. If the different possible modes of operation are considered for each sensor type, an incredibly large amount of data can be extracted from a gas mixture. The use of data treatments in conjunction with arrays of unspecific gas sensors has lead to the concept of gas sensor systems, known as electronic noses.

3. Silicon micromachining

Sensors on silicon are generally made using a combination of thin-film processes used in microelectronics, and specific microfabrication processes, used in microsystems. On one hand, thin film processes on silicon, including deposition, implantation, masking and etching, are well established and fully described in the literature, and will not be reviewed here. For the interested reader, more information on this subject may be found in Refs. [31,60,61]. On the other hand, the field of micromachining applied to sensors is relatively new and less described in the literature. Therefore, this chapter constitutes a summary of the two major categories of techniques used in the field, bulk and surface micromachining.

A vast majority of bulk and surface micromachining is based on single crystal silicon substrates, on which this chapter is focused. Beams, cantilevers, diaphragms and membranes of diverse materials can be released by using silicon micromachining. These microstructures find applications in many fields; such as physical and thermal sensors, and in the field of interest of this thesis, low power gas sensors. Micromachining has grown into a large discipline. Therefore, this chapter is limited to the description of the basic knowledge needed for the understanding of the following scientific papers. The next sections are almost entirely based on the book written by Marc Madou, entitled “Fundamentals of Microfabrication”, published by CRC press in 1997 [62]. More details can also be found in these references [63-65].

3.1 WET BULK MICROMACHINING

In wet bulk micromachining, features are sculpted in the bulk of materials such as silicon, quartz, SiC, GaAs, InP, Ge, glass, and Pyrex by orientation independent (isotropic) and/or by orientation dependent (anisotropic) wet etchants. Bulk micromachining means that three-dimensional structures are etched into the bulk of crystalline and noncrystalline materials. A vast majority of bulk micromachining work is based on single crystal silicon. The technology employs solution-based chemicals as tools, instead of plasma as in the next section. A typical structure fashioned in a bulk micromachining process is shown in Figure 3.1.

This type of membrane structure, a likely base for a pressure sensor or an accelerometer, demonstrated that batch fabrication of miniature components does not need to be limited to integrated circuits (ICs). Despite all the emerging new micromachining technologies (sections 3.2 and 3.3.), Si wet bulk micromachining, being the best characterised micromachining tool, remains the most popular in the industry.

After a short historical note on bulk micromachining, we start with an introduction to the crystal structure of single crystal silicon. Then, some empirical data on wet isotropic and anisotropic etching are reviewed, and models for anisotropic etching behaviour follow. Finally, etch stop techniques are described.

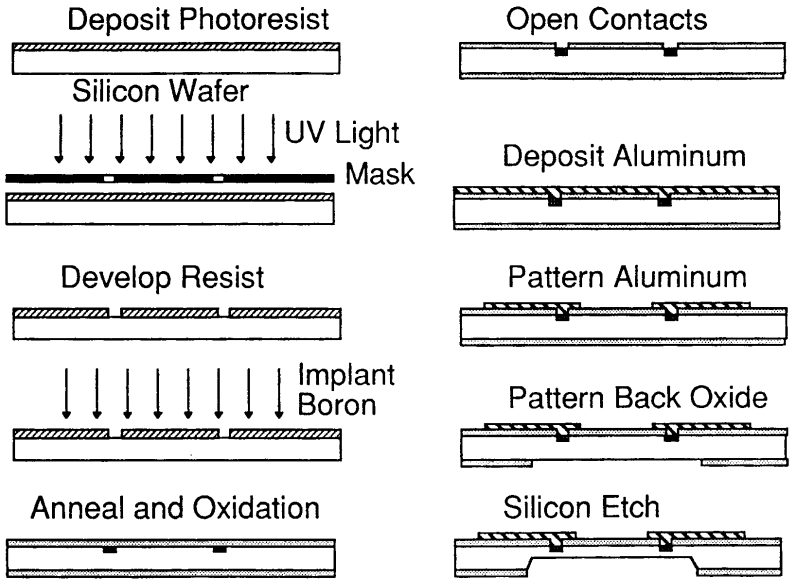

Figure 3.1. A wet bulk micromachining process is used to craft a membrane with piezoresistive elements. Silicon micromachining selectively thins the silicon wafer from a starting thickness of about 400 μm. A diaphragm having a typical thickness of 20 μm or less with precise lateral dimensions and vertical thickness control results [62].

3.1.1 History

The earliest use of wet etching of a substrate, using a mask (wax) and etchants (acid-base), appears to be in the fifteenth century for decorating armour [66]. Engraving hand tools were not hard enough to work the armour, and more powerful acid-base processes became established. The masking in this traditional chemical milling was accomplished by cutting the maskant with a scribing tool and peeling the wax where etching was wanted. In Reference [66], Harris describes in detail all the improvements that, by the mid-1960s,

made this type of chemical milling a valuable and reliable method for manufacturing integrated circuits. Through the introduction of photosensitive masks by Niépce in 1882, chemical milling in combination with lithography became a reality and a new level of resolution and precision came within reach. The more recent applications of lithography-based chemical milling are the manufacture of printed circuit boards, started during the Second World War, and, by 1961, the fabrication of Si-based integrated circuitry. The tolerances for fashioning integrated circuitry are many orders of magnitude smaller than in the chemical milling industry.

In this chapter, we are concerned with lithography and chemical machining used in microfabrication of sensors and actuators. A major difference, compared to the processes used in the IC industry, lies in the aspect ratio (height-to-width ratio) of the features crafted. In the IC industry, one deals mostly with very small, flat structures with aspect ratio of 1 to 2. In the microfabrication field, structures typically are somewhat larger, but aspect ratios might be as high as 400.

Isotropic etching has been used in the silicon semiconductor industry since its beginning in the early 1950s. The usual chemical isotropic etchant used for silicon was HF in combination with HNO_3 with or without acetic acid or water as diluent [67-70]. In the mid-1960s, the Bell Telephone Laboratories started work on development of anisotropic Si etching in mixtures of KOH in water/alcohol and later, in KOH/water solutions. The need for high aspect ratio etching in silicon arose when making dielectric integrated structures in integrated circuits [71-72]. In the mid-1970s, a new surge of activity in anistropic etching was associated with the work on V-groove and U-groove transistors [73-75].

The first use of Si as a micromechanical element can be traced back to a discovery in the mid-1950s, and an idea from early 1960s. The discovery was the existence of large piezoresistance in Si and Ge in 1954 [76]. The idea came in 1961, when a diffusion technique for the fabrication of Si piezoresistive sensors for stress, strain and pressure was proposed [77]. The year after, researchers at Honeywell made the first thin Si piezoresistive diaphragms, of the type shown in Figure 3.1 [78].

In the mid-to late-1970s, there were a few companies commercialising micromachined structures, such as pressure sensors, thermal print head, thermally isolated diode detectors and ink jet nozzle arrays.

Petersen's 1982 paper, extolling the excellent mechanical properties of single crystalline silicon, helped galvanise academia to get involved in Si micromachining in a major way [79]. Before that time, most research efforts would be found in industry, and practical needs were driving the technology. Many scientists are now involved in micromachining research, looking for applications which could one day be commercial breakthroughs

3.1.2 Silicon crystallography

3.1.2.1 Miller indices

The periodic arrangement of atoms in a crystal is called a lattice. The unit cell in a lattice is a segment representative of the entire lattice. For each unit cell, basis vectors (a_1, a_2, and a_3) can be defined such that if that unit cell is translated by integral multiples of these vectors, one arrives at a new unit cell identical to the original. A simple cubic-crystal unit cell for which $a_1 = a_2 = a_3$

and the axes angles are all 90° is shown in Figure 3.2. In this figure, the dimension ‘a’ is known as the lattice constant.

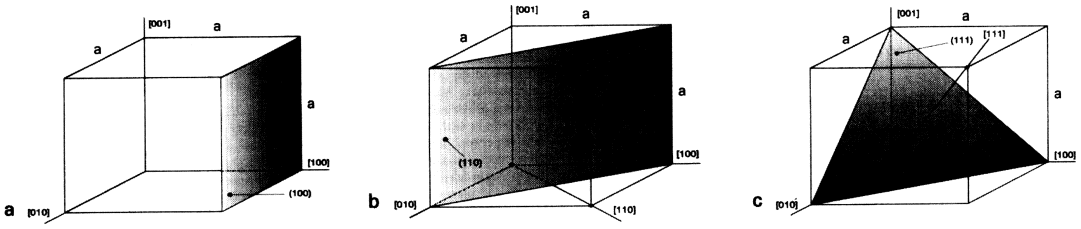

Figure 3.2. Miller indices in a cubic lattice: planes and axes. Shaded planes are: a (100), b (110), c (111) [62].

To identify a plane or a direction, a set of integers h, k, and l,called Miller indices,are used. To determine the Miller indices of a plane, one takes the intercept of that plane with the axes and expresses these intercepts as multiples of the basis vectors a_1, a_2, a_3. The reciprocal of these three integers is taken, and, to obtain whole numbers, the three reciprocals are multiplied by the smallest common denominator. The resulting set of numbers is written down as (hkl).

A direction in the lattice is expressed as a vector with components as multiples of the basis vectors. The Miller indices of an orientation are obtained by translating the orientation to the origin of the unit cube and taking the normalised coordinates of its other vertex. For example, the body diagonal in a cubic lattice as shown in Figure 3.2c is 1a, 1a and 1a or a diagonal along the [111] direction.

Directions [100], [010], and [001] are all crystallographically equivalent, and form the family of <100> directions. A family of faces which bear like relationship to the crystallographic axes — for example, the planes (001),

(100), (010), (001), (100), and (010) — are all equivalent and are marked as {100} planes.

3.1.2.2 Crystal structure of silicon

Crystalline silicon forms a covalently bonded structure, which has the same crystalline arrangement as carbon in diamond form and belongs to the more general zinc-blend classification [80]. Silicon, with its four covalent bonds, coordinates itself tetrahedrally, and these tetrahedrons make up the diamond-cubic structure. This structure can also be represented as two interpenetrating face-centered cubic lattices, one displaced (¼, ¼, ¼)a with respect to the other, as shown in Figure 3.3. The structure is face-centered cubic (fcc), with two atoms in the unit cell and a lattice parameter 'a' for silicon of 5.4309 Å.

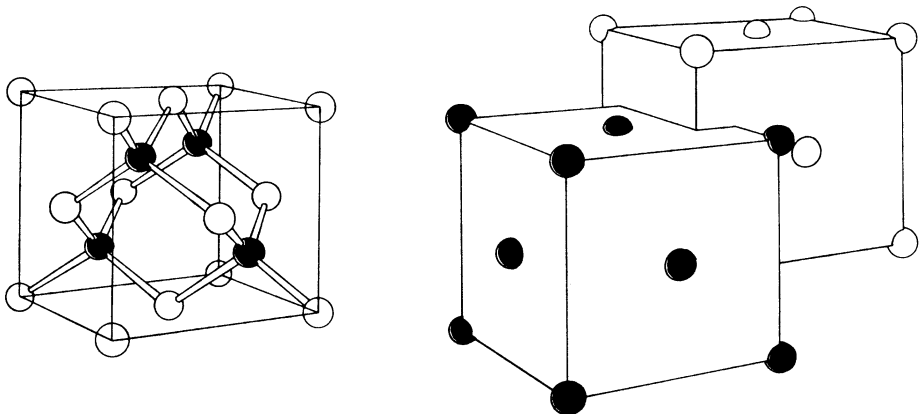

Figure 3.3. The diamond-type lattice can be constructed from two interpenetrating face-centered cubic unit cells. Si forms four covalent bonds, making tetrahedrons [62].

For such a cubic lattice, direction [hkl] is perpendicular to a plane with three integers (hkl), i.e., the Miller indices of a plane perpendicular to the [100]

direction are (100). The {111} planes present the highest packing density and the atoms are oriented such that three bonds are below the plane.

When ordering silicon wafers, the crystal orientation must be specified. The most common orientations used in the IC industry are the <100> and <111> orientation. In micromachining, <110> wafers are used quite often and the <111> wafers are considered generally as useless, as they cannot be etched anisotropically except when using deep plasma etching (Section 3.2) or laser-assisted etching [81]. On a <100> wafer, the <110> direction is often made evident by an orientation flat. They are especially useful to align the structures to be etched with a specific crystallographic direction.

3.1.3 Geometric relationships in the silicon lattice for wet anisotropic etching

To better understand the different three-dimensional shapes resulting from anisotropically etched single crystal Si (SCS), some of the more important geometric relationships between different planes within the Si lattice need further clarification. Silicon wafers with a (100) or a (110) surface plane will be considered. It should also be noted that in anisotropic etching of silicon, the {111} planes, which have the highest packing density, are virtually nonetching compared to the other planes. Therefore, the sidewalls of an etched pit in SCS will ultimately be bounded by this type of plane, if the etch time is long enough for features bounded by other planes to be etched away. The types of planes introduced initially depend on the geometry and the orientation of the mask features.

3.1.3.1 [100]-Oriented silicon

In Figure 3.4, the unity cell of a silicon lattice is shown together with the correct orientation of a [100]-type wafer relative to this cell [82]. It can be seen from this figure that intersections of the nonetching {111} planes with the {100} planes (e.g. the wafer surface) are mutually perpendicular and lying along the <110> orientations.

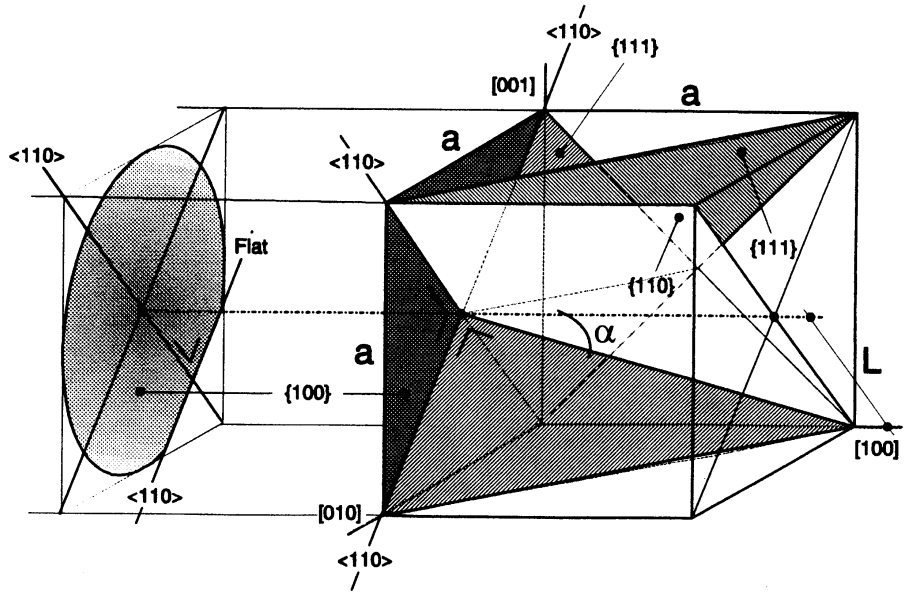

Figure 3.4. (100) silicon wafer with reference to the unity cube and its relevant planes [82].

Provided a square mask opening is accurately aligned with the primary orientation flat, i.e., the [110] direction, only {111} planes will be introduced as sidewalls from the very beginning of the etch. During etching, truncated pyramids deepen but do not widen (Fig. 3.5).

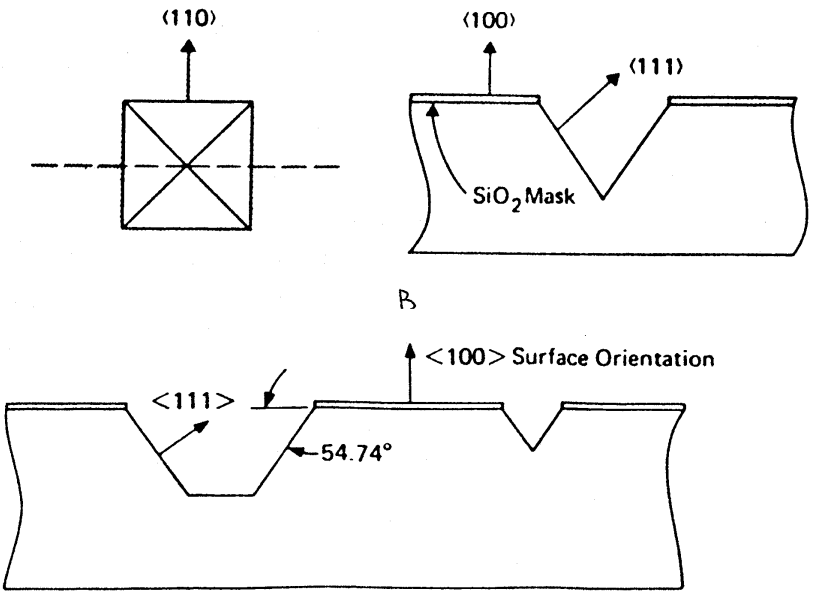

Figure 3.5. Anisotropically etched features in a (100) wafer with a square mask opening [62].

After prolonged etching, the {111} family of planes is exposed down to their common intersection and the (100) bottom plane disappears, creating a pyramidal pit (Fig. 3.5).

For a mask opening with arbitrary geometry and orientation (for example, a circle) and for sufficiently long etch times, the anisotropically etched recess in a {100} wafer is pyramidal, with a base perfectly circumscribing the circular mask opening. Convex corners (> 180°) in a mask opening will always be completely undercut by the etchant after sufficiently long etch times. This can be disadvantageous, for example when making a mesa instead of a pit, or it can be advantageous for undercutting suspended cantilevers or bridges.

The slope of the sidewalls in a cross-section perpendicular to the wafer surface and to the wafer flat is determined by the angle α as in Figure 3.4. This is the

off-normal angle of the intersection of a (111) sidewall and a (100) cross-secting place, and can be calculated from:

$$\tan\alpha = L/a \tag{3.1}$$

with $L = a \times \sqrt{2}/2$ or $\alpha = \arctan \sqrt{2}/2 = 35.26°$, or 54.74° for the complementary angle. The tolerance of this slope is determined by the alignment accuracy of the wafer surface with respect to the (100) plane. Wafer manufacturers typically specify this misalignment to ±1°.

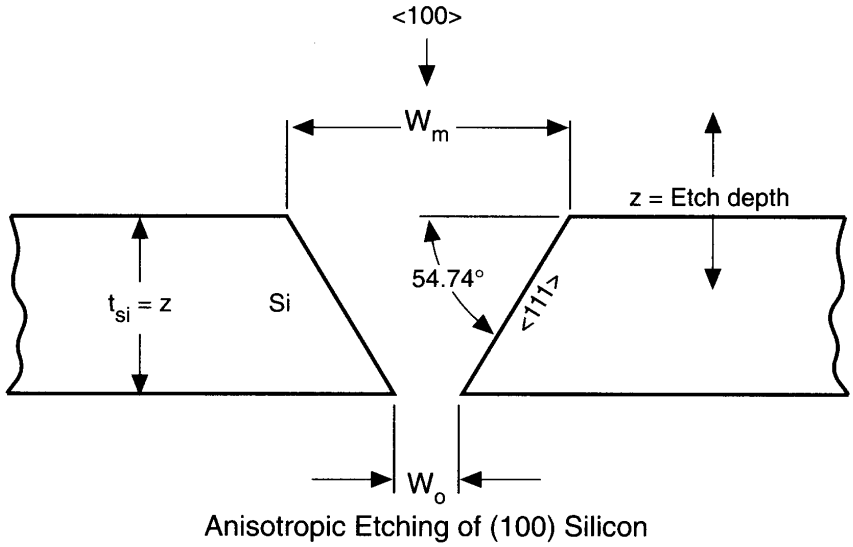

Figure 3.6. Relation of bottom cavity plane width with mask opening width [62].

The width of the rectangular or square cavity, W_0, in the bottom plane in Figure 3.6, aligned with the <110> direction, is completely defined by the etch depth, z, the mask opening, W_m, and the above-calculated sidewall slope:

$$W_0 = W_m - 2\cot(54.74°)z = W_m - \sqrt{2}z \qquad (3.2)$$

The larger the opening in the mask, the deeper the point at which the {111} sidewalls of the pit intersect. The etch stop at the {111) sidewalls' interaction occurs when the depth is about 0.7 times the mask opening.

3.1.3.2 [110]-oriented silicon

In Figure 3.7, we show a unit cell of Si properly aligned with the surface of a (110) Si wafer. Whereas the intersections of the {111} planes with the (100) wafer surface are mutually perpendicular, here they enclose an angle γ in the (110) plane. Moreover, the intersections are not parallel (<110>) or perpendicular (<100>) to the main wafer flat (assumed to be <110> in this case), but rather enclose angles δ or δ + γ. It follows that a mask opening that will not be undercut (i.e., oriented such that resulting feature sidewalls are exclusively made up by {111} planes) cannot be a rectangle aligned with the flat, but has to be a parallelogram skewed by γ – 90° and δ degrees off-axis. The angles γ and δ are calculated as follows [82]:

$$\tan(\beta) = \frac{\frac{1}{2}a\frac{\sqrt{2}}{2}}{\frac{a}{2}} = \sqrt{2}/2 \qquad (3.3)$$

$$\gamma = 180° - 2\beta = 180° - 2\arctan\left(\sqrt{2}/2\right) = 109.47° \qquad (3.4)$$

$$\delta = 90° + \beta = 90° + \arctan\left(\sqrt{2}/2\right) = 125.26° \qquad (3.5)$$

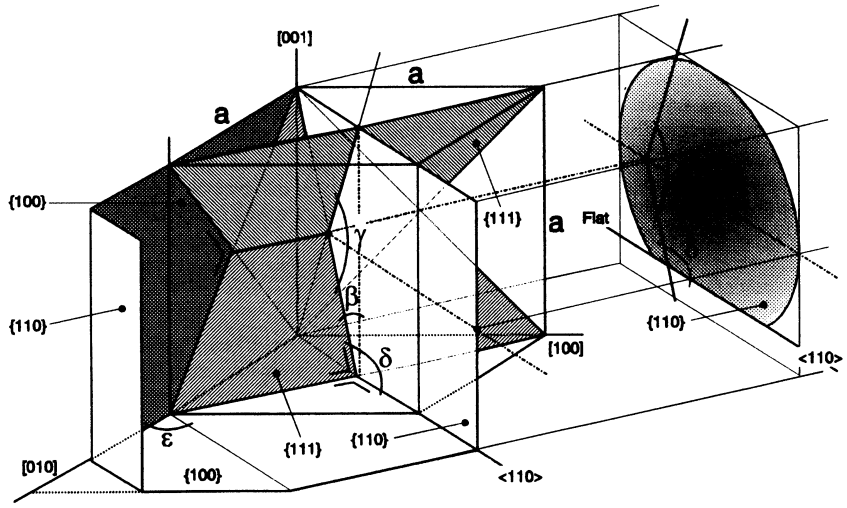

Figure 3.7. (110) silicon wafer with reference to the unity cube and its relevant planes. The wafer flat is in a <110> direction [82].

From Figure 3.7, it can be seen that the {111} planes are oriented perpendicular to the (110) surface. This makes it possible to etch pits with vertical sidewalls. The bottom of the pit would be bounded by {110} and/or {100} planes, depending on the etch time. As the {110} planes are etching slightly faster than the {100} planes, the flat {110} bottom is getting smaller and smaller and a V-shaped bottom bound by {100} planes eventually results.

3.1.3.3 Selection of [100]- or [110]-oriented silicon

In Table 3.1, the main characteristics of etched features in [100]- and [110]-oriented silicon wafers are compared. From this table, it is obvious that for membrane-based sensors, such as micro-hotplates, [100] wafers are preferred for the flat bottoms that result when pits are etched. To also achieve a high component density with anisotropic etches on (100) wafers, the starting silicon wafers must be very thin because of the aspect ratio limitations due to the

sloping sidewalls. Vertical etching in (110) surfaces relaxes the etching requirement dramatically and enables more densely packed structures [83,84].

Table 3.1. Selection of wafer type [62]

[100] Orientation	[110] Orientation
Inward sloping walls (54.74°)	Vertical {111} walls
The sloping walls cause a lot of lost real estate	Narrow trenches with high aspect ratio are possible
Flat bottom parallel to surface is ideal for membrane fabrication	Multifaceted cavity bottom ({110} and {100} planes) makes for a poor diaphragm
Bridges perpendicular to a V-groove bound by (111) planes cannot be underetched	Bridges perpendicular to a V-groove bound by (111) planes can be undercut
Shape and orientation of diaphragms convenient and simple to design	Shape and orientation of diaphragms awkward and more difficult to design
Diaphragm size, bounded by nonetching {111} planes, is relatively easy to control	Diaphragm size is difficult to control; the <100> edges are not defined by nonetching planes

3.1.4 Basics of silicon wet etching

Wet etching of Si is used mainly for cleaning, shaping, polishing, and characterising structural and compositional features [85]. Modification of wet etchant and/or temperature can alter the selectivity to silicon dopant concentration and type and, especially when using alkaline etchants, to crystallographic orientation. Etching proceeds by reactant transport to the surface (1), surface reaction (2), and reaction product transport away from the surface (3). If (1) or (3) is rate determining, etching is diffusion limited and can be increased by stirring. If (2) is the rate-determining step, etching is

reaction rate limited and depends strongly on temperature, etching material, and solution composition. Diffusion-limited processes have lower activation energies than reaction-rate controlled processes, and therefore are relatively insensitive to temperature variations.

Isotropic etchants etch in all crystallographic directions at the same rate. They are usually acidic, such as $HF/HNO_3/CH_3COOH$ (HNA), and lead to rounded isotropic features in single crystalline silicon. They are used at room temperature or slightly above (<50°). Some alkaline chemicals such as $KOH_{(aq)}$ etch anisotropically, i.e., they etch away crystalline silicon at different rates depending on the orientation of the exposed crystal plane. Typically, the pH stays above 12, while more elevated temperatures are used for these slower types of etchants (>50°). Isotropic etchants generally show diffusion limitation, while anisotropic etchants are reaction limited.

3.1.5 Practical aspects of isotropic etching

Since this method was not suited to the fabrication of the microstructures presented in the scientific papers included in this thesis, only basic aspects are summarised in the following lines.

For isotropic etching of silicon, the most commonly used etchants are mixtures of nitric (HNO_3) and hydrofluoric acids (HF). Water can be used as diluent, but acetic acid is preferred because it prevents the dissociation of the nitric acid better and so preserves the oxidising power of HNO_3, which depends on the undissociated nitric acid species for a wide range of dilutions [68]. The etchant is called the HNA system. By the early 1960s, the isotropic HNA silicon etch was well characterised. Iso-etch curves giving the etch rate

of HNA solutions as a function of composition, Arrhenius plots showing the temperature dependence of the etch rate, electrochemical and preferential etching, and masking are presented in Refs. [62,65,67-70].

3.1.6 Practical aspects and models of anisotropic etching

Anisotropic etchants shape or 'machine' desired structures in crystalline materials. When carried out properly, anisotropic etching results in geometric shapes bounded by perfectly defined crystallographic planes. Anisotropic wet etching techniques were developed mainly by trial and error. Going over some experimental data before going in a detail description of etch models, seems fitting. Moreover, we must keep in mind that for higher index planes, most models fail.

The development of anisotropic etchants solved the lateral dimension control lacking in isotropic etchants. Different etch stop techniques needed to control the membrane thickness, such as in the device presented in Figure 3.1, are available, and make these features manufacturable. However, anisotropic etchants are slower, even in the fast etching direction, with etch rates of 1 μm/min or less. Etching through a wafer is therefore a time-consuming process.

3.1.6.1 Anisotropic etchants

A wide variety of etchants have been used for anisotropic etching of silicon, including aqueous solutions of KOH, NaOH, LiOH, CsOH, NH_4OH, and quaternary ammonium hydroxides, with the possible addition of alcohol. Alkaline organics such as ethylenediamine, choline (trimethyl-2-hydroxyethyl

ammonium hydroxide) or hydrazine with additives such as pyrocatechol and pyrazine have been employed as well. Etching of silicon occurs without the application of an external voltage and is dopant insensitive over several orders of magnitude. Alcohols such as propanol, isopropanol, and butanol typically slow the attack of Si [86,87]. The etch rate in anisotropic etching is reaction rate-controlled and therefore temperature dependent. The etch rate for all planes increases with temperature and the surface roughness decreases with increasing temperature, so etching at higher temperatures gives the best results.

The principal characteristics of four different anisotropic etchants are listed in Table 3.2. The most commonly used are KOH [86-91] and ethylene-diamine/pyrocathechol + water (EDP) [92,93]; hydrazine-water is rarely used [94,95]. More recently, quaternary ammonium hydroxide solutions such as tetraethylammonium hydroxide have become more popular [96-99]. Each has advantages and problems and before making a choice, one should consider the extensive literature on the subject.

The simple KOH/water system is the most popular etchant and was used to fabricate the devices presented in this thesis. A KOH etch, in near saturated solutions (1:1 in water by weight) at 60-80°C, produces a uniform and shiny surface. Etch rate non-uniformity gets considerably worse at above 80°C. A large amount of bubbles are seen to evolve from the Si wafer while etching in KOH. The etching selectivity between Si and SiO_2 is not very good in KOH. KOH is also incompatible with the IC fabrication process. The surface roughness continuously decreases with increasing concentration. Since the differences in etch rates for different KOH concentrations are small, a highly

concentrated KOH is preferred to obtain a smooth surface on low index planes.

Table 3.2. Principal characteristics of four different anisotropic etchants [62]

Etchant/Diluent/Additives/ Temperature	Etch Stop	Etch Rate (100) (μm/min)	Etch Rate Ratio (100)/(111)	Remarks	Mask (Etch Rate)
KOH/water, isopropyl alcohol additive, 85°C	$B > 10^{20}$ cm^{-3} reduces etch rate by 20	1.4	400 and 600 for (110)/(111)	IC incompatible, avoid eye contact, etches oxide fast, lots of H_2 bubbles	Photoresist (shallow etch at room temperature); Si_3N_4 (not attacked); SiO_2 (28 Å/min)
Ethylene diamine pyrocatechol (water), pyrazine additive, 115°C	$\geq 5 \times 10^{19}$ cm^{-3} reduces the etch rate by 50	1.25	35	Toxic, ages fast, O_2 must be excluded, few H_2 bubbles, silicates may precipitate	SiO_2 (2–5 Å/min); Si_3N_4 (1 Å/min); Ta, Au, Cr, Ag, Cu
Tetramethyl ammonium hydroxide (TMAH) (water), 90°C	$>4 \times 10^{20}$ cm^{-3} reduces etch rate by 40	1	From 12.5 to 50	IC compatible, easy to handle, smooth surface finish, few studies	SiO_2 etch rate is 4 orders of magnitude lower than (100) Si LPCVD Si_3N_4
N_2H_4/(water), isopropyl alcohol, 115°C	$>1.5 \times 10^{20}$ cm^{-3} practically stops the etch	3.0	10	Toxic and explosive, okay at 50% water	SiO_2 (<2 Å/min) and most metallic films; does not attack Al according to some authors

3.1.6.2 Masking and protection

Etching through a whole wafer (400 to 600 μm) takes several hours (a typical wet anisotropic etch rate being 1.1 μm/min). When using KOH, SiO_2 cannot be used as a masking material for features requiring such a long exposure to the etchants. For prolonged KOH etching, a high density silicon nitride mask has to be deposited. A low pressure chemical vapor deposited (LPCVD) nitride, with an etch rate less than 0.1 nm/min, generally serves this purpose better than a less dense plasma-deposited nitride [100]. If in the overall processing of the devices, nitride deposition does not pose a problem, KOH emerges as the preferential anisotropic wet etchant.

In many cases, it is necessary to protect one side of a wafer from an isotropic or anisotropic etchant. The backside is either mechanically or chemically protected. In the mechanical method the wafer is held in a holder, often made from Teflon. In the chemical method, waxes or other organic coatings are spun onto the wafer side to be protected.

3.1.6.3 Etch stop techniques

In many cases it is desirable to stop etching of silicon when a certain cavity depth or membrane thickness has been reached. Non-uniformity of etched devices due to non-uniformity of the silicon wafer thickness can be quite high. Even with the best wafer quality, the wafer taper is still around ±2 μm. The taper and variation in etch depth lead to intolerable thickness variations in many applications. Moreover, the variation in etch rates becomes critical if one etches membranes down to thicknesses of less than 20 μm; it is almost impossible to etch structures down to less than 10 μm with a time-based technique.

The most widely used etch-stop technique is based on the fact that anisotropic etchants do not attack boron-doped (p+) Si layers to any great extent [101,102]. Experiments show that the decrease in etch rate is nearly independent of boron concentration to the fourth power in all alkaline etchants. It follows that a simple boron diffusion or implantation, introduced from the front of the wafer, can be used to create beams and diaphragms by etching from the back. One disadvantage with this etch stop technique is that extremely high boron concentrations are not compatible with standard CMOS or bipolar techniques.

Alternatively, a second etch-stop method, based on an electrochemical mechanism can be used. In this case, a lightly doped p-n junction is used as an etch stop by applying a bias between the wafer and a counter electrode in the etchant [102-103]. In electrochemical anisotropic etch stop, a p-n junction is made, for example, by epitaxial growth of an n-type layer (phosphorous-doped, $10^{15}cm^{-3}$) on a p-type substrate (boron-doped, 30 Ω•cm). This p-n junction forms a large diode over the whole wafer. The wafer is generally mounted on an inert substrate with the n-type epilayer down and p-type substrate on top, and is partly or wholly immersed in the solution. An ohmic contact to the n-type epilayer is connected to one pole of a voltage source and the other pole of the voltage source is connected via a current meter to a counter electrode in the etching solution. In this arrangement the p-type substrate can be selectively etched away and the etching stops at the p-n junction, leaving a membrane with a thickness defined by the thickness of the epilayer. The incorporation of a third electrode (a reference electrode) in a three-terminal set-up allows a more precise determination of the silicon potential with respect to the solution. A great advantage of this etch stop technique is that it works with low doped Si (levels of the order of $10^{16}cm^{-3}$), allowing the integration of electronic components. A disavantage is the set-up itself, which requires complex fixtures and manual wafer handling. Other electrochemical etching techniques, such as photo-assisted methods, are also used but less frequently [102].

Yet another distinct way to stop etching is by employing a change in composition of material. An example is an etch stopped at a Si_3N_4 diaphragm. Silicon nitride is very strong, hard, and chemically inert, and the stress in the film can be controlled by changing the Si/N ratio in the LPCVD deposition

process. The stress turns from tensile in stoichiometric films to compressive in silicon-rich films. A great number of the materials are not attacked by anisotropic etchants and therefore used as an etch stop. Another example is the SiO_2 layer in a silicon-on-insulator structure (SOI) [102]. A buried layer of SiO_2, sandwiched between two layers of crystalline silicon, forms an excellent etch stop because of the good selectivity of many etchants of Si over SiO_2.

3.1.6.4 Anisotropically etched structures

In Figure 3.8 are compared wet isotropic etch (a) with examples of anisotropic etches (b to e). In the anisotropic etching examples, a square (b and c) and a rectangular pattern (d) are defined in an oxide mask with sides aligned along the <110> directions on a <100>-oriented silicon surface. Etching with the square pattern results in a pit with well-defined {111} sidewalls (at angles 54.74° to the surface) and a (100) bottom. The dimensions of the hole at the bottom of the pit, as we saw above, are given by Equation 3.2. The larger the square opening in the mask, the deeper the point where the {111} sidewalls of the pit intersect. In Figure 3.8a, an undercutting isotropic etch is shown. Misalignment in the case of an anisotropic etch still results in pyramidal pits, but the mask will also be severely undercut. A rectangular pattern aligned along the <110> directions on a <100> wafer leads to long V-shaped grooves (see Fig. 3.8d) or an open slit, depending on the width of the opening in the oxide mask. Using a properly aligned mask on a <110> wafer, holes with four vertical walls ({111} planes) result as shown in Figure 3.8e.

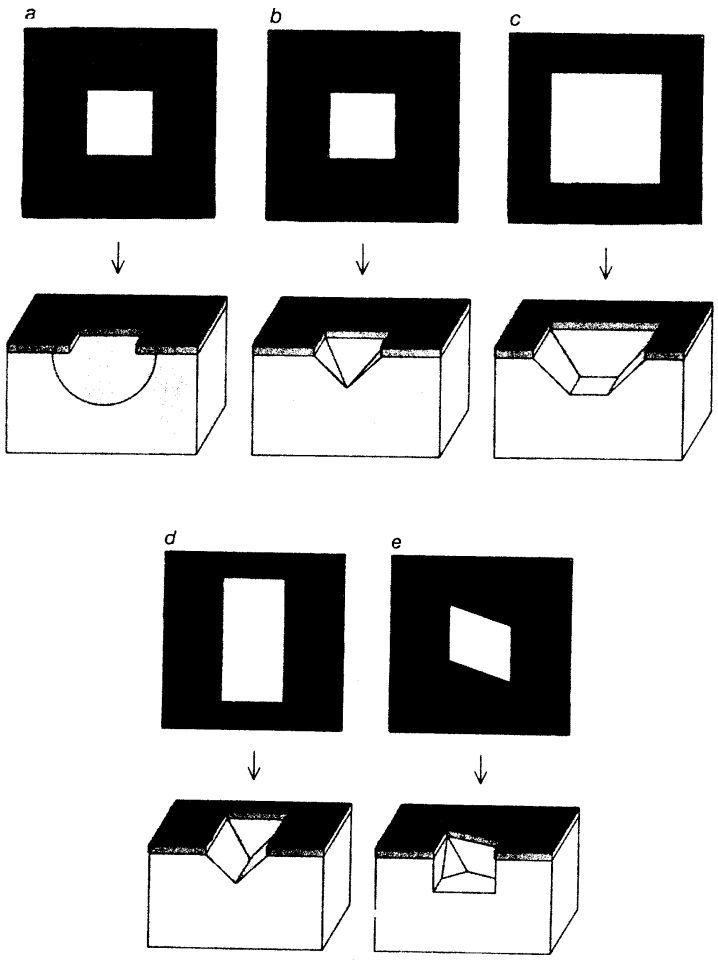

Figure 3.8. Isotropic and anisotropic etched features in <100> and <110> wafers. (a) isotropic etch, (b) to (e) anisotropic etch. (a) to (d) <100> oriented wafers, and (e) <110> oriented wafer [62].

It is also possible to machine surface structures by undercutting. In this case, the orientation of the wafer is of extreme importance. Consider, for example, the formation of a bridge as in Figure 3.9a. When using a (100) surface, a suspension bridge cannot form across the etched V-groove; two independent truncated V-grooves flanking a mesa structure are obtained. To form a suspended bridge, it must be oriented away from the <110> direction. This is

in contrast with a (110) wafer where a microbridge crossing a V-groove will be undercut. Convex corners will be undercut by etchant, allowing formation of cantilevers as shown in Figure 3.9b. When forming a mesa in a (100) wafer, e.g. a mass with perfect 90° convex corners and walls having an angle of 54.7° with the (100) surface, compensation structures must be incorporated in the mask to avoid subsequent undercutting at the convex corners [104-106].

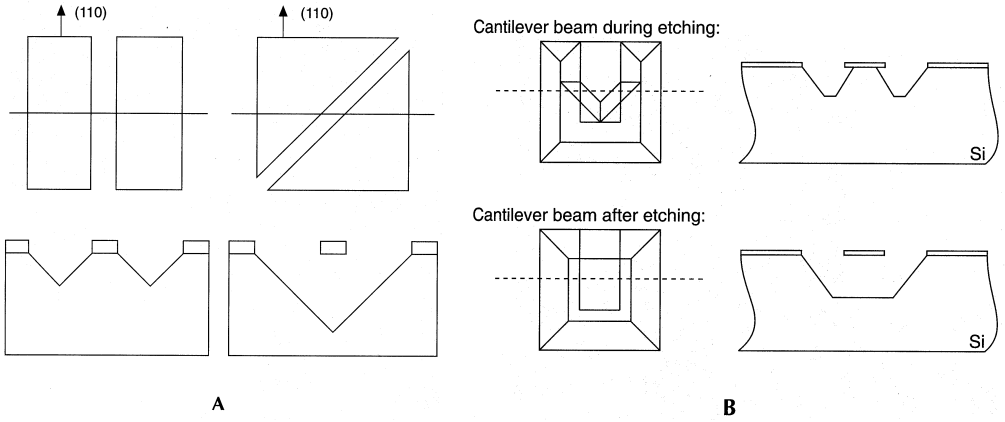

Figure 3.9. How to make (a) a suspension bridge from a (100) Si wafer and (b) a diving board from a (110) Si wafer [107].

By covering the (100)-oriented Si wafer with a dielectric film and using a backside mask opening, it is possible by anisotropic etching of silicon to release a membrane made of this film (see Fig. 3.10a). This technique was used in the following scientific papers to thermally isolate a joule-heating resistor on a dielectric membrane to obtain a micro-hotplate type device. Moreover, with the help of two successive steps of wet anisotropic bulk micromachining of silicon in KOH [108-110], a silicon island was fabricated underneath a dielectric membrane to allow the integration of electronic

devices on a micro-hotplate (Fig. 3.10b). These structures were then used to decrease the power consumption of metal-oxide and MOSFET gas sensors.

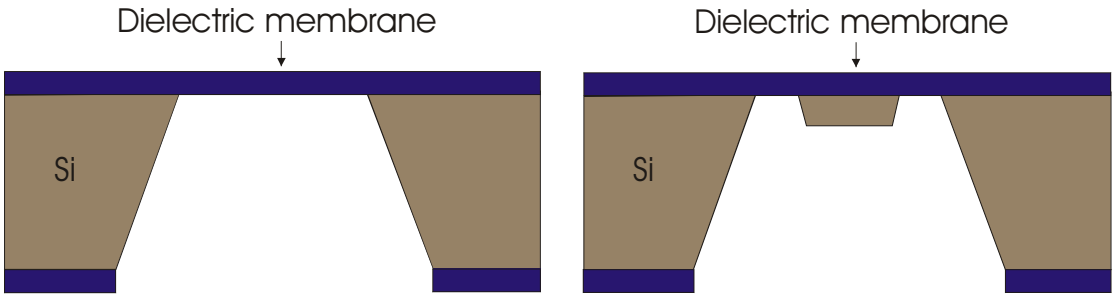

Figure 3.10. Closed dielectric membranes realised using wet anisotropic bulk micromachining of silicon: (a) with and (b) without silicon island.

3.1.6.5 Wet anisotropic etching models

Lots of conflicting data exist in the literature on the anisotropic etch rates of the different Si planes, especially for the higher index planes. This is not too surprising, given the multiple parameters influencing individual results. Temperature, stirring, size of etching feature, KOH concentration, addition of alcohols and other organics, surface defects, complexing agents, surfactants, pH, and cation influence can all affect anisotropic etching.

Several chemical models explaining the anisotropy in etching rates for different Si orientations have been proposed. In this section only the main models are mentioned. Different Si crystal properties have been correlated with the anisotropy in silicon etching.

- It has been observed that the {111} planes present the highest density of atoms per cm^2 to the etchant and that the atoms are oriented such that

three bonds are below the plane. It is possible that these bonds become chemically shielded by the surface bonded (OH) or oxygen, thereby slowing the etch rate.

- It has also been suggested that etch rates correlate with available bond densities, the surfaces with the highest bond density etching faster. The available bond densities in Si and other diamond structures follow the sequence 1:0.71:0.58 for the {100}:{110}:{111} surfaces. However, bond density alone is an unlikely explanation for etch rates because of the magnitude of etching anisotropy (e.g. a factor of 400), compared to the bond density variations of at most a factor of two [84].
- The slow etching of {111} planes was also explained on the basis of their faster oxidation during etching [84]. This does not happen on the other faces, due to the greater distance of the atoms on planes other than (111). Since they oxidise faster, these planes may be better protected against etching. The oxidation rate in particular follows the sequence {111}>{110}>{100}, and the etch rate often follows the reverse sequence. In the most used KOH-H_2O system, however, the sequence is {110}>{100}>{111}.
- In yet another model, it is assumed that the anisotropy is due to differences in activation energies and backbond geometries on different Si surfaces [130].
- Seidel et al.'s model supports the previous explanation [86,87]. They detail a process to explain anisotropy based on the difference in energy levels of backbond-associated surface states for different crystal orientations.

- Finally, Elwenspoek et al. [113] propose that it is the degree of atomic smoothness of the various surfaces that is responsible for the anisotropy of the etch rates. Basically, this group argues that the kinetics of smooth faces (the (111) plane is atomically flat) is controlled by a nucleation barrier that is absent on rough surfaces. The latter, therefore, would etch faster by orders of magnitude.

3.2 DRY BULK MICROMACHINING

Wet anisotropic etching has shown limitations in etching deep structures with high anisotropy in silicon. The ability to etch such features in silicon is of considerable interest in the micromachining community for a variety of applications, including fabricating deep fluidic channels and single-crystal mechanical structures. Deep reactive ion etching and cryogenic dry etching reactors, both using plasma technology, appeared on the market in the 1990s and constitute the latest developments in the field. The information given in the following sections is based on the book by Gregory T.A. Kovacs, "Micromachined Transducers Sourcebook", published by WCB/MaGraw-Hill in 1998 [63].

3.2.1 Basics of silicon dry etching

In this class of "dry" etching reactions, external energy in the form of radio frequency (RF) power drives chemical reactions (taking the place of elevated temperatures or very reactive chemicals). Energetic ions supply the necessary energy such that reactions can occur at low temperatures. This is a very

powerful type of process that can achieve impressive anisotropy (aspect ratios) in the cases where the bombardment of the surface by ions (generally perpendicular to the wafer) drive the etch reaction.

Dry etches were originally developed in the early 1970's for applications in microelectronics. RF energy applied to a pair of plates accelerates stray electrons, increasing their kinetic energy to levels at which they can break chemical bonds in the reactant gases upon impact, forming ions and additional electrons. With ongoing input of RF energy into the chamber, electron/molecule collisions continue to yield ions and electrons, while exposed surfaces within the chamber absorb or neutralise these species. After a number of RF cycles, a steady-state discharge is reached in which generation and loss processes are balanced.

At this point, the discharge is characterised by a central glow or bulk region and dark or sheath regions between the bulk region and the electrodes. It is in the sheath regions where nearly the entire potential drop occurs between the electrodes. The bulk region is electrically semi-neutral. The higher mobility electrons can exit the bulk region more readily than ions in response to the RF cycles. This gives rise to the high-field sheath regions that form to retard the further departure of electrons from the bulk region, thus maintaining charge neutrality.

The DC component of the sheath field (sheath bias) accelerates positive ions originating in the bulk and thus gives rise to the bombardment of the wafers by the resulting highly energetic ions. The DC bias will occur on its own as described above, or it can be controlled using a separate DC power supply typically on the order of 0 to 600 V. This produces a "bias-sputter" or "bias-etch" configuration and allows some control of the electron and ion impact

energies on the wafers. Conceptual illustrations of a dry etching system are shown in Figure 3.11.

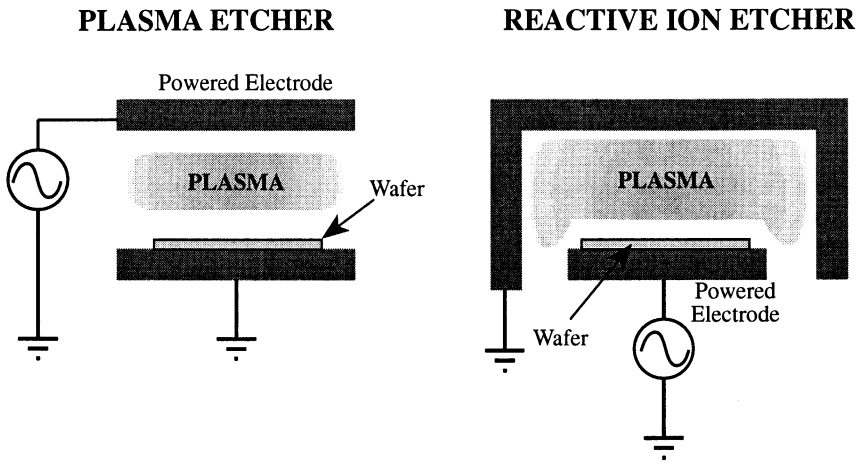

Figure 3.11. Conceptual illustrations of (a) plasma etcher: grounded wafer, symmetrical electrodes, (b) reactive ion etcher: powered wafer, grounded surface area much greater than powered electrode [63].

3.2.2 Deep reactive ion etching

A very high-aspect-ratio method referred to as deep reactive ion etching (DRIE) relies on a high-density, inductively coupled) plasma source and an alternating process of etching and protective polymer deposition to achieve aspect ratios of up to 30:1 (sidewall angles 90±2°), with photoresist selectivities of 50 and 100:1, silicon dioxide selectivities of 120 to 200:1, and etch rates on the order of 2 to 3 μm/min [114,115]. The practical maximum etch depth capability of this approach is on the order of 1 mm, and precise etch depths can readily be obtained using buried SiO_2 etch-stop layers (e.g. using silicon-on-insulator wafers).

A patent covers the concept of alternating between etching and polymer deposition [116]. The etching step uses SF_6/Ar with a substrate bias of –5 to –30 V so that cations generated in the plasma are accelerated nearly vertically into the substrate being etched. After etching for a short time, the polymerisation process is started. A mixture of trifluoromethane (CHF_3) and argon is used (although other fluorocarbons gases such as C_4F_8 combined with SF_6 tend to be utilised in current commercial equipment), and all exposed surfaces (sidewalls and horizontal surfaces) are coated with a Teflon^{TM}-like polymer layer (≈ 50 nm thick). If ion bombardment due to a small applied bias voltage is used during the polymerisation step, the formation of polymer on the horizontal surfaces can essentially be prevented. The etching step is then repeated, and the polymer deposited on the horizontal surfaces is rapidly removed due to ion bombardment and the presence of reactive fluorine radicals.

3.2.3 Cryogenic dry etching

Cryogenic cooling of the wafer can greatly enhance anisotropy of etching. By cooling the chuck to liquid nitrogen temperatures (77 K) and using helium gas flow under the wafer to transfer heat, the wafer's temperature can be maintained at cryogenic temperatures during etching. Apparently, the mechanism is condensation of the reactant gas(es) on the sidewalls of the etched structures (condensing gas at the bottom of the structures is removed by ion bombardment). A potentially important issue with cryogenic dry etching is that if microstructures become thermally isolated due to the etching, cryogenic temperatures (and hence high aspect ratio) may not be maintained

locally. Using pure SF_6, it is possible to obtain aspect ratios on the order of 30:1 and etch all of the way through a full-thickness silicon wafer. Some examples of the application of cryogenic dry etching to micromachining are presented in Ref. [117].

3.3 SURFACE MICROMACHINING

Bulk micromachining means that three-dimensional features are etched into the bulk of crystalline and noncrystalline materials. In contrast, surface micromachined features are built up, layer by layer, on the surface of the substrate. A wet or dry etching photolithographic process defines the surface features in the first layer, which will be the sacrificial layer. Free standing structures are formed by depositing and patterning a second layer over the first, a wet etching releases them from the plane by undercutting. In surface micromachining, shapes in the x-y plane are unrestricted by the crystallography of the substrate and limited to a few microns height in the z direction. The nature of the deposition processes involved results in very planar surface micromachined features. Specifically, the films of polycrystalline silicon (poly-Si), the main structural material in surface micromachining and deposited by low-pressure chemical vapour (LPCVD), are generally only few microns high (low z).

Even with the best possible process control, polysilicon has some material disadvantages over single crystal Si, in that it generates a somewhat smaller yield and has a lower piezoresistivity [118-120]. However, dimensional uncertainties are of greater concern than material issues. Moreover, the wet process for releasing structural elements from a substrate tends to cause

sticking of suspended structures to the substrate, so-called stiction, introducing another disadvantage associated with surface micromachining.

Some of the mentioned problems have recently been resolved by process modifications and/or alternative designs. Surface micromachining has then rapidly gained commercial interest, mainly because it is the most IC-compatible micromachining process developed to date.

In this section, after a brief history, the basic process sequence will be described. The technique is only summarised in the next paragraphs since it was not utilised in the scientific research included in this thesis. However, it can be applied to the field of low-power gas sensors, as will be demonstrated in Chapter 4. More detailed information about thin film mechanical properties, the processing steps, stiction, and sealing of the cavity, and is presented in the Refs. [62,63,121-124].

3.3.1 History

The first example of a surface micromachined device for an electro-mechanical application consisted of an underetched metal cantilever beam for a resonant gate transistor presented in 1967 [125]. By 1970, the first example of a magnetically actuated metallic micromotor appeared in the literature [126]. Because of fatigue problems, metals are rarely used for the fabrication of mechanical components. The surface micromachining method as we know it today was first demonstrated by Howe and Muller in the early 1980s, and relied on polysilicon as the structural material [127]. These pioneers, along with Guckel [128], an early contributor to the field, produced free standing LPCVD polysilicon structures by removing the oxide layers on which the

polysilicon features were formed. Howe's first device consisted of a resonator designed to measure the change of mass upon adsorption of chemicals from the surrounding air. Later mechanical structures, especially hermetically sealed mechanical devices, provided proof that the IC revolution could be extended to electromechanical systems [129]. In these structures, the height (z-direction) typically is limited to less than 10 μm, ergo the name surface micromachining.

The first survey of possible applications of poly-Si surface micromachining was presented by Gabriel et al. in 1989 [130]. In 1991, Analog Devices announced the first commercial product based on surface micromachining, a 50-g accelerometer for activating air-bag deployment [131]. A feature wave of major commercial applications for surface micromachining could be based on the Texas Instruments Digital Micromirror Device™. This surface micromachined movable mirror array is a digital light switch that precisely controls a light source for projection display and hard copy applications [132]. The commercial acceptance of this application will likely determine the future power of the surface micromachining option.

3.3.2 Surface micromachining basic process

A surface micromachining process sequence for the creation of a simple free-standing poly-Si bridge is illustrated in Figure 3.12 [133,134]. A sacrificial layer, also called a space layer or base, is deposited on a silicon substrate coated with a dielectric layer as the buffer/insulation layer (Fig. 3.12a). Phosphosilicate glass (PSG) deposited by LPCVD stands out as the best material for the sacrificial layer because it is etched even more rapidly in HF

than SiO_2. In order to obtain an uniform etch rate, the PSG film must be densified by heating the wafer to 950-1100°C in a furnace or rapid thermal annealer (RTA) [135]. With a first mask, the base is patterned as shown in Figure 3.12b.

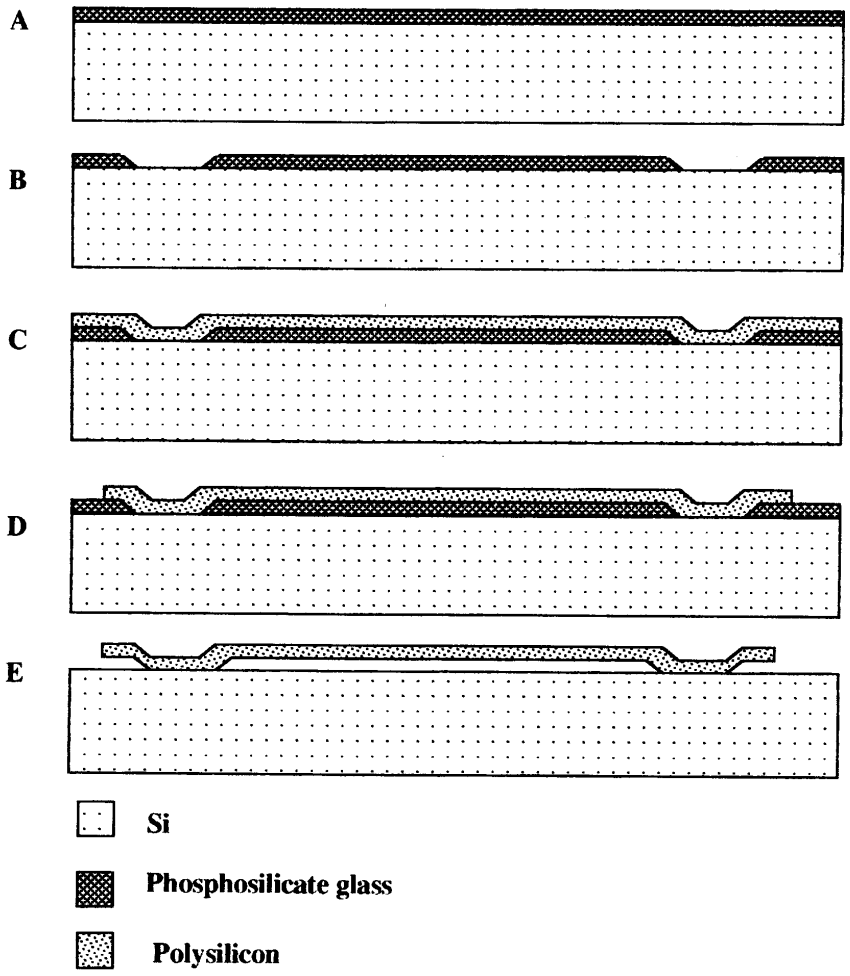

Figure 3.12. Basic surface micromachining process sequence: (a) Space layer deposition, (b) Base patterning with mask 1, (c) Microstructure layer depostion, (d) Pattern microstructure with mask 2, (e) Selective etching of space layer [62].

Windows are opened up in the sacrificial layer and a microstructural thin film, consisting either of polysilicon, metal, alloy, or a dielectric material, is conformally deposited over the patterned sacrificial layer (Fig. 3.12c). Furnace annealing, in the case of polysilicon at 1050°C in nitrogen for one hour, reduces stress stemming from the thermal expansion coefficient mismatch, and the nucleation and growth of the film. Rapid thermal annealing has been found to be effective for reducing stress in polysilicon as well [135]. With a second mask, the microstructure layer is patterned, usually by dry etching in a $CF_4 + O_2$ or $CF_3Cl + Cl_2$ plasma (Fig. 3.12d) [136]. Finally, selective wet-etching of the sacrificial layer, say in 49% HF, leaves a free-standing micromechanical structure (Fig. 3.12e). This surface micromachining technique is applicable to combinations of thin films and lateral dimensions where the sacrificial layer can be etched without significant etching or attack of the microstructure, the dielectric, or the substrate.

3.4 CONCLUSION

In this chapter the main techniques used to structure or ‘micromachine’ silicon were reviewed. These techniques can be separated in two main categories, bulk and surface micromachining. With bulk micromachining techniques, three-dimensional features may be etched into the bulk of crystalline and noncrystalline materials. Wet isotropic or anisotropic etchants can be used. In contrast, surface micromachined features are built up, layer by layer, on the surface of the substrate. Dry etching defines the surface features in the x-y plane, and wet etching releases them from the plane by undercutting.

Beams, cantilevers, diaphragms and membranes of diverse materials can be released by using silicon micromachining. These microstructures find many applications in the development of sensors and actuators, such as in the field of interest of this thesis, low power gas sensors. The next chapter presents the silicon micromachined gas sensors.

4. Micromachined gas sensors

There is a demand for gas sensing devices for many applications, including monitoring for combustible or toxic gases to ensure industrial safety, climate control of buildings and vehicles to improve comfort, and in process control and laboratory analytics. Accurate, high performance gas analysers based on gas chromatography or mass spectrometry are available, but tend to be relatively large and expensive. Their use in thus confined to analytical labs or process control. For other purposes, such as remote monitoring, cheaper, smaller, and user-friendly sensors are required. Hence, a lot of research and development has been done to design small, low-power, and inexpensive gas sensors that possess sufficient sensitivity, selectivity and stability for a given application. A large variety of sensors based on different sensing principles, such as semiconductor gas sensors, optical gas sensors, mass sensitive devices, catalytic sensors, dielectric sensors, and electrochemical sensors, have been reported (see Chapter 2) [6].

On one hand, some types of gas sensors are just by their nature considered as low power gas sensors. As already mentioned, polymer-coated transducers, such as chemo-resistors, MOSFETs, quartz microbalances (QMB) and surface acoustic waves (SAW) fall in this category [15-17,33,43,56,57]. This type of sensor is usually operated at a temperature slightly higher than room temperature. On the other hand, chemo-resistors based on gas-sensitive metal oxide materials and MOSFETs coated with catalytic metals, with operating

temperatures up to 450°C and 200°C, respectively, exhibit high power consumption.

Taguchi was the first to develop metal-oxide gas sensors to the level of an industrial product [137-139]. These Taguchi-type sensors are still on the market. However, most of the commercially available sensors nowadays are manufactured using screen-printing techniques on small and thin ceramic substrates [140-142]. Screen-printing has the advantage that thick films of gas-sensitive metal-oxide sensors are produced in batch processing. This technology is well established, and high performance has been achieved using screen-printed ceramic sensors in various field applications.

However, screen-printed ceramic gas sensors are still in need of improvement, especially with respect to power consumption, mounting technology and selectivity. The power consumption of these sensors is typically in the range of 200 mW to about 1 W [140], which is too much for applications where only battery-driven elements may be used. Moreover, the use of arrays of these sensors, which on the one hand is very promising with respect to improve discrimination between gases in a mixture, can lead on the other hand to the increased size of the sensor elements or combined sensor assemblies and thus, to increased power consumption.

In contrast, MOSFET gas sensors are small in size. In addition, microelectronics-based processing allows the formation of arrays on one substrate. However, their mounting on metallic packages leads to power consumption in the range of 500 mW to 1 W and thus to the same problems as for metal-oxide sensors.

In the last few years, the above mentioned difficulties have led to new developments in substrate technology. The integration of gas-sensitive films in

standard microelectronic processing has been achieved, and has led together with the use of micromachining (see Chapter 3) to micromachined metal-oxide gas sensors like the one shown in Figure 4.1. This technology shows great promise for overcoming the difficulties of screen-printed ceramic sensors. The sensitive layer is deposited onto a thin dielectric membrane of low thermal conductivity, which provides good thermal isolation between the substrate and the gas-sensitive heated area on the membrane. In this way, the power consumption can be kept very low, with typical values on the order of 30–150mW, with the substrate remaining almost at ambient temperature [22, 143-145,159]. This type of thermally heated device is commonly called a micro-hotplate, and is used in different applications [146-149].

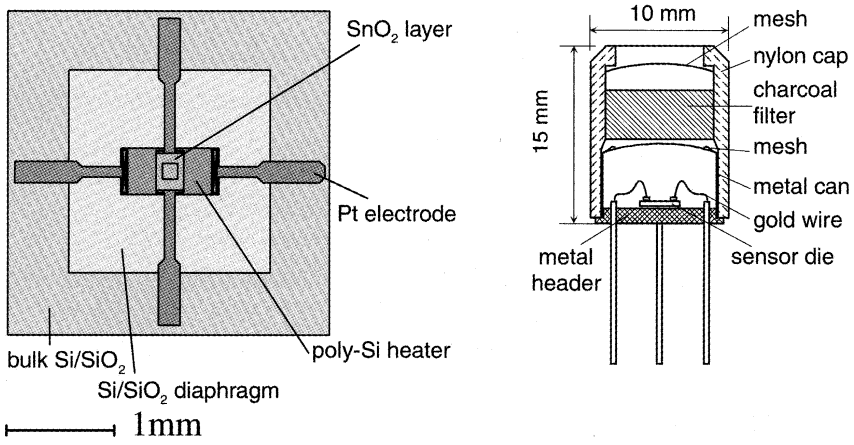

Figure 4.1. Schematic of the micromachined sensor commercialised by MicroChemicalSystems SA (MICS), Corcelles, Switzerland: sensor element on the left and housing on the right.

The mounting of membrane-based sensors is much easier than for an overall hot ceramic sensor element, and control and signal-processing electronics can be integrated on to the same substrate if desired. Moreover, sensor arrays,

which are often needed to overcome the bad selectivity of single sensor elements, can easily be implemented in this technology. The small thermal mass of each micromachined element allows rapid thermal programming, a unique feature, which can be used to study the kinetics of surface processes and to achieve kinetically controlled selectivity [150].

In this chapter, the frequently used technologies in the field of micromachined gas sensors, and the design parameters which influence the thermal and mechanical properties of such devices, are reviewed. The following sections are based mainly on the only review written on the subject by I. Simon et al. [21].

4.1 MICROMACHINED GAS-SENSING PLATFORMS

Several elements have to be considered in the design and processing of micromachined gas sensing platforms. Suitable characteristics for such devices are low power consumption, high mechanical strength, and well-controlled temperature distribution across the sensing layer. The latter is important since both the thermal and mechanical properties of the gas-sensing film are strongly temperature dependent. To reach the given specifications, different combinations of geometries, materials and fabrication techniques can be used.

4.1.1 Technology

4.1.1.1 Membrane

The starting point for the production of micromachined gas sensors is the formation of a thermally isolated heating area on a membrane. In most cases, silicon is used as the substrate and silicon micromachining methods (see Chapter 3) are used to release the dielectric membrane on which are located the active components of the hotplates. In general, there are two different types of structures which the membrane can adopt; one is the closed-membrane-type, the other the suspended-membrane type (Figs. 4.2 and 4.3).

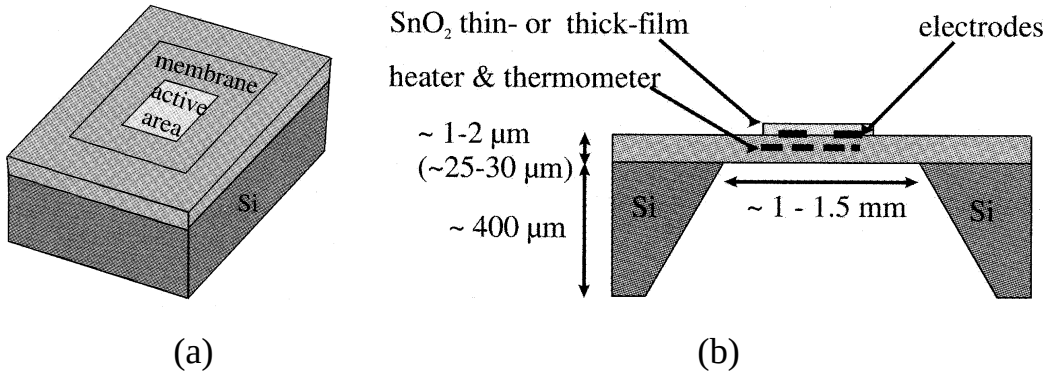

Figure 4.2. Schematic of a closed-membrane-type hotplate: (a) top view, (b) side view [21].

The closed-membrane-type hotplate is formed by anisotropic etching of silicon from the backside (see Chapter 3). In most cases, the membrane is made of silicon nitride and/or silicon oxide thin films. These materials are also used as insulator to cover the heater deposited on the membrane and hence electrically isolate it from the sensing film. Using these sorts of thin films, the typical thickness of the membrane/insulator sandwich is between 1 and 2 μm

[144-146,151]. Another method to form the membrane consists of using nitrided porous silicon with a thickness between 25 and 30 μm, which can be obtained by silicon anodisation followed by nitridation [152]. Silicon oxide, silicon nitride and nitride porous silicon all possess low thermal conductivities and can thus provide good thermal isolation between the heated active area and the membrane rim silicon chip frame [153-155]. Silicon nitride layers generally have large tensile stress and silicon dioxide layers are compressive.

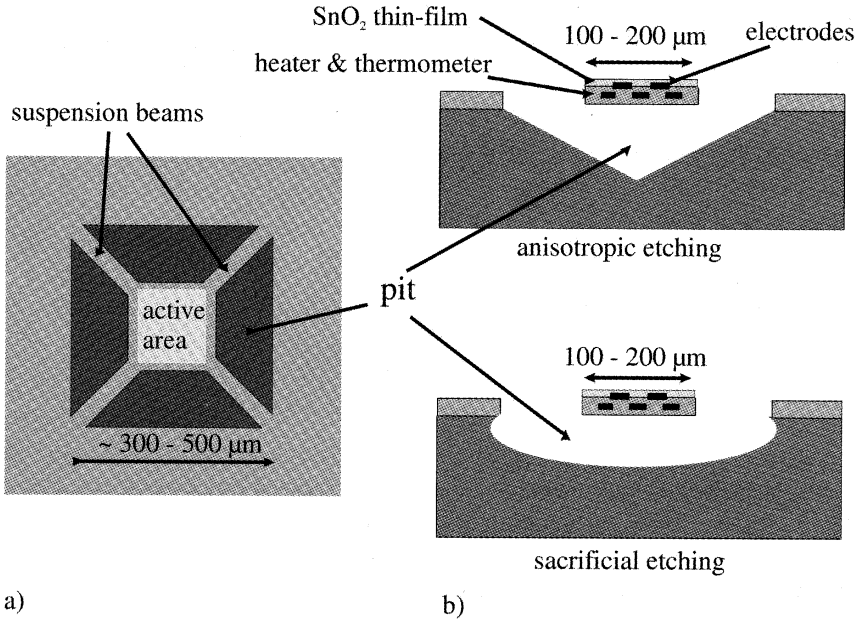

Figure 4.3. Schematic of suspended-membrane-type hotplate: (a) top view, (b) side view [21].

Nevertheless, by appropriate choice of deposition and annealing steps multilayer systems of silicon oxide and/or silicon nitride have proven to be mechanically stable. It is also possible to deposit a so-called low-stress silicon nitride (200-300 MPa) film by low-pressure chemical vapour deposition (LPCVD), which, compared to the previous films, is not fully IC-compatible

[156,157]. The closed-membrane-type has the disadvantage that it requires a double-sided alignment for the bulk silicon etch from the backside. Moreover, sloped sidewalls are obtained by anisotropic etching of silicon, making the lateral dimensions required to form the membrane larger (see Chapter 3). Plasma etching (see Chapter 3) might therefore be an alternative to wet etching if a larger number of sensors on a wafer are desired.

The suspended-membrane-type is completely or partially processed from the front-side. Therefore, it is often claimed that the suspended membrane is more compatible with CMOS processing [158,159]. The suspended membrane is generally released by anisotropic etching of silicon from the front side [158,159]. The membrane is first formed by depositing dielectric layers like silicon dioxide and/or nitride and then patterning to form etched windows. The etching is performed afterwards, or after dicing and packaging [159]. Sacrificial etching of porous silicon is another possibility for obtaining suspended membranes with a greater thickness (few microns) [160]. Another way to fabricate this type of membrane is to use a combination of anisotropic etching from the back with reactive ion etching from the front to form open windows in the membrane. Suspended membranes made of silicon carbide have been processed in this way [161]. The typical lateral dimensions of suspended membranes lie between 100 and 200 μm.

Recently, suspended membranes were also realised on alumina ceramic substrates using bulk and surface-like micromachining of this material [162]. This ceramic approach is based on anodic alumina films with self-organised morphology. The regular porous structure is formed when aluminium is anodised in certain acidic solutions. This anodic alumina can be completely dissolved at pHs lower than 4.2 and higher than 9.9, whereas normal

(polycrystalline) alumina would be subjected only to slight surface etching. Since alumina has a low thermal conductivity, and the solubility of anodic alumina is of a highly anisotropic nature, thermally isolated suspended membranes can be made directly from an alumina substrate without additional layers (Fig. 4.4).

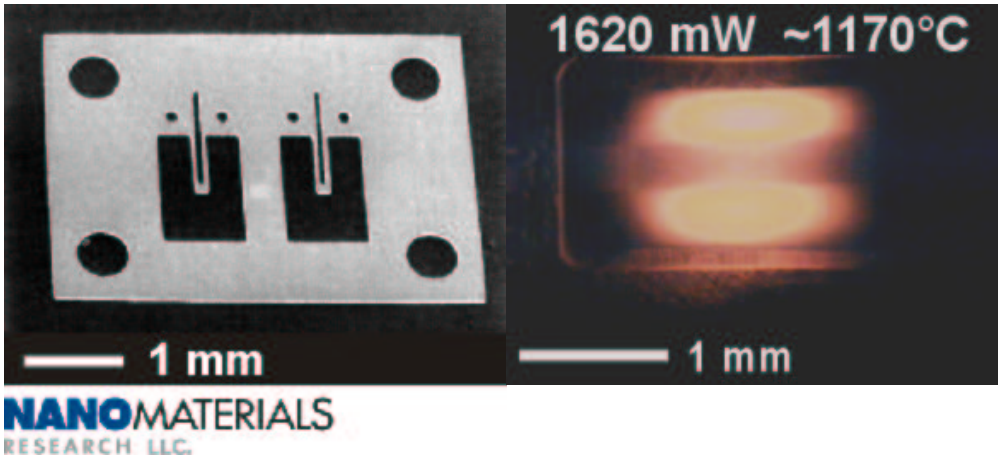

Figure 4.4. Thermally isolated cantilever made from anisotropic etching of an alumina substrate [163]. Courtesy of Nanomaterials Research LLC, Longmont, CO, USA.

Finally, though not as highly developed, suspended membranes made using a surface micromachining process (see Chapter 3) have been reported [154,163]. In one case, polysilicon was used as membrane and heater at the same time and released by etching a sacrificial oxide film, as in the established polysilicon micromachining process [154]. In another case, polysilicon was used as the sacrificial film to release a membrane made of dielectric films (Fig. 4.5) [163].

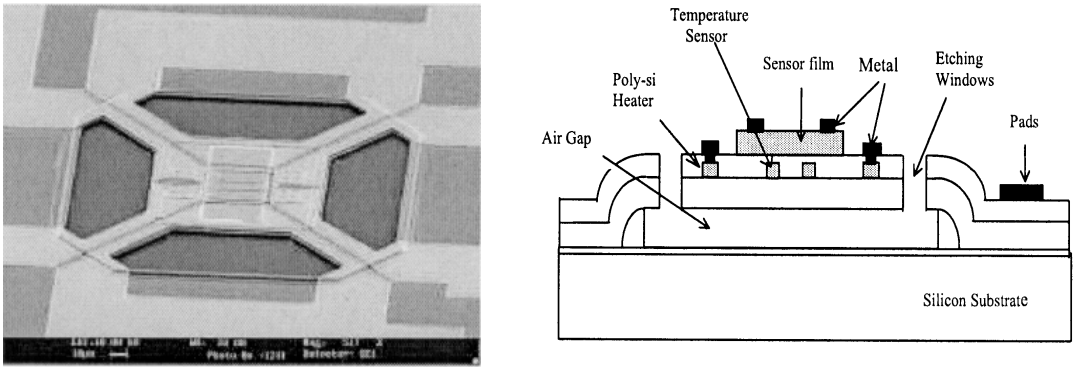

(a) (b)

Figure 4.5. Top view SEM photo and cross-section schematic of a surface micromachined gas sensor [163].

The advantages of such technology are the high density of integration and the possibility to integrate the electronics on to the same chip (CMOS). The problems are mainly caused by the gap (1–2 μm) remaining between the membranes and the substrate. Stiction of the membranes on the substrate might occur and the step to cover by the crossing metal interconnections is large.

4.1.1.2 Integration of heater, temperature sensor and contacts to the sensing layer

Heater and thermometer structures, which are needed to control the sensor operation temperature, can be integrated in two different ways. The first is known as the horizontal approach and is used when the electrodes are made for example of platinum; the heater and thermometer structures can be integrated in the same layer as the electrodes with no additional steps (Fig. 4.6b) [164].

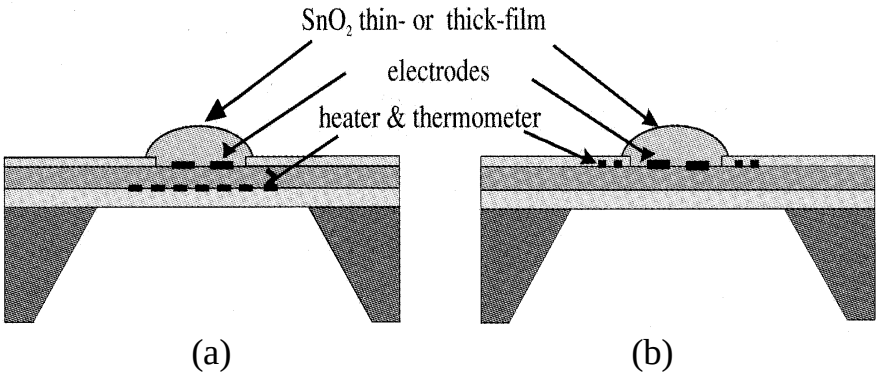

Figure 4.6. Schematic cross-section view of (a) vertical or (b) horizontal approach [21].

However, the design of structures that guarantee both appropriate temperature (resistance) measurements and homogeneous temperature distributions over the active area can represent quite a challenge. The second way is the vertical approach in which the heater and thermometer are made in successive steps as shown in Figure 4.6a. This approach allows more design flexibility [144].

The heater and thermometer are frequently formed in polysilicon, platinum or p++ doped silicon, and embedded in silicon oxide or nitride for electrical isolation [144,147,151,158-160,166-168]. Sometimes these resistive structures act at the same time as heater and thermometer. Polysilicon can be deposited by a standard chemical vapour deposition (CVD) process and patterned using a resist mask and reactive ion etching. Platinum can be evaporated or sputtered, and patterned by a lift-off process or ion beam etching. Whereas polysilicon structures can be easily integrated in an IC-process, platinum elements are generally not [151]. Appropriate thicknesses for polysilicon and platinum are 0.5 and 0.25 μm, respectively. The sheet resistance of the polysilicon can be adjusted by n-type doping with $POCl_3$ [169], and it is possible to fabricate polysilicon with negative temperature coefficient

resistance (TCR). This is a large advantage as negative TCR materials counteract to hot spots whereas heater materials with a positive TCR, such as platinum, have an amplifying effect on hot spots [146]. On the other hand, polysilicon heaters suffer from a lack of reliability at high temperature [170,171]. Another alternative material to form the heater and thermometer is boron-doped (p++) silicon. The structures are located underneath the membrane in the silicon substrate and are preserved during the silicon etching process as p++ etch stop (see Chapter 3) [166,167].

Thermometers have also been realised using aluminium plates with electrical connections for 4-point temperature measurement [159], or by forward biased p-n junctions, since the voltage of diodes operated at constant current is proportional to the absolute temperature [172-173]. The use of aluminium plates improves the temperature uniformity over the active area (high thermal conductivity), but limits the sensor operation and annealing temperatures to values below 500°C.

Electrical connections to the gas-sensitive films are generally made by metal electrodes, deposited on top of the membranes in the so-called active area. The electrodes are located underneath the sensing film most of the time, but their deposition on top of thin gas-sensitive layers has also been realised [174]. The electrode materials usually employed to contact metal-oxide or polymer sensitive films are gold and platinum with an adhesion layer underneath (Cr, Ti, Ta) [22,145,151,162]. In some cases, aluminium and tungsten have also been used for metal-oxide layers [159,175]. Aluminium is commonly employed to contact the catalytic metals of MOSFET sensors. Aluminium is advantageous, as it is the standard metallisation in IC-processes. However, its contact properties to metal-oxide and polymer sensing films are rather bad,

and the maximum operation temperature is limited to about 500°C due to electromigration.

4.1.2 Thermal design

The thermal characteristics of micromachined gas sensors have to be optimised mainly with respect to low power consumption and well-controlled temperature distribution over the sensing area. The physical mechanisms regulating heat losses have to be understood for optimum thermal design of the sensing platforms.

Heat transfer occurs due to conduction, convection and radiation. The different heat transfer pathways of a micromachined platform are illustrated in Figure 4.7. The heat losses from the heated sensing area are due to heat conduction through the membrane, and to losses to the surrounding atmosphere through heat conduction and convection. Radiative losses might also be taken in account depending on the application.

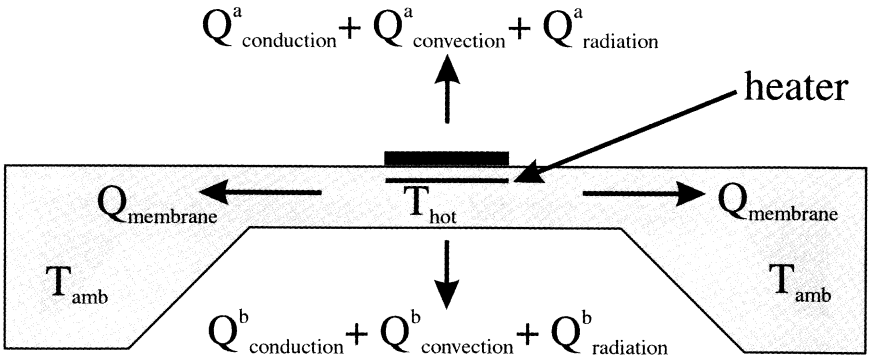

Figure 4.7. Heat pathways of a micromachined sensing platform [21].

According to the different pathways of heat transfer, the determination of the total heat loss and temperature distribution is not an easy task. In the design of

a new device, simple models for basic understanding are necessary and, to minimise the costs of development, extensive simulation studies like FEM (finite element modelling) simulations are required.

Assuming that the different components of heat flow are additive, the total heat flow, Q_{tot}, can be expressed as:

$$\begin{aligned} Q_{tot} &= G_m \times \lambda_m \times (T_{hot} - T_{amb}) \\ &+ G_{air} \times \lambda_{air} \times (T_{hot} - T_{amb}) \\ &+ G_{rad} \times \sigma \times \varepsilon \times (T_{hot}^4 - T_{amb}^4) + \Delta x \end{aligned} \tag{4.1}$$

The first term describes the heat conduction through the closed membrane, the second the heat conduction through the ambient air, the third heat losses due to radiation and the last term, Δx, accounts for unknown heat losses including free convection. G_m, G_{air} and G_{rad} are geometric factors, and are empirical values which contain information about the geometry of the closed or suspended membrane and its effect on heat losses. T_{hot} and T_{amb} denote respectively the temperature of the hot active area and the ambient atmosphere. λ_m and λ_{air} are the thermal conductivity of the membrane and the surrounding atmosphere, respectively, ε the emissivity and σ the Stefan-Boltzmann constant. In the next sections, the different terms are discussed and expressions for the geometric factors are obtained.

4.1.2.1 Heat conduction through the membrane

For the calculation of heat conduction, one has to deal with a 3-dimensional problem. Due to the negligible thickness of the membrane compared to its length, the heat conduction perpendicular to the membrane is generally neglected.

In the case of a suspended membrane, a further reduction to a one-dimensional problem is straightforward, as heat conduction occurs basically only along the suspension beams with length l and sectional area of A_{beam}. Conduction within the membrane plate is negligible in comparison [143] and with 4 beams one obtains:

$$Q_{membrane} = \frac{4 \times \lambda_m \times A_{beam} \times (T_{hot} - T_{amb})}{l} \tag{4.2}$$

$$\text{where} \quad G_m = {}^{4 \times A_{beam}}\!/_{l} \tag{4.3}$$

For a closed membrane, a simple model is obtained by replacement of the square membrane by a round one [144] as depicted in Figure 4.8. This leads to one-dimensional heat conduction problem in cylindrical coordinates which can be easily solved [31]:

$$Q_{membrane} = \frac{2\pi \times \lambda_m \times d \times (T_{hot} - T_{amb})}{\ln(r_a / r_i)} \tag{4.4}$$

$$G_m = \frac{2\pi \times d}{\ln(r_a / r_i)} \tag{4.5}$$

d denotes the thickness of the membrane, and r_a and r_i the radius of the membrane and the heated area, respectively. From equations 4.2 and 4.4, it is

clear that selection of membrane/suspension beam materials of low thermal conductivity and thickness is desirable to achieve low thermal losses. In addition, the length-to-width ratio of the suspension beams and the ratio r_a/r_i, should be chosen as large as possible to minimise heat losses.

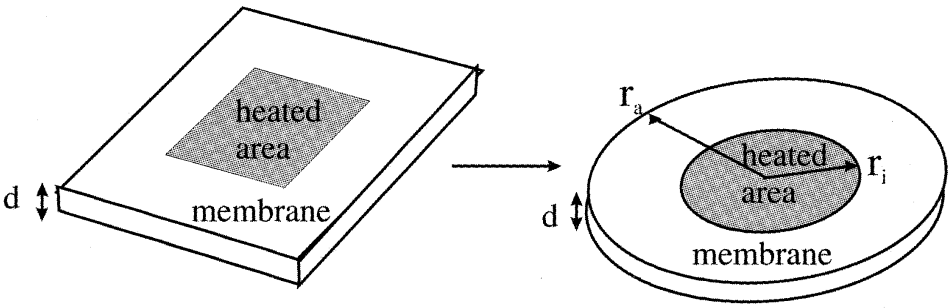

Figure 4.8. Replacement of a square membrane by a one-dimensional circular membrane [21].

In the closed-membrane case, the importance of adequate scaling of the square heating resistor (edge length a) compared with the square membrane (edge length b) has been shown by several authors [151,153,169]. The power consumption as a function of distance between heated area and silicon rim decreases with increasing distance. Nevertheless for a given distance, the thermal isolation is practically not improved further [169], the chip silicon rim remaining close to the ambient temperature. Increasing the membrane size results only in larger devices, reducing the density of integration

Finally, by computing the heat loss in equation 4.2 and 4.4, it can be clearly shown that the suspended membrane type provides lower power consumption than a closed membrane.

4.1.2.2 Heat losses to the air

Heat losses to the surrounding air can occur through two different mechanisms, i.e. fluid motion and conduction. We can distinguish between two different types of heat loss by fluid motion: forced convection or free/natural convection. When there is no fluid motion, heat is transferred only by conduction.

In the following, forced convection is excluded. Nevertheless, due to the coupling of the temperature field and thus the fluid field, the calculation of heat losses to air remains difficult. There are two approaches proposed in the literature to simplify the calculations.

In the first approach, the fluid motion is neglected [143,169,177]. It is assumed that there is no significant contribution of convectional fluid motion because of the small size of the heated structures. The heat transfer to air occurs only by heat conduction. Under this assumption, it is possible to use a simple analytical model as an estimate for heat losses to the air as in Ref. [144]. This model approximates the hot gas sensor and the cold ambient by concentric spheres with radius r_i and $r_{a,}$ respectively. While the model gives a rough estimate of the heat loss by conduction in air, numerical solutions are needed to solve the problem correctly. An additional factor affecting conduction in air, which needs to be considered, is the temperature dependence of the thermal conductivity of air [178]. To optimise the heat losses in air using this approach, the heated area has to be minimised and the distance between the cold die and hot membrane maximised.

Qualitatively, the same can be drawn with the second approach, which takes fluid motion into account. In this case, empirical heat transfer coefficients are

used to describe the heat losses to the air. Heat transfer coefficients are, in general, empirical values and account for heat transfer due to conduction as well as fluid motion. The total heat flow, Q_{air}, from a heated membrane area to the surrounding air can be described as:

$$Q_{air} = \alpha_m \times A \times (T_{hot} - T_{amb}) \tag{4.6}$$

with α_m being the mean heat transfer coefficient. Theoretical determination of heat transfer coefficients requires knowledge of the temperature field and the velocity and is rather difficult. However, for certain problems it is possible to find empirical equations describing heat transfer. Nevertheless, the results should be considered just as estimates for microhotplates, as the empirical equations used are actually evaluated for much larger hotplate sizes. On the other hand, with the help of calculated mean heat transfer coefficients, the total heat flow above a membrane can be easily calculated. Reduction of power consumption saving is accomplished by minimising the heated membrane area and the operation temperature. The latter depends on the properties of the gas-sensing material.

4.1.2.3 Radiation

The expression for radiation in equation 4.1 was obtained with the assumption that the heated membrane area behaves like a grey emitter, i.e. the degree of emission from the heated membrane is set equal to the degree of absorption [176]. Under the assumption that the heated membrane area, A, radiates in all directions, the geometry factor G_{rad} can be set to $G_{rad} = (2 \times A)$. Heat losses due to radiation thus increase with heated membrane area. Generally the heat

losses due to radiation amount to only a few percent of the total heat loss [146,151,153,172]. Nevertheless, due to the T^4 –dependency, radiation should be considered carefully as a potential problem if very high sensor operation temperatures are applied. Radiative losses can be reduced dramatically by coating the membrane backside with glossy materials like gold ($\varepsilon = 0.05$) [179].

4.1.2.4 Key parameters for low power micromachined platforms

From the above discussion, some key parameters for minimising the total power consumption of micromachined gas sensing platforms are:

- thin membranes consisting of materials of low thermal conductivity should be constructed.
- the heated area should be decreased.
- for closed membranes: heater edge length should be adjusted to the size of the membrane.
- for suspended membrane, suspension beams with high length-to-width ratios should be used.
- a large pit depth should be chosen.
- for both types: gold coating at the backside of the membrane.

In this whole discussion, one should not forget that besides low power consumption, the gas sensor's functionality and the mechanical stability have to be maintained.

4.1.2.5 Heater design

The heater design is crucial for control of the temperature distribution over the active area. The geometries of the heater and the substrate have to be adapted carefully to achieve a desired temperature distribution. It should be pointed out that the heating of an active area with constant power per area results in an inhomogeneous temperature profile. The inner part of the heated area loses heat to the ambient air and by radiation, whereas the outer part additionally loses heat by conduction through the membrane. Therefore, the borders of the active area are colder than the inner part, and spatial variation of heating power is needed to compensate it. High thermal conductivity films may also help to improve the uniformity of the temperature distribution.

Two practical approaches have been suggested in the literature to solve this problem. The first one is to use two heaters: an area heater and a ring heater [143,172]. The ring heater serves to compensate of the heat losses through the membrane. One difficulty to this two-heater approach is to determine the compensating heating power required. The other technique is to use a double-spiral structure with variable width as the heater [180,181]. A disadvantage compared to the previous approach is that the temperature homogeneity depends on the heater design and cannot be adjusted later on.

In general, it is very hard to predict the temperature distribution, and numerical calculations are needed.

4.1.2.6 Transient thermal response

A simple expression for the thermal transient response of the sensor can be obtained by assuming the temperature distribution inside the sensor to be

uniform, and by using one overall thermal resistance (R_{th}) and capacity (C_{th}) to describe the thermal behaviour. Heat balance between heating power (P) and heat losses results in the expression:

$$P = C \times \frac{dT(t)}{dt} + \frac{T(t) - T_{amb}}{R_{th}} \qquad (4.7)$$

This equation allows the calculation of the temperature response to an arbitrary heating power input. Solutions can be found using Fourier and Laplace analysis. For instance, the temperature response to a step function is given by:

$$T(t) - T_{amb} = P \times R_{th} \times \left(1 - e^{-t/\tau}\right), \ \tau = R_{th} \times C \qquad (4.8)$$

Because the thermal time constant, τ, obtained in this way depends linearly on thermal resistance and capacity, a sensor with low thermal mass and small thermal resistance will show faster response. Due to the fact that a small thermal resistance also leads to an increase in power consumption, there is a trade-off to make in the choice of the thermal resistance material. Minimisation with respect to thermal capacity is mainly achieved by a reduction of the heated mass. This is why suspended membranes show generally faster thermal response than the larger closed membranes.

4.1.2.7 Thermal simulations [182]

Numerical approximations of the temperature distribution, the total heat loss and the transient response can be obtained by replacing the sensor by a set of points for which temperature is calculated as a function of time. This set of

points is called the computational grid or mesh. The right choice of computational grid is very important to obtain good approximations. An increase of the number of node points result in better accuracy, but leads at the same time to an increase of computational time. Therefore, it is often better to model the parts of the sensor that are subject to large changes in temperature with a narrow grid and regions with few changes with a rather rough grid.

One way to derive the equations for the node temperatures is to divide the sensor into elements and apply the heat balance to each individual element. For each element, a point, e.g. the centre of the element, is selected as a node. Temperature and thus flow variations over the element are neglected. The node temperature is considered to be representative of the entire element. Another possibility is to start with the differential equation, which is the mathematical description of the heat balance of an infinitesimal element, and replace the differentials by finite differences expressed in terms of the node-point temperatures. This method is known as the finite-difference method.

In either case, one has to solve a set of equations relating the temperature at the nodes to each other. A lot of analysis tools that can take over this work are available nowadays. Solutions can be found by describing the thermal system using electrical equivalents and using standard circuit analysis tools such as SPICE.

An alternative is to use advanced finite-element methods (FEM) such as ANSYS. FEM describe the solution for a given geometry (one-, two-, or three dimensional) by means of a finite number of line, surface or volume elements. These can be chosen arbitrarily. FEM can account for complicated boundary conditions and temperature-dependent thermal properties. The node equations can thus become rather complicated. Finite-element methods are therefore

available in the form of complete software packages, which include tools for mesh generation, element definition, equation solving and display of results.

4.1.3 Mechanical design

Micromachined gas sensors are not only a challenge with respect to thermal design but also with respect to mechanical design. With proper design, several modes of failure can be avoided such as:

- large intrinsic or thermal-induced membrane stress, leading to deformation (buckling) /breaking of the membrane.
- plastic deformation at the metal-sensing layer contact area.
- deformation / breaking of the membrane due to deposition of the sensing layer(s).
- bad adherence / peel-off of the sensing layer due to mechanical and thermal stresses.
- mechanical or thermal induced stress in the metallisation.
- thermometer and heater shift or drift due to mechanical and thermal stresses.

To avoid these failures, the right sets of process parameters have to be found and processes need to be well controlled. Thin film mechanical and electrical properties depend strongly on microstructural characteristics like grain size, orientation, density, and stoichiometry, and depend on deposition conditions. Moreover, the microstructures change with number of heat cycles. This can result in the drift of the electrical and/or mechanical characteristics, but also presents the possibility to adjust a layer's properties by annealing steps.

Intrinsic stress in single layer or multilayer systems can occur as results of thermal stress and residual stress [183]. Thermally induced stress is caused by mismatches in the thermal expansion coefficients of the different films, which might lead to deformation of the structure, or by non-uniform temperature distribution, which may in some cases be temperature dependent. The latter points out that thermal and mechanical design are strongly interdependent. Residual stresses are due to the fact that the thin films in their deposited form are not in the most favourable energetic configuration, resulting in compressive or tensile stress.

Residual stresses are generally much more significant than thermal stress, so that control of residual stress in single layers and especially multilayer systems is critical for membrane stability [183]. The resultant residual stress, σ_r, of a stacked membrane can be approximated by:

$$\sigma_r = \frac{\sigma_1 d_1 + \sigma_2 d_2 + \ldots}{d_1 + d_2 + \ldots} = \frac{\sum_{i=1}^{n} \sigma_i d_i}{\sum_{i=1}^{n} d_i} \qquad (4.9)$$

where d_i and σ_i are the thickness and intrinsic stress of the different membrane layers. A low residual tensile stress is favourable for the membrane of a micromachined gas sensor, since the membrane enters in a compressive state (hot in the middle, cold on the chip frame) during operation.

To obtain such low residual stress in single layers is difficult. Frequently used materials such as silicon oxide and silicon nitride show significant compressive and tensile stress, respectively. However, the right combination of these materials can lead to acceptable resultant residual stress [168].

Moreover, by modifying the stoichiometry, a low-stress silicon nitride film can be obtained using low-pressure chemical vapour (LPCVD) deposition [156,157].

The properties of a single layer might change upon annealing and processing of subsequent layers, thus leading to manifestation of different stress properties in the layer within the multilayer system than as a single layer. Therefore, the design and fabrication of a membrane with low intrinsic stress depends on experimental determination of the residual stress. Methods to measure residual stress involve curvature measurements of the whole wafer. In situ stress diagnostic structures like doubly supported beams or Guckel rings, which rely on warping or buckling, may also be used [183]. Such experimental check is not only of interest for the design of stable membranes, but also for achieving the process control required to guarantee reproducible film structures, and thus mechanical as well thermal properties.

A simple, practical measure for the mechanical stability of micromachined gas sensors is the production yield [169]. A more realistic view with respect to mechanical stability under normal sensor operation can be obtained through use of long-term reliability tests [181,184,185]. The importance of thermal stress can then also be determined, the membrane stack expand thermally, leading to additional compressive stress, as mentioned before.

Finally, it should be noted that not only the mechanical properties of thin film layers, but also the macroscopic dimensions of the membrane itself influence the stability of the micromachined sensors. Decreasing the lateral dimensions and increasing the thickness of the membrane and suspension beams can lead to much greater stability. However, as stability is improved, thermal losses are generally increased as discussed in 4.1.2. The choice of membrane dimensions

is therefore a trade-off between high mechanical strength and small thermal heat losses.

4.2 CONCLUSION

In this chapter, the main technologies used in the field of micromachined gas sensors, and the design parameters which influence the thermal and mechanical properties of such devices, were reviewed. Suitable characteristics for such devices are low power consumption, high mechanical strength, and well-controlled temperature distribution across the sensing layer.

The starting point for the production of micromachined gas sensors is the formation of a thermally isolated heating area on a membrane. Silicon micromachining is used to release the dielectric membrane on which are located the active components. In general, there are two different types of structures for the membrane containing the hotplate: one is the close-membrane-type, and the other, the suspended-membrane type. In most cases, the membrane is made of silicon nitride and/or silicon oxide thin films, with the heater and thermometer embedded in between. Metal electrodes deposited on top usually form the electrical connections with the gas-sensitive films.

The thermal characteristics of micromachined gas sensors have to be optimised mainly with respect to low power consumption and well-controlled temperature distribution over the sensing area. The choice of membrane dimensions is a trade-off between small thermal heat losses and high-mechanical strength.

References

[1] D.A. Skoog, F. James Holler, and T.A. Nieman, Principles of instrumental analysis, 5th Ed., Harcourt Brace College Publishers, USA, 1998, pp. 253-271 and pp. 673-777.

[2] J.W. Gardner and P.N. Bartlett, Electronic noses: principles and applications, Oxford University Press, Oxford (UK), 1999.

[3] A. D'Amico, C. Di Natale, and R. Paolese, "Portraits of gasses and liquids by arrays of nonspecific chemical sensors: trends and perspectives", Sensors and Actuators, B 68, pp. 324-330, 2000.

[4] K. Persaud and G. Dodd, "Analysis of discrimination mechanisms in the mammalian olfactory system using a model nose", Nature, 299, pp.352-355, 1982.

[5] H.T. Troy Nagle, S.S. Schifman and R. Gutierriez-Osuna, "The How and Why of Electronic Noses", IEEE Spectrum, Sept. 1998.

[6] W. Göpel, T.A. Jones, M. Kleitz, I. Lundström, and T. Seiyama (Eds),Chemical and biochemical Sensors, Part I, VCH, Weinheim, Germany, 1991, 716 pp.

[7] I. Lundström, "Approaches and mechanisms to solid state based sensing", Sensors and Actuators, B 35-36, pp. 11-19, 1996.

[8] W. Göpel, "Chemical imaging: I. Concepts and visions for electronic and bioelectronic noses", Sensors and Actuators, B 52, pp. 125, 1998.

[9] D.E. Williams, "Semiconducting oxides as gas-sensitive resistors", Sensors and Actuators, B 57, pp. 1-16, 1999.

[10] W. Göpel and K.D. Schierbaum, "SnO_2 sensors: current status and future prospects, Sensors and Actuators, B 26-27, pp. 1-12, 1995.

[11] I. Lundström, A. Spetz, F. Winquist, U. Ackelid, and H. Sundgren, "Catalytic metals and field-effect devices – a useful combination", Sensors and Actuators, B 1, pp. 15-20, 1990.

[12] M. Löfdahl, M. Eriksson, and I. Lundström, “Chemical images”, Sensors and Actuators, B 70, pp. 77-82, 2000.

[13] K.D. Schierbaum, A. Gerlach, M. Haug, and W. Göpel, “Selective detection of organic molecules with polymers and supramolecular compounds: applications of capacitance, quartz microbalance and calorimetric transducers”, Sensors and Actuators, A 31, pp. 130-137, 1992.

[14] A. D’Amico, C. Di Natale, A. Macagnano, F. Davide, A. Mantini, E. Tarizzo, R. Paolese, and T. Boschi, “Technologies and tools for mimicking olfaction: status of the Rome ‘Tor Vergata’ electronic nose”, Biosensors & Bioelectronics, 13, p. 711-721, 1998.

[15] G. Bidan, “Electroconducting conjugated polymers: new sensitive matrices to buld up chemical or electrochemical sensors: A review”, Sensors and actuators, B 6, pp. 45-56, 1992.

[16] Z. Deng, D.C. Stone, and M. Thompson, “Selective detection of aroma components by acoustic wave sensors coated with conducting polymer films”, The Analyst, 121, pp. 671-679, 1996.

[17] K. Domanský, D.L. Baldwin, J.W. Grate, T.B. Hall, J. Li, M. Josowicz, and J. Janata, “Development and calibration of field-effect transistor-based sensor array for measurement of hydrogen and ammonia gas mixtures in humid airAnalytical Chemistry, 70, pp. 473-481, 1998.

[18] M. Haug, K.D. Schierbaum, G. Gauglitz, and W. Göpel, “Chemical sensors based upon polysiloxanes: comparaison between optical, quartz microbalance, calorimetric and capacitive sensors”, Sensors and Actuators, B 11, pp. 383-391, 1993.

[19] T. Eklöv, Methods to improve the selectivity of gas sensors systems, Thesis at Linköping University, Sweden, 1999, 188 pp.

[20] W. Göpel, “Ultimate limits in the miniaturization of chemical sensors”, Sensors and Actuators, A 56, pp. 83-102, 1996.

[21] I. Simon, N. Barsan, M. Bauer, and U. Weimar, "Micromachined metal oxide gas sensors: Opportunities to improve sensor performance", Sensors and Actuators, B 73, pp. 1-26, 2001.

[22] V. Demarne and A. Grisel, "An integrated low-power thin-film CO gas sensor on silicon", Sensors and Actuators, 13, pp. 301-313, 1988.

[23] I. Lundström, S. Shivaraman, C. Svensson, and L. Lundkvist, "A hydrogen-sensitive MOS field-effect transistor", Applied Physics Letters, 26, pp. 55-57, 1975.

[24] M. Johansson, I. Lundström, and L-G. Ekedahl, "Bridging the pressure gap for palladium metal-insulator-semiconductor hydrogen sensors in oxygen containing environments", Journal of Applied Physics, 84, pp. 44-51, 1998.

[25] I. Lundström, "Hydrogen sensitive MOS-structures, Part 1: principles and applications", Sensor and Actuators, 1, pp. 403-426, 1981.

[26] J. Fogelberg and L.-G. Petersen, "Kinetic modelling of the H_2-O_2 reaction on Pd and of its influence on the hydrogen response of a hydrogen sensitive Pd metal-oxide-semiconductor device", Surface Science, 350, pp. 91-102, 1996.

[27] I. Lundström, M. Armgarth, and L-G. Petersson, "Physics with catalytic metal gate chemical sensors", CRC Crit. Rev. Solid State Mater. Sci., 15, pp. 201-278, (1989).

[28] F. Winquist, A. Spetz, M. Armgarth, C. Nylander, and I. Lundström, "Modified palladium metal-oxide-semiconductor structures with increased ammonia gas sensitivity", Applied Physics Letters, 43, pp. 839-841, 1983.

[29] A. Spetz, M. Armgarth, and I. Lundström, "Hydrogen and ammonia response of metal-silicon dioxide structures with thin platinum gates", Journal of Applied Physics, 64, pp. 1274-1283, 1988.

[30] I. Lundström, "Why bother about gas-sensitive field-effect devices", Sensors and Actuators, A 56, pp. 75-82, 1996.

[31] S.M. Sze, Semiconductor devices: physics and technology, John Wiley and Sons, USA, 1985, 523 pp.

[32] M. Josowicz and J. Janata, in Chemical sensor technology, Ed. by T. Seiyama, Elsevier, Amsterdam, 1988, p.153.

[33] M.G.H. Meijerink, M. Koudelka-Hep, N.F. de Rooij, D.J. Strike, J. Hendrikse, W.Olthuis, and P. Bergveld, "Gas-dependent field effect transistor with an electrodeposited conducting polymer gate contact", Electrochemical and Solid-State Letters, 2 (3), pp. 138-139, 1999.

[34] A. Lloyd Spetz, P. Tobias, A. Baranzahi, P. Martensson, and I. Lundström, "Current status of silicon carbide based high-temperature gas sensors", IEEE Transactions on Electron Devices, 46 (3), pp. 561-566, 1999.

[35] A. Lloyd Spetz, P. Tobias, L. Unéus, H. Svenningstorp, L.-G. Ekedahl, and I. Lundström, "High temperature catalytic metal field effect transistors for industrial applications", Sensor and Actuators, B 70, pp.67-76, 2000.

[36] J.P. Colinge, Silicon-on-insulator technology: materials to VLSI, 2nd Ed., Kluwer Academic Publishers, The Netherlands, 1997, 272 pp.

[37] D.R. Walt, T. Dockinson, T. White, J. Kauer, S. Johnson, H. Engelhardt, J. Sutter, and P. Jurs, "Optical sensor arrays for odor recognition", Biosensors & Bioelectronics, 13, pp. 697-699.

[38] J. Homola, S.Y. Sinclair, and G. Gauglitz, "Surface plasmon resonance sensors: review", Sensors and Actuators, B54, pp. 3-15, 1999.

[39] T. Lang, H.-D. Wiemhöfer, W. Göpel, "Carbonate based CO_2 sensors with high performance", Sensors and Actuators, B 34, pp. 383-387, 1996.

[40] J.F. Currie, A. Essalik, and J.C. Marusic, "Micromachined thin solid state electrochemical CO_2, NO_2, SO_2 gas sensors", Sensors and Actuators, B 59, pp. 235-242, 1999.

[41] A. Accorsi, G. Delapierre, C. Vaucher, and D. Charlot, "A new microsensor for environmental monitoring", Sensors and Actuators, B 4,, pp. 539-543, 1991.

[42] M. Zanini, J.H. Visser, L. Rimai, R.E. Soltis, A. Kovalchuk, D.W. Hoffman, E.M. Logothetis, U. Bonne, L. Brewer, O.W. Bynum, and M.A. Richard, "Fabrication and properties of Si-based high-sensitivity microcalorimetric gas sensor", Sensors and Actuators, A 48, pp. 187-192, 1995.

[43] J. Lerchner, D. Caspary, and G. Wolf, "Calorimetric detection of volatile compounds", Sensors and Actuators, B 70, pp. 57-66, 2000.

[44] Ch. Ziegler, W. Göpel, H. Hämmerle, H. Hatt, G. Jung, L. Laxhuber, H.-L. Schimdt, S. Schütz, F. Vögtle, and A. Zell, "Bioelectronic noses: a status report. Part II", Biosensors & Bioelectronics, 13, pp. 539-571, 1998.

[45] J.W. Gardner and P.N. Bartlett, Pattern recognition in gas sensing, in Techniques and & mechanisms in gas sensing, Ed. by P.T. Moseley, S.O.W. Norris and D.E. Williams, The Adam Hilger series on sensors, Bristol (UK), 1991.

[46] D. Gnani, V. Guidi, M. Ferroni, G. Faglia, and G. Sberveglieri, "High-precision neural pre-processing for signal analysis of a sensor array", Sensors and Actuators, B 47, pp. 77-83, 1998.

[47] C. Di Natale, F. Davide, and A. D'Amico, "Pattern recognition in gas sensing: well-stated techniques and advances", Sensors and Actuators, B 23, pp. 111-118, 1995.

[48] M. Holmberg, F. Winquist, I. Lundström, J.W. Gardner, and E.L. Hines, "Identification of paper quality using a hybrid electronic nose", Sensors and Actuators, B 26-27, pp. 246-249, 1995.

[49] T.D. Gibson, O. Prosser, J.N. Hulbert, R.W. Marshall, P. Corcoran, P. Lowery, E.A. Ruck-Keene, and S. Heron, "Detection and simulataneous identification of microorganisms for headspace samples using an electronic nose", Sensors and Actuators, B 44, pp. 413-422, 1997.

[50] K. Esbensen, T. Midtgaard, and S. Schönkopf, Multivariate analysis in practice, Camo A/S, Trondheim, 1994.

[51] R.G. Brereton, Multivariate pattern recognition in chemometrics, Elsevier, Amsterdam, 1992.

[52] E. Kress-Rogers, Handbook of biosensors and electronic noses, CRC Press, Inc., Boca Raton (USA), 1997.

[53] T. Talou and B. Dubreuil, "E-NOSENET: State of the art on patents in electronic nose technology", Conf. Proc. of the of the 6th International Symposium on Olfaction and Electronic Nose, Tübingen, Germany, Sept. 1999, pp. 38-41.

[54] D.J. Strike, M.G.H. Meijerink, and M. Koudelka-Hep, “Electronic noses, a mini review”, Fresenius Journal of Analytical Chemistry, 364, pp. 499-505, 1999.

[55] E. Zubritsky, “E-noses keep an eye on the future”, Journal of Analytical Chemistry, 72 (11), pp. 421A-426A, 2000.

[56] H. Baltes, D. Lange, and A. Koll, “The electronic nose in Lilliput”, IEEE Spectrum, 35, pp. 35-38, 1998.

[57] F. Zee and J.W. Judy, “Micromachined polymer-based chemical gas sensor array”, Sensors and Actuators, B 72, pp. 120-128, 2001.

[58] A. Meckes, J. Behrens, O. Kayser, W. Benecke, Th. Becker, and G. Müller, “Microfluidic system for the integration and cyclic operation of gas sensors”, Sensors and Actuators, A 76, pp. 478-483, 1999.

[59] G. Frye-Mason, R. Kottenstette, P. Lewis, E. Heller, R. Manginell, D. Adkins, G. Dulleck, D. Martinez, D. Sasaki, C. Mowry, C. Matzke, and L. Anderson, “Hand-held miniature chemical analysis system (μChemLab) for detection of trace concentrations of gas phase analytes” Micro Total Analysis Systems 2000, Ed. by A. van den Berg et al., Kluwer Academic Publishers, The Netherlands, 2000.

[60] S.P. Murarka and M.C. Peckerar, Electronic materials: science and technology, Academic Press, Inc. (USA), 1989, 622 pp.

[61] M. Ohring, The material science of thin films, Academic Press, Inc. (USA), 1992, 704 pp.

[62] M. Madoue, Fundamentals of microfabrication, CRC Press, Boca Raton (USA), 1997, 589 pp.

[63] G.T.A. Kovacs, Micromachined transducers source book, WCB/McGraw-Hill (USA), 1998, 911 pp.

[64] M. Köhler, Etching in microsystem technology, Wiley-VCH, 1999, 368 pp.

[65] S.A. Campbell and H.J. Lewerenz, Semiconductor micromachining: vol. 1, Fundamentals of electrochemistry and physics, vol.2 Techniques and industrial applications, John Wiley & Sons, 1996.

[66] T.W. Harris, Chemical milling, Clarendon Press, Oxford (UK), 1976.

[67] H.R. Robbins and B. Schwartz, “Chemical etching of silicon –I. The system HF, HNO_3 and H_2O” Journal of the Electrochemical Society, 106, pp. 505-508, 1959.

[68] H.R. Robbins and B. Schwartz, “Chemical etching of silicon –II. The system HF, HNO_3, H_2O, and $HC_2C_3O_2$” Journal of the Electrochemical Society, 107, pp. 108-111, 1960.

[69] B. Schwartz and H.R. Robbins, “Chemical etching of silicon –III. A temperature study in the acid system”, Journal of the Electrochemical Society, 108, pp. 365-372, 1961.

[70] B. Schwartz and H.R. Robbins, “Chemical etching of silicon –IV. Etching technology”, Journal of the Electrochemical Society, 123, pp. 1903-1909, 1976.

[71] J.H. Foster and J.B. Singleton, “Beam-lead sealed junction integrated circuits” Bell Laboratory Records, 44, pp. 313-317, 1966.

[72] M.P. Lepselter, “Beam lead technology”, Bell Systems Technology Journal, 45, pp. 233-254, 1966.

[73] T.J. Rodgers, W.R. Hiltpold, D. Frederick, J.J. Barnes, F.B. Jenné, and J.D. Trotter, “VMOS memory technology”, IEEE Journal on Solid-State Circuits, vol. SC-12, pp. 515-523, 1977.

[74] T.J. Rodgers, W.R. Hiltpold, J.W. Zimmer, G. Marr, and J.D. Trotter, “VMOS ROM”, IEEE Journal Solid-State Circuits, vol. SC-11, pp. 614-622, 1976.

[75] E.S. Ammar and T.J. Rodger, “UMOS Transistors on (110) silicon”, IEEE Transactions on Electron Devices, ED-27, pp. 907-914, 1980.

[76] C.S. Smith, “Piezoresistance effect in germanium and silicon”, Physical Reviews, 94, pp. 42-49, 1954.

[77] W.G. Pfann, “Improvement of semiconducting devices by elastic strain”, Solid-State Electronics, 3, pp. 261-267, 1961.

[78] O.N. Tuffe, P.W. Chapman, and D. Lomg, “Silicon diffused-element piezoresistive diaphragms”, Journal of Applied Physics, 33, pp. 3322, 1962.

[79] K.E. Petersen, “Silicon as mechanical material”, Proceedings of the IEEE, 70, pp. 420-457. 1982.

[80] C. Kittel, Introduction to solid state physics, John Wiley & Sons, 1976.

[81] M. Alavi, S. Buttgenbach, A. Schumacher, and H.J. Wagner, “Fabrication of microchannels by laser machining and anisotropic etching of silicon”, Sensor and Actuators, A 32, pp. 299-302, 1992.

[82] E. Peeters, Process development for 3D silicon microstructures, with application to mechanical sensors design, Ph.D. Thesis, Catholic University of Louvain, Belgium, 1994.

[83] D.L. Kendall, “On etching very narrow grooves in silicon”, Applied Physics Letters, 26, pp. 195-198, 1975.

[84] D.L. Kendall, “Vertical etching of silicon at very high aspect ratios”, Ann. Rev. Mater. Sci., 9, pp. 373-403, 1979.

[85] A. Uhlir, “Electrolytic shaping of germanium and silicon”, Bell Systems Technology Journal, 35, pp. 333-347, 1956.

[86] H. Seidel, L. Csepregi, A. Heuberger, and H. Baumgartel, “Anisotropic etching of crystalline silicon in alkaline solutions- Part I. Orientation dependence and behavior of passivations layers”, Journal of the Electrochemical Society, 137, pp. 3612-3626, 1990.

[87] H. Seidel, L. Csepregi, A. Heuberger, and H. Baumgartel, “Anisotropic etching of crystalline silicon in alkaline solutions- Part II. Influence of dopants”, Journal of the Electrochemical Society, 137, pp. 3626-3632, 1990.

[88] D.B. Lee, “Anistropic etching of silicon”, Journal of Applied Physics, 40, pp. 4569-4574, 1969.

[89] K.E. Bean, R.L. Yeakley, and T.K. Powell, “Orientation dependent etching and deposition of silicon”, Journal of the Electrochemical Society, 121, pp. 87C, 1974.

[90] P.M. Zavracky, T. Earles, and N.L. Pokrovsky, “Fabrication of vertical sidewalls by anisotropic etching of silicon (100) wafers”, Journal of the Electrochemical Society, 141, pp. 3182-3188, 1994.

[91] K. Sato, M. Shikida, T. Yamashiro, M. Tsunekawa, and S. Ito, “Roughening of single-crystal silicon surface etched by KOH water solution”, Sensors and Actuators, A 73, pp. 122-130, 1999.

[92] R.M. Finne and D.L. Klein, "A water-amine-complexing agent system for etching silicon", Journal of the Electrochemical Society, 114, pp. 965-970, 1967.

[93] A. Reisman, M. Berkenbilt, S.A. Chan, F.B. Kaufman, and D.C. Green, "The controlled etching of silicon in catalysed ethylene-diamine-pyrocathechol-water solution", Journal of the Electrochemical Society", 126, pp. 1406-1414, 1979.

[94] M.J. Declercq, L. Gerzberg, and J.D. Meindl, "Optimization of the hydrazine-water solution for anisotropic etching of silicon in integrated circuit technology", Journal of the Electrochemical Society, 122, pp. 545-552, 1975.

[95] M. Mehregany and S.D. Senturia, "Anisotropic etching of silicon in hydrazine", Sensors and Actuators, 13, pp. 375-390, 1988.

[96] U. Schanakenberg, W. Benecke, and P. Lange, "TMAHW etchants for silicon micromachining", Tech. Digest of the 6th Int. Conf. Solid-State Sensors and Actuators (Transducers '91), San-Francisco (CA), USA, 1991, pp. 815-818.

[97] O. Tabata, R. Asahi, H. Funabashi, K. Shimaoka, and S. Sugiyama, "Anisotropic etching of silicon in T.M.A.H. solutions", Sensors and Actuators, A 34, pp. 51-57, 1992.

[98] A. Merlos, M. Acero,, M.H. Bao, and J. Esteve, "T.M.A.H./IPA anisotropic etching characteristics", Sensors and Actuators, A 37-38, pp. 737-743, 1993.

[99] K. Sato, M. Shikida, T. Yamashiro, K. Asaumi, Y. Iriye, and M. Yamamoto, "Anisotropic etching rates of single crytal silicon for TMAH water solution as a function of crystallographic orientation", Sensors and Actuators, A 73, pp. 131-137, 1999.

[100] R. Puers, "Mechanical silicon sensors at K.U. Leuven", Conf. Proc. Thermadag: SENSOREN, Rotterdam, Netherlands, 1991, pp. 1-8.

[101] C.A. Desmond, C.E. Hunt, and S.N. Farrens, "The effects of process-induced defects on the chemical selectivity of highly doped boron etch stops in silicon", Journal of the Electrochemical Society, 141, pp. 178-184, 1994.

[102] S.D. Collins, "Etch stop techniques for micromachining", Journal of the Electrochemical Society, 144, pp. 2242-2262, 1997.

[103] B. Kloeck, S.D. Collins, N.F. de Rooij, and R.L. Smith, “Study of electrochemical etch-stop for high-precision thickness control of silicon membranes”, IEEE Transactions on Electron Devices, 36, pp. 663-669, 1989.

[104] R. Buser, and N.F. de Rooij, Monolitisches Kraftsensorfeld, VDI Berichte Nr. 667, Sensoren, Technologien und Anwendung, 1988, pp. 115-118.

[105] B. Puers, and W. Sansen, “Compensation structures for convex corner micromachining in silicon”, Sensors and Actuaotors, A 21-23, pp. 1036-1041, 1990.

[106] G.K. Mayer, H.L. Offereins, H. Sandmaier, and K. Kühl, “Fabrication of non-underetched convex corners in anisotropic etching of (100)-silicon in aqueous KOH with respect to novel micromechanics elements”, Journal of the Electrochemical Society, 137, pp. 3947-3951, 1990.

[107] P.W. Barth, P.J. Shlichta, and J.B. Angel, “Deep narrow vertical-walled shafts in <110> silicon” Conf. Proc. 3rd Int. Conf. Solid-State Sensors and Actuators, Philadelphia (PA), 1985, pp. 371-373.

[108] X. Li, M. Bao, and S. Shen, “Maskless etching of three-dimensional structures in KOH”, Sensors and Actuators, A 57, pp. 47-52, 1996.

[109] M. Bao, X. Li, S. Shen, and H. Chen, “A novel micromachining technology for multilevel structures of silicon”, Sensors and Actuators, A 63, pp. 217-221, 1997.

[110] I. Zubel, “Silicon anisotropic etching in alkaline solutions III: On the possibility of spatial structures forming in the course of Si(100) anisotropic etching in KOH and KOH + IPA solutions”, Sensors and Actuators, A 84, pp. 116-125, 2000.

[111] J.B. Price, “Anisotropic etching of silicon with KOH-H_20- Isopropyl alcohol”, Semiconductor Silicon 1973, Chicago (IL), USA, 1973, pp. 339-353.

[112] O.J. Glembocki, R.E. Stahlbush, and M. Tomkiewicz, “Bias-dependent etching of silicon in aqueous KOH”, Journal of the Electrochemical Society, 132, pp. 145-151, 1985.

[113] M. Elwenspoek, “On the mechanism of anisotropic etching of silicon”, Journal of the Electrochemical Society, 140, pp. 2075-2080, 1993.

[114] F. Laermer, A. Schilp, K. Funk, and M. Offenberg, "Bosch deep silicon etching: Improvements uniformity and etch rate for advanced MEMS applications", Conf. Proc. 12th IEEE Int. Conf. On Micro-Electro-Mechanical Systems, Orlando (FL), (USA), 1999, pp. 211-216.

[115] J. Bhardwaj, H. Ashraf, and A. McQuarrie, "Dry silicon etching for MEMS", Conf. Proc. of the 191st Meeting of the Electrochemical Society, Microstructures and Microfabricated Systems III Symposium", Montréal (PQ), Canada, 1997, vol 97-5, pp. 118-130.

[116] F. Larmer and A. Schilp, "Method of anisotropically etching silicon", US-Patent No. 5501893.

[117] M. Esahi, M. Takinami, Y. Wakabayashi, and K. Minami, "High-rate directional deep dry etching for bulk silicon micromachining", Journal of Micromechanics and Microengineering, 5, pp. 5-10, 1995.

[118] M. Biebl and H. von Philipsborn, Fracture and strength of doped and undoped panical filters, Ph.D. Thesis, UC Berkeley, 1993.

[119] S. Greek, F. Ericson, S. Johansson, and J.-A. Schweitz, "In-situ tensile strength measurement of thick-film and thin-film micromachined structures", Conf. Proc 8th Int. Conf. Solid-State Sensors and Actuators (Transducers 1995), Stockholm, Sweden, 1995, pp. 56-59.

[120] M. Le Berre, P. Kleimann, D. Semmache, D. Barbier, and P. Pinard, "Electrical and piezoresian", McWhorter, Eds., Smart Electronics and MEMS, Proc. of the Smart Structures and Materials 1996 Meeting, vol. 2722, SPIE, San Diego (CA), USA, 1996.

[121] C. Linder, L. Paratte, M.-A. Grétillat, V.P. Jaecklin and N.F. de Rooij, " Surface micromachining", Journal of Micromechanics and Microengineering, 2, pp. 122-132, 1992.

[122] P.J. French, "Development of surface micromachining techniques compatible with on-chip electronics", Journal of Micromechanics and Microengineering, 6, pp. 197-211, 1996.

[123] J. Bühler, F-P Steiner, and H. Baltes, “Silicon dioxide sacrificial layer etching in surface micromachining”, Journal of Micromechanics and Microengineering, 7, R1-R13, 1997.

[124] J.M. Bustillo, R.T. Howe, and R.S. Muller, “Surface micromachining for Microelectrochemical systems”, Proc. of the IEEE, vol. 86. no. 8. 1998.

[125] H.C. Nathanson, W.E. Newell, R.A. Wickstrom, and J.R. Davis, “The resonant gate transistor”, IEEE Transactions on Electron Devices, ED-14, pp. 117-133, 1967.

[126] B. Dutta, “Integrated micromotor concepts”. Conf. Proc. of Int. Conf. On Microelectronics Circuits and Systems Theory, Sydney, Australia, 1970, pp.36-37.

[127] R.T. Howe and R.S. Muller, “Polycrystalline silicon micromechanical beams” Spring Meeting of the Electrochemical Society, Montréal (PQ), Canada, 1982, pp. 184-185.

[128] H. Guckel and D.W. Burns, “A technology for integrated transducers”, Conf. Proc. Int. Conf. Solid-State Sensors and Actuators, Philadelphia (PA), USA, 1985, pp. 90-92.

[129] R.T. Howe, “Recent advances in surface micromachining” Tech. Digest 13th Sensor Symposium, Tokyo, Japan, 1995, pp. 1-8.

[130] K. Gabrial, J. Jarvis, and W. Trimmer, “Small machines, large opportunites: A report on the Emerging Field of Microdynamics”, National Science Foundation, 1989.

[131] Editor, “Analog devices combines micromachining with BICMOS”, Semiconductor Internaltional, 14, pp. 17, 1991.

[132] L.J. Hornbeck, “Projection displays and MEMS: Timely convergence for bright future”, Micro-machining and Microfabrication Process Technology, (Proceedings of SPIE), Austin (TX), USA, 1995, pp. 2.

[133] R.T. Howe and R.S. Muller, “Polycrystalline silicon mechanical beams”, Journal of the Electrochemical Society, 130, pp. 1420-1423, 1983.

[134] R.T. Howe, Polycrystalline silicon structures, in Micromachining and Micropackaging of Transducers, Eds. by C.D Fung, P.W. Cheung, W.H. Ko, and D.G. Fleming, Elsevier, NY, USA, 1985, pp. 169-187.

[135] W. Yun, A surface micromachined accelerometer with integrated CMOS detection circuitry, Ph.D. Thesis, U.C. Berkeley, 1992.

[136] A.C. Adams, Dielectric and polysilicon film deposition, in VLSI Technology, Ed. by S.M. Sze, McGraw-Hill, 1988, pp. 233-271.

[137] N. Taguchi, Japanese Patent 45-38200.

[138] N. Taguchi, Japanese Patent 47-38840.

[139] N. Taguchi, US Patent 3 644 795.

[140] Figaro Products Catalogue, Figaro gas sensors 2000-series, Figaro Engineering Inc., European Office, Oststrasse 10, 40211 Düsseldorf, Germany.

[141] FIS, Product list (Specifications: Sb/sp series), FIS Inc. (May 1999).

[142] UST, Product Information (1999), Umweltsensortechnik GmbH, Gewerbegebiet Geschwenda Süd 3, 98716, Geschwenda, Germany.

[143] S. Fung, Z. Tang, P. Chan, J. Sin, and P. Cheung, "Thermal analysis and design of a micro-hotplate for integrated gas-sensor applications", Sensors and Actuators, A 54, pp. 482-487, 1996.

[144] G. Sberveglieri, W. Hellmich, and G. Müller, "Silicon hotplates for metal oxide gas sensors elements", Microsystem Technologies, 3, pp. 183-190, 1997.

[145] J. Gardner, A. Pike, N.F. de Rooij, M. Koudelka-Hep, P.-A. Clerc, A. Hierlemann, and W. Göpel, "Integrated array sensor for detecting organic solvents", Sensors and Actuators, B 26-27, pp. 135-139, 1995.

[146] A. Götz, I. Gràcia, C. Cané, E. Lora-Tamayo, M. Horillo, G. Getino, C. Gràcia, and J. Gutiérrez, "A micromachined solid state integrated gas sensor for detection of aromatic hydrocarbons", Sensors and Actuators, B 44, pp. 483-487, 1997.

[147] D. Briand, O. Guenat, B. van der Schoot, T. Hirata, and N.F. de Rooij, "Micro-hotplate, a useful concept for gas-sensing, fluidics and space applications", Conf. Proc. of Microfabricated Systems and MEMS V, 198th ECS Meeting, 2000, pp. 151-158.

[148] R.J. Reay, E.H. Klaassen, and G.T.A. Kovacs, “Thermally and electrically isolated single crystal silicon structures in CMOS technology”, IEEE Electron Device Letters, 15, pp. 399-401, 1994.

[149] C. Rossi, D. Estève, and C. Mingues, “Pyrotechnic actuator: a new generation of Si integrated actuator”, Sensors and Actuators, A 74, pp. 211-215, 1999.

[150] A.P. Lee and B.J. Reedy, “Temperature modulation in semiconductor gas sensing”, Sensors and Actuators, B 60, pp. 35-42, 1999.

[151] D.-D. Lee, W.-Y. Chung, M.-S. Choi, and J.M. Baek, “Low-power micro gas sensor”, Sensors and Actuators, B 33, pp. 147-150, 1996.

[152] P. Maccagnani, R. Angelucci, P. Pozzi, L. Dori, A. Parisini, M. Bianconi, and G. Benedetto, “Thick porous silicon thermo-insulating membranes”, Sensors and Materials, 11, pp. 131-147, 1999.

[153] S. Astié, A. Gué, E. Schied, L. Lescouzères, and A. Cassagnes, “Optimization of an integrated SnO_2 gas sensor using a FEM simulator”, Sensors and Actuators, A 69, pp. 205-211, 1998.

[154] M. Dumitrescu, C. Cobianu, D. Lungu, D. Dascalu, A. Pascu, S. Kolev, and A. van den Berg, “Thermal simulation of surface micromachined polysilicon hotplates of low power consumption”, Sensors and Actuators, A 76, pp. 51-56, 1999.

[155] M. von Arx, O. Paul, and H. Baltes, “Process-dependent thin-film thermal conductivities for thermal CMOS MEMS”, Journal of Microelectromechanical Systems, 9, pp. 136-145, 2000.

[156] M. Sekimoto, H. Yoshhara, and T. Ohkubo, “Silicon nitride single-layer x-ray mask”, Journal of Vacuum Science Technology, 21, pp.1017-1021, 1982.

[157] C.H. Mastrangelo, Y.-C. Tai, and R.S. Muller, “Thermophysical properties of low-residual stress, silicon-rich, LPCVD silicon nitride films”, Sensors and Actuators, A 21-23, pp. 856-860, 1990.

[158] S. Wessel, M. Parameswaran, S.R. Morrison, and R.F. Frindt, “A CMOS thermally isolated heater structure as a substrate for semiconductor gas sensors”, Microelectronics Journal, 23, pp. 451-456, 1992.

[159] J.S. Suehle, R.E. Cavicchi, M. Gaitan, and S. Semancik, "Tin oxide gas sensor fabricated using CMOS micro-hotplates and in-situ porcessing", IEEE Electron Device Letters, 14, pp. 118-120, 1993.

[160] L. Sheng, Z. Tang, J. Wu, P.C.H: Chan, and J.K.O. Sin, "A low-power CMOS compatible integrated gas sensor using maskless tin oxide sputtering", Sensors and Actuators, B 49, pp. 81-87, 1998.

[161] C. Düsco, E. Vàzsonyi, M .Adám, I. Szabó, I. Bársony, J. Gardeniers, and A. van den Berg, "Porous silicon bulk micromachining for thermally isolated membrane formation", Sensors and Actuators, A 60, pp. 235-239, 1997.

[162] F. Solzbacher, C. Imawan, H. Steffes, E. Obermeier, and H. Möller, "A modular system of SiC-based microhotplates for the application in metal oxide gas sensors", Sensors and Actuators, B 64, pp. 95-101, 2000.

[163] P. Mardilovich, D. Routkevitch, and A. Govyadinov, "Hybrid micromachining and surface microstructuring of alumina surface", Conf. Proc. of Microfabricated Systems and MEMS V, 198th ECS Meeting, 2000, pp. 33-42.

[164] P.C.H. Chan, G.-z. Yan, L.-y- Sheng, R.K. Sharma, Z. Tang, J.K.P. Sin, I.-M. Hsing, and Y. Wang, "An integrated gas sensor technology using surface micromachining", Conf. Proc. of 14th IEEE Int. Conf. on Micro-Electro-Mechanical Systems (MEMS'01), Interlaken, Switzerland, 2001, pp. 543-546.

[165] W.-Y. Chung, J.-W. Lim, D.-D- Lee, N. Miura, and N. Yamazoe, "Thermal and gas-sensing properties of planar-type micro gas sensor", Sensors and Actuators, B 64, pp. 118-123, 2000.

[166] S. Majoo, J.L. Gland, K.D. Wise, and J.W. Schwank, "A silicon micromachined conductometric gas sensor with a maskless Pt sensing film deposited by selected-area CVD", Sensors and Actuators, B 35-36, pp. 312-319, 1996.

[167] Z. Tang, S.K.H. Fung, D.T.W. Wong, P.C.H. Chan, J.K.O. Sin, P.W. Cheung, "An integrated gas sensor based tin oxide thin-film and improved micro-hotplate", Sensors and Actuators, B 46, pp. 174-179, 1998.

[168] C. Rossi, P. Temple-Boyer, and D. Estève, “Realization and performance of thin SiO_2/SiN_x membrane for microheater applications”, Sensors and Actuators, A 64, pp. 241-245, 1998.

[169] A. Götz, I. Gràcia, C. Cané, and E. Lora-Tamayo, “Thermal and mechanical aspects for designing micromachined low-power gas sensors”, Journal of Micromechanics and Microengineering, 7, pp. 247-249, 1997.

[170] N.R. Swart and A. Nathan, “Reliability study of polysilicon microhotplates”, Conf. Proc. Solid-State Sensor and Actuator Workshop, Hilton Head, South Carolina, USA, 1994, pp. 119-122.

[171] O. Grudin, R. Marinescu, L. Landsberger, D. Cheeke, and M. Kahrizi, “Microstructure release and test techniques for high temperature micro hotplate”, Conf. Proc. of the IEEE Canadian Conference on Electrical an Computer Engineering, Edmonton (Alberta), Canada, 1999, pp. 1610-1615.

[172] P. Hille and H. Stack, “A heated membrane for a capacitive gas sensor”, Sensors and Actuators, A 32, pp. 321-325, 1992.

[173] C. Saul and J. Zemel, “Diode-based microfabricated hot-plate sensor”, Sensors and Actuators, A 65, pp. 128-135, 1998.

[174] M. Hausner, J. Zacheja, and J. Binder, “Multi-electrode substrate for selectivity enhancement in air monitoring”, Sensors and Actuators, B 43, pp. 11-17, 1997.

[175] S. Semancik and R.E. Cavicchi, “Kinetically controlled chemical sensing using micromachined structures”, Accounts of Chemical Research, 31, pp. 279-287, 1997.

[176] H. Baehr and K. Stephan, Wärme- und Stoffübertragung, 3rd Edition, Springer, 1998.

[177] A. Van Herwaarden and G. Meijer, Thermal sensors, in S.M. Sze (Ed.) Semiconductor Sensors, John Wiley & Sons Inc, 1994, pp. 331-382.

[178] U. Grigull and H. Sandner, Wärmerleitung, Springer Verlag, 1979.

[179] S. Möller, J. Lin, and E. Obermeier, “Material and design considerations for low-power microheater modules for gas-sensor applications”, Sensors and Actuators, B 24-25, pp. 343-346, 1995.

[180] R. Aigner, M. Dietl, R. Katterloher, and V. Klee, “Si-planar-pellistor: design for temperature modulated operation”, Sensors and Actuators, B 33, pp. 151-155, 1996.

[181] V. Guidi, G. Cardinali, L. Dori, G. Faglia, M. Ferroni, G. Martinelli, P. Nelli, and G. Sberveglieri, “ Thin-film gas sensor implemented on a low-power consumption micromachined silicon structure”, Sensors and Actuators, B 49, pp. 88-92, 1998.

[182] G. Meijer and A. van Herwaarden, Thermal Sensors, Sensors Series, Institute of Physics, Publishing Bristol and Philadelphia, 1994.

[183] C. Mastrangelo and W. Tang, Semiconductor sensor technologies, in S.M. Sze (Ed.) Semiconductor Sensors. John Wiley & Sons Inc, 1994, pp. 17-95.

[184] H. Low, M. Tse, and M. Chiu, “Thermal induced stress on the membrane in intergrated gas sensor with micro-heater”, Conf. Proc. 1998 IEEE Honk-Kong Electron Devices Meeting, 1990, pp. 140-143.

[185] J. Bosc, Y. Guo, V. Sarihan, and T. Lee, “Accelerated life testing for micro-machined chemical sensors”, IEEE Transactions on Reliability, 47, pp. 135-141, 1998.

Summary of papers

In this work, the power consumption of metal-oxide and MOSFET gas sensors was lowered using a combination of thin film and micromachining processes. Devices with improved thermal and gas sensing properties were designed, fabricated and simulated. The published articles and manuscripts that have emerged from the results of the experimental work are compiled in the upcoming papers. The following paragraphs summarise the topics covered by the papers, as well as their contributions to the field.

Paper I. Design and fabrication of high temperature micro-hotplates for drop-coated gas sensors

The first paper deals with the design and fabrication of micro-hotplates for drop-coated metal-oxide gas sensors for high temperature operation. Different dimensions, geometries and materials were investigated with the aim of lowering power consumption, improving temperature distribution and withstanding operation at high temperature. Micro-hotplates which could withstand annealing temperatures and temperature-pulsed modes of operation up to 700°C were demonstrated. Regarding the fabrication, deep reactive ion etching of silicon was used to increase the integration density, and a silicon island was added underneath the membrane to obtain a homogeneous temperature distribution over the sensing area.

Paper II. Thermally isolated MOSFET for gas sensing application

The concept of a micro-hotplate having a silicon island presented in the previous paper was used to thermally isolate MOSFETs for gas sensing applications. An implanted resistor and a diode, used respectively as heater and temperature sensor, and 4 MOSFETs were integrated on a micro-hotplate. The thermal efficiency of the device was 2°C/mW, with a thermal constant less than 100 ms. This low-thermal mass device allowed the operation of the sensors in a pulsed or cycled temperature mode, and the monitoring of the field and thermal effects in the presence of sample gases.

Paper III. A low-power micromachined MOSFET gas sensor

This paper is an extension of the communication presented in paper II. More details are given about how the combination of microelectronics and MEMS (silicon micromachining) processing technologies was used to fabricate the sensor.

Paper IV. New modes of operation for MOSFET gas sensors using low-power devices

The pulsed and modulated modes of operation for MOSFET gas sensors were investigated using the low-power, micromachined MOSFET device. Cycling the temperature during gas exposure modified the kinetics of the gas reactions with the sensing film. The way in which sensor response was modified

depended on the nature of the analyte gas and the catalytic sensing film. Pulsing the temperature higher after gas exposure was found to reduce the recovery time in specific applications. It was also possible to discriminate between gases in a gas mixture by using a sinusoidal-type of temperature modulation. Perspectives on new modes of operation are also presented. Silicon-on-insulator (SOI) technology is introduced as a good candidate to both reduce the power consumption of MOSFET sensors and to increase their operating temperature.

Paper V. Thermal optimisation of micro-hotplates having a silicon island

Thermal measurements and finite-element-modelling (FEM) were performed with the aim of optimising the power consumption and temperature distribution of micro-hotplates for metal-oxide and MOSFET gas sensors. The work concentrated mainly on micro-hotplates having a silicon island underneath the sensing area. The thickness of the silicon island was optimised to lower the power consumption of the devices and still maintain a homogeneous temperature distribution over the sensing area. The thermal conductivity of the silicon and the dielectric membrane, the operating temperature, the geometry and area of the heater, and the processing of the silicon island were considered in the optimisation process.

Paper I

DESIGN AND FABRICATION OF HIGH TEMPERATURE MICRO-HOTPLATES FOR DROP-COATED GAS SENSORS

Danick Briand[1], Andreas Krauss[2], Bart van der Schoot[1], Udo Weimar[2], Nicolae Barsan[2], Wolfgang Göpel[2], and Nicolaas F. de Rooij[1]

[1]Institute of Microtechnology, University of Neuchâtel, Rue Jaquet-Droz 1, P.O. Box 3, CH-2007 Neuchâtel, Switzerland

[2]Institute of Physical Chemistry, University of Tübingen, Auf der Morgenstelle 6, 72076 Tübingen, Germany

ABSTRACT

This paper reports on the optimisation of micromachined hotplates for gas-sensing applications designed to withstand high temperature coating processes and modes of operation. Different thin film materials, geometry and dimensions have been investigated regarding to their power consumption, their temperature distribution over the sensing area and their robustness when annealed at high temperature. In comparison with oxide films, the micro-hotplates made of nitride were the most robust. They withstood annealing temperatures up to 700°C and a pulsed temperature mode of operation. Their robustness allowed the sensing area be heated up to a high temperature (550-700°C). These micro-hotplates are therefore suitable for the annealing "on-chip" of the gas-sensitive materials deposited in a drop coating procedure. Sensors coated with a Pd-doped tin oxide drop and annealed using the

Published in Sensors and Actuators, B 68, pp. 223-233, 2000

integrated heater have been tested under different concentrations of CO and CH_4 in air.

1.1 INTRODUCTION

Micro-hotplates have a tremendous importance in the field of high-temperature gas-sensing devices (e.g. metal oxide) since they allow the reduction of the sensor power consumption and the use of new modes of operation such as temperature cycling due to their low thermal mass [1-6]. SnO_2-based nanocrystalline thick film deposited on micromachined hotplates have been investigated during the past years at the Institute of Physical Chemistry (IPC), University of Tübingen, Tübingen, Germany as a combination of thick film and thin film technology for gas detection [6,7]. Thick film technology is well established in the field of the gas-sensitive materials. Moreover the use of micro-hotplates as substrate makes this technology suitable for markets where low-power consumption, low-cost and reliable devices are needed, such as in the portable instruments and in the automotive industry.

The micro-hotplates previously fabricated at the Institute of Microtechnology (IMT), University of Neuchâtel, Neuchâtel, Switzerland, could be annealed at temperatures not higher than 550°C and were unsuitable for long-term operation in a pulsed temperature mode [7,8]. The adhesion of the coating and the stability of the sensors were limited by the lack of robustness of the devices at very high temperature. In this communication, we report on the design, fabrication and characterisation of micro-hotplates, used in a drop-

coating procedure of the gas sensitive materials, with the aim of improving their performance at high temperatures.

The design has been supported using thermal finite element modeling (FEM) simulations (MEMCAD software from Microcosm Technologies Inc.) [9]. The micro-hotplates are made using backside bulk micromachining of silicon. The annealing of chemically vapor deposited (CVD) oxide films (to obtain a low-stress film), the adding of a localised silicon island underneath the membrane and the use of deep reactive ion etching (DRIE) to release the membrane have been investigated. Micro-hotplates having an improved temperature distribution over the sensing area and a higher density of integration are presented. The optimised devices withstand high annealing temperatures (700°C) and a pulsed temperature mode of operation.

Moreover, they allow the annealing "on chip" of the coating material, which was not possible before. The annealing "on chip" of the coating is very interesting for device packaging, as it will be discussed in the following pages. The first results concerning the gas sensitivities (CO, CH_4, %RH) of a Pd-doped tin oxide film annealed "on chip" are also reported.

1.2 DESIGN

1.2.1 Power consumption and robustness

In the aim of reducing the gas sensors power consumption, the micro-hotplates were made using backside silicon micromachining in KOH to release a thin dielectric membrane (Fig. 1.1). The membrane thermally isolated the heated sensing area from the silicon chip frame.

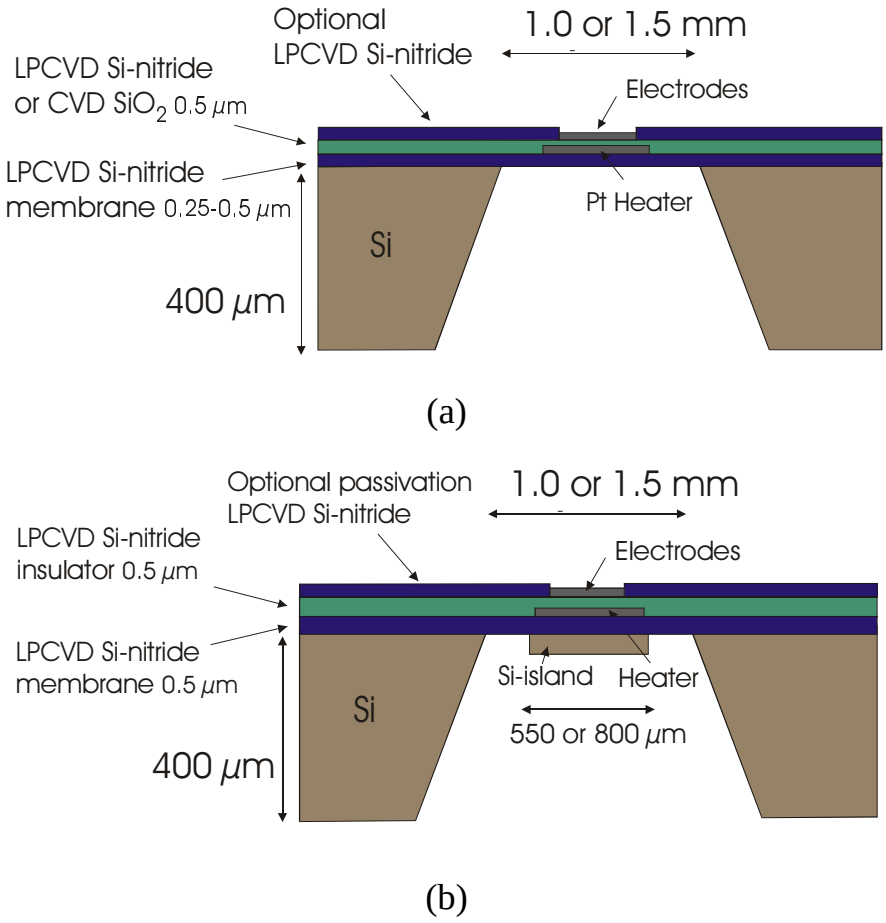

Figure 1.1. Micro-hotplates schematic without (a) and with (b) Si-island.

The micro-hotplates were made up of a heater stacked between a membrane and an insulator, on which the interdigited electrodes (IDE 5-50 μm) were laid. The membrane sizes investigated were 1.0 × 1.0 and 1.5 × 1.5 mm^2. The heater and electrode areas were respectively 500 × 500 μm^2 and 750 × 750 μm^2. These dimensions have been chosen with regard to the results of previous works reported in the literature concerning the decrease of micro-hotplate power consumption [2,10-12] and were limited by the minimum droplets size (400 × 400 μm^2) used in the coating procedure of the gas-sensitive material.

Different thin film materials of varying thickness have been investigated to improve robustness (Fig. 1.1). The membrane was made up of a low-stress LPCVD silicon nitride with a film thickness between 0.25 and 0.5 μm. Platinum (250 nm) with an adhesive layer of tantalum (20 nm) was used for the heater (≅ 150-190 Ω at RT, TCR = 0.0020/°C) and the electrodes (150 nm). The insulation layer consisted of a low-stress LPCVD silicon nitride or an annealed CVD oxide film (0.5 μm). Annealing of the CVD oxide films was performed to stabilise their microstructures at a high temperature with a residual tensile stress. The passivation layer consisted of a low-stress LPCVD nitride (0.2 μm). PECVD silicon nitride thin films were avoided. From our previous experiences, they were not suitable for annealing and operating at a temperature higher than 500-550°C [7].

1.2.2 Temperature distribution

The temperature distribution was optimised by studying different heater geometry such as simple and double meander. On a series of devices, a ≅ 10-μm-thick silicon island was added underneath the membrane (Fig. 1.1b) to improve the homogeneity of the temperature distribution on the sensing area, which was confirmed by using FEM simulation [9].

1.2.3 Density of integration

Holes having vertical walls can be etched by DRIE of silicon. Using this technology to release the membranes, the densities of the devices fabricated were increased compared to using wet anisotropic etching of silicon. DRIE also gives more flexibility in the design of the device in such a way that the

crystal planes of the silicon wafer do not restrict the geometry of the membrane. Moreover, no protection of the wafer frontside was needed during the silicon etching if the gas-sensitive material was deposited prior to the silicon micromachining.

1.3 TECHNOLOGY

1.3.1 Micro-hotplates fabrication

The standard fabrication process was as follows. The starting material was a (100) double-sided polished silicon wafer with a thickness of 400 μm. A thermal oxide of 50 nm was grown in the case where the hotplates were made by wet chemical etching of silicon. The 0.25–0.5-μm-thick membrane film (LPCVD nitride) was then deposited and followed by the lift-off of platinum (0.25 μm) to make the heater. The heater was covered up with a 0.5-μm-thick insulation layer (LPCVD nitride or annealed CVD oxide). After the opening of the contact areas, the Pt electrodes (0.15 μm) were patterned by lift-off and the devices were covered by an LPCVD nitride passivation film (0.15 μm). The latter protects both sides of the wafer during the silicon etching in KOH (40%, 60°C). Once the membrane was released in KOH, the wafer was dipped in BHF to totally remove the oxide underneath the membrane. Then, the passivation film was completely or partially (on the sensing area and the pads) removed by RIE depending on the application. Finally, the wafers were covered with resist and then diced. The dicing procedure did not affect either the fabrication yield or the performance of the devices.

The silicon oxide film used as insulation between the heater and the electrodes were deposited at 400°C by APCVD. After deposition, the films were densified (15 min : 625°C/N_2) and showed a remaining stress of about 215 MPa (TENCOR instrument). Subsequent annealing of the CVD oxide films at 625° (up to 1 h) and at 800°C (15 min–1 h) were performed to stabilise them before the following processes done at higher temperatures: the LPCVD at 800°C and the drop coating at 700°C. The annealing temperatures chosen were compatible with the standard fabrication processes used at IMT. In this way, it was possible to vary the stress in the layer between 250 MPa to 5 MPA (625°C : 1h; 800°C : 1h). CVD oxide films with three different stresses of about 5, 75 and 165 MPa were used as insulator in the micro-hotplates fabrication (see results in Table 1.1.).

Table 1.1. Stress in annealed CVD oxide films.

CVD silicon dioxide anneals (530 nm)	Stress before annealing	Stress after annealing
Anneal a : 625°C 15 min	250 MPa	213 MPa
Anneal b : 625°C 1 h	250 MPa	167 MPa
Anneal c : 625°C 1 h + 800°C 15 min	250 MPa	76 MPa
Anneal d : 625°C 1 h + 800°C 1 h	250 MPa	7 MPa
Anneal e : 625°C 1 h + 800°C 4 h	250 MPa	-85 MPa

Variations in the processing were either the DRIE of silicon or the fabrication of a silicon island underneath the membrane using two etching steps in KOH. With respect to the DRIE of silicon, the passivation nitride film was not necessarily on the wafer frontside. A photoresist film (AZ-4562) was used to

protect the wafer backside during the silicon etching. The thermal oxide, 300 nm thick for this process, acts as the membranes' etch stop.

In the case where there is a silicon island remaining under the membrane, the island is made with two successive KOH etching steps using different masking, instead of a heavy boron implantation (etch stop) as presented in Ref. [13]. The process is similar to the one used at IMT to thermally isolate GasFETs (Gas-sensitive FETs) from the silicon chip frame [14] and is presented in Figure 1.2.

Firstly, 10 μm of silicon was etched in KOH (40%, 60°C) to define the silicon island that was protected by the thermal oxide film. The LPCVD Si-nitride film served to protectt the surrounding silicon (Fig. 1.2a). Secondly, after removing the oxide mask in BHF, the silicon was etched in 52% KOH (60°C) all over the window opened in the silicon nitride (Fig. 1.2b). The silicon island formed during the first etching step is then vertically and horizontally etched respectively along the <100> and <311> cristallographic axes, respectively [15]. Therefore, a concentration of 52% of KOH was used to perform the second silicon etching to decrease the (311) planes' etch rate to obtain the desired island width (covering the sensing area). Since the lateral planes (311) forming the silicon island sides have a higher etch rate than the planes appearing at the corners (410), no compensation structures were needed [15] (Fig. 1.2a). The process ended when the membrane was reached. Time was critical since there was no etch stop to preserve the silicon island thickness.

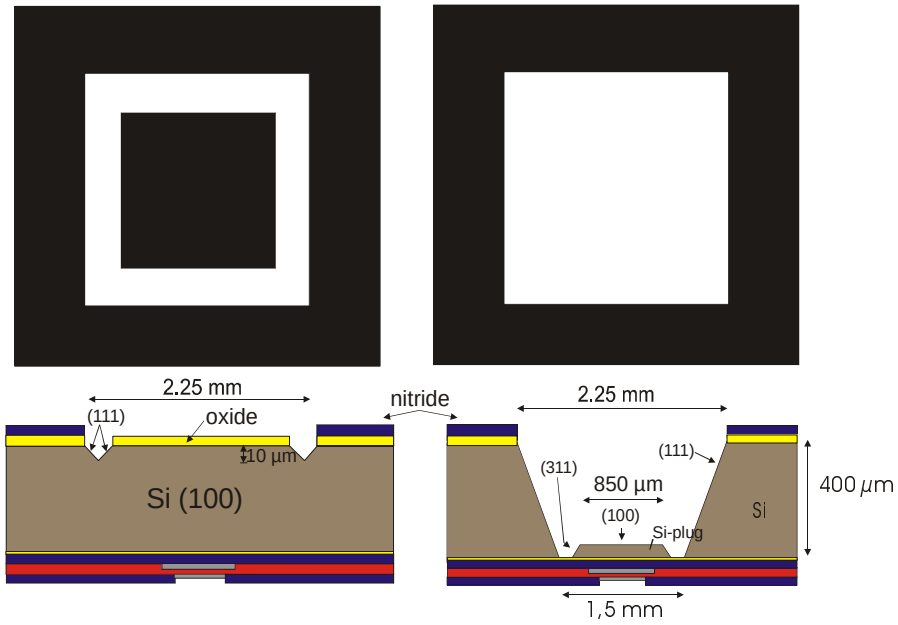

Figure 1.2. Fabrication process of the silicon island using wet anisotropic etching of silicon with two masks: (a) with an oxide mask to define the 10 µm thick silicon island in 40% KOH, (b) with the oxide remove to release the membrane in 52% KOH.

1.3.2 Drop coated gas sensor fabrication

The annealing of the drop gas-sensitive coating can be performed in a belt oven or “on chip” using the integrated heater. In the case where a belt oven was used, the hotplates were first cleaned (acetone/isopropanol) and then coated. A reproducible drop of coating material with a diameter between 400 and 700 µm depending on the film preparation and the hotplate diameter was added using a drop-coating method. More information about the preparation of the sensitive material can be found in Refs [16,17]. The chip was then annealed up to 700°C (10–20 min). The typical resistance of the coated device

was between 1 kΩ to 10 MΩ. Differences in value depend on the doping (e.g. Pt, Pd, undoped) and on the electrodes gaps.

The chips were mounted in a TO-5 package. The devices were glued using the conductive glue (No. CW2200MTP from Chemtronics, USA). All the contacts of the device (two sensor and two heater contacts) are connected to the four-pin TO-5 socket using a glue drop for each connection. The glue fixes the dice mechanically and provides the electrical connections. Figure 1.3 shows a micro-hotplate mounted in a packaging and coated with tin oxide.

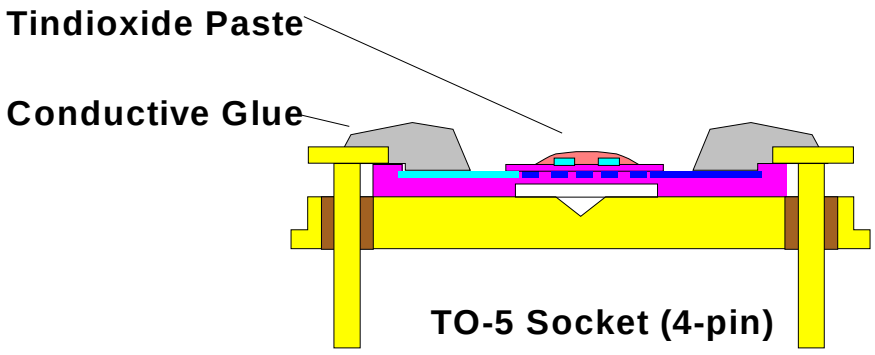

Figure 1.3. Schematic cross-section view of a packaged sensor.

In the case of the annealing “on chip” of the drop-coated films, the micro-hotplates were packaged before the annealing. The packaging and the coating were performed using the procedures explained before. Micro-hotplates having a 1.5 × 1.5-mm^2 membrane (0.5 μm) and an insulation (0.5 μm) film made up of low-stress LPCVD were used due to their high robustness. Four sensors (S1, S2, S3, S4) with interdigited electrodes (50 μm) were coated with a spot of 2% Pd-doped nanocrystalline tin dioxide material (diameter of about 400 μm). The annealing “on chip” was performed with a heater (190 Ω) voltage of 6 (S0), 7 (S1, S2) and 8 V (S3, S4). The annealing time was 10 s for

S1 and S3 and 10 min for S0, S2 and S4. The shortest time was selected to test another annealing condition, which would be compatible with a later manufacturing process, and the other to have one sensor processed similar to a belt oven-annealing procedure. The power consumption during the annealing at 7 V and 8 V were about 115 mW and 160 mW and corresponded to a temperature of about 500°C and 600°C, respectively.

1.4 CHARACTERISATION AND RESULTS

1.4.1 Micro-hotplates: robustness, power consumption and temperature distribution

The micro-hotplates mechanical properties were characterised, from the yield and robustness to the pulsed temperature operation and high annealing temperatures. The fabrication yield is considered as the percentage of micro-hotplates with their membranes not broken during the fabrication process. The Si-nitride micro-hotplates have higher fabrication yield (98–100%). Concerning the micro-hotplates with a CVD oxide film as insulation layer, the passivation layer has to be partially removed on the sensing area after the etching in KOH to increase their yield and their robustness. Annealing of the oxide film at 625°C: 1h or 600°C: 1h + 800°C: 15 min (stress of ≅ 165 MPa and 75 MPa) provides the highest fabrication yield (90–95%) and mechanical robustness. CVD oxide films annealed successively at 625°C: 1h and 800°C: 1h with no nitride passivation film remaining gave the lowest results with a yield of about 40%.

Switching (100 cycles) of the heater voltage (0–9.5 V / ≅700°C) has shown that nitride micro-hotplates are very robust (none broke of the 16 tested). Nitride / oxide micro-hotplates are less robust (at 9.5 V, three broke of the 14 tested). Both designs were also able to stand the annealing process used in a drop-coating process of the gas-sensitive element: 350°C: 4 min; 550°C: 8 min; 700°C: 10–20 min; 550°C: 8 min; and 350°C: 4 min in a belt oven. Micro-hotplates with silicon island are more brittle and, in operation, their breakdown occurred at about 500–550°C.

The evaluation of the thermal properties, such as the power and the temperature distribution, were made using the integrated heater and an infrared camera AVIO 2100, with a pixel resolution of 12.5 × 20 μm^2. Thermal observations were recorded at ambient pressure and at room temperature. The resistance dependence on the voltage $R(V)$ and the maximum temperature $R(T_{max})$ under these conditions were monitored. Figure 1.4 presents the variation of the temperature as a function of power consumption for nitride micro-hotplates with membrane area of 1.0 × 1.0 and 1.5 × 1.5 mm^2.

Micro-hotplates with an area of 1.0 × 1.0 mm^2 consume less than the 1.5 × 1.5 mm^2. This could be explained by their smaller heating area, which reduces the power lost by convection. At an operating temperature of 300 °C, the power consumption for the 1.0 × 1.0- and 1.5 × 1.5-mm^2 micro-hotplates are 55 and 75 mW, respectively. An optimised design should have a 500 × 500 μm^2 heating area on a 1.5 × 1.5-mm^2 micro-hotplate to reduce the power also lost by conduction through the membrane. No significant difference has been observed concerning the power consumption of micro-hotplates made with

CVD oxide as insulator. This could be explained by the similar thermal conductivity of the silicon oxide and the rich silicon nitride films (respectively 1.5 and 3.2 W m^{-1} K^{-1}), and by the heat loss mechanism, which is mainly due to convection [9,18].

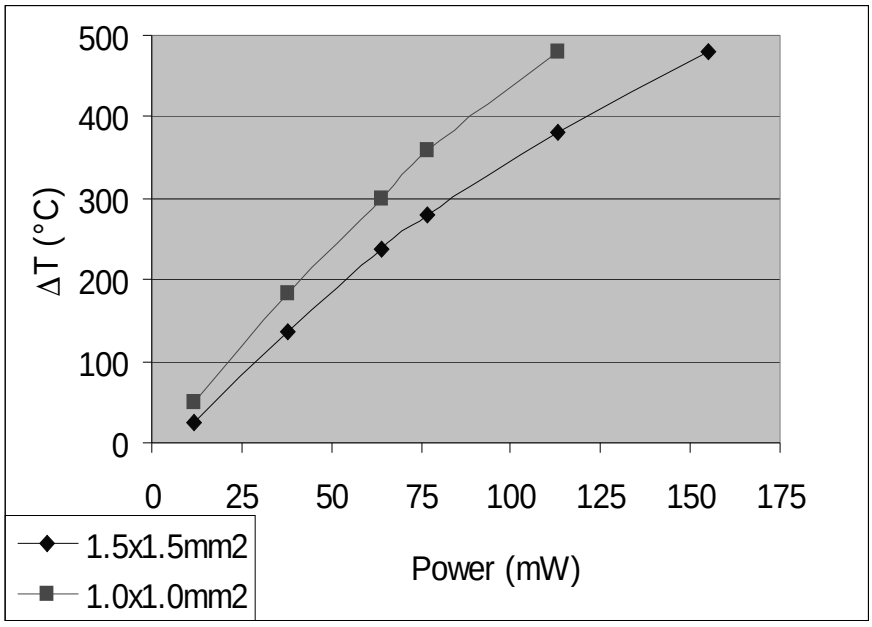

Figure 1.4. Variation of the temperature as a function of the power consumption for nitride micro-hotplates.

As shown by other groups before, the double-meander heater gives a more uniform temperature distribution over the sensing area than the simple-meander heater, as described in Refs [9,12]. It was possible from the IR measurements to show the uniformity of the temperature on the micro-hotplates with a silicon island. The measurements were made on structures with the heater alone stacked between nitride films. The temperature distribution on a whole micro-hotplate could not be measured with enough precision due to the resolution of the camera, which is comparable to the

heater and the electrode finger width. More details concerning the optimisation of the temperature distribution and power consumption of micro-hotplates with or without silicon island are given in Ref. [9].

1.4.2 Drop coated SnO_2 thick film gas sensors: annealing and gas sensitivities

To perform the gas sensitivity measurements, a gas-mixing station with eight channels was used. The system was completely realised in stainless steel using Tylan flow controllers (model 270) and additional electromagnetic valves. The first channel of the system was used for synthetic air, the second channel was equipped with a humidifier delivering 98–99% relative humidity, channel 2,3 and 4 were connected to bottled test gases (3% CH_4/50 ppm CO). The measurement chamber for eight sensors was realised in brass coated with Teflon; the volume of the chamber is about 140 ml. A diffusion barrier was realised using sintered glass with a thickness of 3 mm and a porosity of 200 μm dividing the chamber into a flow-exposed section and a sensor section. Thus, influences of the flow on the temperature of the membranes could be reduced. The flow was kept constant at 200 ml/min. Each measurement started without test gases for 3–5 h to adjust the humidity and get the sensors to a stable baseline. Test gases and synthetic air alternated afterwards every 30 min. The sensors were heated with a power supply having 10 channels, using individually adjustable linear voltage regulators. The voltage was measured directly at the sensors to eliminate voltage drop on the power lines. The resistance of the sensors was measured using a Keithley 199 DMM.

The sensors annealed at 6 V showed a long-term baseline drift. Therefore, the sensors were annealed at a higher temperature to stabilise their baseline. The sensors annealed at 8-V heating voltage showed heavy noise slowly appearing during several measurement runs in the gas-mixing set-up (Fig. 1.5).

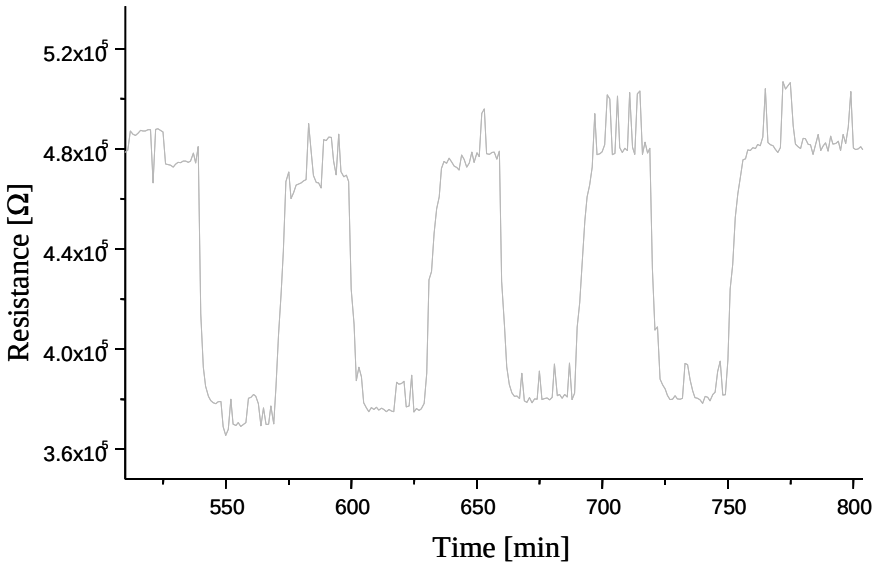

Figure 1.5. Gas response under 4000 ppm CH_4 (30% r.h.) of a sensor (S4) coated with 2% Pd-doped tin oxide, annealed on chip at 8V for 10 s and operated at 4V.

This indicates contact problems between the substrate and the sensitive layer. This effect is certainly induced by the extreme bending of the membrane during the annealing step at a high temperature. The bending was estimated at 400 μm at 700°C in an optical microscope. The dices heated evenly in an oven did not show this effect (membrane and frame expanding together) nor did the sensors (S1, S2) annealed at lower temperature (7 V). The following results concern only the sensors annealed at 7 V since they do not show any of the unwanted effects, i.e. baseline drift and heavy noise, described before.

Figure 1.6 presents a typical sensor (S2: annealing 7 V / 10 min) measurement curve operating at 4.5 V. The sensor shows a stable baseline and a fast response time, $t_{90} < 150$ s, which is, in fact, limited by the flow set-up and the glass diffusion barrier in the measurement chamber.

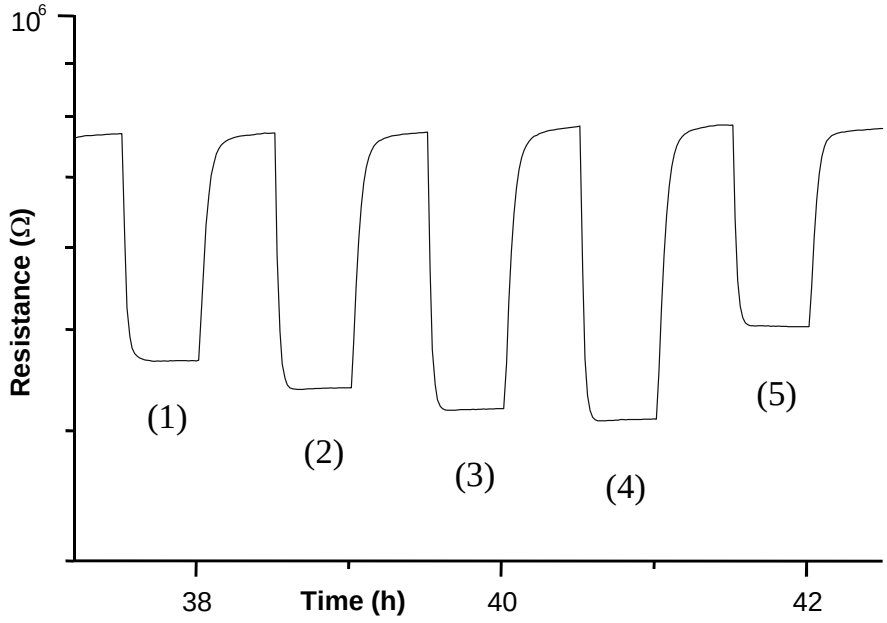

Figure 1.6. Typical sensor measurement curve. The sensor is coated with 2% Pd-doped tin oxide, annealed on chip at 7V for 10 min and operated at 4.5V. (1) 5ppm CO + 500 ppm CH_4, (2) 5ppm CO + 1000 ppm CH_4, (3) 5 ppm CO + 1500 ppm CH_4, (4) 5 ppm CO + 2000 ppm CH_4, (5) 5 ppm CO.

Figure 1.7 shows the gas-flow protocol corresponding to the sensor tests presented in Figures 1.8 and 1.9.

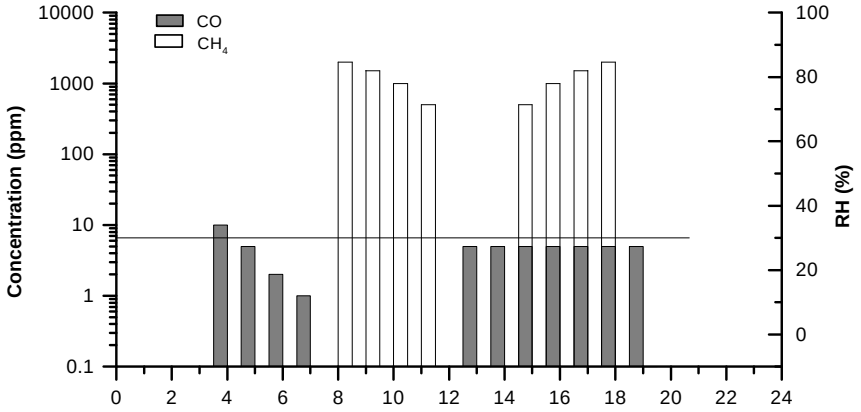

Figure 1.7. Gas protocol for the gas sensing measurements showed in Figures 1.8 and 1.9.

Figure 1.8 shows the response of the sensors annealed at 7 V during 10 s and 10 min for different concentrations of CO and CH_4 (30% RH).

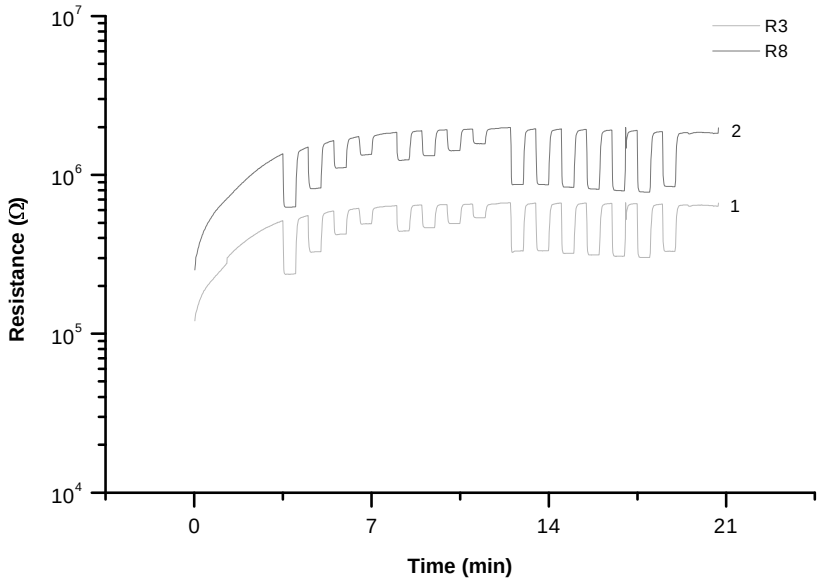

Figure 1.8. Gas sensing measurements (protocol in Fig. 1.7) on a sensor coated with 2% Pd-doped tin oxide, annealed on chip at 7V for 10 s (S1) and for 10 min (S2) at an operating voltage of 4V.

The sensor was measured for the first time after annealing. This caused the drift at the beginning of the measurement. For both sensors (S1, S2), G_{gas}/G_{air} is 2.2 for 10 ppm CO and 1.4 for 2000 ppm CH_4. In the measured mixtures of CO and CH_4 (Fig. 1.8), the concentration of CH_4 could not be fixed out of the measurement data. Although with a higher heating voltage (4.5 V), the mixtures of CO and CH_4 can clearly be determined with the best results obtained at 0% RH (Fig. 1.9).

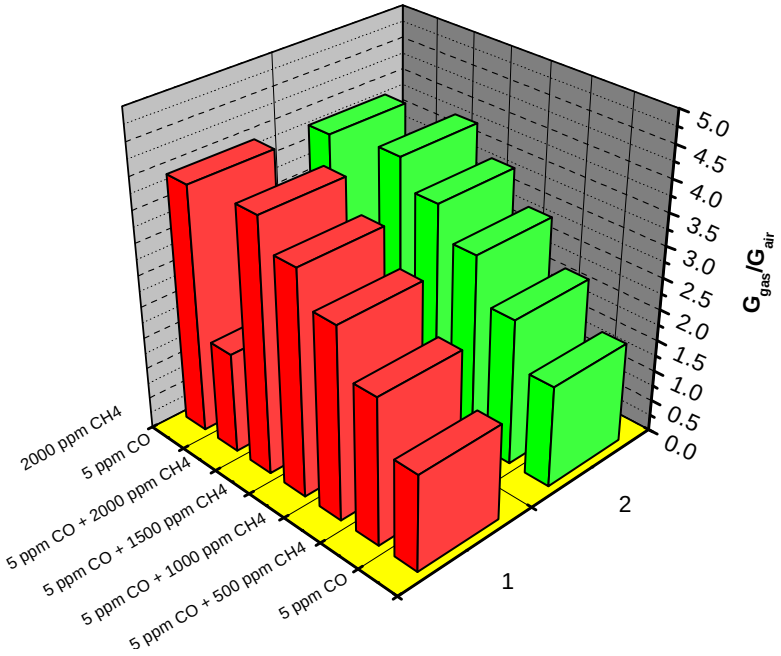

Figure 1.9. Gas sensing measurements (protocol in Fig. 1.7) on a sensor coated with 2% Pd-doped tin oxide, annealed on chip at 7V for 10 s (S1) and for 10 min (S2) at an operating voltage of 4.5 V.

Humidity has no significant effect on the CO response, and, concerning the methane, the signal decreases with the humidity going up to 50% RH (Figs. 1.10 and 1.11), following the same behaviour described in Ref. [19]. The same

figures also show that the annealing time has no influence on the sensors' gas sensitivities.

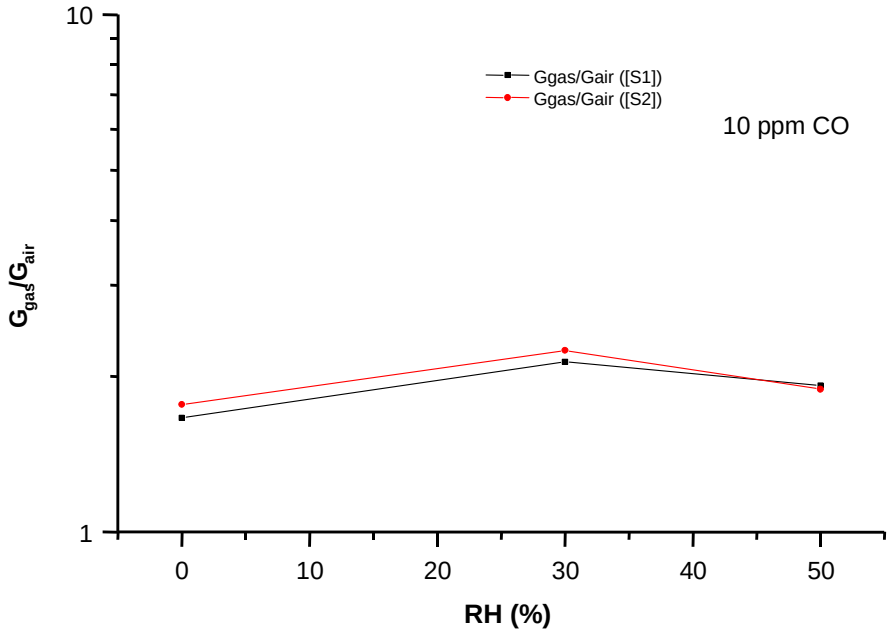

Figure 1.10. Influence of the humidity on the sensors signals in CO. The sensors are coated with 2% Pd-doped tin oxide, annealed on chip at 7V for 10 s (S1) and for 10 min (S2) at an operating voltage of 4.5 V.

To summarise, the micro-hotplates made of nitride films were shown to be suitable for operation at a high temperature. The annealing "on chip" of the tin oxide coating material was performed. The obtained results showed that sensors annealed with a heater voltage of 7 V either during 10 s or 10 min and operating at a heater voltage of 4.5 V (≈ 300°C) give the best gas responses to CO and CH_4. More experiments are under progress to optimise the annealing "on chip" of the gas-sensing materials. In terms of performance (sensitivity,

selectivity and stability), sensors made using this technique are comparable to the ones annealed in a belt oven at 700°C.

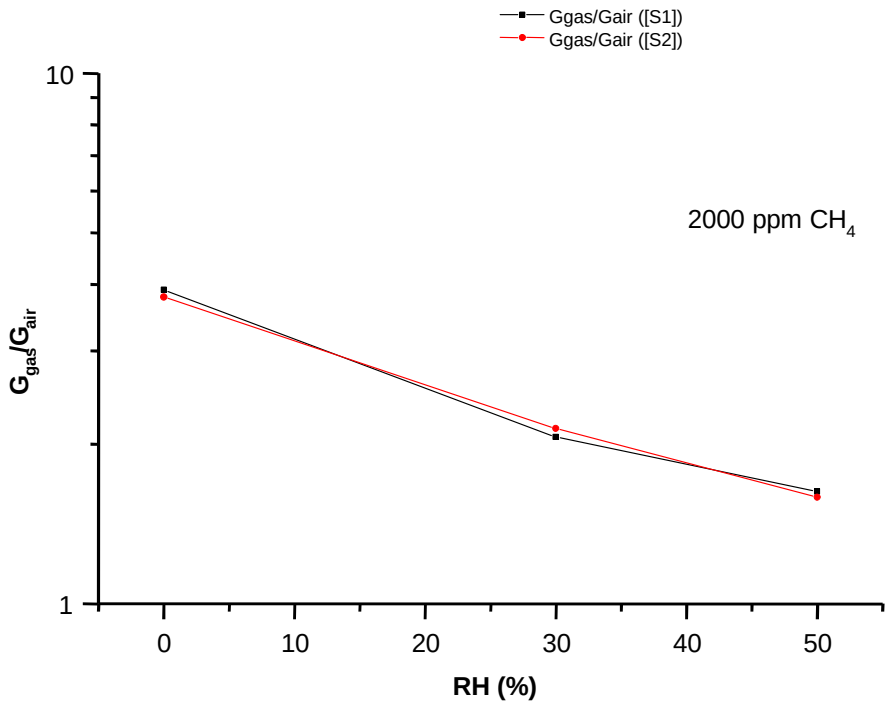

Figure 1.11. Influence of the humidity on the sensors signals in CH_4. The sensors are coated with 2% Pd-doped tin oxide, annealed on chip at 7V for 10 s (S1) and for 10 min (S2) at an operating voltage of 4.5 V.

1.5 CONCLUSION

The standing high temperatures of these micro-hotplates are of great interest for drop-coated thick film gas sensors. Compared to previous works they allow the annealing of the coating material at higher temperatures (up to 700°C), which improves the performance of these sensors. They also give the

opportunity to proceed at the annealing "on chip" of the coating material. The chip can be coated and mounted by flip-chip bonding directly on a PCB, a very cheap technology for the automotive and similar mass markets, and can finally be annealed using the "integrated" electronic.

1.6 ACKNOWLEDGEMENTS

This project was financially supported by the European program Brite-Euram III (n° BRPR-CT96-0194) and by the Fonds pour la formation des Chercheurs et l'Aide à la Recherche (FCAR) from the Quebec Government. We are grateful to the technical staff of the Institute of Microtechnology (IMT-samlab), University of Neuchâtel, Neuchâtel, Switzerland, for the fabrication of the devices, and to Dr M.-A. Grétillat (IMT) for its help with the finite element modeling simulations. We would like also to thank Dr. E. Scheid, Laboratory for Analysis and Architecture of Systems (LAAS), Toulouse, France, for the IR thermal measurements.

1.7 REFERENCES

[1] V. Demarne and A. Grisel, "An integrated low-power thin-film CO gas sensor on silicon", Sensors and Actuators, 13, pp. 301-313, 1988.

[2] U. Dibbern, "A substrate for thin-film gas sensors in microelectronic technology", Sensors and Actuators, B 33, pp. 63-70, 1990.

[3] S. Wessel, M. Parameswaran, S. R. Morrison, and R.F. Frindt, "A CMOS thermally isolated heater structure as a substrate for semiconductor gas sensor", Microelectronics Journal, 23, pp. 451-456, 1992.

[4] J.S. Suehle, R.E. Cavicchi, M. Gaitan, and S. Semancik, “Tin oxide gas sensor fabricated using CMOS micro-hotplates and in-situ processsing”, IEEE Electron Device Letters, 14 (3), pp. 118-120, 1993.

[5] R.E. Cavicchi, J.S. Suehle, K.G. Kreider, M. Gaitan, and P. Chaparala, “Optimized Temperature-pulse sequences for the enhancement of chemically specific response patterns from micro-hotplates gas sensors”, Sensors and Actuators, B 33, pp. 142-146, 1996.

[6] J.W. Gardner, A. Pike, N.F. de Rooij, M. Koudelka-Hep, P.-A. Clerc, A. Hierlemann, and W. Göpel, “Integrated array sensor for detecting organic solvents”, Sensors and Actuators, B 26-27, pp. 135-139, 1995.

[7] A. Heilig, N. Barsan, U. Weimar, M. Schweizer-Berberich, J.W. Gardner, and W. Göpel, “Gas identification by modulating temperatures of SnO2 based thick film sensors”, Sensors and Actuators, B 43, pp. 45-51, 1997.

[8] A. Heilig, N. Barsan, U. Weimar, and W. Göpel, “Selectivity enhancement of SnO_2 gas sensors: simultaneous monitoring of resistances and temperatures”, in Conf. Proc. of Eurosensors XII, pp. 633-636, 1998.

[9] D. Briand, M.-A. Grétillat, B. van der Schoot, and N.F. de Rooij, “Thermal management of micro-hotplates using MEMCAD as simulaiton tool”, in Conf. Proc. of the 3rd Int. Conf. on the Modeling and the Simulation of Microsystems (MSM’00), pp. 640-643, 2000.

[10] M. Gall, “The Si planar pellistor : a low-power pellistor sensor in Si thin-film technology”, Sensors and Actuators, B 4, pp. 533-538, 1991.

[11] A. Götz, I Gràcia, C Cané, and E Lora-Tamayo, “Thermal and mechanical aspects for designing micromachined low-power gas sensors”, Journal of Micromechanics and Microengineering, 7, pp. 247-249, 1997.

[12] V. Guidi, G.C. Cardinali, L. Dori, G. Faglia, M. Ferroni, G. Martinelli, P. Nelli, and G. Sberveglieri, "Thin-film gas sensor implemented on a low-power consumption micromachined silicon structure", Sensors and Actuators, B 49, pp. 88-92, 1996.

[13] A. Götz, I. Gràcia, C. Cané, E. Lora-Tamayo, M.C. Horrillo, J. Getino, C. Garcia, and J. Gutiérrez, "A micromachined solid state integrated gas sensor for the detection of aromatic hydrocarbons", Sensors and Actuators, B 44, pp. 483-487, 1997.

[14] D. Briand, B. van der Schoot, S. Jeanneret, P.-A. Clerc, and N.F. de Rooij, H. Sundgren, I. Grahn, and I. Lundström, "Novel low-power consumption MOSFET array gas sensor. Tech. Digest of 10^{th} Int. Conf. Solid-State Sensors and Actuators (Transducers'99), pp. 938-941, 1999.

[15] X. Li, M. Bao, and S. Shen, "Maskless etching of three-dimensional silicon structures in KOH", Sensors and Actuators, A 57, pp. 47-52, 1996.

[16] A. Diéguez, A. Romano-Rodriguez, J.R. Morante, U. Weimar, M. Schweizer-Berberich, and W. Göpel, "Morphological analysis of nanocrystalline SnO_2 for gas sensor applications", Sensors and Actuators, B 31, pp. 1-8, 1996.

[17] J. Kappler, N. Barsan, U. Weimar, A. Diéguez, J.L. Alay, A. Romano-Rodriguez, J.R. Morante, and W. Göpel, "Correlation between XPS, Raman and TEM measurements and the gas sensitivity of Pt and Pd doped SnO_2 based gas sensors", Fres. Journal Anal. Chem, 361, pp. 110-114, 1998.

[18] C. H. Mastrangelo, Y.-C. Chong, and R. S. Muller, "Thermophysical properties of low-residual stress silicon rich LPCVD silicon nitride films", Sensors and Actuator, A 21-23, pp. 856-860, 1990.

[19] J. Kappler, N. Barsan, U. Weimar, and W. Göpel, "Influence of water vapour on nanocrystalline SnO_2 to monitor CO and CH_4", in Conf. Proc. of Eurosensors XI, pp. 1177-1180, 1997.

Paper II

THERMALLY ISOLATED MOSFET FOR GAS-SENSING APPLICATION

Danick Briand[1], Hans Sundgren[2], Bart van der Schoot[1],
Ingemar Lundström[2], and Nicolaas F. de Rooij[1]

[1]Institute of Microtechnology, University of Neuchâtel,
P.O. Box 3, CH-2007 Neuchâtel, Switzerland
[2]S-SENCE and Laboratory of Applied Physics, Linköping University,
S-581 83 Linköping, Sweden

ABSTRACT

This work reports on thermally isolated electronic components for gas sensing applications. The device is composed of an array of 4 MOSFETs, a diode and a semiconductor resistor integrated on a micro-hotplate, which is fabricated using bulk micromachining of silicon. The thermal efficiency of the device is 2°C/mW with a thermal constant less than 100 ms. Holes are made in the passivation film over the gates of the MOSFET and gas-sensitive films deposited on top of the gate insulator. The low thermal mass device realised allows new modes of operation for MOSFET gas sensors such as a combination of the field and thermal effects and a pulsed temperature mode of operation.

Published in IEEE Electron Device Lettters,22(1), pp. 11-13, 2001

2.1 INTRODUCTION

During the last decade, sensors based on electronic components thermally isolated on dielectric membranes have been reported [1-5]. Most of these devices were used as thermal sensors to measure for instance the temperature, the pressure and the gas flow [1-3]. Only recently, thermally isolated electronic devices were reported for gas sensing applications such as capacitors [4], but none have been reported on MOSFET gas sensors. In this type of sensors, the gate insulator has to remain uncovered after the processing of the electronic components. A gas sensitive film is then deposited on top of the insulator to form the gate of the transistor. The replacement of the standard MOSFET gate by a gas sensitive material, such as a catalytic metal (e.g. Pd, Pt, Ir), a metal-oxide or a polymer, allows the detection of several gases such as hydrogen, ammonia, carbon monoxide and organic vapours [6-8].

Gas-sensitive FETs (GasFETs) operate normally at temperatures higher than 100°C and are limited to 175-200°C since they are made on standard silicon. The integration of an array of four GasFETs on a micro-hotplate has reduced to 20 mW the power consumption of a single MOSFET sensor operating at 170°C. The developed low-power MOSFET array allows new modes of operation for MOSFET gas sensors such as a pulsed temperature mode of operation and the monitoring of the heat exchange. These modes of operation are of great interest to reduce the power consumption of the sensors or to enhance their selectivity to specific gases [9].

2.2 DESIGN AND FABRICATION

An array of 4 MOSFETs, including a diode and semiconducting resistor, has been designed for gas sensing applications (Fig. 2.1). The MOSFETs were used as field-effect gas sensors, the diode as temperature sensor and the resistor as heater.

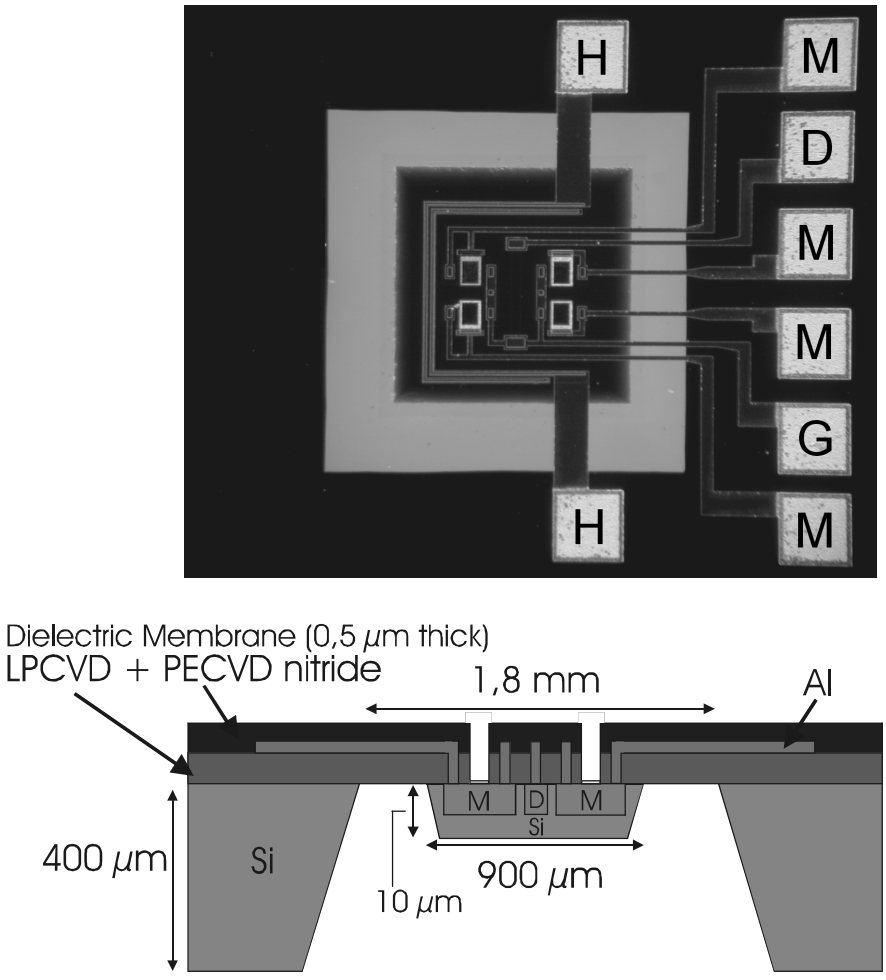

Figure 2.1. Top view photograph and cross-section schematic of the low-power MOSFET array gas sensor: M stands for MOSFET, D for Diode, H for Heater and G for Ground.

The channel length of the MOSFET was 10 μm with a width/length = 30. Since they operate in a constant current mode (100 μA) between the source and the drain, the GasFETs had their drain and gate connected together.

The electronic components: MOSFET, diode, resistor were fabricated in the 5 μm IMT NMOS process using a p-well technology [10]. The process started with the implantation of boron in a 100 mm silicon substrate (25 Ω•cm, n type, 400 μm thick, double face polished) to define the MOSFET p-well, the p-doped region of the diode and the resistive heater. The transistor sources/drains and the diode were made in a single diffusion step of doping atoms (phosphorus and boron) from CVD oxide films. The p-well implant resulted in a sheet resistance of ~20 kΩ/□, and the sheet resistance of the p+ (channel stop) and n+ (source/drain) diffusions was respectively of ~1 kΩ/□ and of ~20 Ω/□. A gate oxide of 100 nm was grown next to provide a gate dielectric.

The active devices were thermally isolated from the bulk silicon to reduce the major conduction paths for the heat. The GasFETs, the heating resistor and the diode were located in a silicon island isolated from the chip frame by a dielectric membrane (Fig. 2.1). The membrane size was 1.8×1.8 mm^2. The silicon island had an area of about 900×900 μm^2 and a thickness of about 10 μm. The membrane was made of LPCVD low-stress silicon nitride film. A PECVD silicon oxi-nitride film was used as passivation layer on the aluminum metallisation. After the patterning of the passivation film on three of the MOSFETs' gates, thin catalytic metals, 80 nm of Pt, Ir and Pd, were deposited and patterned directly on the gate oxide. Three GasFETs having

different catalytic metals were fabricated and the fourth one had an aluminium gate and could be used as a reference device.

The thermal isolation was achieved by using two successive backside silicon micromachining steps [11]. Firstly, the silicon island was protected by a thermal oxide film during the etching of 10 μm of silicon in KOH (40%, 60°C) to define the silicon island thickness. Secondly, after the removal of the protective oxide, the silicon was etched in KOH (52%, 70°C) until the dielectric membrane was reached, leaving a 10 μm thick silicon island underneath. A concentration of 52% is used to decrease the ratio of the etch rate of the island's sides, formed by (311) planes, with respect to the etch rate of its bottom, defined by the (100) plane [11]. In the aim of having a precise control on the silicon island thickness, electrochemical etch-stop could be used as done by other research groups [3,4].

2.3 CHARACTERISATION AND DISCUSSION

The electrical characterisation of the electronic components was performed using the HP4156A Semiconductor Parameter Analyser from Hewlett Packard. The power consumption was evaluated by measuring the temperature using an infrared camera AVIO 2100. The gas sensing measurements were performed using the gas mixing system and electronic nose at the Swedish Sensor Center (S-SENCE), Linköping University, Linköping, Sweden.

The threshold voltage for the MOSFET covered with aluminium was 0.9 V. Figure 2.2 presents the I-V curves of the suspended MOSFETs with an aluminium gate. The operating voltage for a drain current of 100 μA (gate and

drain connected) was of about 1.1 V for the MOSFETs with an Al gate and went up to about 1.3, 1.7 and 2.9 V respectively for the MOSFETs having Ir, Pt and Pd gates.

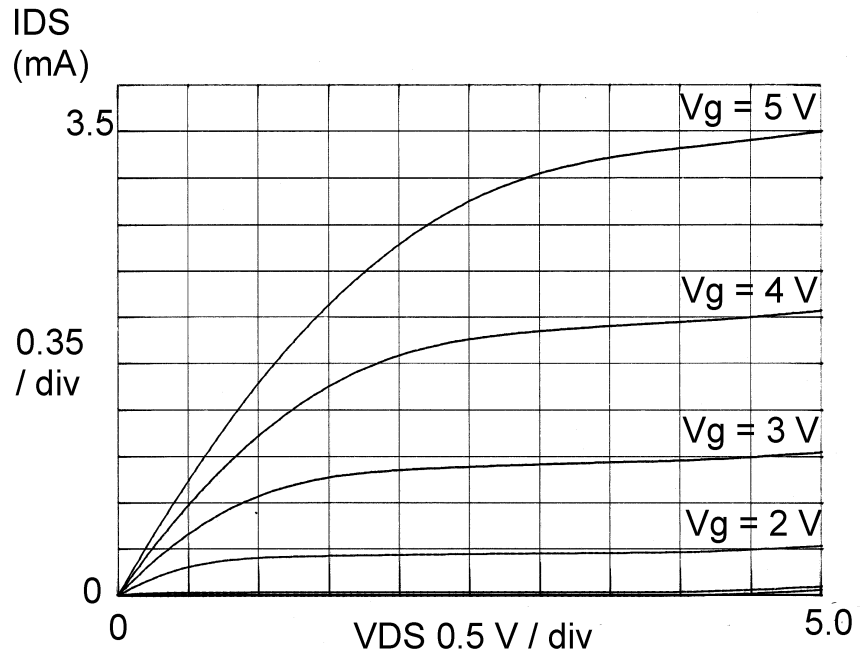

Figure 2.2. Output characteristics of a MOSFET with an aluminium gate at room temperature (W/L = 300 µm/10 µm), VG = 0 to 5 V, step of 1 V.

The MOSFETs and the diode have shown to be suitable for gas sensing at temperatures up to 200°C for an operating current of 100 µA. An increase of this current can even allow an operation at higher temperature (e.g. 225°C at 200 µA, see Fig. 2.3).

The temperature sensitivity of the diode measured in an oven was - 2.4 mV/°C. The value of the heating resistor was 225 ohms at room temperature. The resistance increases from room temperature to reach a maximum at about

150°C, to then decrease as expected for a semiconductor and as shown in Ref. [12].

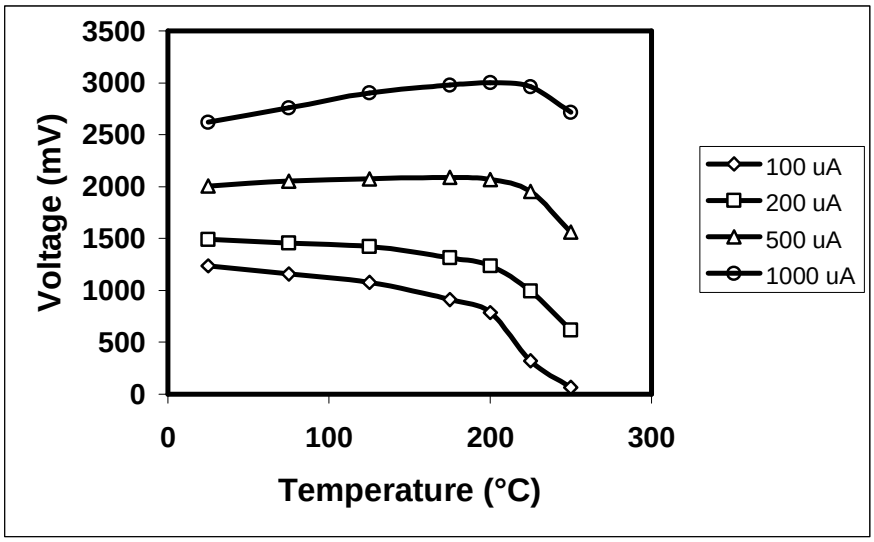

Figure 2.3. Voltage at the connected gate and drain of a MOSFET with an aluminium gate as a function of temperature for different drain currents.

A low power consumption of 80 mW was achieved for an operating temperature of 170°C for the array of 4 GasFETs compared to 0.5-1.0 W for one standard bulk GasFET (Fig. 2.4). The power consumption could be lowered using microelectronics and micromachining processes having a higher definition. The thermal time constant to go to room temperature up to 170°C was in the order of 65 ms for the rising time and of about 100 ms for the cooling time, which allowed the operation of the sensor in a cycled or pulsed temperature mode. Moreover, the low-thermal mass makes possible to use the device as a thermal sensor, monitoring the variation of the thermal

conductivity in the presence of the sample gas and the heat exchange generated by the chemical reactions occurring on the catalytic films.

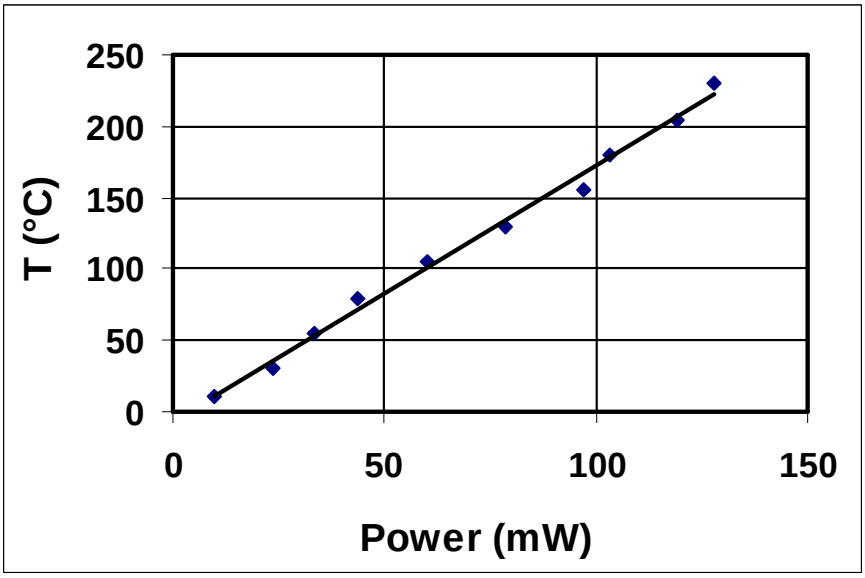

Figure 2.4. Variation of the device temperature as a function of the power dissipated by the heater.

The value and the behaviour of the gas sensitivities to hydrogen, ammonia and ethanol of these low-power devices were comparable with the standard MOSFET gas sensors [13]. For instance, at a typical operating temperature of 140°C, the MOSFET sensors covered with Pt had a response of 182 mV to 20 ppm of NH_3 and 60 mV to 250 ppm of H_2. The response for the same two gases was respectively of 165 mV and 103 mV for the MOSFET covered with Ir. The sensor characteristics: the electrical and the gas sensing properties, show promise in using the device in electronic noses and hand-held gas monitors for gas mixture analysis.

2.4 CONCLUSION

The combination of microelectronics and MEMS (silicon micromachining) processing was used to fabricate thermally isolated MOSFET for gas sensing applications. An implanted resistor and a diode, used respectively as heater and temperature sensor, and 4 MOSFETs are located in a silicon island thermally isolated from the sensor chip frame by a dielectric membrane. The thermal efficiency of the device is 2°C/mW with a thermal constant less than 100 ms. This low-thermal mass device allows the operation of the sensors in a pulsed or cycled temperature mode and the monitoring of the field and thermal effects in the presence of the sample gas. A CMOS compatible process and the silicon-on-insulator (SOI) technology are envisaged in the future developments.

2.5 ACKNOWLEDGEMENTS

The financial support of the Brite-Euram III European program (BRPR-CT96-0194) and Nordic Sensors Technologies (NST, Linköping, Sweden), the help of the technical staff from the Institute of Microtechnology (IMT-samlab), University of Neuchâtel, Neuchâtel, Switzerland, and from the Swedish Sensor Center (S-SENCE), Linköping University, Linköping, Sweden and the scientific advices of A. Lloyd Spetz (S-SENCE) and P. Martensson (NST) are gratefully acknowledged.

2.6 REFERENCES

[1] P.M. Sarro, A.W. van Herwaarden, and W. van der Vlist, “A silicon silicon-nitride membrane fabrication process for smart thermal sensors”, Sensors and Actuators, A 41-42, pp. 666-671, 1994.

[2] M.A. Gajda, H. Admed, and J. Dodgson, “CMOS-compatible silicon devices on thin SiO2 membranes”, Electron. Lett., 30, pp. 28-30, 1994.

[3] R.J. Reay, E.H. Klaassen, and G.T.A. Kovacs, “Thermally and Electrically Isolated Single Crystal Silicon Structures in CMOS Technology”, IEEE Electron Device Lett., 15 (10), pp. 399-401, 1994.

[4] C. Hagleitner, A. Koll, R. Vogt, O. Brand, and H. Baltes, “CMOS capacitive chemical microsystem with active temperature control for discrimination of organic vapors”, in Transducers’99 Tech. Dig., 1999, pp. 1012-1015.

[5] J.S. Suehle, R.E. Cavicchi, M. Gaitan, and S. Semancik, “Tin oxide gas sensor fabricated using CMOS micro-hotplates and in-situ processing”, IEEE Electron Device Lett., 14, pp. 118-120, 1993.

[6] I. Lundström, M.S. Shivaraman, C.M. Svensson, and L. Lundkvist, “Hydrogen sensitive MOS field-effect-transistor”, Appl. Phys. Lett., vol. 26, pp. 55-57, 1975.

[7] I. Lundström, A. Spetz, F. Winquist, I Ackelid, and H. Sundgren, “Catalytic metals and field-effect devices – a useful combination”, Sensors and Actuators, B 1, pp. 15-20, 1990.

[8] M.G.H. Meijerink, M. Koudelka-Hep, N.F. de Rooij, D.J. Strike, J. Hendrikse, W. Olthuis and P. Bergveld, “Gas-Dependent field effect transistor with an electrodeposited conducting polymer gate contact”, Electrochem. and Solid-state Lett., 2 (3), pp. 138-139, 1999.

[9] A.P. Lee, and B.J. Reedy, “Temperature modulation in semiconductor gas sensing”, Sensors and Actuators, B 60, pp. 35-42, 1999.

[10] P. Arquint, Integrated blood gas sensor for pO_2, pCO_2 and pH based on silicon technology. Thesis at the University of Neuchâtel, Switzerland, 1994, pp. 84-86.

[11] D. Briand, A. Krauss, B. van der Schoot, N. Barsan, U. Weimar, W. Göpel, and N.F. de Rooij, “Design and fabrication of high temperature micro-hotplates for drop coated gas sensors”, in Proc. of Eurosensors XIV, 1999, pp. 357-358, Sensors and Actuators, B 68, pp. 223-233.

[12] K. Somogyi, “Some critical conditions of thermal breakdown in semiconductors”, Sensors and Actuators, A71, pp. 58-62, 1998.

[13] I. Lundström, “Why bother about gas-sensitive field-effect devices?”, Sensors and Actuators, A 56, pp. 75-82, 1996.

Paper III

A LOW-POWER MICROMACHINED MOSFET GAS SENSOR

Danick Briand[1], Bart van der Schoot[1], Hans Sundgren[2],
Ingemar Lundström[2], and Nicolaas F. de Rooij[1]

[1]Institute of Microtechnology, University of Neuchâtel,
P.O. Box 3, CH-2007 Neuchâtel, Switzerland
[2]S-SENCE and Laboratory of Applied Physics, Linköping University,
S-581 83 Linköping, Sweden

ABSTRACT

This paper reports on the design, fabrication and characterisation of the first low-power consumption MOSFET gas sensor. The novel MOSFET array gas sensor has been fabricated using anisotropic bulk silicon micromachining. A heating resistor, a diode used as temperature sensor and four MOSFETs are located in a silicon island suspended by a dielectric membrane. The membrane has a low thermal conductivity coefficient and, therefore, thermally isolates the electronic components from the chip frame. This low thermal mass device allows the reduction of the power consumption to a value of 90 mW for an array of four MOSFETs at an operating temperature of 170°C. Three of the MOSFETs have their gate covered with thin catalytic metals and are used as gas sensors. The fourth one has a standard gate covered with nitride and could

act as a reference. The sensor was tested under different gaseous atmospheres and has shown good gas sensitivities to hydrogen and ammonia. The low-power MOSFET array gas sensor presented is suitable for applications in portable gas sensor instruments, electronic noses, and automobiles.

3.1 INTRODUCTION

Gas-sensitive field-effect (GasFETs) devices have been studied for about 25 years [1]. The replacement of the MOSFET gate by materials having catalytic properties (Pd, Pt, Ir…) allows the detection of several gases such as hydrogen, ammonia, carbon monoxide and, alcohols [2,3]. Over the years they have been shown to be suitable for different applications such as hydrogen monitors and leak detectors, and in electronic noses [4].

Portable instruments and automobiles are products in which low-cost and low-power consuming devices are needed. During the last decade, a lot of work has been done in the gas sensor field on reducing the power consumption of metal-oxide sensors [5-9]. Silicon micromachining combined with thin-film technology was used to fabricate micro-hotplates having a good thermal insulation and a low-thermal mass. These devices have allowed new modes of operation for metal-oxide gas sensors such as a modulated and pulsed-temperature mode. These modes of operation can be of great interest to reduce the power consumption of the sensors or to enhance their selectivity to specific gases [10-13].

Some research groups have recently worked on thermally isolating electronic components on membranes using silicon micromachining and CMOS

technologies [14-16], but none has been reported on MOSFET-type gas sensors. In this type of sensors, the gate insulator has to remain uncovered after the processing of the electronic components. A gas-sensitive film, such as a catalytic metal, a metal-oxide or a polymer, is then deposited on top of the insulator to form the gate of the transistor.

MOSFET gas sensors operate usually at a temperature over 100 °C and are limited to 175-200°C due to the use of standard silicon technology [17]. The power consumption of a bulk sensor realised using a standard silicon processing is of about 0.5–1.0 W. A silicon island containing the electronic devices was, therefore, added to the micro-hotplate concept to reduce the MOSFET sensor power consumption [18]. The developed low-power GasFET arrays allows new modes of operation for this type of gas-sensing devices and makes this technology more competitive with the others on the market.

3.2 DESIGN

3.2.1 Sensor chip

The MOSFET sensor realised has been designed in the aim of reducing the source/drain leakage currents and the power consumption of this type of gas sensors. Each device consists of 4 GasFETs, a temperature sensor (diode), and a heater as shown in Figure 3.1. The chip size is 4.0×4.0 mm^2 and has not been optimised in this paper since the throughput was not an important issue.

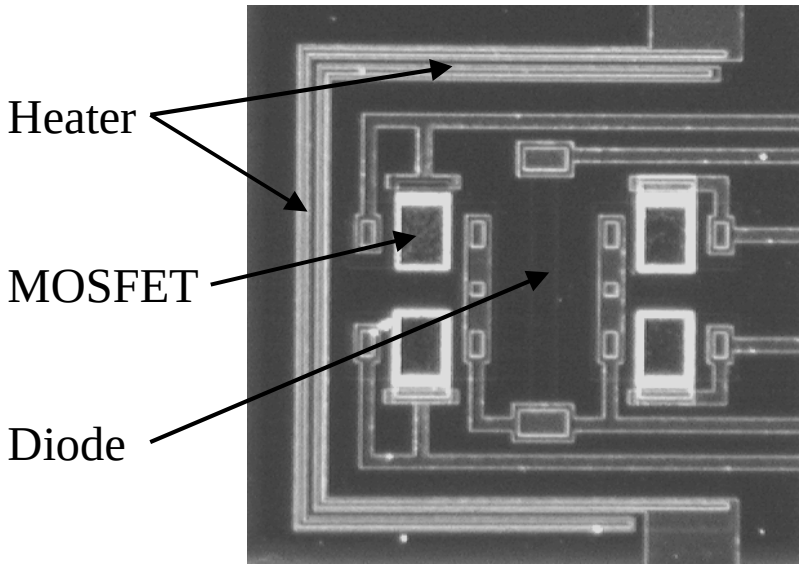

Figure 3.1. Photograph of the "bulk" MOSFET array gas sensor, on which are the four MOSFETs (W/L = 30, L = 5 μm) surrounded by the heater (U-shape) and with the diode in the middle.

3.2.2 Electronic components

The electronic components are realised using the Institute of Microtechnology (IMT), University of Neuchâtel, Neuchâtel, Switzerland, NMOS processing technology [19]. NMOS transistors and diodes are realised in an implanted p-well technology. The transistor sources/drains and the diode are made in a single diffusion step of doping atoms (Phosphorus and Boron) from CVD oxide films. Therefore, the minimum channel length for the transistors is 5.0 μm due to the diffusion process used. The heater is a semiconducting resistor, which is made during the p-well implantation. The target value of the heater's resistance at room temperature was 120 Ω.

Two arrays with 4 medium or small MOSFETs have been designed with a channel length of 10.0 and 5.0 μm, respectively, both with W/L = 30. Their

source/drain leakage currents have been limited by minimising the p-n junction surface at the source and the drain regions. Therefore the metal/semiconductor contacts are directly taken on the source and the drain just beside the gate. The GasFETs have their drain and gate connected together. They operate with a constant current between the source and the drain. On the test chips used for evaluating the MOSFET electrical properties, the drain and gate were not connected together to allow more flexibility during the characterisation.

3.2.3 Power consumption

The thermal mass and, therefore, the power consumption of the sensor, are minimised by the design. The GasFETs heater and diode are located in a silicon island thermally isolated from the chip frame by a dielectric membrane (Figs. 3.2 and 3.3).

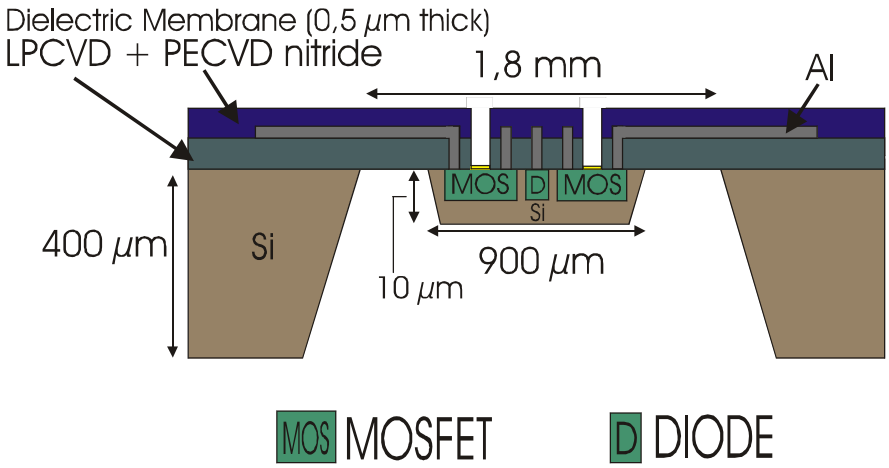

Figure 3.2. Schematic cross-section view of the low-power MOSFET array gas sensor. The electronic components are located in a silicon island thermally isolated from the silicon chip.

The membrane is made of LPCVD low-stress (nonstoichiometric) silicon-nitride film. A PECVD silicon nitride or oxi-nitride film is used as passivation layer on the aluminum metallisation. The membrane size is 1.8 × 1.8 mm^2. The silicon island has an area and a thickness respectively of about 900 × 900 μm^2 and 10 μm.

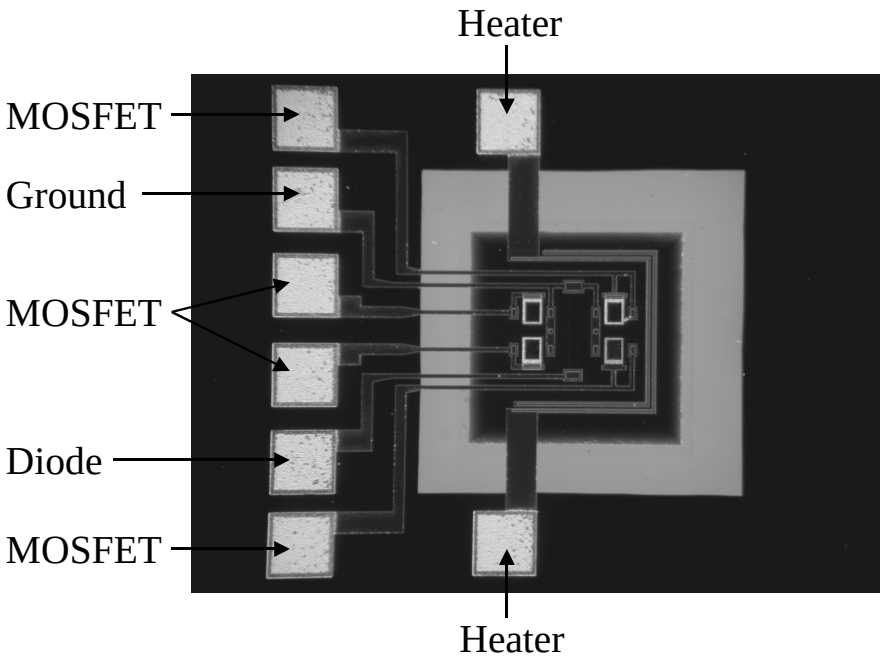

Figure 3.3. Photograph of the low-power micromachined MOSFET gas sensor showing the electronic devices in the silicon island suspended by a dielectric membrane.

3.3 FABRICATION

The processing consists of the following three main parts:

- fabrication of the doped regions in the silicon to make the electronic components;

- gate oxide growth and deposition of the membrane, metallisation, and passivation films;
- releasing of the membrane and the formation of the silicon island by wet anisotropic etching of silicon.

3.3.1 Electronic components

The process starts with the implantation of boron in a 100-mm silicon substrate (25 Ω•cm, n type 400-μm-thick double-face polished) to form the MOSFET p-well, p-doped region of the diode, and resistive heater. The deposition and patterning of boron and phosphorus doped CVD oxide films followed by the diffusion of the doping atoms to define the n+ (diode, source/drain) and p+ (channel stop) regions of the electronic devices are also included in this first part.

3.3.2 Membrane, metallisation and passivation

The second part starts with the growth of a thermally gate oxide (100 nm) followed by the deposition of a low-stress LCPVD silicon-nitride film. Then, the gate and contacts are defined in the nitride. The metallisation is deposited by e-beam evaporation of aluminium, which is annealed later on to obtain ohmic contacts on silicon. A PECVD reactor is used to deposit a silicon nitride/oxi-nitride passivation layer (low stress/tensile). After the patterning of the passivation film, thin catalytic metals (CM: Pt, Ir, Pd) are deposited, patterned, and annealed. Therefore, GasFETs having three different catalytic metals were fabricated and the fourth one had an aluminium gate and could be used as a reference.

3.3.3 Silicon bulk micromachining

Since the deposition of the CM layers is done prior to the silicon bulk micromachining, the frontside of the wafer is protected during the backside etching of silicon in KOH. Firstly, the thermally grown oxide film on the wafer backside is patterned to define the silicon island area. The oxide film acts as a mask in the standard KOH solution (40% at 60°C) during the etching of 10-μm depth of silicon, corresponding to the silicon island thickness. Secondly, after removing the protective oxide, the silicon is entirely etched using 52% KOH (solubility limit of KOH in water at room temperature) at 60°C. Figure 3.4 shows the backside view of the final silicon island formed by anisotropic etching of silicon. A KOH solution with a concentration of 52% is used to decrease the etch rate of the (311) planes, forming the side of the silicon island, compared to the etching rate of the (100) plane, forming the bottom of the silicon island. The ratio between the etching rates in the direction parallel (the <311> direction projected on the (100) surface) and perpendicular <100> to the wafer surface (100) is about 1.4 for this specific KOH solution [20, 21].

Despite the fact that the nitride and oxide layers used as membrane are slowly etched in KOH compared to silicon, the release of membrane has to be done with a precise time control of the silicon etch rate to obtain the desired silicon island thickness of 10 μm. In the aim of having a precise control on the silicon island thickness, electrochemical etch stop could be used, as done by other research groups [15, 16].

The whole fabrication process is done using 11 masks, which are used in 14 photolithography steps (4 of them for the CM films). The fabrication process

is compatible with the use of different gate insulators such as silicon nitride (Si_3N_4), aluminum oxide (Al_2O_3) and tantalum oxide (Ta_2O_5). The last two need one more mask.

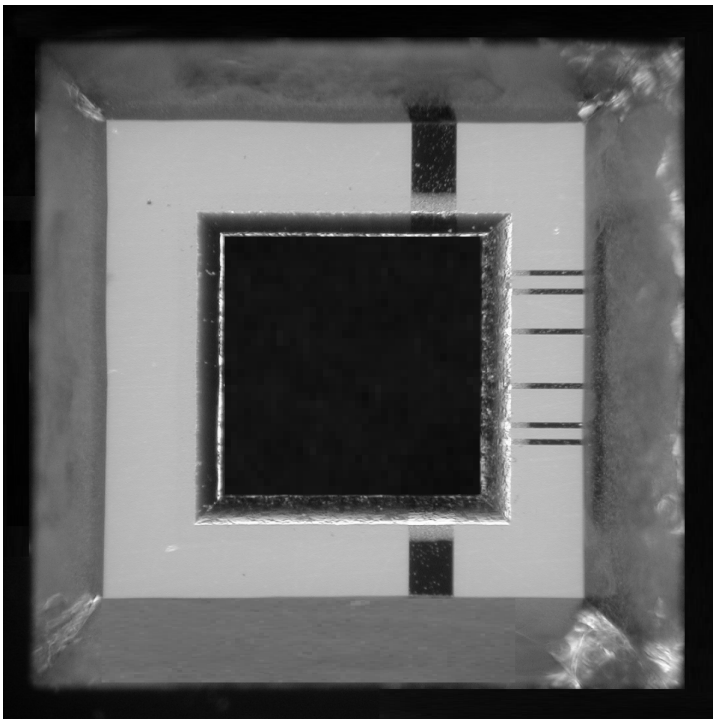

Figure 3.4. Photograph of the backside of the sensor chip showing the silicon island.

3.4 PACKAGING

The bulk MOSFET devices (not on membranes) were mounted on a whole metal dual in line (DIL) 16-p-i-n package with an external heating resistor and SiC diode temperature sensor. Concerning the low-power MOSFET sensors suspended on membranes, they were mounted on a TO-8 16-p-i-n package. The components in both cases were fixed using glue (epo-tek 3081). The pads

on the devices were connected to the package p-i-n's by using ultrasonic bonding of gold or aluminium wires.

3.5 CHARACTERISATION

The electrical characterisation of the electronic components was performed using the Hewlett-Packard HP4156A Semiconductor Parameter Analyser. The thermal time constant was determined by applying a square-wave voltage (Philips PM 5705 pulse generator, 0.1 Hz–10 MHz) on the heater and monitoring both the pulse signal and the diode voltage at 100 μA on an oscilloscope (Tektronix TPS 380, 400 MHz). The power consumption versus temperature was evaluated by measuring the temperature using an infrared camera AVIO 2100, with a pixel resolution of 12.5 × 20 μm^2. Thermal observations were recorded at ambient pressure and room temperature. The dependence of the resistance on the voltage $R(V)$ and on the maximum temperature $R(T_{max})$ were monitored.

The gas sensing measurements were performed using the gas mixing system and electronic nose at the Swedish Sensor Center (S-SENCE), Linköping University, Linköping, Sweden. The gas mixing system allows the mixing of up to 4 sample gases with a carrier gas. Hydrogen (250, 125, 62.5 ppm) and ammonia (40, 20, 10 ppm) were used as sample gas and the carrier gas was dry synthetic air, with a total flow of 100 ml/min. The length of the sample pulse was set to 30 s and the recovery time in carrier gas only to 300 s. These are typical values used for applications in an electronic nose. The sensors are connected to a printed circuit board (PCB), which enables the operation of the

sensors and the data acquisition. A current of about 100 μA was used to drive both the temperature sensor (the diode) and MOSFET sensors. The temperature was set successively at about 140 and 170°C, which are typical operating temperatures for this type of sensors. The whole setup is managed by using a PC and the date acquisition was carried out in Senstool Software (Nordic Sensor Technologies, Linköping, Sweden).

3.6 RESULTS AND DISCUSSION

3.6.1 Electrical properties

The electrical characterisation of the MOSFETs and the diode has shown that they are suitable for operation at temperatures up to 200°C at a current of 100 μA. An increase of this current can even allow an operation at higher temperature (225°C at 200 μA). Another option is to use a retrograded p-well to minimise the leakage current at high temperature [22]. The temperature sensitivity of the diode measured in an oven is –2.4 mV/°C. The membrane bends during the internal heating of the sensor and, therefore, the diode signal is also influenced by the deformation of the silicon island due to its piezoresistive properties. Therefore, the diode is calibrated before operation to define the voltage vs. temperature law and the working points corresponding to 140 and 170°C. The value of the heating resistor was higher than expected at 225 ohms at room temperature. The resistance could be adjusted at 120 ohms by proceeding at minor modifications to the design and the processing since the technology was characterised. The heating resistor value as a

function of temperature has the behaviour expected for a semiconductor. It increases from room temperature to reach a maximum at about 150°C, to then decrease as shown in Ref. [17].

3.6.2 Thermal properties

A low power consumption of 90 mW is achieved for an operating temperature of 170°C for the array of four GasFETs compared to 0.5–1.0 W for one standard GasFET. Figure 3.5 shows the variation of the sensor temperature as a function of the power dissipated by the heater.

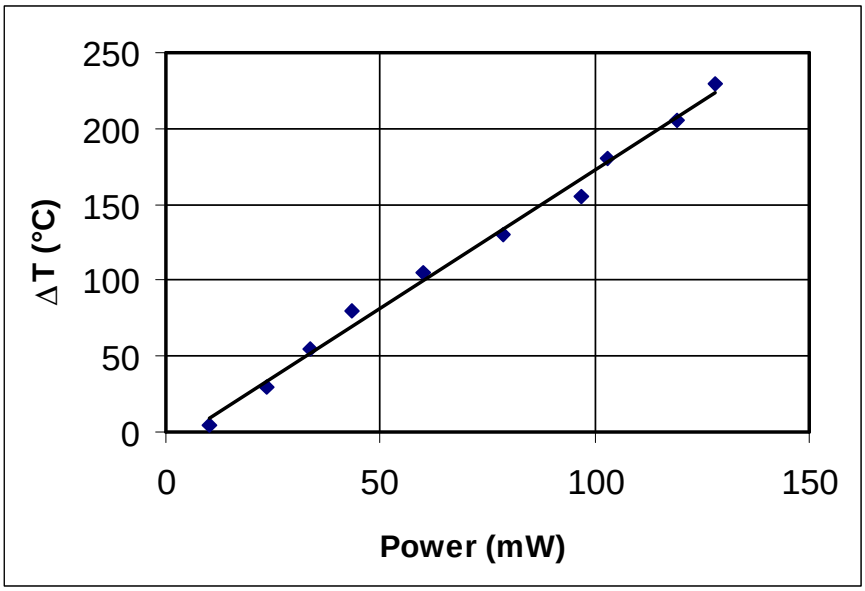

Figure 3.5. Variation of the temperature as a function of the power consumption for the micromachined MOSFET sensor.

The power consumption could be lowered using microelectronic processes having a higher definition. A silicon micromachining process that gives a better control on the dimensions of the silicon island could be used as well,

such as electrochemical etch stop. A thinner and narrower silicon island could be achieved reducing the heat loss by conduction and convection, which are, respectively, related to the distance between the silicon island and the chip frame and to the area of the silicon island [23].

The thermal time constant when the heater is pulsed (square wave) at 6 V (70 mW) is in the order of 65 ms for the rising time and of about 100 ms for the cooling time. Figure 3.6 shows the variation of the heater and the diode voltages (at a constant current of 100 μA) as a function of time.

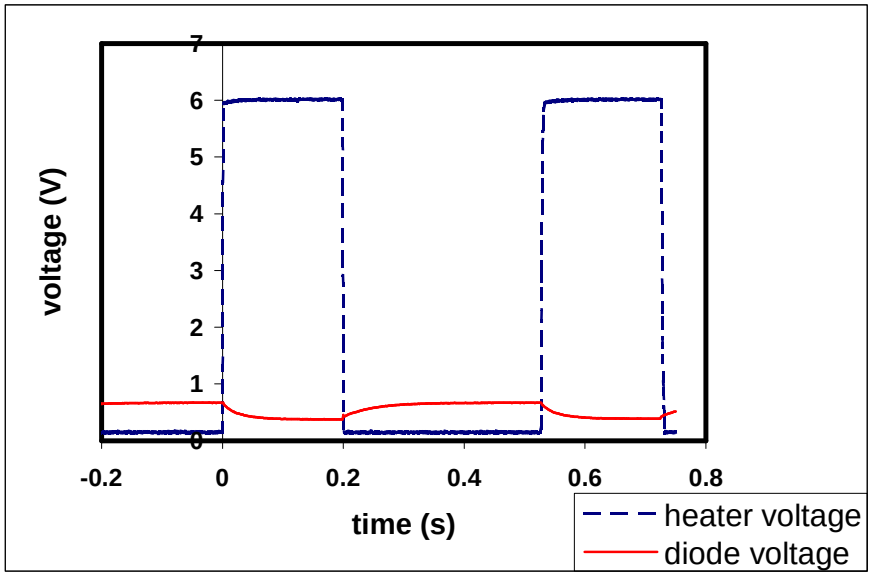

Figure 3.6. Square wave voltage applied on the heater and voltage on the temperature sensor (diode) as a function of time.

The low thermal mass allows the operation of the sensor in a pulsed or cycled temperature mode, which lowers the power consumption and could influence the selectivity, as in metal-oxide gas sensors [10-13]. The silicon island ensures a uniform temperature distribution all over the active area [24], which was confirmed using FEM simulations [23].

3.6.3 Gas sensitivities

The low-power MOSFET sensors have slightly smaller gas response levels than the standard bulk MOSFET sensors used at the S-SENCE, but in a useful range for gas-sensing applications. The different processing steps used to make the membrane and the quality of the catalytic metals deposited at IMT might be the cause of the differences observed. Figure 3.7 presents the gas sensitivities to hydrogen and ammonia for two low-power MOSFETs coated with Ir and Pt thin films, 8-nm-thick, at a temperature of about 140°C. Good gas sensitivities were also obtained at 170°C.

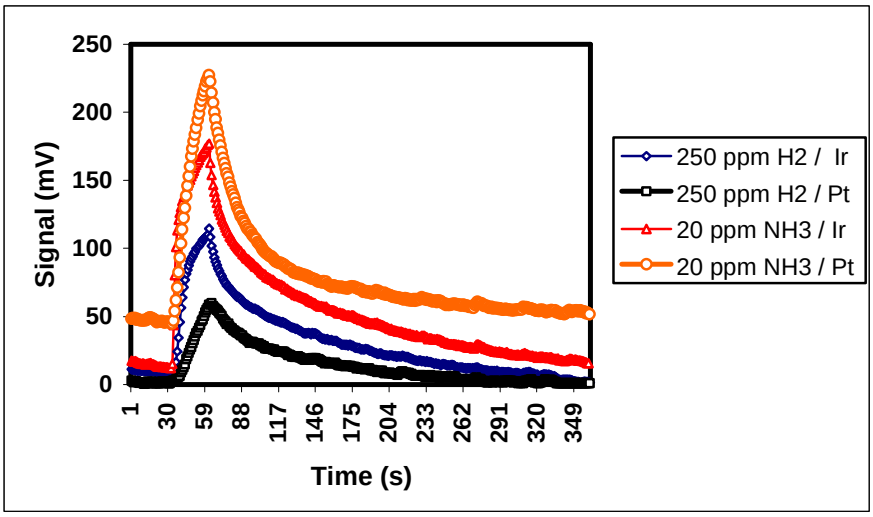

Figure 3.7. Gas response of two of the low-power micromachined MOSFET sensors to hydrogen (250 ppm) and ammonia (20 ppm) at a temperature of about 140°C.

In regard to the results obtained, the low-power MOSFET sensor is suitable for applications in electronic noses. Further investigations are needed to evaluate the effect of different temperature profiles during the gas

measurements in the aim of improving the gas sensitivity and selectivity. More measurements have to be performed before a conclusion can be drawn about the way the signal from the reference sensor can be used.

3.7 CONCLUSION

The design, fabrication and characterisation of a low-power consumption MOSFET array gas sensor has been presented. The sensor consists of a heating resistor, diode temperature sensor, and four GasFETs located in a silicon island thermally isolated from the chip frame by a dielectric membrane. The combination of microelectronics and MEMS (silicon micromachining) processing technologies was used to fabricate the sensor. The array of four GasFETs shows a low-power consumption of 90 mW at an operating temperature of 170°C. The low thermal mass of the device allows the operation of the sensors in a temperature cycling mode. Gas sensitivity of the micromachined device in this mode of operation is under evaluation. Moreover, we suggest that silicon-on-insulator (SOI) technology should be a good candidate to increase the working temperature of these sensors and to simplify the silicon micromachining process by having a precise control of the silicon thickness forming the island.

3.8 ACKNOWLEDGEMENTS

This work was partly done in the context of the Chemical Imaging for Automotive (CIA) project of the Brite-Euram III European program (contract

no°BRPR-CT96-0194) and in collaboration with the Swedish Sensor Centre (S-SENCE), Linköping University, Linköping, Sweden and Nordic Sensors Technologies (NST), Linköping, Sweden. The authors wish to thank the Fonds pour la Formation de Chercheurs et l'Aide à la Recherche (FCAR) from the Quebec Government for its financial support. The authors are grateful to the Institute of Microtechnology (IMT-samlab), University of Neuchâtel, Neuchâtel, Switzerland, and the S-SENCE technical staffs, respectively, for the help in the fabrication and the characterisation of these devices. The authors would like to thank Dr. Per Martensson from NST for useful discussions and also Dr. E. Scheid, Laboratory for Analysis and Architecture of Systems (LAAS), Toulouse, France, for performing the IR temperature measurements.

3.9 REFERENCES

[1] I. Lundström, M. S. Shivaraman, C. M. Svensson, and L. Lundkvist, "Hydrogen sensitive MOS field-effect-transistor", Apply Physics Letters, 26, pp. 55-57, 1975.

[2] I. Lundström, A. Spetz, F. Winquist, I Ackelid, and H. Sundgren, "Catalytic metals and field-effect devices – a useful combination", Sensors and Actuators, B 1, pp. 15-20, 1990.

[3] J.W. Gardner and P.N. Bartlett, Sensors and Sensory Systems for an Electronic Nose. The Netherlands, Kluwer Academic, 1992, pp. 303-319.

[4] I. Lundström, T. Ederth, H. Kariis, H. Sundgren, A. Spetz, and F. Winquist, "Recent developments in field-effect gas sensors", Sensors and Actuators, B 23, pp. 127-133, 1995.

[5] V. Demarne and A. Grisel, "An integrated low-power CO gas sensors on silicon", Sensors and Actuators, 13, pp. 301-313, 1988.

[6] S. Wessel, M. Parameswaran, S. R. Morrison, and R. F. Frindt, "A CMOS thermally-isolated heater structure as a substrate for semiconductor gas sensors", Microelectronics Journal, 23, pp. 451-456, 1992.

[7] J.S. Suehle, R.E. Cavicchi, M. Gaitan, and S. Semancik, "Tin oxide gas sensor fabricated using CMOS micro-hotplates and in-situ processing", IEEE Electron Device Lett., 14, pp. 118-120, 1993.

[8] U. Dibbern, "A substrate for thin-film gas sensors in microelectronic technology", Sensors and Actuators, B 33, pp. 63-70, 1990.

[9] D. Briand, A. Krauss, B. van der Schoot, N. Barsan, U. Weimar, W. Göpel, and N.F. de Rooij, "High temperature micro-hotplates for drop coated gas sensors", in Conf. Proc. of Eurosensors XIII, pp. 703-704, 1999.

[10] G. Faglia, E. Comini, A. Cristalli, G. Sberveglieri, and L. Dori, "Very low-power consumption micromachined CO sensors", Sensors and Actuators, B 55, pp. 140-146, 1999.

[11] A. Heilig, N. Barsan, U. Weimar, M. Schweizer-Berberich, J.W. Gardner, and W. Göpel, "Gas identification by modulating temperatures of SnO2 based thick film sensors", Sensors and Actuators, B 43, pp. 45-51, 1997.

[12] M. Jaegle, J. Woellenstein, T. Meisinger, H. Boettener, G. Mueller, T. Becker, and C. Bosh-v.Braunmühl, "Micromachined thin film SnO_2 gas sensors in temperature pulsed operation mode", in Conf. Proc. of Eurosensors XII, pp. 225-228, 1998.

[13] R.E. Cavicchi, J.S. Suehle, K.G. Kreider, M. Gaitan, and P. Chaparala, Optimized Temperature-Pulse Sequences for the Enhancement of Chemically Specific Response Patterns from Micro-Hotplates Gas Sensors, Sensors and Actuators, B 33, pp. 142-146, 1996.

[14] M.A. Gajda, H. Admed, and J. Dodgson, "CMOS-compatible silicon devices on thin SiO_2 membranes", Electron. Lett., 30, pp. 28-30, 1994.

[15] E.H. Klaassen, R.J. Reay, C. Stroment, and G.T.A. Kovacs, "Micromachined thermally isolated circuits", Sensors and Actuators, A 58, pp. 43-50, 1997.

[16] C. Hagleitner, A. Koll, R. Vogt, O. Brand, and H. Baltes, "CMOS capacitive chemical microsystem with active temperature control for discrimination of organic vapors", in Conf. Proc. of the 10th Int. Conf. Solid-State Sensors and Actuators (Transducers'99), pp. 1012-1015, 1999.

[17] K. Somogyi, "Some critical conditions of thermal breakdown in semiconductors", Sensors and Actuators, A 71, pp. 58-62, 1998.

[18] D. Briand, B. van der Schoot, S. Jeanneret, P.-A. Clerc, N.F. de Rooij, H. Sundgren, I. Grahn, and I. Lundströom, "Novel low-power consumption MOSFET array gas sensor", in Tech. Digest. of 10th Int. Conf. Solid-State Sensors and Actuators (Transducers'99), pp. 938-941, 1999.

[19] P. Arquint, Integrated Blood Gas Sensor for pO_2, pCO_2 and pH based on Silicon Technology, Thesis at the University of Neuchâtel, Switzerland, 1994, pp. 84-86.

[20] X. Li, M. Bao, and S. Shen, "Maskless etching of three-dimensional silicon structures in KOH", Sensors and Actuators, A 57, pp. 47-52, 1996.

[21] M. Bao, X. Li, S. Shen, and H. Chen, "A novel micromachining technology for multilevel structures of silicon", Sensors and Actuators, A 63, pp. 217-221, 1997.

[22] M. Wilander and H. L. Hartnagel, High temperature electronics. London, Chapman & Hall, 1997, pp. 67-119.

[23] D. Briand, M.-A. Gretillat, B. van der Schoot, and N.F. de Rooij, "Thermal management of micro-hotplates using MEMCAD as simulation tool", in Conf. Proc. of 3rd Int. Conf. on Modelling and Simulation of Microsystems (MSM'00), pp. 640-643, 2000.

[24] A. Götz, I. Gràcia, C. Cané, E. Lora-Tamayo, M.C. Horrillo, J. Getino. C. Garcia, and J. Gutiérrez, "A micromachined solid-state integrated gas sensors for the detection of aromatic hydrocarbons", Sensors and Actuators, B 44, pp. 483-487, 1997.

Paper IV

NEW MODES OF OPERATION FOR MOSFET GAS SENSORS USING LOW-POWER DEVICES

Danick Briand[1], Helena Wingbrant[2], Hans Sundgren[2], Bart van der Schoot[1], Lars-Gunnar Ekedahl[2], Ingemar Lundström[2], and Nicolaas F. de Rooij[1]

[1]Institute of Microtechnology, University of Neuchâtel,
P.O. Box 3, CH-2007 Neuchâtel, Switzerland
[2]S-SENCE and Laboratory of Applied Physics, Linköping University,
S-581 83 Linköping, Sweden

ABSTRACT

This communication presents new modes of operation for MOSFET gas sensors. A low-power micromachined device allows pulsing the temperature of MOSFET gas sensors with a time constant less than 100 ms. Cycling the temperature during the gas exposure modifies the kinetics of the gas reactions with the sensing film. The way the sensor response is modified by the temperature modulation depends on the nature of the analyte gas and of the catalytic sensing film. Pulsing the temperature up just after the gas exposure can reduce the recovery time for specific applications. Cycling the temperature can allow the discrimination between different gas mixtures. The small thermal mass of the device also enables to monitor the heat exchange in the presence of the sample increasing the amount of information obtained from MOSFET gas sensors.

Published in Conf. Proc. of Eurosensors XIV, Copenhagen, Denmark, Aug. 2000, pp. 737-740, manuscript in preparation.

4.1 INTRODUCTION

Miniaturisation and reduction of the power consumption were of primary interest in the field of gas sensors during the 90's. The micro-hotplate concept allows battery operation and the use of arrays, opening a route to the concept of portable electronic noses [1]. New modes of operation, such as pulsed or modulated temperature modes, were investigated for these small thermal devices. Using these modes, desorption of water, discrimination of gases in a mixture and lower power consumption were achieved [2-4]. These findings yield some information about how temperature changes affect to chemical reactions on a sensor surface. However, these modes of operation were mainly applied to metal oxide gas sensors [5].

In this paper, we report on the gas sensing properties of low-power micromachined MOSFET gas sensors operated in a modulated temperature mode. The design and fabrication of a low-power micromachined MOSFET gas sensor was reported recently [6]. The thermal isolation of electronic devices on a micro-hotplate has reduced the sensor power consumption to 90 mW for an array of four Gas-sensitive Field-Effect Transistors (GasFET) working at 170°C. The small thermal mass of these devices allowed the modulation of sensor temperature and the monitoring of the variation of the heat exchange in the presence of sample gases [7,8]. The modulated temperature mode of operation was used to reduce the sensor recovery time, and to discriminate between gases in a gas mixture using a single sensor. The low-power devices also bring new modes of operation for MOSFET sensors, the potential of which is discussed. The next section presents the basic sensing mechanisms of MOSFET sensors, an understanding of which is necessary to

explain the behaviour of these sensors in a modulated temperature mode of operation.

4.2 MOSFET SENSORS

4.2.1 Gas sensor characteristics

The gas sensor is in most cases not specific to a certain molecule. Many gaseous species can induce a sensor response. It is therefore not possible to determine the identity of a gas only by observing if the sensor gives a signal in its presence or not. Another important property of gas sensors is that they usually exhibit a non-linear response; the change in the response is not proportional to the change in the gas concentration. This non-linear effect is due to saturation. The number of available adsorption sites on the sensor surface is limited and the higher the concentration is, the smaller the fraction of total number of molecules will be able to adsorb on the surface. The temperature of the sensor surface also influences the response. The sensor sensitivity to a certain gas and sensor selectivity for the same gas can be modified by changes in its operating temperature. Chemical reaction rates, and therefore the sensor response and recovery time, also depend on temperature. Therefore, modulating sensor temperature may lead to variations in the chemical reaction kinetics. The results of this mode of operation applied to MOSFET sensors are presented in this paper.

4.2.2 MOSFET sensor characteristics

The GasFET sensor is a traditional MOS field effect transistor with a gas sensitive film, such as a catalytic metal, a polymer, or a metal oxide, as the gate material [9-12]. Only the case where a catalytic metal constitutes the gas-sensitive film will be discussed here. The hydrogen sensitivity of the sensor when using palladium as the gate material has been known for more than 25 years [13]. Extensive research has been performed since the introduction of the GasFET to understand the chemical reactions taking place on its surface and how to improve its performance. It has been shown that the sensitivity of the sensor depends on the nature of the catalytic metal, the structure of the metal film and the operating temperature [14]. By changing these parameters, the sensor has proven to be highly sensitive not only to hydrogen, but to a number of other gas species like ammonia and ethanol.

The typical structure of the sensor is schematically shown in Figure 4.1. The bulk material is made of p-doped silicon, in which there are two n-doped silicon regions, the source and the drain. An insulating layer of silicon dioxide forms a bridge between the source and the drain, on top of which the catalytic metal, the gate, is deposited. Due to the physical properties of silicon, the sensor can only be operated at rather low temperatures. The upper limit depends on the design and is usually of about 200°C.

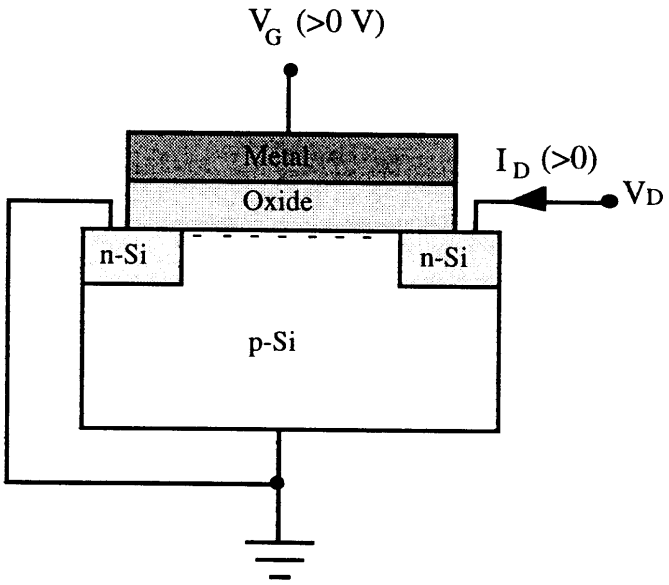

Figure 4.1. Schematic cross-section view of a MOSFET sensor structure.

The MOSFET sensor is operated with a constant current between the source and the drain, with the latter connected to the gate. During gas detection, the voltage between the source and the drain is measured, and the change in this voltage is recorded as the sensor signal. Molecules in a gas may interact with the catalytic surface and give rise to a shift in the current-voltage (IV) curve so that the voltage at a certain current decreases (Fig. 4.2.). The theory behind this is described in the next section.

4.2.3 MOSFET sensor response

Certain molecules have the ability to interact with the surface of the MOSFET sensor, causing a shift in the sensor operating voltage (at constant current) (Fig. 4.2). In the following, an explanation of this shift will be given, for the case where hydrogen is the gas being detected.

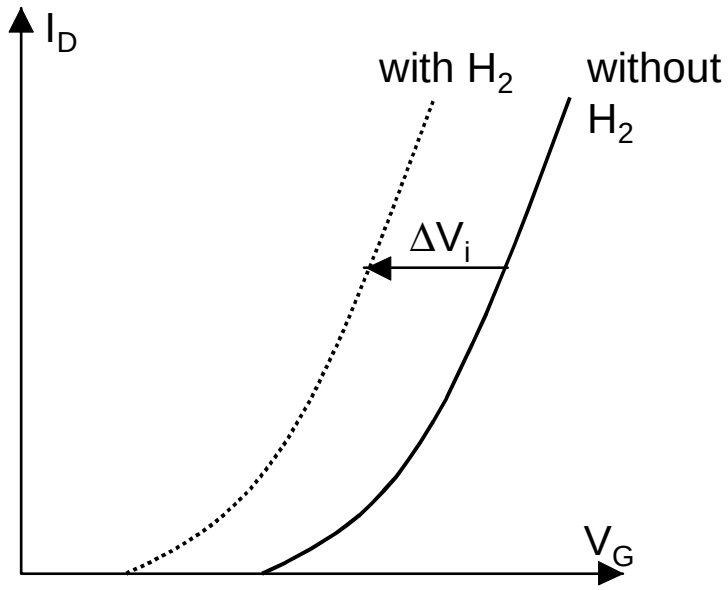

Figure 4.2. Shift in the IV curve of the MOSFET sensor due to its interaction with hydrogen.

When a flow of hydrogen molecules passes over the catalytic metal surface, a fraction of the molecules that contact the metal stick to it and dissociate on the outer surface. The hydrogen atoms then diffuse through the metal and enter the metal-insulator interface, the inner surface, where they become polarised. The hydrogen atoms preferably adsorb on the SiO_2 side of the surface rather than on the metal [11]. The polarisation gives rise to an increase in the electric field across the insulator and increases the concentration of electrons at the semiconductor surface. Since the sensor is operated at a constant current, this causes a decrease in the sensor voltage between the drain/gate and the source.
When a molecule contains a few hydrogen atoms, the voltage shift appears to be due to the ability of the catalytic surface to dehydrogenate the molecules. When dehydrogenation has occurred, the hydrogen atoms diffuse through the metal as in the case of pure hydrogen. The detection of this kind of molecule

is highly dependent on the temperature, though, since the dehydrogenation reaction will not occur unless sufficient energy is added.

A typical gas sensor response when exposed to a rectangular sample gas pulse is shown in Figure 4.3. The required time for the sensor response to reach a plateau may be of the order of several minutes. This time strongly depends on the type and the concentration of the gas, together with the type of catalytic metal and the operating temperature of the sensor. The plateau is commonly regarded as a steady state in the different chemical reactions taking place on the sensor surface.

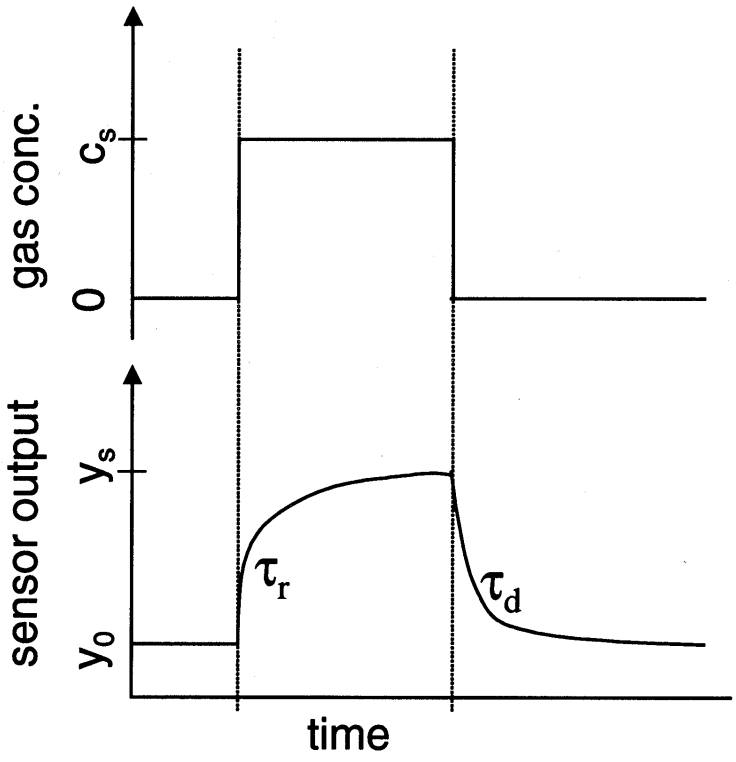

Figure 4.3. A typical transient sensor response when exposed to a rectangular gas pulse of test gas with height c_s. The sensor baseline value is y_0, the sensor output at sample gas off is y_s, and the sensor rise time and decay time are τ_r and τ_d, respectively.

The long rise time is believed to be due to the slow rates at which trapping of the molecules and chemical reactions on the surface occur, rather than the diffusion across the metal layer. The time it takes for the molecules to leave the surface, the recovery time, is even longer than the rise time. This time may be due to the same phenomena as for the rise time, but is also dependent on the large activation energy that is needed for the molecules to leave the metal-insulator interface [15,16]. The energy diagram with the heat of adsorption at the outer and the inner surface for hydrogen in a Pd-MOS device is presented in Figure 4.4 [17].

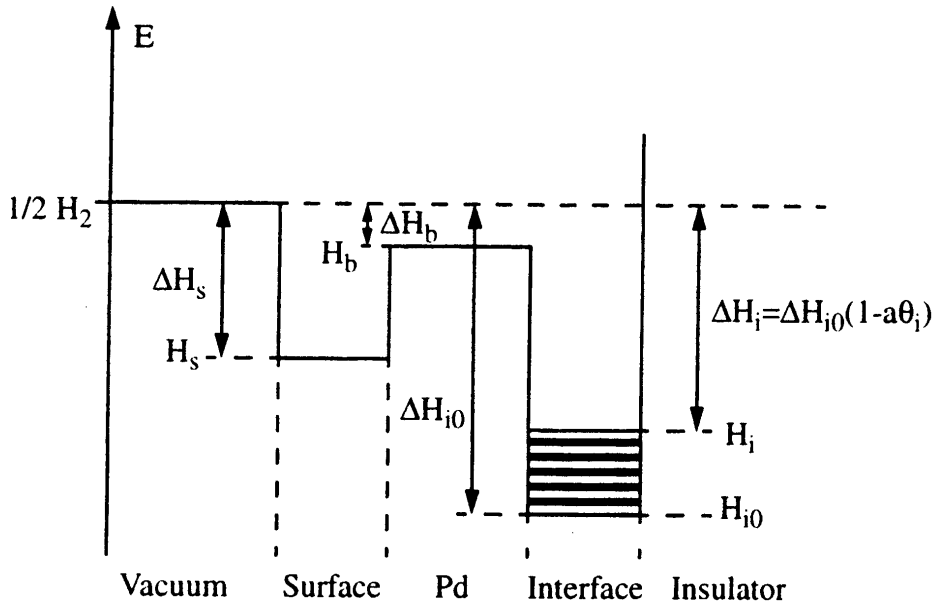

Figure 4.4. Energy diagram for hydrogen in Pd-MOS device. The heat of adsorption for hydrogen on the outer Pd surface is ΔH_s and the absorption potential for hydrogen into the Pd bulk is ΔH_b. The heat of adsorption for hydrogen at the Pd-insulator interface is ΔH_i [17].

4.2.4 Temperature dependence of the reaction kinetics

If air is present between or during the hydrogen gas pulses, this means that when hydrogen molecules reach the sensor surface, it is covered with oxygen atoms. The hydrogen atoms that stick to the surface and dissociate may then either react with the oxygen atoms on the surface to form water, or diffuse through the metal. The rate of all the reactions taking place on the sensor surface or at the interface between the metal and the insulator may be described as

$$r_{OH} = N\alpha\theta_O\theta_H \qquad (1)$$

where r is the reaction rate, N the number of available adsorption sites, α is the rate constant, and θ_O and θ_H are the fractions of all the available adsorption sites that are occupied by two types of molecules, oxygen and hydrogen [16]. θ_O and θ_H are also called the coverage of oxygen and hydrogen, respectively. When the coverage of both molecular oxygen and hydrogen, as in (1), is kept constant, the reaction rate depends on the temperature of the sensor surface through the rate constant:

$$\alpha = \upsilon \exp\left\{-\Delta E_{OH} \middle/ kT\right\} \qquad (2)$$

where υ is a frequency factor, ΔE_{OH} the required activation energy for a reaction between oxygen and hydrogen, T the temperature and k the Boltzmann constant [16]. This expression tells us that the rate constant will increase with increase of temperature, which means that the reaction will

become faster as the temperature rises. The reaction rates on the sensor surface are related to the number of molecules present at the metal-insulator interface. The expressions above can thus be related to the sensor signal. However, from this mathematical model, it is not easy to determine exactly how the sensor signal will behave when the temperature is changed. All reactions have different rate constants at a certain temperature. This is due in part to the different heat of adsorption for the different chemical species and adsorption sites. It should be also noted that adsorption sites at the interface are assumed to follow a Temkin isotherm [15]. In this isotherm, the heat of adsorption depends linearly on the coverage. This indicates that the influence of the change in temperature is also dependent on the degree of coverage on the surface at a certain instant.

It was mentioned above that the reaction rate depends on the temperature of the sensor surface through the rate constant, provided that the coverage of both molecule x and y are kept constant. This restriction was given to simplify the relation between the reaction rate and the temperature. However, the coverage of a molecule is also dependent on the temperature. This dependence is related to changes in the adsorption rate, the desorption rate and the reaction rate that occur when the temperature is altered. At a constant gas concentration and when the reactions on the sensor surface have reached equilibrium, the coverage of a molecule on a surface increases when the temperature is decreased [18].

4.2.5 Temperature modulation

4.2.5.1 General aspects

The effects of cycling or pulsing the temperature of MOSFET sensors have not been studied before, due to large thermal mass. However, the influence of the temperature on their sensitivity is well known.

An obvious advantage of using the new low-power MOSFET devices is that they offer the possibility to reduce the number of sensors used in a sensor array. A single sensor could be switched between different operating temperatures during the course of a measurement. This may give even more information about the species in the sample gas than in the case of different bulk sensors working at fixed, individual temperatures.

Also, when changing the temperature rapidly over time, the conditions for reaction of chemical species with each other and the surface are changed. Both low-temperature and high-temperature reactions will be favoured. Species that normally only exist at a low temperature may react with species that occur frequently at higher temperatures. The products from these reactions, or the high-temperature species themselves, may give rise to a change in the voltage shift. This will give impart new features to the sensor response.

However, it must be recalled that the electronic properties of MOS field-effect transistors are also a function of temperature. The main temperature-dependent parameters are the threshold voltage, the channel mobility, and the junction leakage currents [19]. Therefore, modulating the temperature changes the sensor signal even if no sample gas is present.

4.2.5.2 Reduction of the recovery time

A possible advantage of improving the performance of the MOSFET sensor through temperature modulation is to shorten both the sensor rise and recovery time. This is important e.g. for on-line monitoring. In typical operating conditions, the rise and recovery times for the bulk MOSFET sensor are both long, on the order of 30 and 320 s, respectively, so that a single measurement lasts more than five minutes. Faster measurements can be achieved by choosing the right temperature conditions for the reactions occurring on the sensor surface. As previously discussed in section 4.2.4, the rates of the reactions on the surface depend on the temperature, and are expected to increase with increasing temperature. The optimum conditions would probably be to operate the sensor at a high temperature, such as 300°C, throughout the measurement. This would make the molecules on the surface reach equilibrium faster. However, because of the degradation of the electronic devices, the sensor cannot be operated at such high temperatures for long periods of time. A solution to this problem would be to apply a short heating pulse at the beginning of the gas pulse and the recovery period (Fig. 4.5).

4.2.5.3 Discrimination of gas mixtures

In this work, a study of the information content in a sensor response operated in a cycled temperature mode is also presented. The aim was, firstly, to see if it was possible to discriminate between four gas mixtures by using only one sensor. Secondly, it was of interest whether rapid temperature cycling gave a signal with higher information content than slow temperature modulation.

Certainly, the effects of temperature cycling on the MOSFET sensor is of interest since it has not been studied before, but it is also important from another more practical aspect. When using the device in an electronic nose, purified air is applied between samples. This requirement leads to a test system which is technically more complex. However, if the device is operated in a cycled temperature mode at a constant sample gas flow, with at least the same amount of information being collected as when the sample gas is pulsed, the use of purified air would lose its importance.

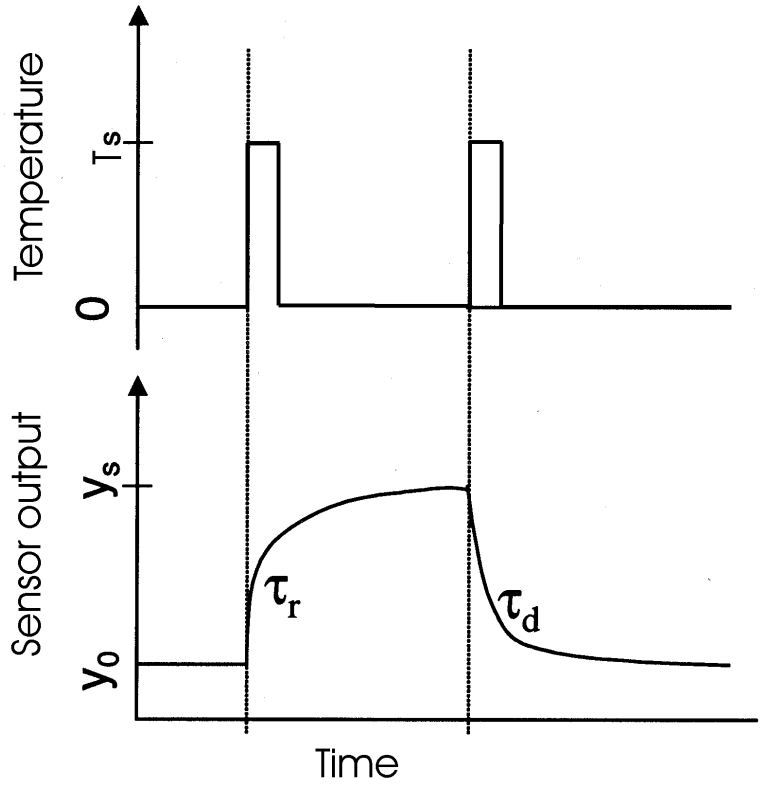

Figure 4.5. One possible way to shorten the rise and recovery time for the MOSFET sensor would be to apply temperature pulses shortly after the sample gas pulse has been either turned on or off.

4.3 EXPERIMENTAL

4.3.1 Low-power MOSFET array sensor

An array of 4 MOSFETs coated with different catalytic metals (GasFETs) was designed and fabricated (Fig. 4.6) [6]. The transistors have a channel length of 5 µm with W/L (width/length) = 30. They are suitable for gas sensing applications at temperatures up to 225°C.

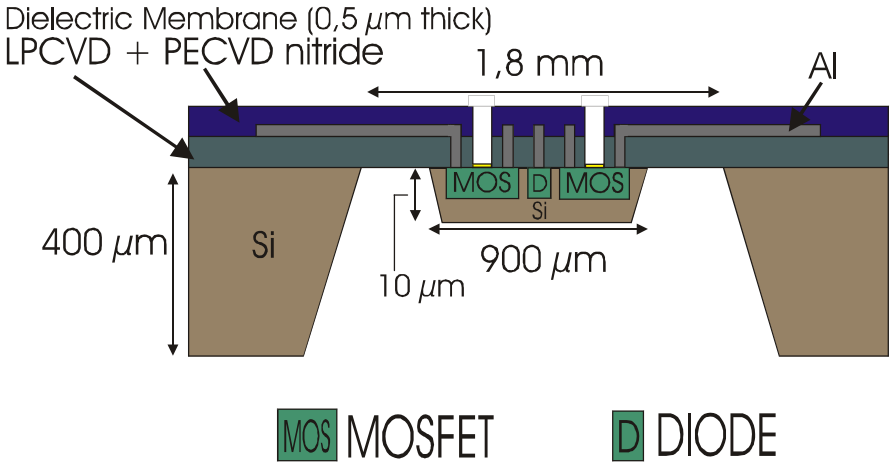

Figure 4.6. Schematic cross-section of a thermally isolated micromachined MOSFET array gas sensor.

The GasFETs composing the array have their gate insulator covered with catalytic metals: Ir/8nm, Pt/8nm and Pd/6.5nm. The fourth one has a gate made of Al and could act as a reference sensor. The low-power GasFET sensor is heated using an integrated silicon or platinum resistor with a thermal time constant of less than 100 ms. Platinum has the advantage that it allows operating temperatures higher than 200°C. The temperature of the array is monitored using an integrated diode.

4.3.2 Gas mixing system and acquisition set-up

The gas measurements were performed using the gas mixing system and electronic nose at the Swedish Sensor Centre (S-SENCE, Linköping, Sweden). Each sensor chip was mounted on a 16-pin socket and placed in a metal chamber with a gas inlet and outlet. The device was connected by an adapter to a printed circuit board, and the gas inlet and outlet were connected to the tubes of a gas mixing system.

The gas mixing system had a maximum flow capacity of 100 ml/min. The system made it possible to mix several different gases with a carrier gas. The printed circuit board contained the necessary electronics to measure the voltage from the diode and the sensors, and to apply well-defined currents and voltages to the components of the chip. The whole set-up was controlled using a PC, and the data acquisition was carried out using the software LabVIEW 5.1. The sensor chip temperature was controlled via a PID regulator and the maximum sample rate was 16 Hz. SensLab 10 (AppliedSensor AB, Sweden) and MatLab 5.3 (The MathWorks Inc., USA) were used for data evaluation.

4.3.3 Gas measurements

The background gas in all the measurements was synthetic air (Airliquide, Sweden), with a composition of 20% oxygen and 80% nitrogen (purity of 99,99%). The sample gases hydrogen (200, 100 and 25 ppm) and ammonia (40, 20, 10 and 5 ppm) were mixed with the synthetic air to achieve the desired concentrations. The work was limited to the study of hydrogen and ammonia since their effects on the sensor surface have been extensively studied [11,13-18], and they are known to produce the highest response in Pt

and Ir MOSFET sensors. A total flow of 100 ml/min was used. The length of the sample pulse was set to 30–60 s and the recovery time in the carrier gas to 320–420 s. These are typical values used for applications in an electronic nose. A current of 120 µA and 100 µA was used to drive the temperature sensor (diode) and the MOSFET sensors, respectively. The voltage on the heater could be changed with a maximum frequency of 16 Hz.

4.3.4 Standard gas response

The micromachined devices were first tested under the various gas atmospheres at constant operating temperatures, varying from 50 to 190°C. The upper limit was regarded to be low enough not to damage the device. The upper limits of the concentrations were chosen because higher concentrations yielded only small or virtually no changes in the final response, due to saturation of the sensor surface. The concentrations and temperatures that were found to maximise the final response were later used as basic settings in all other measurements.

4.3.5 Temperature modulation

The reduction of recovery time and the discrimination of gases in a mixture using MOSFET sensors in a modulated temperature mode were the two goals of the experiments described below. Square and sinusoidal temperature pulses were applied in the experiments. The response patterns under these modes of operation were recorded for different gaseous atmospheres (single sample gas or mixtures) for the sensors coated with Ir and Pt catalytic metals.

4.3.5.1 Minimising the recovery time

Square-shaped temperature pulses of different duration (in the range of 0.5 to 30 s) and height (in the range of 200 to 300°C) were applied 10 to 210 s after the end of the sample gas pulse. The duration of the sample gas pulse was 30 s. The time between two different sample gas pulses was 320 s. The gas mixing system caused a delay in the gas pulse of approximately 5 s. The gas was assumed to be completely finished from the tubes 10 s after it was shut off. This was the reason why the temperature pulse was applied at least 10 s after the gas pulse. These temperature pulses were also applied when no sample gas was present in order to study the effects of the temperature change on the sensor baseline.

4.3.5.2 Cycling the temperature to discriminate between gas mixtures

The aim in the second part of the work was to study the possibility of discriminating between four gas mixtures using one sensor. Only the sensor coated with Ir as catalytic metal was used in these experiments due to its higher level of response.

The sensor was operated in a constant flow of carrier gas (100 ml/min) with either one of the four gas mixtures presented in Table 4.1. The constant gas flow was chosen primarily for practical reasons. That is, it facilitated both the interpretation of the results and the handling of the gas mixing system. The temperature was kept constant at 180°C for 500 s in order to allow the reactions on the surface to reach equilibrium. After this period of time, the temperature was cycled for 2000 s with a sinusoidal waveform. Three sets of experiments with similar settings for this waveform were chosen. The

temperature range and frequency for these experiments are presented in Table 4.2. The limits of the temperature were chosen to be low enough to not damage the device.

Table 4.1. Types of gas mixtures used in the experiments with cycled temperatures.

Type of gas	**Gas concentrations in air (ppm)**			
	Mixture 1	**Mixture 2**	**Mixture 3**	**Mixture 4**
Hydrogen	0	100	0	100
Ammonia	0	0	10	10

Table 4.2. Properties of the sinus waves used in the experiments with cycled temperatures.

Sinus wave properties	**Experiments**		
	Set 1	**Set 2**	**Set 3**
Frequency (Hz)	0.01	0.25	0.01
Temperature range (°C)	150-200	150-200	100-200

Every gas mixture was measured three times in each set of experiments. This is the minimum number of measurements that is needed to make meaningful data evaluation possible. The experiments were made randomly in order to make memory effects less significant.

4.3.5.3 Data processing

The purpose of the first experiments was to minimise the recovery time by varying the values of the duration and magnitude of the temperature pulse. The sensor response was used for data evaluation. The voltage over the sensor with no gas sample present constituted the zero level. The voltage shift caused by the presence of a test gas was treated as a positive signal (Fig. 4.3). A change in sensor response is thus comparable to a change in the absolute voltage over the sensor. The sensor response increases when the voltage over the sensor decreases and vice-versa.

In the case of discrimination between gases, one measurement used for data evaluation consisted of the last 1000 s of each of the experiments (16000 variables). This was chosen mainly for two reasons: 1) the same number of variables was always available for data processing, 2) generally the signal required 1500 s to return to baseline. The data from each measurement was stored in a file, and Fourier transformed and visualised using the program SensLab. The software utilises Mathlab for performing calculations and has functions for computing fast-Fourier transform (FFT) and principal component analysis (PCA) plots [20,21]. The number of frequencies obtained from the Fourier transform was only half the number of points from the time domain, since half of the amplitude spectrum in the frequency domain is a mirror image of the other half. The absolute values of the complex-valued Fourier transform were used for PCA calculations. Both the data from the FFT calculation and the original samples from the time domain were visualised in PCA plots, and the most highly differentiating mode of operation for the sensor was determined.

4.4 RESULTS AND DISCUSSION

4.4.1 Standard gas response

On one hand, it was observed that scaling down the GasFETs and lowering their power consumption have had an effect on their gas sensitivity. This was slightly lower than for standard devices, but still in a useful range for gas detection. An explanation could lie in the processing steps used to fabricate the micromachined MOSFET gas sensors, which are different than those used for standard bulk sensors. The study of the influence of device fabrication on MOSFET gas sensitivity is in progress. The dependence of the final response on temperature and concentration of the two sample gases on the final response for the Ir sensor is shown in Figure 4.7.

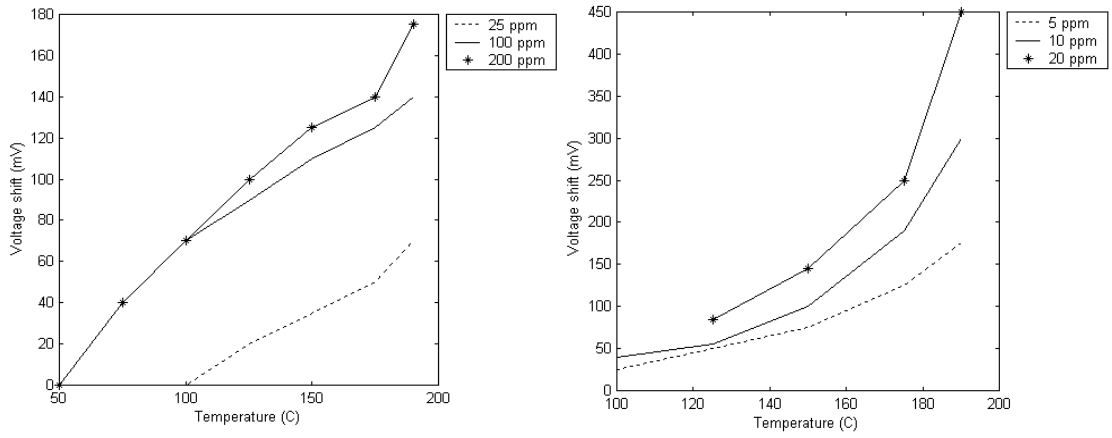

(a) (b)

Figure 4.7. Final response for the Ir sensor in (a) hydrogen and (b) ammonia (60 s gas pulse) as a function of temperature.

In the temperature range and gas concentration tested, no saturation of the response to hydrogen and ammonium occurred. The optimum gas response was obtained for a high working temperature. It was observed that the change in the shape of the response curve when the temperature was increased was slightly different from hydrogen to ammonia. The rise and recovery times generally became shorter at higher temperatures. However, it was not possible to draw similar conclusions for the sensors coated with Pt, due to their lack of reproducibility and stability.

4.4.2 Temperature modulation for minimising the recovery time

The working point of the MOSFET sensor, the voltage at constant current, depends on the nature of the catalytic metal and the operating temperature (section 4.2.5.1). Therefore, the sensor baseline (signal without sample gas) is expected to change during modulation of the sensor operating temperature. Another possible cause for this modification could be the piezoresistive properties of silicon, since the device membrane bends a few μm during its operation.

Modification of the response of a MOSFET sensor using a temperature pulse was recently reported [7]. Figure 4.8 shows the response of a MOSFET device when a square-shaped temperature pulse was applied randomly, overlapping the sample gas exposure (ammonia) and the recovery periods.

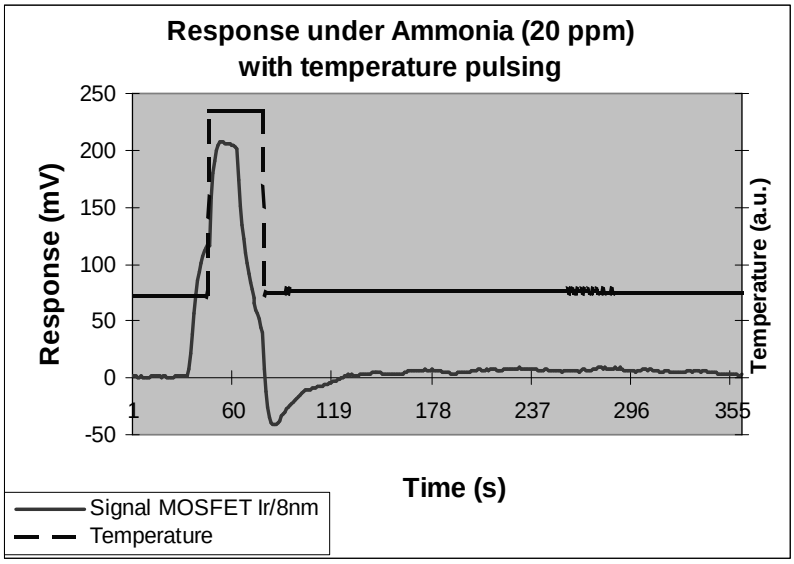

Figure 4.8. Modified response curve for a micromachined MOSFET sensor when a temperature pulse (45 s) was applied during the sample gas exposure (30 s) and recovery periods.

The curve obtained is clearly different than the usual response, schematically represented in Figure 4.3. It was observed that pulsing the temperature after gas exposure could accelerate the recovery time. However, some questions were raised regarding the effects that led to these first results. What were the contributions of the electrical and chemical effects produced by the temperature pulse to the modification of the sensor signal? What pulse length and height would be optimum to shorten the sensor recovery time? In the following sections, some mechanisms to explain sensor behaviour are discussed, and the results of recovery time minimisation presented for hydrogen and ammonia.

4.4.2.1 Pulsing of the temperature without sample gas

Square-shaped temperature pulses were applied to the sensors during the baseline (without sample gas) period, with the aim of determining the electrical contribution of the temperature pulse to the sensor response.

The Al sensor was first tested to determine the electrical contribution to the sensor signal when the temperature is pulsed. The Al sensor response increases with an increase of the temperature pulse (in fact, the voltage on the sensor goes down). At temperatures higher than 235°C, the shift in the sensor response can reach a few hundred milliVolts (Fig. 4.9), due to the leakage current increasing drastically in these devices [28].

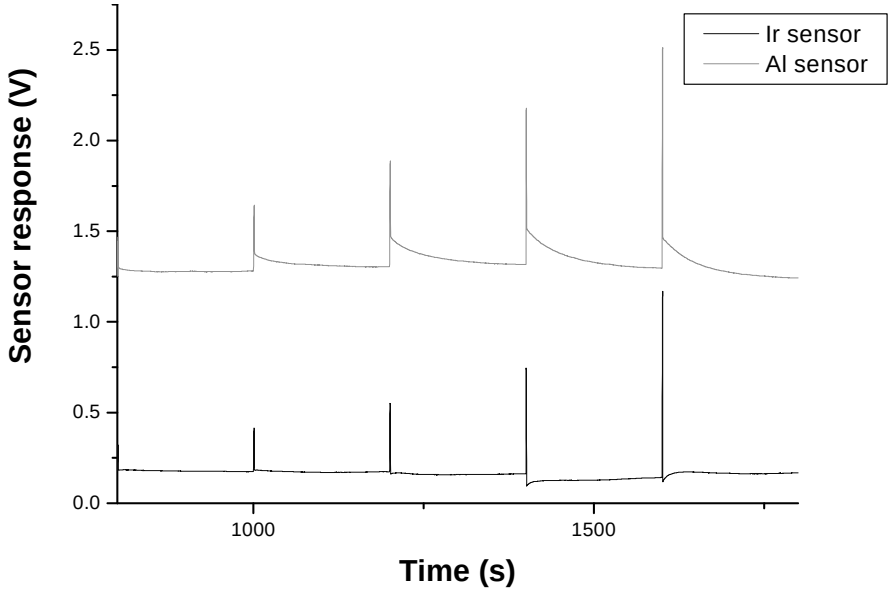

Figure 4.9. Application of temperature pulses (one second long, from 200 to 240, 250, 260 and 270°C, respectively) to on Ir and Al sensors in the absence of sample gas.

However, after the application of the temperature pulse, the Al sensor signal exhibits an unexpectedly large relaxation time. Some investigation is still required to identify the mechanisms related to this phenomenon.

The desired behaviour of the Al sensor was that it would give the same signal as the Ir sensor in pure synthetic air. This would have made it possible to erase the electrical effect of the temperature pulse on the Ir sensor response by using the Al sensor as a reference. However, the responses of the two sensors were not comparable. The long relaxation time constant was not observed for the Ir sensor. Moreover, the Ir sensor response sometimes dipped below the baseline after the pulse was applied, something that was not observed for the Al sensor (Fig. 4.9). Different Ir and Pt sensors were also used for studying the influence of the temperature pulse (Fig. 4.10).

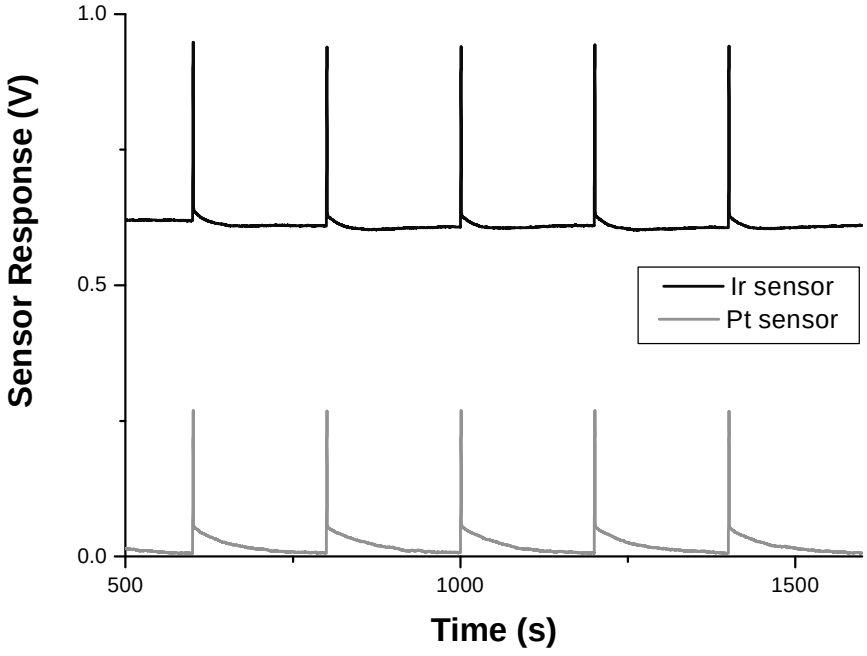

Figure 4.10. Application of temperature pulses (one second long, from 190 to 240°C) to Ir and Pt sensors in the absence of sample gas.

It was observed that the perturbation of the baseline caused by the temperature change was specific to each device, depending on its chemical 'state' (history) when the pulse was applied, and on the pulse shape. It was also noted that the temperature could cause positive or negative deviations in the baseline, as illustrated in Figure 4.11.

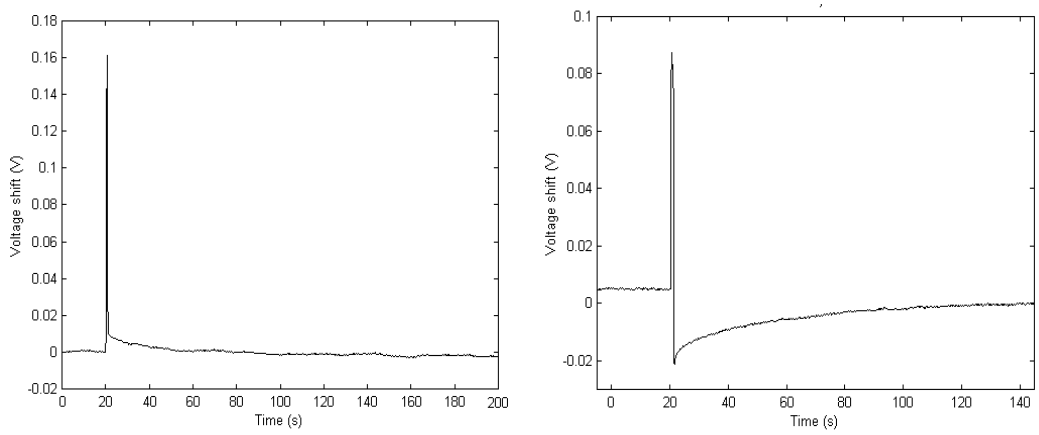

(a) (b)

Figure 4.11. Application of a temperature pulse (one second long, from 190 to 240°C) in the absence of sample gas caused either a (a) positive or (b) negative change in the baseline for an Ir sensor.

It was mentioned above (section 4.2.4) that the adsorption sites at the interface are assumed to follow a Temkin isotherm [15]. This indicates that the influence of the temperature change is also dependent on surface coverage at the time of application. This could explain the different behaviour of the Ir sensor noticed in Figures 4.9 and 4.11. Depending on the coverage of the outer surface (metal), transfer of chemical species to the inner surface (interface metal/insulator) (high coverage), or desorption of species to the outer surface (low coverage), could dictate response for a given shape of the temperature pulse (see Fig. 4.4.).

At the beginning of the temperature pulse, the energy transferred to the system would activate the adsorption of atoms in the background on the outer surface (see Fig. 4.4). However, if the temperature pulse is long or large enough, the desorption of chemical species from the inner surface would become predominant.

On one hand, since the temperature pulse is applied in air, the outer surface should be relatively clean, and the desorption of molecules from the inner surface should rapidly dominate. In this case, the inner surface, where the polarisation giving rise to the sensor signal occurred (section 4.2.3), is empty of hydrogen during the temperature pulse. When the temperature pulse is turned off, the sensor signal is lower and goes back to the initial value with a certain time constant due to reactions with molecules in the background (Fig. 4.11b).

On the other hand, when the outer surface is covered by chemical species, the transfer of these species to the inner surface will first dominate, and the sensor signal should slightly increase. If the temperature pulse is too short or small, the desorption will not occur more rapidly than adsorption at the inner surface. Therefore, the sensor voltage after application of the gas pulse would be slightly higher than before, as shown in Figure 4.11a.

When studying this effect on the Pt sensor, it was found that the dip in response was not present (Fig. 4.10). Unfortunately, it was not possible to speculate any further on the effect of the temperature modulation on Pt sensor response due to their lack of stability.

Applying a temperature pulse in the presence of carrier gas after a pulse of ammonia showed that the temperature pulse in itself caused a tailing of the sensor baseline (Fig. 4.14). The tailing lasted for more than 5 minutes, as the

baseline had to drop by about 250 mV to return to its original level. In this case, it was believed that some impurities remained in the tubing/sensing cell, so that the transfer of chemical species to the inner surface was predominant. It can be clearly seen from Figure 4.14 that the electrical effect of the temperature pulse was to cause a quick shift in sensor response of about 200 mV, and that the response continued to increase until the temperature pulse was switched off. Therefore, the sensor response dropped 200 mV due to the electrical effect upon termination of the pulse, but remained at a higher level than before, due to the increased coverage of chemical species at the inner interface.

This effect had made impossible to reproduce the results suggested in Figure 4.8, that the recovery time of the sensor after an ammonia gas pulse could be reduced by a temperature pulse. It is known that it is harder to interpret the chemical sensing mechanisms related to ammonia since the molecules tend to exhibit a "sticking" effect. The measurement set-up design would have to be reconsidered to improve the cleanliness of the system. However, the results obtained gave some indications about the nature of interactions between the chemical species and the gas sensor itself.

4.4.2.2 Minimising the recovery time in the presence of hydrogen

Hydrogen was chosen for the first set of experiments because hydrogen atoms are generally easier to remove from a sensor surface than ammonia (faster chemistry). An attempt was made to find a magnitude and duration of the temperature pulse that minimised the recovery time without taking perturbation profile into account. This kind of temperature pulse was tested only in the carrier gas for temperatures in the range of 200 to 300°C. In order

to decrease the induced Ir sensor baseline perturbation, the duration of the temperature pulse was lowered drastically to last for 0.5 to 4 s.

The resulting baseline shift was not as pronounced as for a pulse lasting 30 s, and was considered acceptable below temperatures of 240°C, where the amount of leakage current is significantly reduced. However, though a temperature pulse of 200°C did not induce any baseline shift, it was not powerful enough to increase reaction rates on the surface, since the sensor was operated at 190°C.

The outcome from all the tests was that a longer heat pulse (4 s) induced a disturbance that had a negative effect on the recovery time and a shorter pulse (0.5 s) did not seem to be long enough to decrease the recovery time. It was also clear that the minimum recovery time should be determined when the temperature pulse was higher than or equal to 240ºC. A question that remained was to determine when this temperature pulse should be applied in the recovery time period.

A temperature pulse of 240°C that lasted for 1 s was then applied 60 s after a pulse of 200 ppm hydrogen. It was found to cause a non-significant change in the sensor recovery time. In order to study more closely its effect on the response curve, the temperature pulse was applied as close to the gas pulse as possible in all further experiments. The reason for this was that the maximum final response was often between 50 and 100 mV, and the response decreased quickly after the gas had been shut off. The possible effect of a temperature pulse was more clearly visible if it was applied before many of the molecules had desorbed from the sensor. Finally, it was found that the minimum recovery time was observed when the duration of the pulse was 1 s, its height

50°C (from 190 to 240°C), and when it was applied 10 s after the sample gas has been shut off (Fig. 4.12).

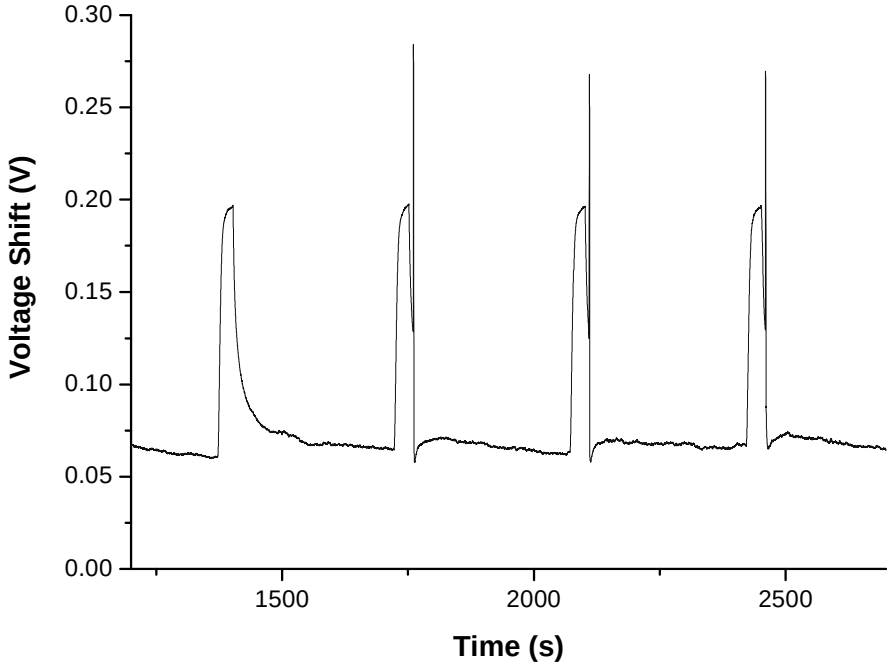

Figure 4.12. Ir sensor response at 190°C to 4 gas pulses of 200 ppm H_2 (30 s), first cycle with no temperature pulse after the gas pulse, following cycles with a temperature pulse to 240°C that lasted for 1 s and applied 10 s after the gas pulse,.

4.4.2.3 Minimising the recovery time in the presence of ammonia

The first attempt to decrease the recovery time of the sensor when exposed to ammonia was made using the same parameters tested for hydrogen. The influence of temperature pulses on ammonia was found to be negligible in all these experiments, which we explained, as previously mentioned, by the presence of the impurities remaining in the chemical background. In fact, a temperature pulse of 240°C that lasted for 4 s made the recovery time even

longer (Fig. 4.13). Shorter pulses at lower temperatures did not seem to have any effect on the response.

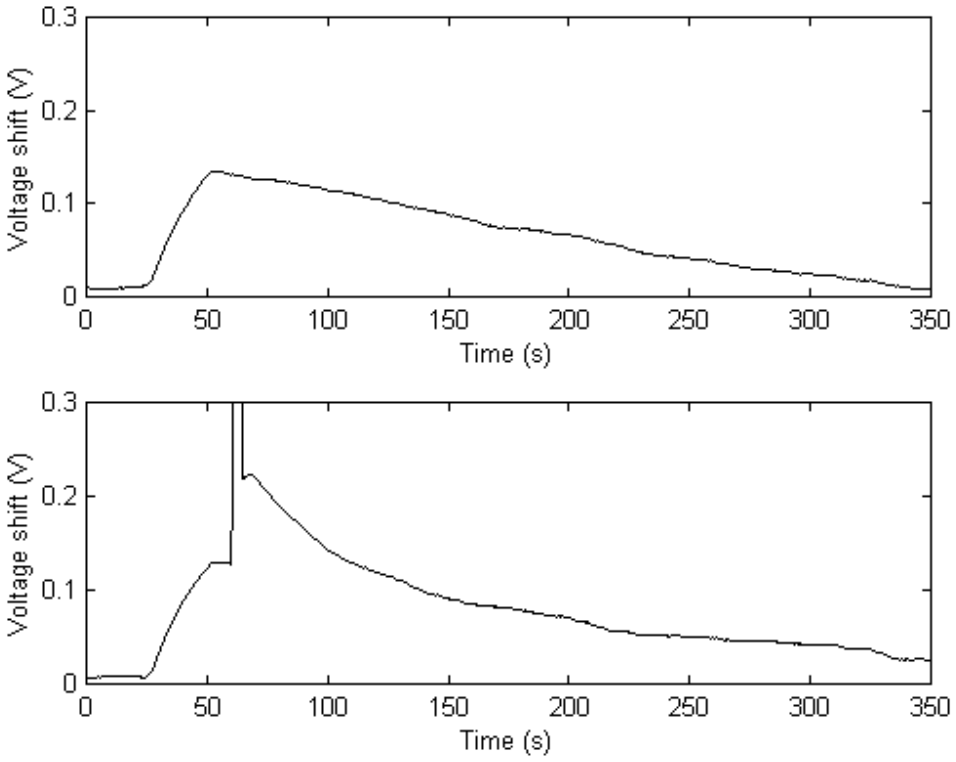

Figure 4.13. (a) No temperature pulse applied, sensor at 190°C (b) a temperature pulse of 240°C that lasted for 4 s was applied 10 s after a pulse of 20 ppm ammonia.

A longer temperature pulse than for hydrogen was therefore believed to be required to show the feasibility to decrease the recovery time. A temperature pulse of 230°C that lasted for 30 s was applied 210 s after the sample gas had been shut off (Fig. 4.14).

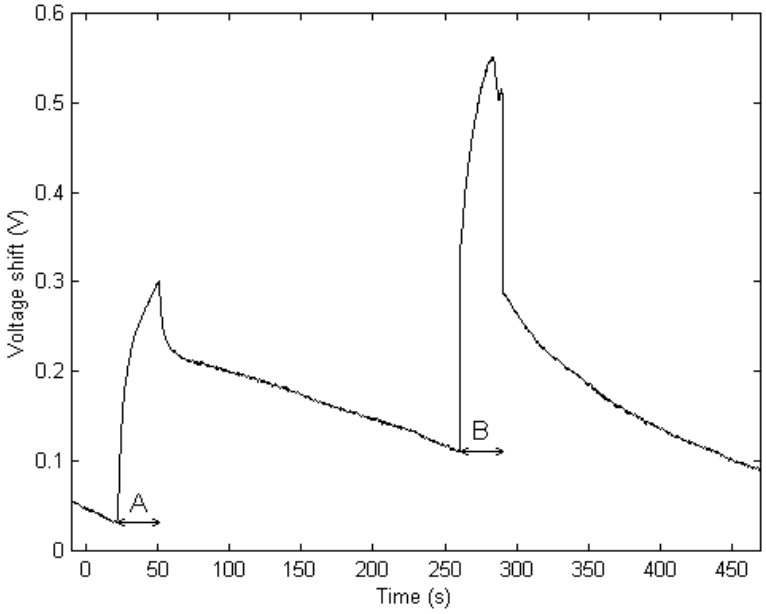

Figure 4.14. A temperature pulse (B) of 230°C that lasted for 30 s was applied 210 s after a pulse of ammonia (A) that lasted for 30 s. This caused an increase in the recovery time rather than a decrease.

When looking at Figure 4.14, it is apparent that the desorption of molecules occurred more rapidly after the temperature pulse was applied, but the significant shift of the sensor signal (250 mV) increases the recovery time. When the temperature pulse was applied, sensor response increased (chemical background effect, see section 4.4.2.1). However, during the last part of the temperature pulse, the sensor signal started to decrease, corresponding to a desorption of species from the inner surface dictating sensor response. This result confirms that a temperature pulse could reduce the recovery time of a sensor exposed to ammonia. In these experiment conditions, a longer temperature pulse could finally result in the desorption of species from the inner surface at a faster rate than their adsorption. Another solution could be to increase the temperature of the sensor pulse.

4.4.2.4 Discussion about temperature modulation for minimising the recovery time

Different effects were suggested to explain the behaviour of the sensor signal when the temperature pulse was applied either during the baseline or recovery period. They include electrical effects due to the intrinsic properties of MOSFET transistors, as well as chemical effects. A device with an aluminium gate was used to determine the electrical effects. The chemical effects were studied by applying a temperature pulse to a device coated with a sensing film in synthetic air. Different processes such as adsorption and desorption of chemical species seem to occur at the outer and inner sensor surfaces. By an adjustment of the temperature pulse length and height, the recovery time for hydrogen could be improved under specific conditions.

The recovery time for ammonia could not be improved in any of the experiments performed in this work. This is partly due to the fact that ammonia is difficult to remove from the tubes of the gas mixing system. This means that the long recovery time observed may be an effect of ammonia molecules slowly leaching from the tubes of the gas mixing system. This also explains why the recovery time was seemingly not improved by temperature changes on the sensor surface, since the adsorption of chemical species at the inner surface was greater than the desorption. The long rise and recovery times observed for ammonia may also be influenced by slow reaction rates. However, temperature variations are expected to affect these reactions more than what was seen in the experiments described here. Pulses that last for longer times or having higher temperatures might activate species desorption from the inner surface to a greater extent as shown in Figure 4.8.

These experiments were performed at a typical operating temperature for these sensors, 190°C. To avoid long term damage to the device and especially the strong baseline shift when the temperature pulse is applied, further tests should be performed at lower operating temperatures. The aim would be to reduce the temperature of the gas pulse to values where leakage currents are less apparent.

In summary, the figures presented in this section show that different kinetics can be obtained by varying the temperature during gas exposure, due to the dependence of the reaction constants on temperature. The way the sensor response is modified by a given temperature profile differs, depending on the nature of the sample pulse (analyte gas) and the sensing catalytic metal. Depending on the application, a temperature pulse applied after gas exposure could be used to shorten the sensor recovery time. Moreover, a modulated temperature mode of operation could be of interest for discrimination between gases in a mixture, as presented in the next section.

4.4.3 Temperature modulation for discriminating gas mixtures

As mentioned in section 4.3.5.2, only sensors coated with Ir as catalytic metals were investigated in these experiments to discriminate gaseous in mixture.

4.4.3.1 Results from the first set of experiments

Typical shapes of sensor voltage for each gas mixture from the first set of measurements (Table 4.2) can be found in Figure 4.15. Three similar measurements have been averaged and two complete temperature cycles have

been chosen. All the figures in this section present the absolute value of the sensor voltage.

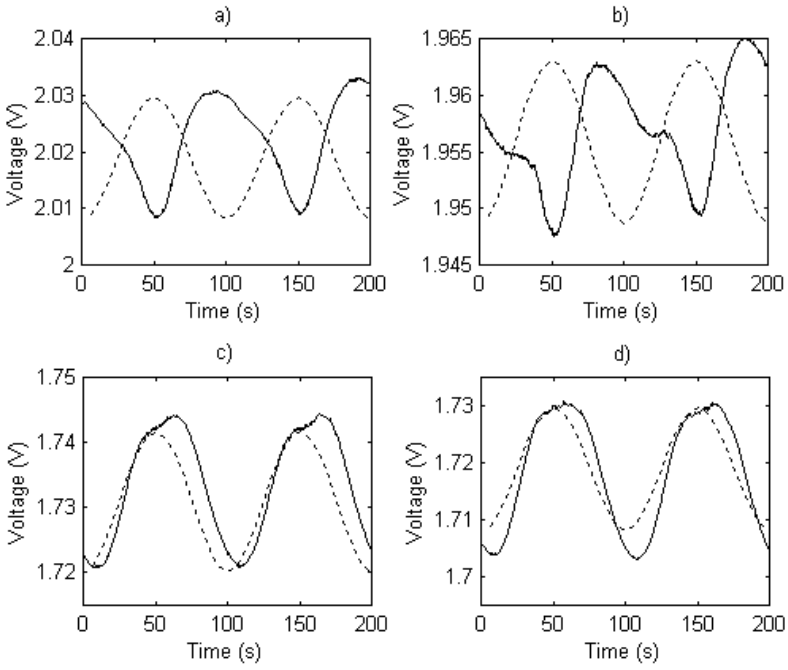

Figure 4.15. Ir sensor voltage (continuous line) at a temperature variation between 150 and 200°C at 0.01 Hz (dotted line) in the presence of (a) pure synthetic air, (b) 100 ppm H_2, (c) 10 ppm NH_3, (d) 10 ppm NH_3 and 100 ppm H_2.

As Figure 4.15a shows, the sensor voltage in the presence of synthetic air showed the same characteristics as expected when only electrical effects are influencing the voltage. That is, the sensor voltage reached its lowest value when the temperature was high and became high at a low temperature. The sensor voltage when 100 ppm of hydrogen was present was similar to the case with only synthetic air. A difference in its fluctuation appeared when the temperature was raised (Fig. 4.15b.). The samples with NH_3 were very similar to each other in that they both caused the same type of sensor voltage shift

compared to the temperature variation (Figs. 4.15c and 4.15d). The voltage increased when the temperature was high. The amplitude in these samples was slightly higher than when hydrogen alone was present. The voltage difference between the samples with NH_3 and those without NH_3 was in the range of 300 mV. This was larger than the difference in voltage between, for example, the samples with 100 ppm hydrogen and those with only synthetic air.

The waveforms were further investigated by using the measurements made only in synthetic air as a reference for all the other measurements (Fig. 4.16). The absolute value of the sensor voltage in the presence of pure synthetic air was subtracted from the absolute values of all the other measurements. The three runs for each mixture were averaged before the calculation was done. The negative voltages in Figure 4.16 are due to the sensor voltage in the reference signal being higher than in all other measurements.

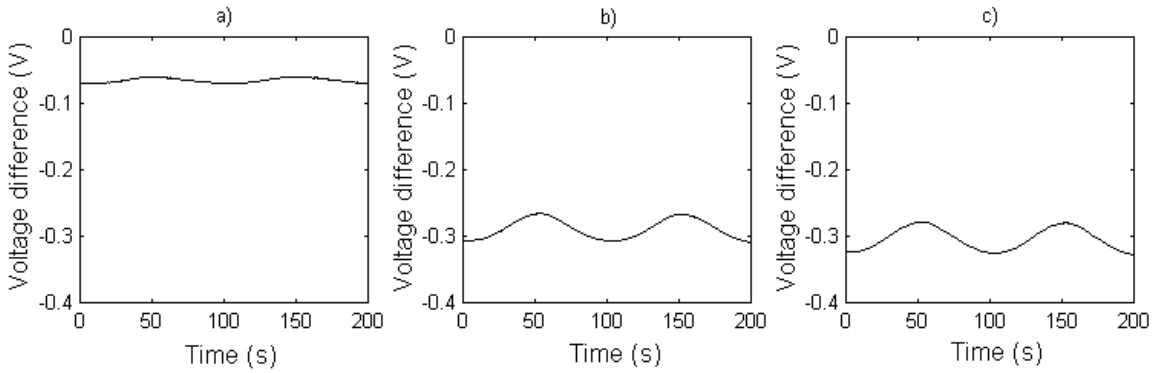

Figure 4.16. Normalised Ir sensor voltage for an operating temperature cycled between 150 and 200°C at 0.01 Hz using synthetic air as a reference for (a) 100 ppm H2, (b) 10 ppm NH_3, and (c) 100 ppm H_2 and 10 ppm NH_3.

These results showed that even the sensor voltage in the presence of hydrogen reached its highest value when the temperature was high. It should also be noted that all the normalised voltage curves have a shape that resembled to a sinusoidal waveform. The differences between the normalised sensor outputs suggest that it could be possible to discriminate between samples with a pattern recognition method. To investigate this further, the data was Fourier transformed and visualized in PCA plots. The PCA plots obtained, with the variables plotted as distinct times and as frequencies, can be found in Figure 4.17.

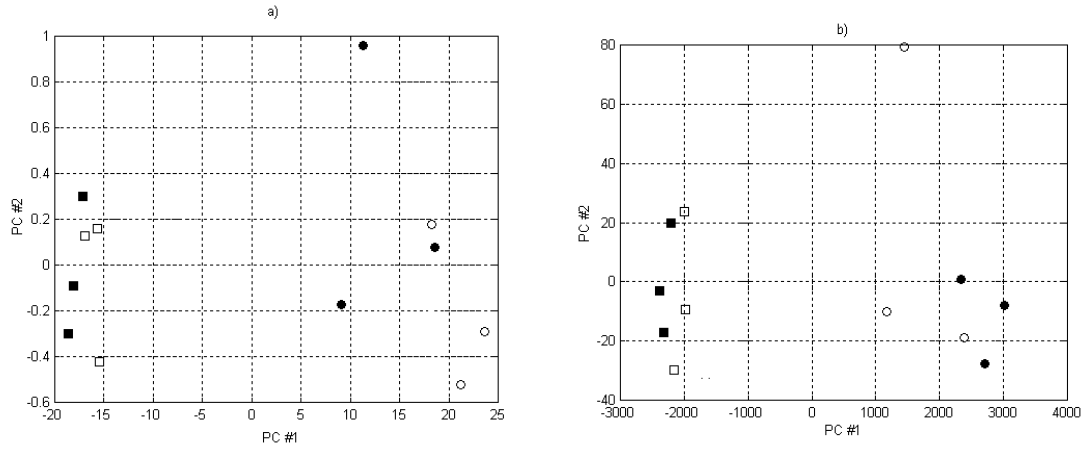

Figure 4.17. PCA plots from the data in the first set of the experiments using (a) distinct times and(b) frequencies from the Fourier transform as variables. ●: Pure synthetic air. ○: 100 ppm H_2. □: 10 ppm NH_3. ■: 100 ppm H_2 and 10 ppm NH_3.

A rule of thumb for determining if it is possible to build a valid Partial Least Squares (PLS) or Artificial Neural Networks (ANN) model from the data is that it should be possible to draw straight lines between the groups in the PCA plots. As it can be seen in the plots, the discrimination between different gas mixtures was poor for both choices of variables and no straight lines could be

drawn between the groups. There was a clear distinction between the samples with ammonia and the samples without ammonia. However, there was no separation between the groups within these two categories.

4.4.3.2 Results from the second set of experiments

In order to improve the discrimination, a second set of experiments was performed. In these experiments, the frequency of the sinusoidal temperature modulation was increased to 0.25 Hz. It turned out that the shorter period of the waveform changed the behaviour of the recorded signals. Firstly, the amplitude of all the voltages decreased. Secondly, the NH_3 curves no longer exhibit their apparent phase shift. However, when using the synthetic air measurement as a reference, it turned out that most of the phase shift still remained in all the samples (Fig 4.18).

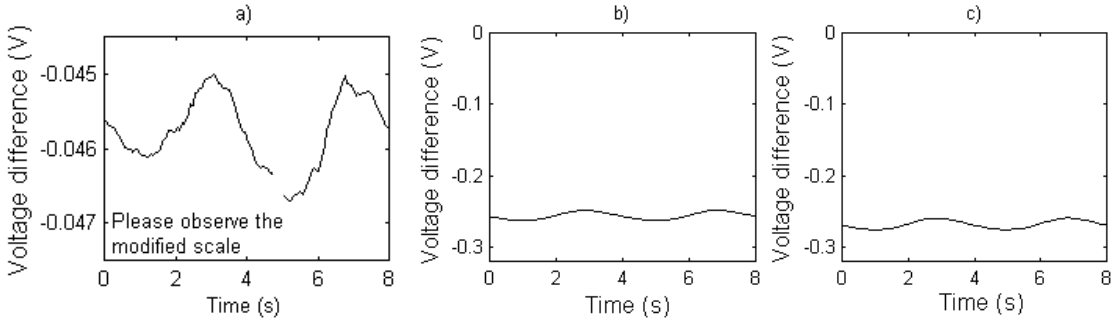

Figure 4.18. Normalised Ir sensor voltage for an operating temperature cycled between 150 and 200°C at 0.25 Hz using synthetic air as a reference for (a) 100 ppm H_2, (b) 10 ppm NH_3, and (c) 100 ppm H_2 and 10 ppm NH_3.

The data from these measurements were processed and visualised in PCA plots as for the first measurements. The changed frequency of the temperature modulation did not improve the separation between the groups.

4.4.3.3 Results from the third set of experiments

In the third set of experiments, the temperature range was 100 to 200°C and the frequency 0.01 Hz. The extended temperature range was expected to increase the amount of information obtained from the reactions at the sensor surface. They would therefore yield better discrimination between the gas mixtures. However, the voltage curves from these experiments looked almost identically as in Figure 4.15. Most of the features from the first set of experiments seemed to be preserved. Normalised sensor voltages when using synthetic air as a reference signal can be seen in Figure 4.19.

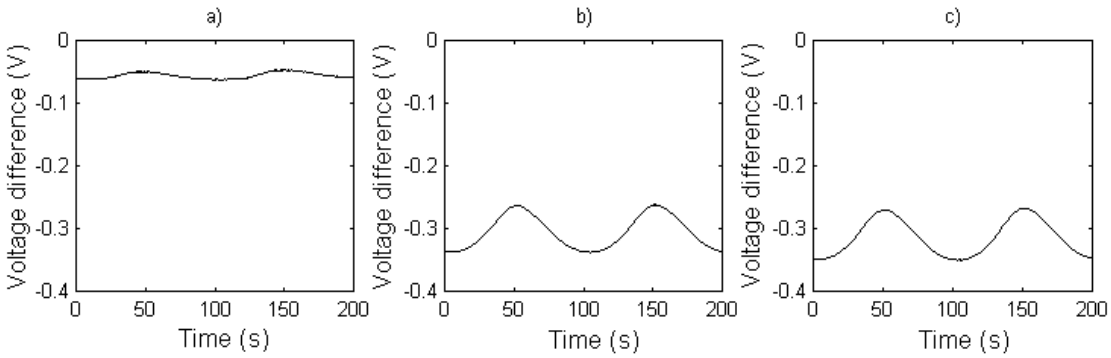

Figure 4.19. Normalised sensor voltages for an operating temperature cycled between 100 and 200°C at 0.01 Hz using synthetic air as a reference for a) 100 ppm H_2 b) 10 ppm NH_3 and c) 100 ppm H_2 and 10 ppm NH_3.

The data from these experiments were visualised in PCA plots in a manner similar to the two earlier data sets. The PCA plot that was based on discrete

samples from the time domain did not show any improvements with regard to the ability to discriminate between the gas mixtures (Fig. 4.20a). However, a separation was obtained between the groups of measurements that had been Fourier transformed. The separation was good enough to make it possible to draw straight lines between the gas mixtures, as can be seen in Figure 4.20b. The differences between these groups of measurements were not large, but the possibility of drawing lines between the groups implies that the four types of gases may be separated. However, the number of measurements for each gas sample was small.

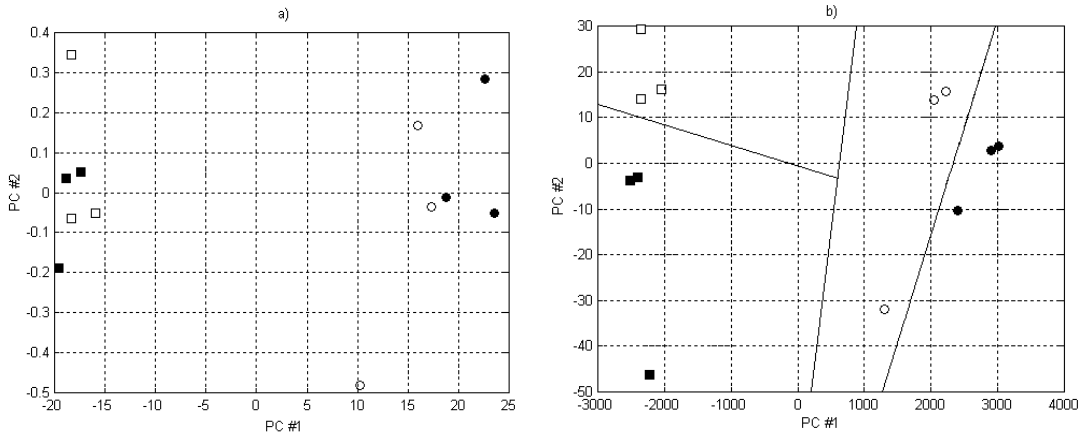

Figure 4.20. PCA plots from the data in the third set of experiments using (a) distinct times, and (b) frequencies from the Fourier transform as variables. ●: pure synthetic air. ○: 100 ppm H_2. □: 10 ppm NH_3. ■: 100 ppm H_2 and 10 ppm NH_3.

4.4.3.4 Discussion about temperature modulation for gas mixture discrimination

It should be emphasised that the sensor voltage patterns obtained in the cycled operating mode were different from those from the experiments described in

section 4.4.2, as they were obtained at constant gas concentrations (no sample gas pulse). This means that the sensor voltage pattern from each experiment was not dependent on the gas concentration but only on the change in temperature. It should also be noted that the absolute value of the sensor voltage, instead of the voltage shift, was used in all these experiments for both data visualisation and evaluation.

An increase in the temperature decreases the voltage over a sensor operated in synthetic air. This is due to the electrical effect of the temperature on the sensor. However, operating the device in a cycled temperature mode in the presence of a sample gas adds a chemical effect to the sensor voltage. This effect can be studied separately if the sensor voltage is normalised by subtracting the sensor voltage in synthetic air is subtracted from the sensor voltage in the presence of a sample gas (Figs. 4.16, 4.18 and 4.19). In these experiments, the effect of the sample gas was larger at a low temperature than at a high temperature. This means that the total coverage of test gas molecules reached its lowest value at a high temperature. This is in accordance with previous theoretical findings [18].

The normalised voltage from the sensor decreases when the frequency of the sinusoidal waveform is increased. This implies that the reactions on the sensor surface are too slow for this frequency. They do not get enough time to reach their original value after every period. It was originally thought that this mode of operation would yield better discrimination between the gas mixtures than a slower modulation of the temperature, but that result was not achieved.

When studying the samples in the time domain, it is clear that the samples with 10 ppm NH_3 (with or without hydrogen) lie very close to each other. The same is true for samples without ammonia. The same behaviour is observed in

the PCA plot. The separation between samples with and without NH_3 is very good, but not within these groups. The small difference between samples of just synthetic air and both synthetic air and hydrogen implies that not many hydrogen atoms interfere with the sensor surface. This also explains why the difference between the NH_3 samples is very small. The separation between the four groups of measurements would probably have been better if the sensors have been more sensitive to hydrogen.

As could be seen in the PCA plot from the third set of experiments, when using frequencies as variables, it was possible to draw straight lines between the four groups of measurements. The separation between the four gas mixtures was better when frequencies from the Fourier transform were used instead of distinct times. This may be due to the ability of the FFT to extract useful information from the signals linked to the shape of the voltage curve. The time domain yields mostly information about the difference in voltage between the four curves. However, the distance between the groups in the corresponding PCA plot was rather small, and more measurements are required in order to determine the validity of this result. This small distance and measurements over a long period would probably be sufficient for differentiating between the four gas mixtures using a pattern recognition method like PLS or ANN.

4.5 OULOOK FOR OTHER MODES OF OPERATION

Further experiments are underway to evaluate the potential of this new information, with the aim of applying these modes of operation for specific gas-sensing applications. With the low-power micromachined MOSFET gas,

new ways of combining different gas sensing principles using different modes of operation emerge. The results obtained indicate that an “intelligent” combination of sample and temperature pulses could be used to expand the information content in sensor response considerably. In the following paragraphs, a few possibilities will be described.

4.5.1 Thermal/calorimetric sensor

The small thermal mass MOSFET sensor opens up the opportunity to monitor the heat exchange during exposure to a gas. This parameter could contain relevant information for applications such as electronic noses [22]. The heat exchange during gas exposure is produced by chemical reactions between the analyte gases and the catalytic metals, and/or by the heat transfer by convection between the sensor surface and the gaseous atmosphere. The latter is due to the change in thermal conductivity of the ambient atmosphere when impurities are introduced. It was previously shown that traces of certain gases could be identified using thermal sensors [23,24].

In our case, it could be useful to combine the heat exchange effect due to chemical reactions and the field-effect to improve the selectivity of MOSFET gas sensors. From a practical point-of-view, this means that the power needed to keep the MOSFET sensor at a constant temperature has to be monitored.

Moreover, an array of hotplates could be designed to combine the low-power MOSFET with thermal sensors and microcalorimeters. In this way, information could be obtained about the thermal conductivity of the gases and the enthalpy changes during the chemical reactions. Depending on the location of the microcalorimeters and MOSFET sensors, a distributed chemical sensor

system could be made, in which the gas mixture would be modified along the flow direction as described in ref. [25].

4.5.2 Combination of thermal/calorimetric, resistive and field-effect sensing mechanisms

Moreover, a gas-sensitive polymer or a metal-oxide film could replace the gate material [9,10,12]. In order to obtain more information, the resistance of the film could be monitored under various gaseous atmospheres to obtain a resistive, calorimetric, and field-effect gas-sensing device.

4.5.3 Operating at high temperature, sensing at low temperature

Since the more stable gaseous compounds (e.g. NO_2, hydrocarbons) require higher temperatures to be decomposed by the catalytic metals, another mode of operation to investigate would be pulsing of the device temperature at temperatures higher than the working temperature of the transistors (>200°C). As an example, at higher temperatures hydrocarbons would in general be decomposed to release hydrogen, which diffuses through the catalyst layer to reach the metal/insulator interface, where they absorb to form electric dipoles [11]. By cooling the temperature rapidly to a normal operating temperature (140-170°C), the signal given by the MOSFET gas sensor could contain information about these compounds. The desorption of the adsorbed hydrogen is in most cases slow enough to allow a sufficient amount of hydrogen to remain after the cooling period [15]. Typical recovery time constants of the devices at 140-170°C are of the order of 1-10 s (see Fig. 4.12).

4.5.4 Self-heating mode of operation

The low-thermal mass of these devices means that they could be used as self-heating MOSFET gas sensors. The MOSFET could be used as heater and as field-effect gas sensor at the same time. However, it would be harder to separate the thermal and field effects in this operational mode, since both have a direct influence on MOSFET electrical parameters. Considering the actual design, high voltages would also be needed to meet the power requirement (90 mW / 4 = 22.5 mW per MOSFET) and to keep the MOSFET drain current as low as possible. Some additional drift problems might appear. To lower the power consumption, more precise microelectronics and micromachining processes could be used to scale down the MOSFET and the silicon island [6]. Another way to accomplish this would be to use the silicon-on-insulator (SOI) technology as proposed in the next paragraph.

4.5.5 Silicon-on-insulator technology

The use of SOI technology allows the fabrication of micro-hotplates with a reduced silicon island thickness. We have shown that the power consumption and the thermal time constant could be reduced by at least a factor 2 and 5, respectively, for the same array on micromachined SOI substrates [26]. Moreover, MOSFETs made on SOI could operate at higher temperatures, up to 300-350°C [27]. Concerning the self-heating mode, the MOSFETs on SOI could be thermally isolated by the local oxidation of silicon (LOCOS). They could therefore be locally self-heated, in contrast to devices made on standard silicon, in which the whole silicon island is heated.

4.6 CONCLUSION

A low-power micromachined device allows new modes of operation for MOSFET gas sensors. The working temperature of the sensor can be modulated with a time constant smaller than 100 ms. Modulation of the temperature during gas exposure modifies the kinetics associated with gas response mechanisms. The different response patterns obtained in these modes of operation depend on the analyte sensed and on the catalytic sensing film.

A pulse of the sensor temperature after gas exposure can reduce its recovery time under specific operating conditions. A competition between the adsorption of chemical species from the outer to the inner surface, and their desorption from this inner surface, was suggested as an explanation of the sensor response behaviour. Cycling the temperature can allow discrimination between different gas mixtures, with effective resolution at a temperature modulation of 'low' frequency and large amplitude. The data were Fourier transformed before the evaluation was done. Further experiments are underway to evaluate further the potential use of these effects, with the aim of applying these modes of operation for specific gas sensing applications.

Other possible modes of operation were discussed. The small thermal mass could allow monitoring of the heat exchange during gas exposure, increasing the amount of information obtained from MOSFET gas sensors. SOI technology was also suggested as a good candidate to improve the performance of MOSFET gas sensors, by allowing higher temperatures of operation, lower power consumption, and smaller thermal time constants.

4.7 ACKNOWLEDGEMENTS

This work was done in collaboration with the Swedish Sensor Centre (S-SENCE) and Applied Sensor (former NST), both located in Linköping, Sweden. We wish to thank AppliedSensor and the Fonds pour l'aide aux Chercheurs et à la Recherche (FCAR), from Quebec Government, for their financial support. We are grateful to the IMT-samlab, Institute of Microtechnology, Neuchâtel, Switzerland, and the S-SENCE technical staffs respectively for technical support in the fabrication, and for the characterisation of these devices. We would like to thank Dr. Per Martensson and Tomas Eklöv from AppliedSensor, and Dr. Anita Lloyd-Spetz, Dr. Mats Eriksson and Martin Holmberg from S-SENCE for useful discussions.

4.8 REFERENCES

[1] I. Simon, N. Barsan, M. Bauer, and U. Weimar, "Micromachined metal oxide gas sensors: Opportunities to improve sensor performance", Sensors and Actuators, B 73, pp. 1-26, 2001.

[2] R.P Lyle, H.G. Hughes, and D. Walters, "Micromachined silicon CO gas sensors", in Conf. Proc. Microstructured and microfabricated systems III, 191st ECS Meeting, pp. 188-198, 1997.

[3] A. Heilig, N. Barsan, U. Weimar, M. Scheweizer-Berberich, J.W. Gardner and W. Göpel, "Gas identification by modulating temperatures of SnO_2-based thick film sensors", Sensors and Actuators, B 43, pp. 45-51, 1997.

[4] G. Faglia, E. Comini, A. Cristalli, G. Sberveglieri, and L. Dori, "Very low power consumption micromachined CO sensors", Sensors and Actuators, B 55, pp. 140-146, 1999.

[5] A.P. Lee and B.J. Reedy, “Temperature modulation in semiconductor gas sensing” Sensors and Actuators, B 60, pp. 35-42, 1999.

[6] D. Briand, H. Sundgren, B. van der Schoot, I. Lundström, and N.F. de Rooij. A low-power micromachined MOSFET gas sensor, Journal of Microelectromechanical Systems, 9(3), pp. 303-308, 1999.

[7] D. Briand, B. van der Schoot, H. Sundgren, L.-G. Ekedahl, I. Lundström, and N. F. de Rooij, “New response patterns for MOSFET gas sensors using low-power devices”, in Conf. Proc. of Eurosensors XIV, pp. 737-740, 2000.

[8] H. Wingbrant, 'The effect of temperature modulation on a low-power MOSFET gas sensor', diploma work LITH-IFM-Ex-942, Linköping University, 2001, 52 pp.

[9] M.G.H. Meijerink, M. Koudelka-Hep, N.F. de Rooij, D.J. Strike, W. Olthuis, and P. Bergveld, “Gas-dependent field effect transistor with an electrodeposited conducting polymer gate contact”, Electrochemical and Solid-State Letters, 2, pp. 138-139, 1999.

[10] S.K Andreeva and L.I. Popova, “Modelling the gas-sensing behaviour of SnO_2-gate FETs”, Sensors and Actuators, B 19, pp. 540-542, 1994.

[11] I. Lundström and L.-G. Peterson, “Chemical sensors with catalytic metal gates”, J. Vac. Sci. Technol., A 14, pp. 1539-1545,1996.

[12] J.A. Covington, J.W. Gardner, D. Briand, and N. F. de Rooij, “A polymer gate FET sensor array for detecting organic vapours”, Sensors and Actuators, B 77, pp. 155-162, 2001.

[13] I. Lundström, S. Shibaraman, C. Svensson, and L. Lundkvist, “A hydrogen-sensitive MOS field-effect transistor’, Applied Physics Letters, 26 (2), pp. 55-57, 1975.

[14] I. Lundström, T. Ederth, H. Kariis, H. Sundgren, A. Lloyd Spetz, and F. Winquist, “Recent developments in field-effect gas sensors”, Sensors and Actuators, B 23, pp. 127-133, 1995.

[15] L.-G. Ekedahl, M. Eriksson, and I. Lundström, “Hydrogen sensing mechanisms of metal-insulator interfaces”. Accounts of Chemical Research, 31, pp. 249-256, 1998.

[16] M. Johansson, I. Lundström, and L.-G. Petersson, “Kinetic modelling of the H_2-O_2 reaction on Pd and of its influence on the hydrogen response of a hydrogen sensitive Pd metal-oxide-semiconductor device”, Surface Science, 350, pp. 91-102, 1996.

[17] M. Johansson, I. Lundström, and L.-G. Ekedahl, “Bridging the pressure gap for palladium metal-insulator-semiconductor hydrogen sensors in oxygen containing environments”, Journal of Applied Physics, 84 (1), pp. 44-51, 1998.

[18] L.-G. Petersson, H.M. Dannetum, J. Fogelberg, and I. Lundström, “Hydrogen adsorption states at the external and internal palladium surfaces of a palladium-silicon dioxide-silicon structure”, Journal of Applied Physics, 58 (1), pp. 404-413, 1985.

[19] F. Schoucair, W. Hwang, and P. Jain, “Electrical characteristics of large scale integration (LSI) MOSFETs at very high temperatures, Part I: Theory”, Microelectronics and Reliability, 24 (3), pp. 465-485, 1984.

[20] R.G. Brereton, “Fourier transform: use, theory and applications to spectroscopic and related data”, Chemometrics and Intelligent Laboratory Systems, 1, pp. 17-31, 1986.

[21] K.R. Beebe, R.J. Pell, and M.B. Seasholtz, Chemometrics – A practical guide, New York, Chichester, Wiley, USA, 1998.

[22] J. Lerchener, D. Caspary, and G. Wolf, “Calorimetric detection of volatile organic compounds”, Sensors and Actuators, B 70, pp. 57-66, 2000.

[23] C.K. Saul and J.N. Zemel, “Diode-based microfabricated hot-plate sensor”, Sensors and Actuators, A 65, pp. 128-135, 1998.

[24] M.A. Gajda and H. Ahmed, “Applications of thermal silicon sensors on membranes”, Sensors and Actuators, A 49, pp. 1-9, 1995.

[25] T. Eklöv and I. Lundström, “Gas mixture analysis using a distributed chemical sensors system”, Sensors and Actuators, B 57, pp. 274-282, 1999.

[26] D. Briand, O. Guenat, B. van der Schoot, T. Hirata, and N.F. de Rooij, "Micro-hotplate, a useful concept for gas-sensing, fluidics and space applications", in Conf. Proc. of Microfabricated systems and MEMS V, 198th ECS Meeting, pp. 151-158, 2000.

[27] J.P. Colinge, Silicon on insulator technology: materials to VLSI, 2nd Ed. Kluwer academic publisher, 1997, 272 pp.

[28] D. Briand, H. Sundgren, B. van der Schoot, I. Lündström, and N.F. de Rooij, "Thermally isolated MOSFET for gas-sensing application", IEEE Electron Device Letters, 22(1), pp. 11-13, 2001.

Paper V

THERMAL OPTIMISATION OF MICRO-HOTPLATES HAVING A SILICON ISLAND

Danick Briand, Stephan Heimgartner, *Marc-Alexis Grétillat,

Bart van der Schoot, and Nicolaas F. de Rooij

Institute of Microtechnology, University of Neuchâtel,
P.O. Box 3, CH-2007 Neuchâtel, Switzerland
*currently at Intersema Sensoric SA, Bevaix, Switzerland

ABSTRACT

Thermal measurements and electrothermal simulations (FEM) were performed in the aim of optimising the power consumption and the temperature distribution of micro-hotplates for gas-sensing applications. A silicon island was added underneath the micro-hotplate's membrane to improve the temperature distribution of drop-coated metal oxide gas sensors and to thermally isolate MOSFET gas sensors. The temperature distribution over the sensing area and the power consumption depend on the silicon island thickness, which was optimised for both applications using the software MEMCAD from Microcosm Technologies. The thermal conductivity of silicon and dielectric membrane, the operating temperature, the geometry and the area of the heater, and the processing of the silicon island were considered

Published in Conf. Proc. Of 3rd Int. Conf. on Modelling and Simulation of Microsystems, San-Diego, California, U.S.A., March 2000, pp. 640-643, manuscript in preparation.

in the optimisation process. The thickness of the silicon island was optimised to ensure a good temperature distribution over the gas-sensing area for metal-oxide and MOSFET gas sensors with specific geometry.

5.1 INTRODUCTION

Micro-hotplates are of great interest in the gas sensor field since they allow reduction of the power consumption and new modes of operation [1-3]. The main device characteristics which require optimisation are the power consumption, the temperature distribution over the sensing area, and the device robustness. They operate generally at high temperatures (i.e. 200-450°C) and heat losses are generated by conduction through the membrane, by radiation and by convection in the surrounding atmosphere. Different authors have reported on the modelling of the thermal behaviour of micro-hotplates [4-7]. In this paper, the focus is on the optimisation, based on finite element modelling (FEM), of the power consumption of micro-hotplates having a silicon island with the aim of achieving a uniform temperature distribution over the sensing area.

We have recently reported on fabrication and characterisation of micro-hotplates for gas-sensing applications [8,9]. A 10-µm thick silicon island was added underneath the micro-hotplate's membrane, using a two-step bulk micromachining process, to improve the temperature distribution of drop-coated metal-oxide gas sensor. The design also allowed the integration of electronic devices and was used to lower the power consumption of MOSFET gas sensors. Here, we report on thermal measurements and electrothermal FEM simulations to optimise the thickness of the silicon island, with the aim

of reducing the power consumption of these micro-hotplates and still have a homogeneous temperature distribution over the gas sensing area. A uniform temperature over the sensing area would improve the gas sensitivity and selectivity of the sensor. A decrease of the silicon island thickness would facilitate the use of standard etch stop techniques for its fabrication.

A FEM simulator is a useful tool to determine the thermal behaviour of these devices. So far, the main CAD packages used for this purpose were ANSYS [10,11], SESES [12], COSMOS [13], and SOLIDIS-ISE [14]. In this work, the silicon island thickness was optimised using the MEMCAD (4.8) FEM simulator from Microcosm Technologies, Inc [15]. The Mechanical-Electro-Thermal module, MemETherm, was used to simulate the thermal behaviour of the devices. This Joule heating module computes the thermal and electrical potential field distributions resulting from an applied voltage or current through a resistive element. The mechanical coupling was not included in the simulations, though this could be of interest when designing thermal actuators [16]. The simulation manager, SimMan, was used to investigate the influence of silicon island thickness and thermal conductivity on the thermal properties of the micro-hotplates. Infrared (IR) thermal measurements were performed, and the results combined with those from the simulator to determine the physical parameters necessary for the simulations.

5.2 DESIGN AND FABRICATION

5.2.1 Micro-hotplates for metal-oxide sensors

The micro-hotplates for the metal-oxide gas sensors consisted of a heater sandwiched in between a membrane and an insulator, on top of which sensing electrodes were integrated. A low-stress LPCVD silicon nitride film was used as membrane and insulator, which thermally isolates the heated sensing area from the silicon chip frame as illustrated in Figure 5.1.

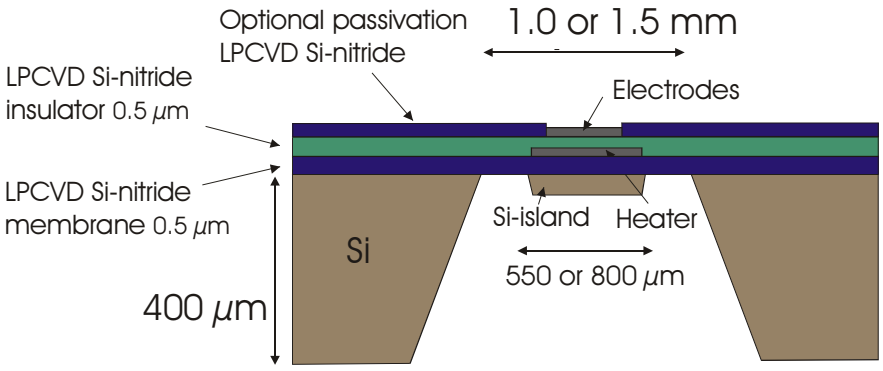

Figure 5.1. Micro-hotplate with a silicon island for metal-oxide gas sensors.

A two-step silicon bulk micromachining process was used to release the dielectric membrane and to define the 10-µm thick silicon island. The thickness was limited at 10 µm since the fabrication process does not provide precise control over the remaining thickness of the silicon island remaining after the second etching step. The heater (100 Ω at 0°C) and the electrodes (sensing area) were made of platinum (TCR=0.00185/°C). More details concerning the design and fabrication of these micro-hotplates with and without silicon island are presented in Ref. [8].

The gas sensitivity of a metal-oxide sensor to a specific reducing or oxidising gas is spread over a certain temperature range. Since the electrodes are completely covered with the metal-oxide, a temperature gradient as small as possible is needed over the whole sensing area to improve their selectivity. In the case investigated here, a temperature gradient of less than 10°C is considered as ideal. Moreover, these micro-hotplates can withstand operation at high temperatures (up to 700°C), and allow the annealing "on chip" of the gas-sensitive material used in the drop-coating process [8]. Therefore, the temperature distribution over the gas-sensing area is an important parameter to optimize, so that the gas-sensitive material can be annealed in the same way as in a belt oven, where temperature gradients are minimised. With an optimized temperature gradient for the hotplate, it should be possible to achieve the same gas-sensing characteristics using both annealing techniques.

5.2.2 Micro-hotplates for MOSFET sensors

The micro-hotplates with thermally isolated Gas-sensitive Field-Effect Transistors (GasFETs) also have a membrane made of low-stress LPCVD nitride, which was released using a two-step silicon micromachining process as described above [8]. An array of 4 MOSFET gas sensors was located in the silicon island, thermally isolated from the chip frame (Fig. 5.2) [9].

The array was surrounded by a heater laid out in a U-shape. The heater resistor was made either of doped silicon or evaporated platinum. A diode was used as temperature sensor. The metallisation was made of aluminium and covered with a PECVD silicon oxynitride film. Windows were opened over the MOSFET gate oxides and gas-sensitive catalytic metals, such as Ir, Pt and

Pd, were deposited to form the GasFETs. Since many sensor arrays can be used at different temperatures, as in electronic noses, the temperature gradient between the 4 sensing areas covered by the catalytic metals (size of 60 × 70 μm^2) has to be minimized. A temperature gradient less than 10°C has to be reached, 5°C is considered as an ideal value.

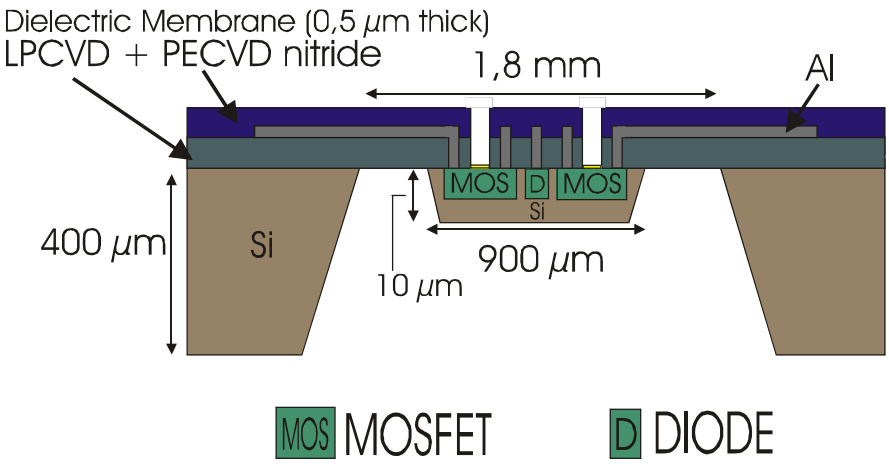

Figure 5.2. Schematic cross-sectional view of a micro-hotplate for MOSFET gas sensors. The electronic components are located in a silicon island thermally isolated from the silicon chip.

5.3 EXPERIMENTAL

5.3.1 Characterisation

The device temperature was measured using an infrared (IR) camera AVIO 2100, with a pixel resolution of 12.5 × 20 μm^2. IR thermal measurements of the micro-hotplates were performed in both an ambient atmosphere and in vacuum. The dependence of the resistance on the applied voltage and on the

maximum temperature at the center of the heater under these conditions was monitored. Then, from these results, the temperature coefficient of the resistance (TCR) was calculated. Finally, using the value of the resistance at room temperature, and the TCR, the relation between the power consumption and the temperature was obtained. This way, the problem of the determination of material emissivity was avoided.

Because of the camera pixel size being similar to heater width and this difficulty of determining a value of emissivity for the materials in the different regions, precise mapping of the temperature over the whole heated area was rather difficult. It was concluded that simulations could yield more reliable results about the temperature distribution if the thermal properties of the materials were defined.

5.3.2 Optimisation and simulation

For the metal-oxide gas sensors, the temperature distribution over the sensing area of micro-hotplates without silicon islands was first investigated. Different heater geometries such as simple and double meander were studied (Fig 5.5). It was found that the power consumption was lowered by adjusting the membrane and heater size, but this was not the main goal of the work presented here. As mentioned before, the focus was on the optimisation of the hotplates having a silicon island. Membranes having two sizes were considered: 1.0×1.0 mm^2 and 1.5×1.5 mm^2, with a heater/sensing area of 450×450 μm^2 and 750×750 μm^2, respectively. In the case of the MOSFET gas sensors, the geometry was fixed, with 1.5×1.5 mm^2 for the membrane

and $750 \times 750\ \mu m^2$ for the active area, since the technology used in house for the processing did not allow for a higher density of integration [8].

The thickness of the silicon island was optimised for both types of micro-hotplates staking hotplate geometry and fabrication into account. Simulations were performed to determine the minimum thickness of silicon necessary to have a uniform temperature distribution over the sensing area. The boundary conditions and the parameters were set as follows:

- The chip frame temperature was set at 30°C in accordance with the IR observations;
- The heat was dissipated by convection in the gaseous atmosphere on the front ($h = 250\ W \bullet m^{-2}K^{-1}$) and backside ($h = 125\ W \bullet m^{-2}K^{-1}$) surfaces of the membrane [12];
- The thermal conductivity (k) of the silicon rich LPCVD nitride film was set in the range of 3.2–22 $W \bullet m^{-1}K^{-1}$, of platinum at 71 $W \bullet m^{-1}K^{-1}$, and of silicon between 50 and 150 $W \bullet m^{-1}K^{-1}$, depending on its level of doping [11,12,18-20];
- An operating temperature in the range of 200-400°C was considered for the metal-oxide sensors;
- A maximum operating temperature of 200°C was considered for the MOSFET sensors;
- To simplify the simulation, the heater was made of platinum sandwiched in between nitride films for both types of devices.
- The temperature gradient in the z direction and the radiation were considered negligible [3,12];

- The forced gas flow, used for instance in electronic noses, was assume to have no influence on the temperature distribution [17];
- The dependence of the thermal conductivity on temperature was not considered;

The different designs on which the simulations were performed are described in Table 5.1. S1 and S2Si correspond to two types of metal-oxide micro-hotplate, without and with a silicon island, respectively. S2Si without silicon island is named S2. S3Si is the only design investigated for the MOSFET micro-hotplate.

Table 5.1. The different designs simulated for metal-oxide and MOSFET micro-hotplates with and without silicon island.

	S1	S2Si*	S3Si
Sensor type	Metal-oxide		MOSFET
Membrane area (mm^2)	1.0 × 1.0	1.5 × 1.5	1.5 × 1.5
Sensing area (μm^2)	450 × 450	750 × 750	750 × 750
Si-island area (μm^2)	———	800 × 800	800 × 800
Membrane thickness (μm)	0.25 + 0.75		0.25 + 0.25
Pt-heater geometry	Simple and double meander		U-shape
Pt-heater thickness (μm)	0.25		

*S2Si without silicon island is named S2

5.4 RESULTS AND DISCUSSION

5.4.1. Thermal measurements

The thermal measurements were performed on micro-hotplates for metal-oxide and MOSFET sensors [8,9]. Here, the results are presented only for the micro-hotplates for metal-oxide sensors since there was no variation of the dimensions for the MOSFET sensors (design S3Si only, see Table 5.1).

At an operating temperature of 300 °C, the power consumption of the micro-hotplates without silicon islands was of about 50 mW for the 1.0 × 1.0 mm^2 design (S1) and of about 75 mW for the 1.5 × 1.5 mm^2 (S2). The lower power consumption of the micro-hotplates with a membrane area of 1.0 × 1.0 mm^2 could be explained by their smaller heating area, which reduces the absolute heat lost by convection. A way to optimise the power consumption would be to minimise the heating area in relation to the membrane size as shown in refs. [3,10-12]. In the review published by Simon et al. [3], ratios of 2.6 and 3.0, corresponding to the radius of the heated area to the radius of the membrane, are given for minimum power consumption. In our case, this would mean combining a heating area of 500 × 500 μm^2 with a membrane size of 1.5 × 1.5 mm^2. However, in a commercial production, a compromise between the power and the density of integration has to be reached.

The power consumption for micro-hotplates having a 10-μm thick silicon island (S1Si and S2Si) was about 45% higher at an operating temperature of 300°C. At a given operating temperature, the heat dissipated while maintaining a uniform temperature over the sensing area would be lowered by optimising the thickness of the silicon island to be less than 10 μm.

In the case of the metal-oxide micro-hotplates without silicon islands (S1, S2), the thermal observations indicated that the temperature distribution over the sensing area was more homogeneous for the double meander heater than for the simple meander (Fig. 5.3).

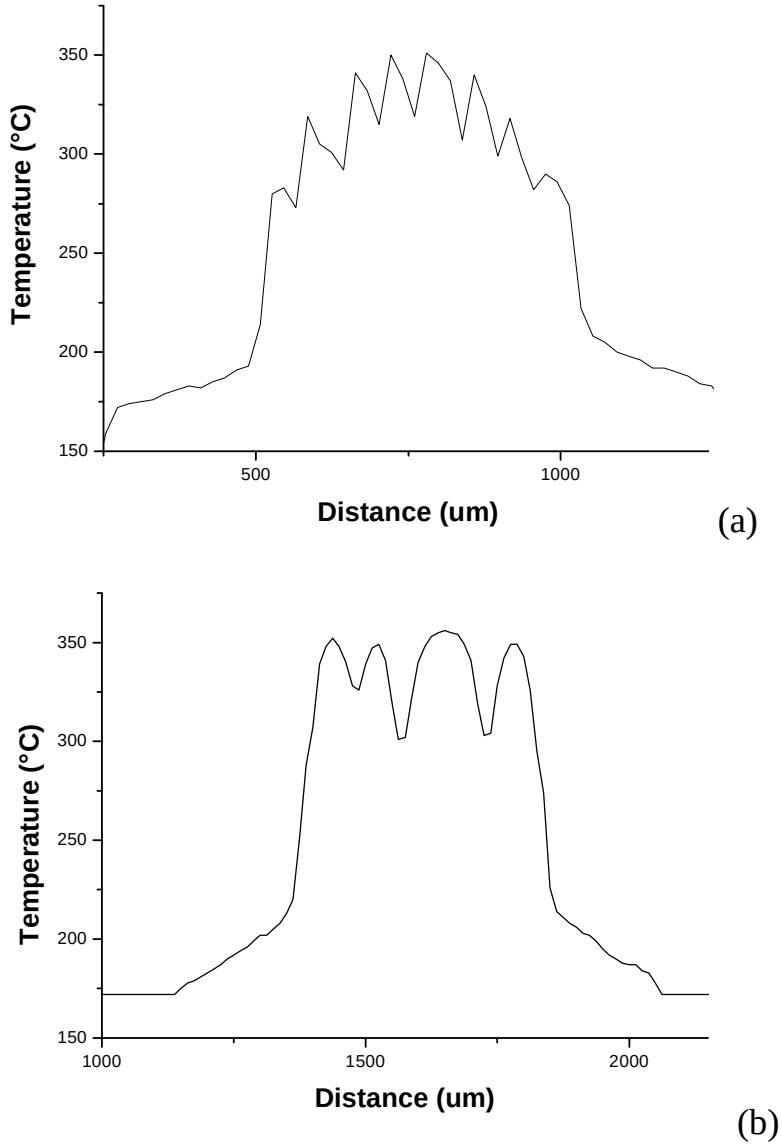

Figure 5.3. Cross-section of the temperature distribution for a metal-oxide micro-hotplate with (a) simple and (b) double meander heaters (S1), from IR thermal measurements.

The hollows in the Figure 5.3 are due to the difference of emissivity value between the arms of the platinum heater and the silicon nitride membrane. The value of emissivity could not be adjusted locally on the system used for the measurements and therefore the graphs in Figure 5.3 are representative of the two different heater designs.

The thermal measurements also suggested that the silicon plug added underneath the membrane improves the temperature distribution over the sensing area as shown in Figure 5.4. The curve obtained presented a smoother shape than those in Figure 5.3, taken on devices without silicon island, since the radiation intensity measured by the IR-camera is mainly coming from the silicon island.

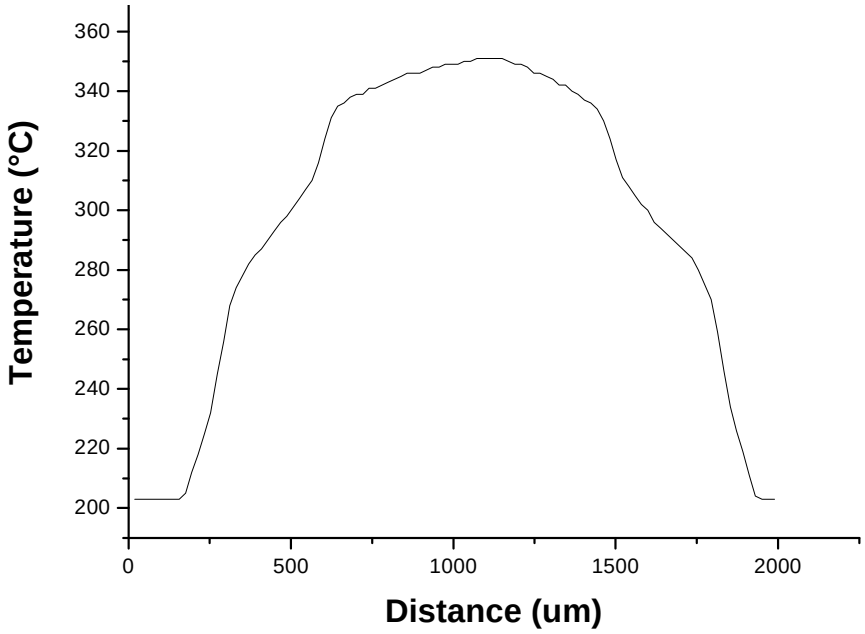

Figure 5.4. Cross-section of the temperature distribution over the sensing area for a metal-oxide micro-hotplate with a simple meander heater and a silicon island (S2Si), obtained by IR thermal measurements.

5.4.2 FEM simulations

5.4.2.1 Micro-hotplates without silicon island

The FEM simulations confirmed the indications obtained from the thermal measurements about the temperature distribution for the different heater designs. The temperature distribution over the sensing area was more homogeneous for the double meander heater than for the simple meander as shown in Figure 5.5 and in Table 5.2 for the 1.0 × 1.0 mm^2 design (S1).

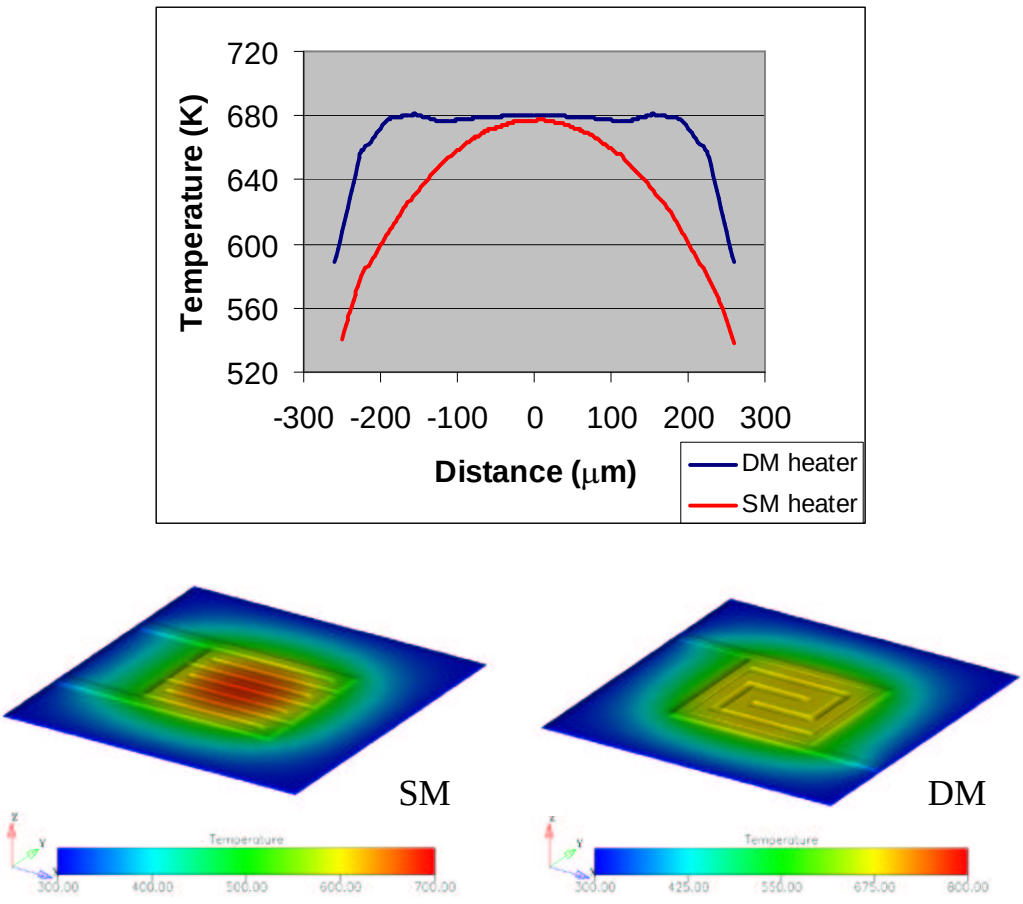

Figure 5.5. Temperature distribution at 400°C for the simple (SM) and double meander (DM) heaters on a membrane of 1.0 × 1.0 mm^2 (S1, $k_{nitride}$ =22 $W \bullet m^{-1}K^{-1}$).

At an operating temperature of 400°C ($k_{nitride}$ =22 W•m^{-1}K^{-1}), the temperature gradient between the center and the edge of the sensing area is 100°C and 23 °C for the simple and double meander, respectively (Fig. 5.5 and Table 5.2). Therefore, for a metal-oxide micro-hotplate without silicon island, the double meander heater definitely provides the best performance. The double meander structure gives more flexibility in the design of the heater It can be adapted to different thermal conductivity of the membrane material (silicon nitride in this case) by changing the width of its elements and/or the distance between them.

Table 5.2. Influence of the operating temperature (200, 300 and 400°C) on the temperature gradients of simple and double meander heaters on a 1.0 × 1.0 mm^2 membrane (S1).

Simple meander heater $k_{nitride}$=22 W•m^{-1}K^{-1}				**Simple meander heater** $k_{nitride}$=3.2 W•m^{-1}K^{-1}		
V [V]	T_{max} [°C]	ΔT_{max} [°C]		V [V]	T_{max} [°C]	ΔT_{max} [°C]
2.25	207	45		1.70	204	47
2.75	297	75		2.10	299	67
3.25	405	100		2.45	398	91
Double meander heater $k_{nitride}$=22 W•m^{-1}K^{-1}				**Double meander heater** $k_{nitride}$=3.2 W•m^{-1}K^{-1}		
V [V]	T_{max} [°C]	ΔT_{max} [°C]		V [V]	T_{max} [°C]	ΔT_{max} [°C]
2.50	200	10		1.70	198	8
3.15	302	15		2.20	315	15
3.70	406	23		2.50	398	20

Figures 5.6, as well as the results given in Table 5.2, show that the temperature gradient on the sensing area depends also on the temperature of operation. The temperature gradient is larger for a higher operating

temperature. Moreover, in the case of the designs considered here, maintaining the ratio of heater area radius to membrane radius constant, the size of the heater area influenced the temperature gradient over the sensing area for the metal-oxide hotplate, as presented in Figure 5.7. The gradient was larger for the larger design, S2, than for S1.

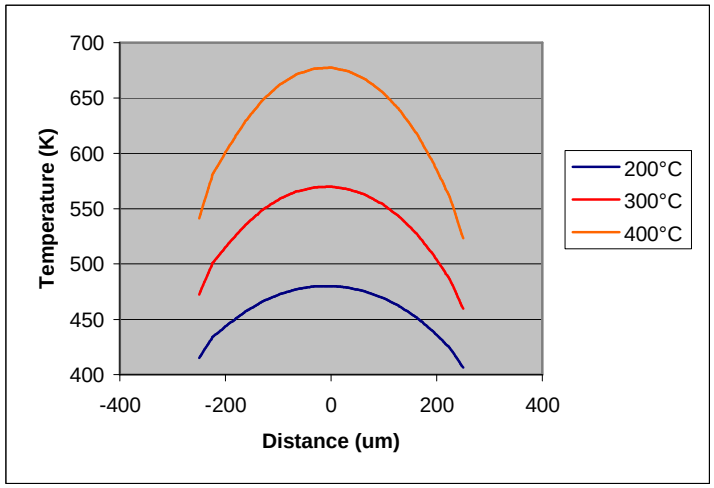

(a)

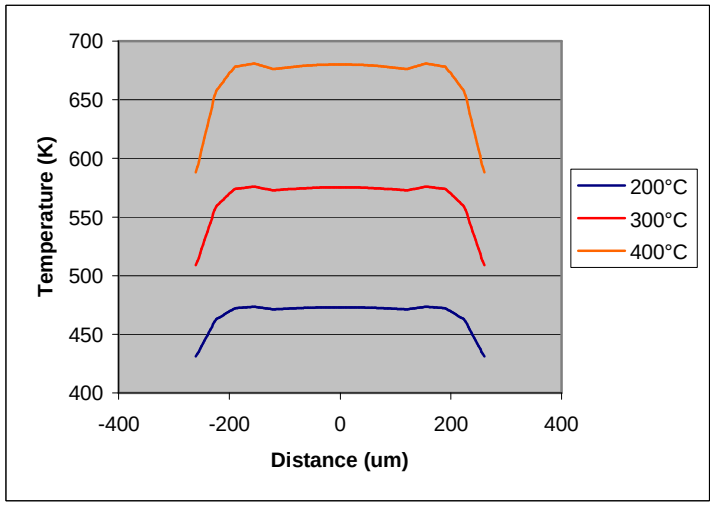

(b)

Figure 5.6. Influence of the operating temperature on the temperature gradient between the centre and the edge of the sensing area for the metal-oxide micro-hotplate (S1, $k_{nitride}$ = 22 $W \bullet m^{-1}K^{-1}$) with (a) simple meander and (b) double meander heater

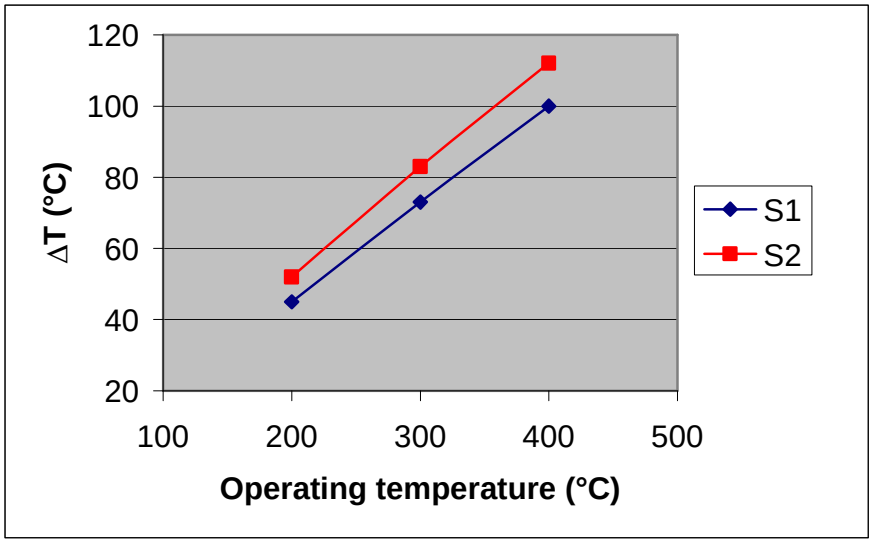

Figure 5.7. Influence of the heater area (S1 and S2) on the temperature gradient between the centre and the edge of the sensing area for the metal-oxide micro-hotplate with a simple meander heater ($k_{nitride}$=22 W•m^{-1}K^{-1}).

Depending on the technology and applications, different types of heater geometry have been proposed during the last years [10,12,21-23]. However, to our knowledge, a temperature gradient lower than 10°C has not been reported so far for closed-membranes. Since the temperature gradient between the center and the edge of the sensing area can reach a value of about 110°C for a simple meander heater operating at 400°C on a 1.5 × 1.5 mm^2 membrane (S2) (see Figure 5.7), this was considered as our worse case to optimise. A 10-µm thick silicon island (k=100 W•m^{-1}K^{-1}) was added underneath the membrane of this design (S2Si, simple meander heater) to improve the temperature homogeneity over the sensing area.

5.4.2.2 Micro-hotplates with silicon island

A 10-μm thick silicon island was added to the metal-oxide micro-hotplate with a simple meander heater (S2Si) with the hope of reaching a temperature gradient less than 10°C over the heating/sensing area. The FEM simulations confirmed the experimental results presented in Figure 5.4. Using this design, a uniform temperature distribution (< 5°C) over the sensing area was obtained all over the silicon island surface as shown in Figure 5.8a. Another interesting point is that temperature distribution was found to be almost independent of the heater geometry. This is evident in Figure 5.8b which shows the homogeneous temperature distribution over the sensing area for a U-shaped heater on a silicon nitride membrane with the silicon island underneath.

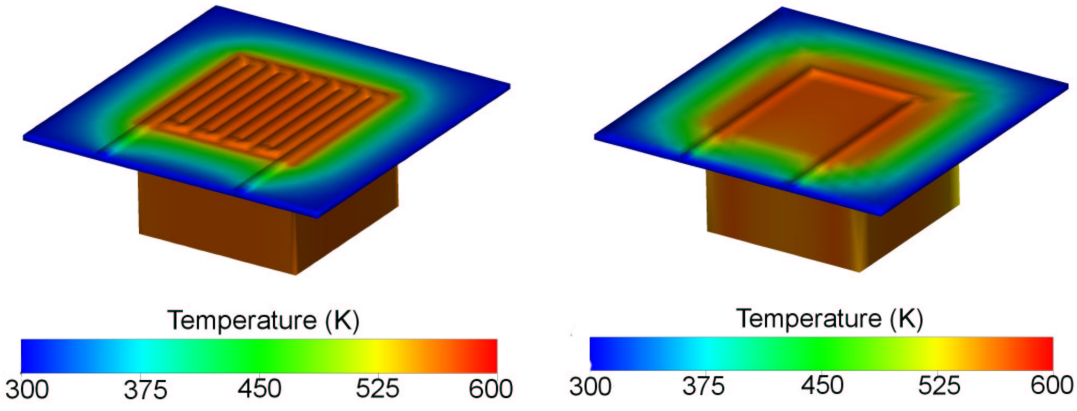

(a) (b)

Figure 5.8. FEM simulations of a micro-hotplate with a silicon island (S2Si, S3Si) for (a) simple meander, and (b) U-shape heater (z-axis x 50, temperature = 300°C, k_{Si}= 100 W•m^{-1}K^{-1}, $k_{nitride}$= 3.2 W•m^{-1}K^{-1}).

Therefore, the heater and the electrodes (Pt) could be defined in one fabrication step using the same mask level [23].

Moreover, a semiconducting heater having a U-shape was adopted for the MOSFET sensor (S3Si). This heater geometry gives more flexibility in the layout, which is an important issue due to the high number of electrical connections for this device.

5.4.3 Optimisation of the silicon island thickness

The optimum silicon island thickness to minimise the power consumption and maintain a uniform temperature distribution over the sensing area was determined by simulation. The metal-oxide sensor with a simple meander heater (S1Si and S2Si) and a MOSFET sensor with a U-shaped heater (S3Si) were considered. Different parameters, such as the heater area, operation temperature, thermal conductivity of the materials used, and silicon island fabrication, were taken into account.

5.4.3.1 Heating area and operating temperature

As presented in Figure 5.7 for metal-oxide micro-hotplates, the heater area can have an influence on the temperature gradient depending on the design. The gradient was larger for the larger design, S2, than for S1. Therefore, the silicon island thickness was optimised for the design S2Si, with assumption that the results could be transferred to S1 with slight improvement. The thickness of the silicon island for the MOSFET micro-hotplates was minimised for the only design considered here, S3Si.

Figures 5.6, as well as the results given in Table 5.2, show that the temperature gradient on the sensing area depends also on the temperature of operation. The temperature gradient is larger for a higher operating

temperatures. Indeed, the temperature of operation of metal-oxide gas sensors depends on the nature of the gas to be detected and typically varies from 200°C (e.g. NO_2) to 400°C (e.g. CH_4). This effect is less important for MOSFET sensors since their temperature of operation is limited to 225°C, due to the appearance of leakage currents at higher temperatures. The simulations to optimise the silicon island thickness were performed at a specific operating temperature of 300°C and 200°C for the metal-oxide and MOSFET sensors, respectively.

5.4.3.2 Materials thermal conductivity

The temperature distribution over the sensing area depends also on the thermal conductivity of the silicon forming the island, which is related to the fabrication process. Simulations were performed considering different levels of doping of the silicon. The thermal conductivity (k) was set at 150 $W \bullet m^{-1}K^{-1}$ for pure silicon, and at 100 $W \bullet m^{-1}K^{-1}$ and 50 $W \bullet m^{-1}K^{-1}$ for doped silicon used in electrochemical (n-type) and boron (p++) etch stop processes, respectively [11,20]. The influence of the thermal conductivity of the silicon on the temperature gradient is shown for the metal-oxide micro-hotplate in Figure 5.9.

Since the thermal conductivity of a thin film is not easy to determine, a low value of 3.2 $W \bullet m^{-1}K^{-1}$ (low-stress) and a high value of 22 $W \bullet m^{-1}K^{-1}$ (standard) were taken from the literature for the silicon nitride film used as membrane [11,18]. Its influence on the temperature distribution over the sensing area is also presented in Figure 5.9. The high value gives a higher temperature gradient over the sensing area as expected. The micro-hotplates optimised

here have a low-stress silicon nitride as membrane. A thermal conductivity of 3.2 $W \bullet m^{-1}K^{-1}$ was therefore chosen to perform the simulations with the aim of minimising the silicon island thickness. However, one should be aware that the value of this parameter should be experimentally determined to confirm the following results.

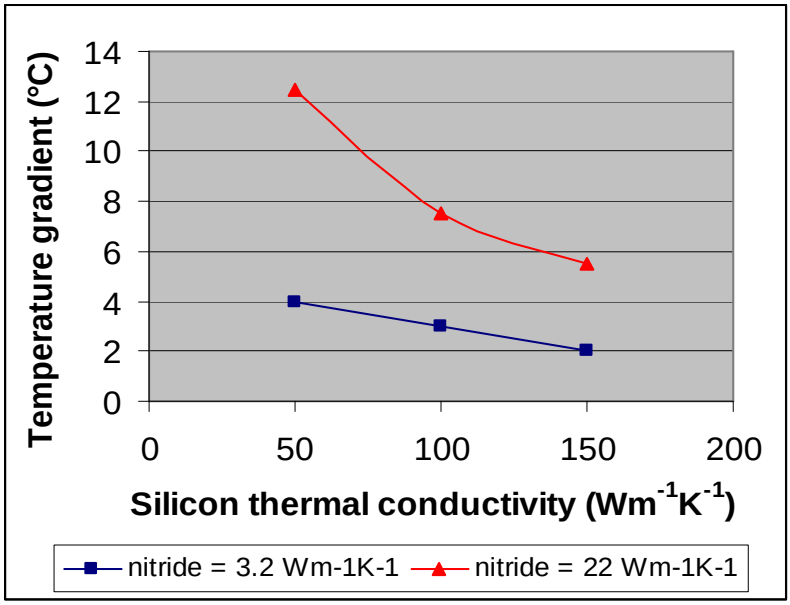

Figure 5.9. Influence of the silicon thermal conductivity on the temperature gradient for metal-oxide micro-hotplates having a silicon island (5 µm thick) and operating at 300°C (S2Si with simple meander heater, $k_{nitride}$ = 3.2 $W \bullet m^{-1}K^{-1}$ and 22 $W \bullet m^{-1}K^{-1}$).

5.4.3.3 Optimised silicon island thickness for metal-oxide micro-hotplates

In the case of metal-oxide sensors, the temperature gradient has to be optimised to improve the sensitivity and selectivity of the gas sensitive coating over the electrodes. This means that the temperature gradient has to be

minimised over the entire sensing area. Figure 5.10 shows the influence of the silicon island thickness on the temperature gradient over the sensing area for a simple meander heater. A 2.0–2.5-µm-thick silicon island (k = 50 W•m^{-1}K^{-1}) is enough to reduce the temperature gradient over the sensing area (750 × 750 µm^2) to a value of about 10°C. Therefore, the two-step silicon bulk micromachining process used to fabricate the 10 µm-thick silicon island could be replaced by a high concentration boron etch stop (p^{++}) made by implantation.

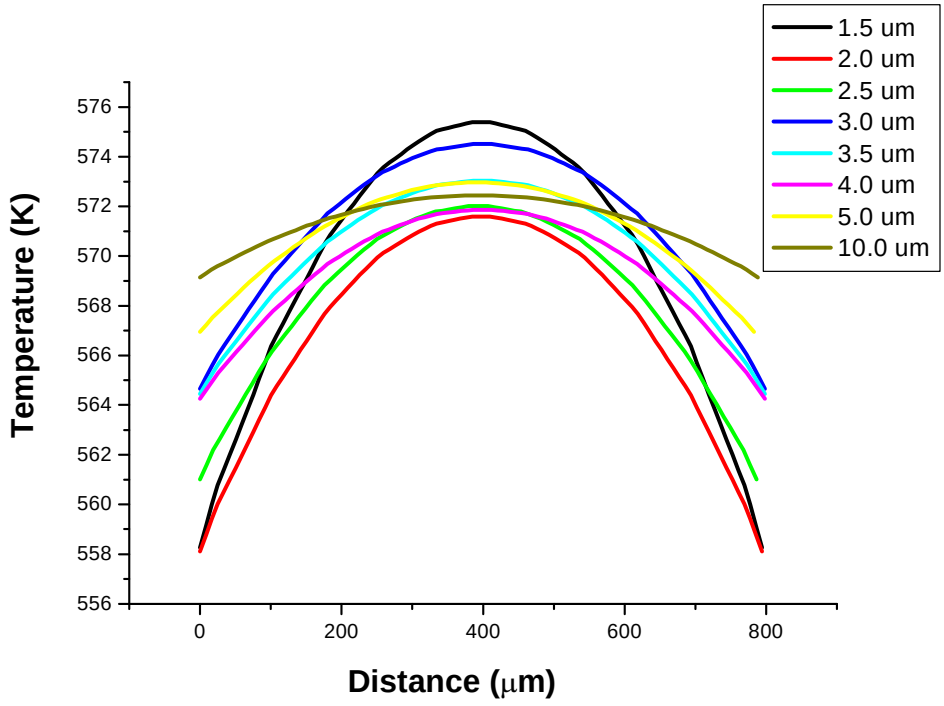

Figure 5.10. Temperature distribution over the sensing area (section in the middle) of a metal-oxide micro-hotplate as a function of the silicon island thickness (k = 50 W•m^{-1}K^{-1}) for an operating temperature of 300°C (S2Si with simple meander heater, $k_{nitride}$ = 3.2 W•m^{-1}K^{-1})

5.4.3.4 Optimised silicon island thickness for metal-oxide micro-hotplates

The MOSFET array sensor contains four different sensitive areas (60 × 70 μm^2) that should operate at the same temperature (Fig 5.11). Therefore, the silicon island thickness has to be minimised with the aim of obtaining a temperature gradient on individual devices (on 60 × 70 μm^2) and between the devices that does not exceed 5°C**.** The array of devices has a symmetric 2 × 2 configuration and is placed in between the U-shaped heater**.**

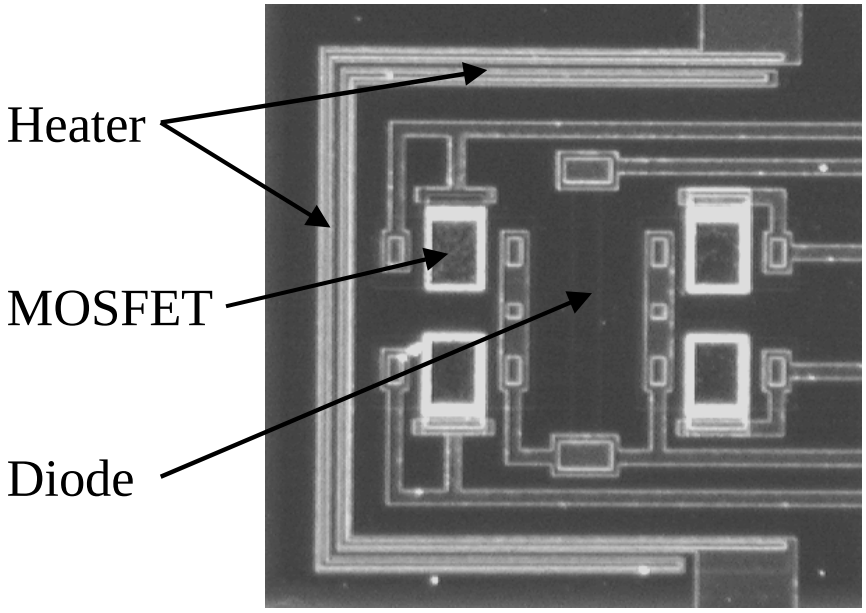

Figure 5.11. Photograph of the MOSFET array gas sensor, on which are the four MOSFETs surrounded by the heater (U-shape) and with the diode in the middle (temperature sensor).

For a minimum silicon island thickness of 1.5 μm, Figures 5.12 and 5.13 show that the gradient is less than 5°C on an individual sensor and also between two sensors in a symmetric position with respect to the heater (the two on the left

or on the right in Fig. 5.11). However, for a given silicon island thickness, a comparison of Figures 5.12 and 5.13 is necessary to determine the temperature gradient between the two sensors on the left and the two on the right on Figure 5.11. It was found that a silicon island (k = 100 $W \bullet m^{-1}K^{-1}$) with a minimum thickness of 2.0 μm provides a homogenous temperature for the sensor array. The temperature gradient is less than 5°C.

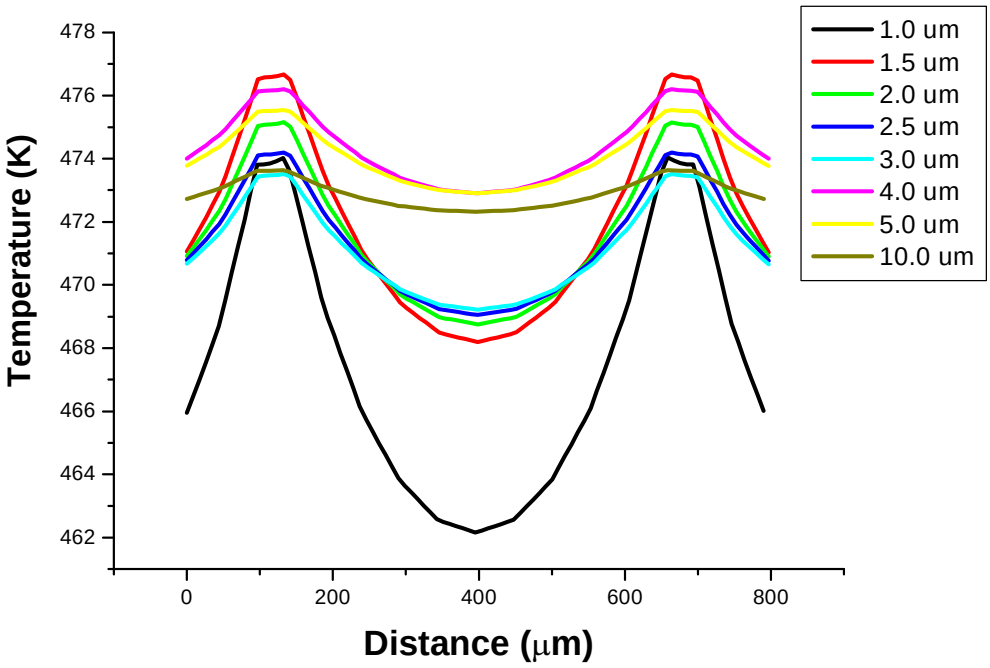

Figure 5.12. Temperature distribution (cross-section on the two sensors on the left in Fig. 5.11) over a MOSFET micro-hotplate as a function of the silicon island thickness (k = 100 $W \bullet m^{-1}K^{-1}$) for an operating temperature of 200°C (S3Si with U-shaped heater, $k_{nitride}$ = 3.2 $W \bullet m^{-1}K^{-1}$).

An electrochemical etch stop process could be used to fabricate the silicon island. In this case, a boron etch stop is not suitable since it is not compatible with the integration of electronic components in the silicon island.

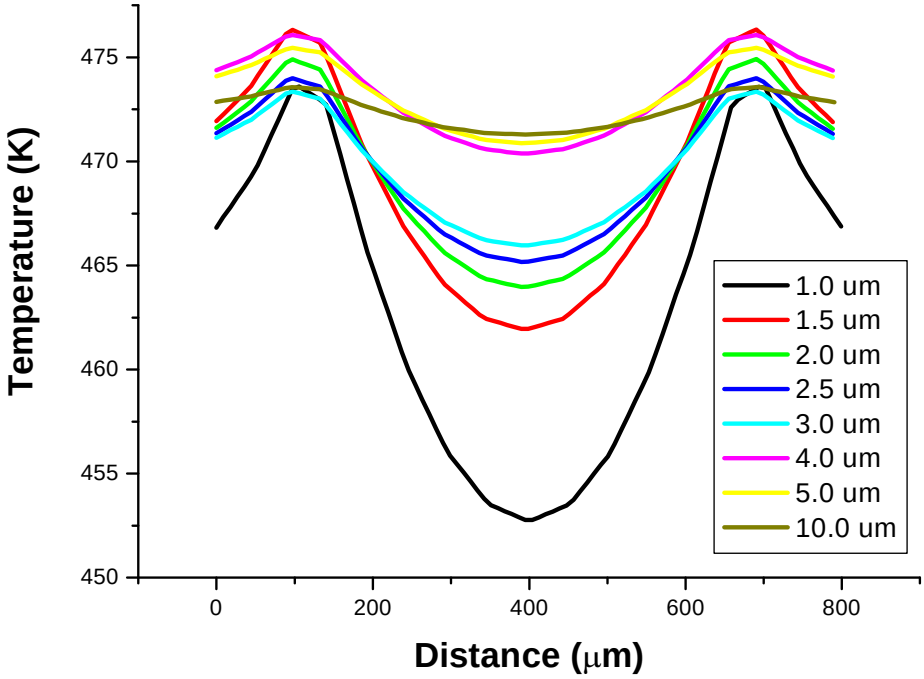

Figure 5.13. Temperature distribution (cross-section on the two sensors on the right in Fig. 5.11) over a MOSFET micro-hotplate as a function of the silicon island thickness (k = 100 $W \bullet m^{-1}K^{-1}$) for an operating temperature of 200°C (S3Si with U-shaped heater, $k_{nitride}$ = 3.2 $W \bullet m^{-1}K^{-1}$).

5.5 CONCLUSION

The power consumption and the temperature distribution of micro-hotplates having a silicon island were optimised by using MEMCAD to simulate their thermal behaviour. Optimised silicon island thicknesses were determined by

simulation, to improve the temperature distribution over the sensing areas of low power metal-oxide and MOSFET gas sensors. The specific operating temperatures, heater geometry and thermal conductivity were considered in the simulations.

A 10-µm-thick silicon island was found to be suitable for the design of micro-hotplates with no restrictions introduced by heater geometry. Therefore, the platinum heater and electrodes for the metal-oxide micro-hotplates could be defined in one photolithographic step. Optimisation by simulation of the silicon island thickness to decrease power consumption and facilitate its fabrication was performed for specific applications. Two-steps silicon bulk micromachining in KOH to make the silicon island could be replaced by a boron or an electrochemical etch stop process for metal-oxide and MOSFET micro-hotplates, respectively.

We are looking at the influence of a thin layer of silicon on the temperature distribution over the gas sensing area to evaluate the use of silicon-on-insulator (SOI) substrates. SOI technology provides an integrated etch-stop for the silicon island in the form of a buried oxide layer. Increased operating temperatures for of the MOSFET sensors should also be made possible using this technology.

5.6 ACKNOWLEDGEMENTS

The European program Brite-Euram III (n° BRPR-CT96-0194), AppliedSensor (former NST, Linköping, Sweden) and the Fonds pour la formation des Chercheurs et l'Aide à la Recherche (FCAR) from the Quebec Government have financially supported this project. We are grateful to IMT-

samlab, Institute of Microtechnology, University of Neuchâtel, Neuchâtel, Switzerland, technical staff for the support in the fabrication of the devices. We would like also to thank Dr. E. Scheid, Laboratory for Analysis and Architecture of Systems (LAAS), Toulouse, France, for the IR thermal measurements and Dr. P. Martensson from AppliedSensor, Linköping, Sweden, and Dr. N. Barsan and A. Krauss, University of Tübingen, Tübingen, Germany, for helpful discussions.

5.7 REFERENCES

[1] G. Sberveglieri, W- Hellmich, and G. Müller, “Silicon hotplates for metal oxide gas sensor elements”, Microsystem Technologies, 3, pp.183-190, 1997.

[2] A.P. Lee and B.J. Reedy, “Temperature modulation in semiconductor gas sensing”, Sensors and Actuators, B 60, pp. 35-42, 1999.

[3] I. Simon, N. Barsan, M. Bauer, and U. Weimar, “Micromachined metal oxide gas sensors: Opportunities to improve sensor performance”, Sensors and Actuators, B 73, pp. 1-26, 2001.

[4] U. Dibbern, “A substrate for thin-film gas sensors in microelectronic technology”, Sensors and Actuators, B 2, pp. 63-70, 1990

[5] W. Lang, “Heat transport from a chip”, IEEE Trans. on Electron Devices, 37(4), pp. 958-963, 1990.

[6] U. Dillner, “Thermal modeling of multilayer membranes for sensors applications”, Sensor and Actuators, A 41-42, pp. 260-267, 1994.

[7] A. Pike and J.W. Gardner, “Thermal modelling and characterisation of micropower chemoresistive silicon sensors”, Sensors and Actuators, B 45, pp. 19-26, 1997.

[8] D. Briand, A. Krauss, B. van der Schoot, U. Weimar, N. Barsan, W. Göpel, and N.F. de Rooij, "High temperature micro-hotplates for drop-coated gas sensors", Sensors and Actuators, B 68, pp. 223-233, 1999.

[9] D. Briand, B. van der Schoot, H. Sundgren, I. Lundström, and N.F. de Rooij, A low-power micromachined MOSFET gas sensor, Journal of Micro-Electro-Mechanical Systems, 9(3), pp. 303-308, 2000.

[10] A. Gotz, I. Gràcia, C. Cané, and E. Lora-Tamayo, "Thermal and mechanical aspects for designing micromachined low-power gas sensors", Journal of Micromechanics and Microengineering, 7, pp. 247-249, 1997.

[11] C. Rossi, E. Scheid, and D. Estève, "Theoretical and experimental study of silicon micromachined microheater with dielectric stacked membranes", Sensors and Actuators, A 63, pp. 183-189, 1997.

[12] S. Astié, A.M. Gué, E. Scheid, L. Lescouzères, and A. Cassagnes, "Optimisation of an integrated SnO_2 gas sensor using a FEM simulator", Sensors and Actuators, A 69, pp. 205-211, 1998.

[13] M. Dumitrescu, C. Cobianu, D. Lungu, D. Dascalu, A. Pascu, S. Kolev, and A. van den Berg, "Thermal simulation of surface micromachined polysilicon hot plates of low power consumption", Sensors and Actuators, A 76, pp. 51-56, 1999.

[14] L. Chih-Cheng, D. Setiadi, F. Udrea, W. Milne, J.A. Covington, and J.W. Gardner, "3D therm-electro-mechanical simulations of gas sensors based on SOI membranes", in Conf. Proc. of 3rd Int. Conf. on Modeling and Simulation of Microsystems (MSM'00), pp. 297-300, 2000.

[15] Microcosm Technologies Inc., Development Center, 101 Rogers St., Suite 213, Cambridge, MA 02142, USA.

[16] D.J. Silversmith, and J.R. Reid, "Joule heating simulations of polysilicon microactuators", in Conf. Proc. of 2nd Int. Conf. on Modeling and Simulation of Microsystems (MSM'99), pp. 613-615, 1999.

[17] P. Mielle, "Managing dynamic thermal exchanges in commercial semiconducting gas sensors", Sensors and Actuators, B 34, pp. 533-538, 1996.

[18] C.H. Mastrangelo, Y.-C. Tai, and R.S. Muller, “Thermophysical properties of low-residual stress, silicon-rich, LPCVD silicon nitride films”, Sensors and Actuators, A 21-23, pp. 856-860, 1990.

[19] R.P. Manginell, D.A. Rosato, D.A. Benson, and G.C. Frye-Mason, “Finite element modelling of a microhotplate for microfluidic applications”, in Conf. Proc. Of the 2nd Int. Conf. On Modeling and Simulations of Microsystems (MSM’99), pp. 663-666, 1999.

[20] G. Slack, “Thermal conductivity of pure and impure silicon, silicon carbide, and diamond” J. Appl. Phys., 35(12), pp. 3460-3466, 1964.

[21] V. Guidi, G.C. Cardinali, L. Dori, G. Faglia, M. Ferroni, G. Martinelli, P. Nelli, and G. Sberveglieri, “Thin-film gas sensor implemented on a low-power-consumption micromachined silicon structure” Sensors and Actuators, B 49, pp. 88-92, 1998.

[22] R. Aigner, M. Dietl, R. Katterlober, and V. Klee, “Si-planar-pellistor: designs for temperature modulated operation“, Sensors and Actuators, B 33, pp. 151-155, 1996.

[23] W.-Y. Chung, J.-W. Lim, D.-D. Lee, N. Miura, and N. Yamazoe, “Thermal and gas-sensing properties of planar-type micro gas sensor”, Sensors and Actuators, B 64, pp 118-123, 1999.

List of publications

List of publications

Referred articles

D. Briand, H. Windgrant, H. Sundgren, B. van der Schoot, L.-G. Ekedahl, I. Lundström, and N. F. de Rooij, “New modes of operation for MOSFET gas sensors using low-power devices”, manuscript in preparation.

D. Briand, S. Heimgartner, M.-A. Grétillat, B. van der Schoot, and N.F. de Rooij, “Thermal optimisation of micro-hotplates having a silicon island”, manuscript in preparation.

R. Tamadori, J.W. Gardner, A. Krauss, U. Weimar, D. Briand, B. van der Schoot, H. Sundgren, I. Besnard, P. Barttlet, L. Gier, and S. Cosensa, “A cabin air analyser”, submitted.

J.A. Covington, J.W. Gardner, D. Briand, and N. F. de Rooij, “A polymer gate FET sensor array for detecting organic vapours”, Sensors and Actuators, B 77, pp. 155-162, 2001.

D. Briand, H. Sundgren, B. van der Schoot, I. Lündström, and N.F. de Rooij, “Thermally isolated MOSFET for gas-sensing application”, IEEE Electron Device Letters, 22(1), pp. 11-13, 2001.

D. Briand, B. van der Schoot, H. Sundgren, I. Lundström, and N.F. de Rooij, “A low-power micromachined MOSFET gas sensor”, Journal of Micro-Electro-Mechanical Systems, 9(3), pp. 303-308, 2000.

D. Briand, A. Krauss B. van der Schoot, U.Weimar, N. Barsan, W. Göpel, and N.F. de Rooij, “Design and fabrication of high temperature micro-hotplates for drop coated gas sensors”, Sensors and Actuators, B 68, pp. 223-233, 2000.

O. Renault, D. Briand, G. Delabouglise, J. F. Currie, and M. Labeau, “Integration of a sensitive material to a silicon-based device for CO detection”, Sensors and Actuators, A 74, pp. 225-228, 1999.

D. Briand, M. Labeau, J. F. Currie, and G. Delabouglise, “Pd-doped SnO_2 thin films deposited by CVD assisted ultrasonic spraying for gas-sensing: selectivity and effect of annealing”, Sensors and Actuators, B 48, pp. 395-402, 1998.

Conferences and workshop proceedings

J.W. Gardner, S.M. Lee, D.C. Dyer, P.N. Bartlett, S. Guerin, D. Briand, and N.F. de Rooij, “Silicon planar microcalorimeter employing nanostructured films”, Tech. Digest of Transducers’01, Munich, Germany, pp. 820-823, 2001.

D. Briand, O. Guenat, B. van der Schoot, T. Hirata, and N.F. de Rooij, “Micro-hotplate, a useful concept for gas-sensing, fluidics and space applications”, Conf. Proc. of Microfabricated Systems and MEMS V, 198th ECS Meeting, pp. 151-158, 2000.

L. Dellmann, T. Akiyama, D. Briand, S. Gautsch, B. Guldimann, P. Luginbuhl, C. Marxer, U. Staufer, and N. F. de Rooij, “Microsystems for diverse applications using recently developed microfabrication techniques”, Conf. Proc. SPIE vol. 4176, Micromachined Devices and Components VI, pp. 16-27, 2000,

O. T. Guenat,T. Hirata, D. Briand, P.-A. Clerc, G. Mondin, U. Kroll, and N. F. de Rooij, "Pneumatic conveyance systems for micro-parts transportation", Conf. Proc. of the 2nd International Workshop on Microfactories, pp. 43-46, 2000.

D. Briand, B. van der Schoot, H. Sundgren, L.-G. Ekedahl, I. Lundström, and N. F. de Rooij, "New response patterns for MOSFET gas sensors using low-power devices", Proc. of Eurosensors XIV, pp. 737-740, 2000.

J.A. Covington, J.W. Gardner, C. Toh, P.N. Bartlett, D. Briand, and N.F. de Rooij, "Array of MOSFET devices with electrodeposited conducting polymer gates for vapour and odour sensing", Conf. Proc. of the 7th International Symposium on Olfaction and Electronic Nose, 2000.

D. Briand, M.-A. Gretillat, B. van der Schoot, and N.F. de Rooij, "Thermal management of micro-hotplates using MEMCAD as simulation tool", Conf. Proc. of 3rd Int. Conf. on Modelling and Simulation of Microsystems, pp. 640-643, 2000.

D. Briand, B. van der Schoot and N.F. de Rooij, A. Krauss, U.Weimar, N. Barsan, and W. Göpel, "High temperature micro-hotplates for drop-coated gas sensors", Conf. Proc. of Eurosensors XIII, pp. 703-704, 1999.

D. Briand, B. van der Schoot, S. Jeanneret, P.-A. Clerc, and N.F. de Rooij, H. Sundgren, I, Grahn, and I. Lundström, "Novel low-power consumption MOSFET array gas sensor", Tech. Digest of Transducers'99, pp. 938-941, 1999.

O. Renault, D. Briand, G. Delabouglise, J. F. Currie, and M. Labeau, "Integration of a CO sensitive film on silicon", Conf. Proc. of EMRS-Meeting, Symposium: Materials for Microsystems, 1998.

D. Briand, M. Labeau, G. Delabouglise, and J. F. Currie, "Pd-doped SnO_2 thin films deposited by CVD assisted ultrasonic spraying for gas-sensing: selectivity and effect of annealing", Conf. Proc. of Eurosensors XI, pp. 451-454, 1997.

D. Briand, G. Delabouglise, A. Lecours, J. F. Currie, and M. Labeau, "Pd-doped SnO_2 thin films for CO detection", Conf. Proc. of the 2^{th} International Symposium on New Materials for Fuel Cell and Modern Battery System, Montréal, Canada, July 1997, pp 911-914.

Patent

D. Briand, H. Sundgren, B. van der Schoot, I. Lundström, and N.F. de Rooij, GasFET devices integrated on micro-machined hotplates and methods for their fabrication, submitted.